Understanding historical and future changes in mean and extreme rainfall in Australia

A thesis submitted for the degree of Doctor of Philosophy of The Australian National University

Raktima Dey

June 2020

Fenner School of Environment and Society

Australian National University, Canberra, ACT, Australia

Declaration

This thesis is submitted as a Thesis by Compilation in accordance with the Australian National University policies https://policies.anu.edu.au/ppl/document/ANUP_003405.

I declare that the research presented in this thesis represents original work that I carried out during my candidature at the Australian National University, except for contributions to multi-author papers incorporated in the thesis where my contributions are specified in this Statement of Contribution.

Publication declaration

Chapter 2, 3, and 6 are published, chapter 5 is in manuscript form, and chapter 5 is under review. Below is the list of papers, including my contribution in each article.

Chapter 2: **Dey R**, Lewis SC, Arblaster JM, & Abram NJ. 2019. A review of past and projected changes in Australia's rainfall. *Wiley Interdisciplinary Reviews: Climate Change* **10**: e577.doi:10.1002/wcc.577.

Author	Nature of contribution	Extent of contribution in research	Extent of contribution in writing
Raktima Dey	Led project designing, data analysis, writing, and carried out all revisions.	80%	70%
Sophie C. Lewis	Helped with project designing, and manuscript editing.	10%	15%
Julie M. Arblaster	Helped with project designing, and manuscript editing.	5%	10%
Nerilie J. Abram	Helped with project designing, and manuscript editing.	5%	5%

Chapter 3: **Dey R**, Lewis SC, Abram NJ, 2018. Investigating observed northwest Australian rainfall trends in Coupled Model Intercomparison Project phase 5 detection and attribution experiments. *Int J Climatol.*;1–16. https://doi.org/10.1002/joc.5788

Author	Nature of contribution	Extent of contribution in research	Extent of contribution in writing
Raktima Dey	Led project designing, data analysis, writing, and carried out all revisions.	70%	80%
Sophie C. Lewis	Helped with project designing and manuscript editing.	15%	5%
Julie M. Arblaster	Helped with project designing and manuscript editing.	10%	10%
Nerilie J. Abram	Helped with project designing and manuscript editing.	5%	5%

Chapter 4: **Dey R,** Bador M, Alexander LV, Lewis SC. The timing and drivers of extreme rainfall events in Australia (Under review).

Author	Nature of contribution	Extent of contribution in research	Extent of contribution in writing
Raktima Dey	Led project designing, data analysis, writing, and carried out all revisions.	85%	80%

Margot Bador	Helped with project designing and manuscript editing.	10%	10%
Lisa V. Alexander	Helped with project designing and manuscript editing.	5%	5%
Sophie C. Lewis	Helped with project designing and manuscript editing.	-	5%

Chapter 5: **Dey R**, Lewis SC. Understanding extreme rainfall scaling rates in Australia in historical climate and future projections (In preparation).

Author	Nature of contribution	Extent of contribution in research	Extent of contribution in writing
Raktima Dey	Led project designing, data analysis, writing, and carried out all revisions.	85%	75%
Sophie C. Lewis	Helped with project designing and manuscript editing.	15%	25%

Chapter 6: **Dey R**, Gallant AJ, Lewis SC (2020). Evidence of a continent-wide shift of episodic rainfall in Australia. *Weather and Climate Extremes*, 29, 100274. doi:https://doi.org/10.1016/j.wace.2020.100274

Author	Nature of contribution	Extent of contribution in research	Extent of contribution in writing
Raktima Dey	Led project designing, data analysis, writing, and carried out all revisions.	80%	70%
Ailie J. Gallant	Helped with project designing, writing, and manuscript editing.	15%	20%
Sophie C. Lewis	Helped with project designing and manuscript editing.	5%	10%

Acknowledgement

First, I want to acknowledge that the last year of my PhD, 2020 has been exceptionally hard for everyone. I am incredibly grateful for being safe and healthy. I am thankful for the great support provided by the Australian National University.

I want to express great appreciation to Dr. Sophie Lewis for her continuous supervision and support for the last three and a half years. Prof. Julie Arbalester has a great contribution to my research and publications, even the briefest interactions with her have proven to be extremely helpful. I want to thank Prof. Nerilie Abram, for guiding me through my PhD project. I greatly appreciate my supervisors' contributions and efforts in mentoring me. I want to thank Prof. Saul Cunningham for kindly agreeing to become my chair of the panel and supporting me with administrative hurdles at ANU. Apart from my supervisory panel, I have enjoyed many kind gestures by scientists towards me during my PhD. Especially, I want to thank Dr. Ailie J. Gallant for her time and rigorous support which continued even through maternity leave. Lastly, I want to thank Dr. Margot Bador and Prof. Lisa Alexander for their support and collaborative research.

I am extremely grateful to be a part of the Centre of Excellence for Climate System Science. The Centre of Excellence has given me many opportunities to meet scientist and students from different institutes, and build academic skills through various workshops. Also, through the support of the Centre, I had the opportunity to visit NOAA, and NCAR, where networking opportunities have been most enjoyable and beneficial.

My experience would not have been so satisfying without a fantastic group of friends and colleagues in Fenner. In the last three years, I have received great support from my lovely friends Depi, Soy, and other PhD students through many office chats, and "shut up and write" sessions.

I want to thank my three compassionate friends – Astha, Anukriti and Ankur. Sharing our PhD journeys with lots of laughs have made my PhD journey a lot smoother. Cooking, hosting dinners, and weekend trips with two amazing housemates Ankuriti, Astha and dear friend Chirag have given me memories for a lifetime. I want to thank Preetha, who has been a pillar of strength in this journey and for always feeding me homecooked food. Thank you to Mahesh for being so loving and always guiding me as an elder brother and friend. I want to thank

Nicholas Schepel for his unconditional love, support, and patience. I cannot thank him enough. These people have been a family away from family in India.

Finally, I want to thank Maa (Kabita) and Baba (Nabakumar) for teaching me everything I have learnt. My sister (Moumita AKA Didi) has been a constant mood uplifter. Thank you so much for always giving me positivity, support, and love. Didi has been a second mother to me. Thank you my two little cousin brothers Arush and Rishan who bring constant joy in my life. I also want to thank my grandmother (Purabi) for so much love and care every time I visit India, my Uncle (Mithun) and Aunt (Moumita) for their love and care.

This thesis is dedicated to my family in India, whom I love and miss very much.

Abstract

Understanding anthropogenic changes in rainfall in Australia is difficult as Australia experiences one of the highest variable rainfall climates in the world. In general, detecting long-term robust changes in rainfall, particularly rainfall extremes, is challenging due to short observational records, discrepancies in datasets, varying methodologies and the influence of many large-scale drivers modulating Australia's rainfall.

There are three main goals of this thesis. Firstly, this research aims to understand the observed historical changes in various characteristics of mean and extreme rainfall in Australia. Secondly, the research aims to understand the role of anthropogenic forcing and large-scale variability in driving changes in mean and extreme rainfall in Australia. Lastly, this research aims to identify the shortcomings of existing methods to study historical and future changes in rainfall and develop robust new approaches.

The major outcomes from each of the result chapters are summarised below:

1. A comprehensive review of the persistent increase in rainfall in northwest Australia (NWA) since 1950, and a strong decrease in the southwest of Western Australia (SWWA) and southeast Australia (SEA), finds there are still significant knowledge gaps in our understanding of underlying mechanisms behind some of these changes. Extreme rainfall follows a similar trend to mean rainfall; however, very few regions show significant long-term historical changes in extreme rainfall. In addition, there is low confidence in extreme rainfall projections.
2. Anthropogenic forcings play a significant role in modulating rainfall in NWA. Investigation using a set of the Coupled Model Intercomparison Project phase 5 (CMIP5) models shows that the persistent increase in mean and extreme rainfall in NWA is better captured when aerosol forcings are incorporated. While aerosols lead to increased rainfall, greenhouse gases lead to a decrease in rainfall, resulting in an offsetting impact between aerosols and greenhouse gases. This study indicates the importance of correct representation of the interaction between natural drivers and all anthropogenic forcings (i.e. not just greenhouse gases) in climate models.
3. Previous research shows that large-scale Pacific drivers (the El Niño-Southern Oscillation (ENSO) and the Interdecadal Pacific Oscillation (IPO)) modulate both rainfall intensity and frequency in Australia. This research presented in this thesis indicates that the timing of

extreme rainfall varies largely depending on the phases of ENSO and IPO and their interaction, particularly in SEA. Australia has a clear north and south distinction in the timing of extreme rainfall. Extreme rainfall in the north usually occurs in the summer, while in the south it typically occurs in late autumn/winter. The area of summer extreme rainfall extends southward (northward) during a negative phase of IPO (positive IPO). Variability in the timing of extreme rainfall is largest in SEA, indicating that extremes can occur at any time of the year in this region. During El Niño years, SEA receives extreme rainfall in late autumn/winter, and during La Niña years extremes usually occur in spring/summer months. Overall, large-scale drivers, such as ENSO and IPO, both play major roles in modulating the timing of extreme rainfall. Understanding these relationships have major implications on improving seasonal prediction of extremes.

4. The relationship between extreme rainfall and temperature, the scaling rate, has been used in previous studies to provide robust projections for extreme rainfall. However, there are large regional variations in scaling rates, with a rate higher than expected from the Clausius-Clapeyron (C-C) relationship found in the tropical north and south of Australia. Further decomposition into dynamic and thermodynamic drivers of extreme rainfall shows that dynamics play a key role in the high scaling rate in the north, while thermodynamic drivers of extreme rainfall play a crucial role in the south of Australia. Scaling rates in future simulations are higher than in historical simulations. This non-stationary nature of scaling rates makes it challenging to project extreme rainfall. Overall, the use of scaling rates in projecting extreme rainfall remains questionable.
5. Lastly, a novel approach to detect long-term changes in rainfall characteristics is developed. By studying rainfall events (defined as consecutive n number of rain days), a continent-wide increase in the frequency and intensity of short duration (1-2 day) events is found and is evident across all seasons. In tropical north Australia (north of 20°S), there is an increase in the frequency of long persistent (> 6 days) rainfall events, whereas the drought-prone regions in the south (below 20°S) show a decrease in the frequency of rainfall events of duration > 2 days. Results using this method are spatially more coherent than other methods used previously. In addition, the method can be used to explain some of the observed historical changes in rainfall.

Table of Contents

List of Figures

List of Tables

Chapter 1

Introduction

1.1 Background

Australia is a semi-arid country with a population of more than 25.4 million (Australian Bureau of Statistics; 31st Dec 2017). On average, the maximum total rainfall is received along the coast, making these regions habitable and sustaining major industries such as agriculture, and livestock. Australia has one of the highest variable rainfall in the world (Nicholls *et al.*, 1997), and large swings in rainfall totals have been observed in instrumental and pre-instrumental records (Freund *et al.*, 2017). Therefore, understanding changes in rainfall characteristics is vital for water management policies, and livelihood of the growing population of Australia.

In addition to the changes in mean rainfall, extreme rainfall has enormous impacts on a country's socio-economic growth. The annual average damage due to floods in Australia between 1967 and 2013 was $943 million, excluding human fatalities and injuries (Handmer *et al.*, 2018). The 2010-2011 Queensland flood resulted in $6.63 billion direct loss of properties and 35 deaths, and thousands of people were homeless (Ladds *et al.*, 2017). Profit from a typical cropping farm can reduce by $370,000 because of a switch from a year with average rainfall to a dry year (Hughes *et al.*, 2019).

The general consensus is that wet extremes have intensified and have become more frequent, globally and in Australia (Guerreiro *et al.*, 2018; Prein *et al.*, 2017; Trenberth *et al.*, 2003). The effects of increasing dry and wet extremes are already observed in Australia and are expected to continue to intensify in future. Climate models project a future intensification and increased frequency of extreme rainfall events globally (Fischer & Knutti, 2016). However, in Australia, models only show high confidence in a future rainfall decline in SWWA (Andrys *et al.*, 2017). For other regions, climate models show low confidence in future changes (Evans *et al.*, 2017). The possible reasons for models failing to capture/project robust changes in extreme rainfall at a regional scale include a lack of model skill and/or high natural variability compared to the climate change signal (Hawkins *et al.*, 2020). Thus, more research is required to better

understand and model the variability in mean and extreme rainfall, and to improve our understanding of the drivers of rainfall changes in Australia. The research presented in this thesis contributes to this need.

1.2 Aims

There are three major goals of this thesis:

1. Understand the observed historical changes in various characteristics of mean and extreme rainfall in Australia.
2. Investigate the role of anthropogenic (greenhouse gas and aerosols) and natural forcings (large-scale drivers such as El Niño-Southern Oscillation (ENSO) and Inter-decadal Pacific Oscillation (IPO)) in changing rainfall characteristics.
3. Examine existing approaches to study mean and extreme rainfall and come up with novel approaches to detect robust long-term changes in rainfall characteristics.

These three objectives are addressed in five result chapters. The first aim is addressed in chapter 2, the second aim is addressed in chapters 3 and 4, and the last aim is addressed in chapters 5 and 6. Finally, the conclusions and future work are discussed in chapter 7.

1.3 Overview of chapters

Rainfall in Australia is modulated by various large-scale drivers such as the ENSO, the IPO, the Indian Ocean Dipole (IOD), the Southern Annular Mode (SAM), the Subtropical ridge (STR), and the Madden Julian Oscillation (MJO). A large number of remote drivers contribute to the high variability of Australia's rainfall. These large-scale drivers modulate large-scale/regional rainfall systems, such as Monsoon, Tropical Cyclones (TCs), fronts, and East Coast Lows (ECLs).

Previous research shows that some regions in Australia have experienced significant changes in rainfall post-1950. The north of Australia has experienced a see-saw type trend in rainfall. The strongest increase is seen in northwest Australia (NWA), most evident in summer months (December- February) (Berry *et al.*, 2011b; Clark *et al.*, 2018). On the other hand, a decrease in summer rainfall is observed in northeast Australia (NEA) and is strongest in the southeast of Queensland (Li *et al.*, 2012). Consistent with the rainfall trends, an increase in monsoonal rainfall has occurred in NWA, and a simultaneous decrease is seen in NEA (Cai *et al.*, 2010; Li *et al.*, 2012). The decrease in rainfall in NEA is explained by an eastward shift of

Walker circulation along with a break down in the connection between ENSO and Australia's rainfall due to the positive phase of IPO (Cai *et al.*, 2010). However, the monsoonal rainfall increase in the northwest cannot be explained by large-scale drivers that affect this region (Shi *et al.*, 2008).

The south of Australia has experienced a decrease in rainfall, that is strongest in the autumn (March-May) and winter (June-August) months. Rainfall in the southwest of Western Australia (SWWA) has declined in a step-wise manner, experiencing a drop in average rainfall in the 1970s and again in the 2000s (Hope & Ganter, 2010). The decline in rainfall in SWWA is strongest in winter. Southeast Australia (SEA) has experienced a gradual decrease in rainfall since the 1970s, with the strongest decrease in autumn (Murphy & Timbal, 2008; Pepler *et al.*, 2019).

Chapter 2 of this thesis provides an in-depth review of the mechanisms of the observed changes in mean and extreme rainfall in Australia for regions where a significant change in rainfall has been observed. In addition to rainfall trends in the instrumental period, a section of the chapter consolidates the recent observed changes in rainfall in a paleoclimate context. This helps to put the recent observed changes into long-term context and understand the full range of natural climate variability. The chapter also summarises how large-scale drivers and their teleconnections have changed historically and the impacts this has had on Australia's rainfall. This study provides state of the art knowledge of the projections of mean and extreme rainfall in Australia by synthesising recent global and regional scale modelling studies. Overall, this research outlines the knowledge gaps and proposes future avenues for research in the field of mean and extreme rainfall, some of which are addressed in this PhD work.

There have been many studies looking at changes in mean and extreme rainfall in SEA (Gallant *et al.*, 2007; Pepler *et al.*, 2014; Timbal, 2009) and SWWA (Cai *et al.*, 2011d; Feng *et al.*, 2010; Hope *et al.*, 2010), and various hypotheses have been proposed to explain these changes. However, relatively fewer studies have explored rainfall trends in the north. Studies show that the recent increase in summer rainfall in NWA since 1990 is unusual in the last ~2000 years (O'Donnell *et al.*, 2015; Rouillard *et al.*, 2016). Chapter 3 of this thesis examines the possible mechanisms behind the rainfall increase in NWA by investigating the role of anthropogenic (greenhouse gas, anthropogenic aerosols) and natural forcings in an increase in mean and extreme summer rainfall in this region. A range of datasets including station data, observational gridded products and the Coupled Model Intercomparison Project phase 5 (CMIP5; (Taylor *et*

al., 2012)) detection and attribution experiments were used for this study. Although a persistent, robust change in both mean and extreme rainfall are historically observed, there is very little confidence in rainfall projections for this region in CMIP5 models (Brown *et al.*, 2016). A new study by Narsey *et al.* (2020) shows that although the uncertainty in future monsoonal rainfall projection in this region has reduced in CMIP6 models compared to CMIP5, the direction of change remains uncertain. This chapter further investigates the projections in both mean and extreme rainfall in NWA using CMIP5 representative concentration pathway (RCP) 8.5 simulations.

Although various large-scale drivers impact Australia's rainfall, no single driver explains more than 20% of Australia's rainfall variability (Risbey *et al.*, 2009). ENSO is known as the biggest source of rainfall variability, impacting rainfall in large areas of Australia (Lim *et al.*, 2017; Risbey *et al.*, 2009). During La Niña (El Niño) years, Australia usually receives above (below) average rainfall. However, the relationship between ENSO and Australia's rainfall undergoes significant decadal variability (Lim *et al.*, 2017; Power *et al.*, 1999) due to an ENSO-like phenomenon, known as the IPO (Henley *et al.*, 2015). Both ENSO and IPO have significant impacts on the mean (Power *et al.*, 1999) as well as extreme rainfall (King *et al.*, 2013). However, these relationships are challenging to study because of high rainfall variability and the short observational record.

As discussed above, large-scale drivers impact various aspects of rainfall, however, most studies simply focus on the intensity and frequency of extremes. Australia is one of the most arid habitable continents on Earth (Preston, 2009). Long, persistent dry conditions and droughts are not unlikely in this continent (Freund *et al.*, 2017). Often droughts lasting over a few months to multiple years in Australia are followed by extreme rainfall events that bring drought-breaking rain (King *et al.*, 2020). Thus, moderate to very extreme rainfall events can cause large-scale flooding, but can also act as a relief from drought, supporting the agriculture sector and maintain water storage in Australia. Figure 2 of Jackson *et al.* (2018) (included in this thesis as Fig. 4.1) highlights the wheat and sheep zone of Australia, mainly situated in the southern latitudes that heavily depends on winter rainfall. However, recent research shows that the winter rainfall has decreased significantly in this region, whereas a slight increase in summer rainfall has been observed in SWWA (Philip & Yu, 2020). Chen *et al.* (2019) have shown that the persistent decline in rainfall in the south of Australia has resulted in a southward shift of the wheat yield. Thus, specific information about if the timing of mean and extreme

rainfall has shifted is essential for the agricultural industry. Globally, the season in which extreme rainfall occurs has shifted later in the year (Marelle *et al.*, 2018). There has not been any study yet in Australia investigating the timing of extreme rainfall and its variability.

Chapter 4 of this thesis answers the question, "when does extreme rainfall usually occur in Australia"? In this study, a relatively moderate extreme index such as the maximum consecutive 5-day rainfall (Rx5; (Zhang *et al.*, 2011)) is used. Previous studies show that Pacific variability plays a large role in the intensity and frequency of extreme events (King *et al.*, 2013). Chapter 4 looks at the relationship between the large-scale Pacific drivers such as ENSO and IPO and the timing of extreme rainfall in Australia. In addition, the study investigates the role of the interaction of ENSO and IPO in modulating the timing of extreme rainfall. Understanding these relationships is challenging because of the short observational record. Robust conclusions are drawn in this chapter using the Australian Water Availability Project (AWAP; (Jones *et al.*, 2009)) data and the Twentieth Century Reanalysis (20CR; (Compo *et al.*, 2011)) 56 ensemble members. The year to year variability in the timing of extreme rainfall, conditioned on ENSO and IPO phases are analysed. Understanding the relationship between the timing of extreme rainfall and large-scale drivers has substantial implications for improving seasonal prediction of mean and extreme rainfall in Australia.

Climate models often struggle to replicate observed trends in rainfall (Flato *et al.*, 2014). Chapter 2 of this thesis shows that in Australia, SWWA is the only region where climate models capture a significant decline in rainfall in the historical period. However, similar to historical changes, there is only low confidence in rainfall projections in most regions in Australia, except for SWWA (Alexander & Arblaster, 2009; Alexander & Arblaster, 2017); confidence in extreme rainfall projections is even less. On the other hand, climate models show robust evidence of a ubiquitous increase in surface temperature (Power & Delage, 2019). Thus, recent research focuses on using the relationship between temperature and extreme rainfall (scaling rate) to project extreme rainfall. From theory, we expect a 7% increase in extreme rainfall per degree of warming in the atmosphere (Clausius-Clapeyron (C-C) equation). However, the observed scaling rates do not match the expected $7\%°C^{-1}$ rate (Bao *et al.*, 2017; Roderick *et al.*, 2019; Wasko & Nathan, 2019). The scaling rate values calculated using surface temperature in the north of Australia is below $-21\%°C^{-1}$, which is consistent in gridded and observational datasets (Bao *et al.*, 2017; Hardwick Jones *et al.*, 2010). More recent research shows that surface temperature is not an appropriate parameter to study scaling rates (Ali *et al.*,

2018; Ali & Mishra, 2017). An increasing body of literature suggests that the dominant mechanism behind the strong negative scaling rates using surface temperature in north Australia is the lack of moisture availability at high temperatures (Ali *et al.*, 2018; Barbero *et al.*, 2018; Bui *et al.*, 2019; Hardwick Jones *et al.*, 2010; Lenderink *et al.*, 2018; Roderick *et al.*, 2019; Wasko *et al.*, 2018; Zhang *et al.*, 2019). Instead, dew point temperature (DPT) is a more suitable indicator for studying scaling rates as it takes into account both temperature and the available moisture in the atmosphere (Ali *et al.*, 2018; Ali & Mishra, 2017).

In Chapter 5, the scaling rates in Australia are further investigated using DPT in climate model datasets. The scaling rates using DPT are consistent with the C-C relationship (Ali *et al.*, 2018; Ali & Mishra, 2017; Wasko *et al.*, 2018). In this research, mechanisms behind the regional variations of scaling rates in Australia are investigated by studying the relationships between DPT and the thermodynamic and dynamic drivers of extreme rainfall. This chapter further examines the applicability of scaling rates to extrapolate extreme rainfall into the future, and the associated challenges are discussed.

Although Australia's reliable rainfall observational record began in 1900 (Jones *et al.*, 2009), only a few regions in Australia show long-term robust changes in rainfall, and even fewer regions show significant trends in extreme rainfall. The reasons behind this are high variability in rainfall due to various large-scale drivers modulating Australia's rainfall, inhomogeneities in datasets, and inconsistent methods. This chapter discusses the shortcomings of the existing approaches to study mean and extreme rainfall characteristics that are traditionally used. For example, wet day percentiles are sensitive to the number of rain days (Schär *et al.*, 2016), while all-day percentiles usually account for moderate extreme events (Pendergrass, 2018). The extreme events calculated over an arbitrary fixed number of days, such as Rx5 can be drawn from one long persistent event or can be calculated combining multiple weather systems. Therefore, there is a need for a robust approach which can be applied to various observed and model datasets to improve our understanding of changes in rainfall characteristics.

In chapter 6, a novel approach is used over the period 1911-2016 to study long-term changes in rainfall characteristics using rainfall events, defined as n consecutive rain days (days when rainfall is $\geq$ 1 mm). The rainfall events are further segregated into four categories based on rainfall duration, 1-2 day events, 3-4 day events, 5-6 day events, and >6 day events. Rainfall event intensity is defined as the average rainfall over the event duration. Next, frequency and

intensity trend analyses were performed using AWAP data at annual as well as seasonal time scales. The trends were verified against high-quality Lavery *et al.* (1997) station dataset. Overall, the goal in this chapter is to come up with an approach to detect robust long-term trends in rainfall which was not found previously using existing methods. This method also helps to identify possible mechanisms behind the observed changes in rainfall in Australia.

The overall summary of the thesis is discussed in chapter 7, section A. Section B of chapter 7 suggests new research avenues following the conclusions of this thesis that would improve our understanding of mean and extreme rainfall.

Chapter 2

A review of past and projected changes in Australia's rainfall

Abstract

There has been much attention given to the spatial and temporal characteristics of changes in mean and extreme rainfall over Australia during the past century. As Australia is the second driest continent on Earth, reliable projections around the trends and variability in future rainfall are crucial for policymakers and water resource management. This paper comprehensively reviews the current published literature on trends in Australia's rainfall from pre-instrumental and instrumental records, the climatic drivers of Australia's rainfall variability, attribution of the long-term trends, extreme rainfall attribution methods with particular reference to a recent case study (2010-2012 east Australia rainfall event) and projected changes of mean and extreme rainfall over Australia during the 21st century. Notable trends in the observational record of rainfall in Australia are a decrease in mean rainfall in southwest and southeast Australia and an increase in northwest Australia since 1950. The general consensus of research into Australia's future rainfall is that mean rainfall will continue to decrease in southwest Australia in a warming world, while changes over northern and eastern Australia remain uncertain. There are still significant knowledge gaps around the causes of observed trends in rainfall both in the mean and extremes, the ability of climate models to accurately represent rainfall in the Australian region and future rainfall projections. These gaps are identified, and avenues for future research directions are proposed.

2.1 Introduction

Australia's rainfall facilitates established agricultural industries and supports a population of approximately 24.5 million (Australian Bureau of Statistics; 31st Dec 2017), but is amongst the most variable rainfall in the world (Nicholls *et al.*, 1997). This variability can lead to droughts and floods that have widespread impacts on various sectors, such as food production, human health, and water management.

Although there is no single definition of drought (IPCC, 2012), the Bureau of Meteorology (BOM) defines drought as a period of three months or above when rainfall is below the 10th percentile on record. A succession of below average rainfall years can lead to a significant reduction in crop productivity and an associated decline in the Gross domestic product (GDP). While relatively short periods of drought interrupt the balance between the water supply vs demand relationship, long-term droughts may require far more substantial changes in resource allocations and water storage management strategies in order to sustain the supply of resources to the growing population of Australia. Similarly, periods of above average rainfall can cause floods, damage crops, and lead to human health issues due to water contamination. While shorter periods of above average rainfall (extreme rainfall) are destructive, a long-term persistent increase in rainfall could, in some parts of Australia, reinvigorate the agricultural industry (Cai *et al.*, 2011b). This may in turn help compensate for agricultural losses due to drought in other parts of the continent. However, a regime shift in either direction would be difficult to adapt to.

The anthropogenic influence on aspects of rainfall change is not clear. Recently we have experienced an increase in both greenhouse gas (GHG) emissions and the number of observed extreme events in various regions (IPCC 2013). Furthermore, Global Climate Models (GCMs) simulate a 1.5-2% K^{-1} increase in global mean rainfall in response to surface warming (Allen & Ingram, 2002). Globally, extreme rainfall is generally expected to intensify and become more frequent under increased warming, whereas the light to moderate events are expected to become less frequent (Trenberth *et al.*, 2003). Recent studies suggest an intensification of extreme rainfall events over Australia since the 1950s (e.g. Contractor *et al.* (2018)), however, it is still uncertain to what extent we can quantify humans' influence on these changes.

The current article reviews the recent scientific literature on rainfall in the pre-instrumental and instrumental period over Australia, including the underlying mechanisms (e.g. impact of anthropogenic changes, and natural variability) of the regional and seasonal variations and future projections. We discuss progress in detection and attribution of rainfall trends and extremes and future avenues in this field. While there is a wide body of literature available looking at mean and extreme rainfall changes at both regional and continental scales, a consolidated summary of recent research is useful to identify the major knowledge gaps and suggest future avenues for research in this field. Furthermore, an assessment for the whole country is necessary for understanding potential vulnerabilities to future climate change. This

is particularly pertinent for policymakers, various government agencies dealing with water management and urban planners who need to manage potential changes in variability in extremes of rainfall and other changes across the country.

The article is organised as follows. We first review the datasets available for studying both mean and extreme rainfall across Australia and its main characteristics, systems and drivers. We then review studies attributing observed rainfall trends and extremes as well as projected changes. We conclude with a summary and suggestions for further research.

2.2 Observed and reconstructed datasets of rainfall

2.2.1 Gridded and station datasets over Australia

Observational rainfall data from pioneering meteorologists and Indigenous Australian knowledge is available from before the establishment of the BOM in 1908 (Zillman, 2001). However, pre-1900 data are sparse, particularly in central Australia and parts of South Australia (Jones *et al.*, 2009).

There has been much attention given to improving the observational network and providing high-quality gridded and spatially aggregated datasets by combining station data. A set of 191 stations was used to provide a high-quality daily dataset for Australia (Lavery *et al.*, 1992). This dataset was created using strict quality control checks to provide long-term statistically reliable, homogenous data to monitor climate change and rainfall trends. However, the dataset has limited spatial coverage and various issues with quality control. For example, these station datasets show untagged weekend accumulations recorded erroneously against individual days in 102 out of 191 stations (Viney & Bates, 2004), and some stations showed anomalously high frequent extreme rainfall events on Mondays and too few extreme events on Sundays (King *et al.*, 2013a). These quality control factors lead to a range of uncertainties in intensity and frequency of wet or dry spells and therefore need to be considered when drawing conclusions based on these datasets.

Another issue with the dataset is the unavailability of station data in various regions, making it difficult to study long-term trends or climatological averages across large parts of Australia, particularly on the daily timescale. On monthly timescales, a high-quality rainfall dataset comprised of 379 stations was developed by including shorter duration rainfall records and by using a composite of two or more neighbouring stations (Lavery *et al.*, 1997).

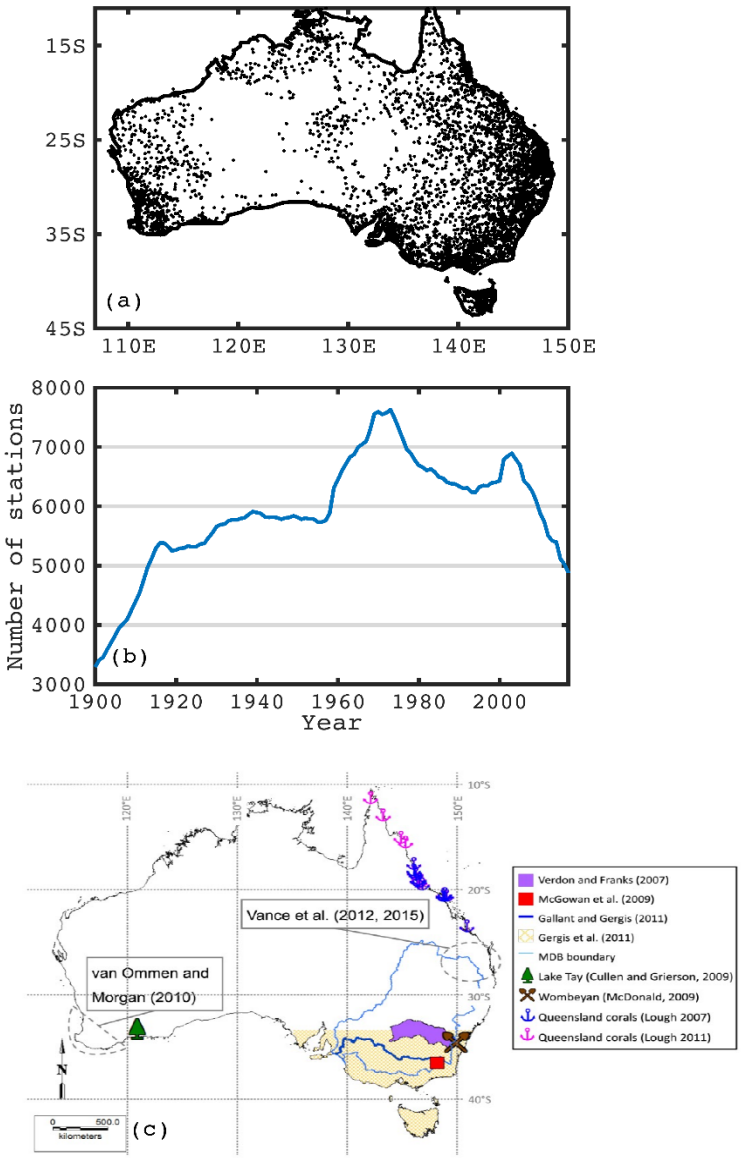

Figure 2.1 Rainfall data availability across Australia. (a) Station network of AWAP dataset over the period 1988-2017, (b) time series of the number of stations contributing to the AWAP daily rainfall dataset, (c) locations of rainfall and streamflow reconstructions until 2015. Dashed regions show reconstruction regions of rainfall variability based on Antarctic ice core record. Figure 2.1 (a) and (b) produced using station information provided by BOM, updated with permission from Jones et al. (2009). Figure 2.1(c) is reprinted with permission from Ho et al. (2015a), Copyright @ John Wiley and Sons.

All available in situ observations were used in the development of the Australian Water Availability Project (AWAP) data (Jones *et al.*, 2009). AWAP data are available at horizontal resolutions of 0.25˚×0.25˚ and 0.05˚×0.05˚ over the period 1900-2015 [http://www.bom.gov.au/jsp/awap/rain/index.jsp]. Although such gridded datasets are useful for many analyses, the AWAP dataset is known to underestimate the intensity and overestimate

the frequency of extreme events (King *et al.*, 2013a). There are some issues in assessing long-term trends using the AWAP dataset as the changing number of in situ observations and gridding methods as well as the quality control issues mentioned above may result in spurious trends over data-sparse regions (Alexander & Arblaster, 2017). Furthermore, the density of observed rainfall data is spatially inhomogeneous: southeast and southwest Australia, for example, have a dense observed network, while north and central Australia are comparatively sparse. Fig. 2.1a, b show the spatial distribution of stations (over the period 1980-2017) and the time-series of the number of stations respectively that goes into the AWAP rainfall dataset. King *et al.* (2013a) pointed out that changes in the station distribution can produce artificial wet or dry trends. Thus, it is recommended to mask regions of uncertainty to avoid artefacts in the data. We have masked two regions (121º-134ºE, 18º-34ºS and 136º-139ºE, 23º-29ºS) with less data coverage (Fig. 2.2), following Chung and Power (2017).

In addition, gridded products suffer from uncertainties due to various gridding techniques. Contractor *et al.* (2015) showed using various stations, satellites and gridded products that, although all the datasets show similar local distributions of rainfall for light to moderate events (less than 20 mm per day), they can show large differences for very extreme events.

Extreme rainfall has been examined using AWAP (e.g. Alexander and Arblaster, 2017) and there are also specialised extreme event datasets available (e.g. HadEX, HadEX2, GHCNDEX; http://www.climdex.org/datasets.html). HadEX (Alexander *et al.*, 2006) is a gridded dataset containing extreme rainfall indices defined by the Expert Team on Climate Change Detection and Indices (ETCCDI) group (Zhang *et al.*, 2011), and HadEX2 (Donat *et al.*, 2013a) is updated with an increase in the number of stations, available over the period 1901-2010. GHCNDEX is a set of extreme indices calculated from daily data of the station based Global Historical Climatological Network (GHCN) (Donat *et al.*, 2013b), available since 1951-present. GHCNDEX has better spatial coverage than HadEX2 for rainfall indices over Australia (Dittus *et al.*, 2015). For HadEX, HadEX2 and GHCNDEX, the indices are calculated at the station level first and then gridded (Alexander *et al.*, 2006; Donat *et al.*, 2013b; Donat *et al.*, 2013a). The order of operation of calculating these indices can influence the data significantly in combination with various interpolation techniques (Avila *et al.*, 2015), for example, angular distance weighting method showed the maximum influence due to the order of operation whereas natural neighbour and cubic spline interpolation showed the least impact.

Rainfall extremes are generally calculated at observation sites and then gridded, whereas, in climate models, the extreme indices are calculated based on grid values. This leads to a scaling problem, and the values from climate models are not directly comparable with the observed data (Avila *et al.*, 2015). The scaling might result in large differences in values in extreme indices; for example, Avila *et al.* (2015) reported a doubling in monthly maximum 1-day precipitation (Rx1day) values in some cases. In conclusion, extremes can be sensitive to definition and dataset choice, and it is necessary to understand the uncertainties in both gridded and station datasets in order that appropriate conclusions can be drawn.

2.2.2 Pre-instrumental period reconstructions of Australia's rainfall

This section summarises long-term reconstructed rainfall data available in Australia established using proxy data. Observations of Australia's rainfall (since 1900) are unlikely to cover the full range of variability of the hydrological cycle (Palmer *et al.*, 2015), and reconstructed paleoclimate datasets from tree rings, ice-core, coral and sediment cores are necessary to examine the full range of hydroclimatic variability (Tozer *et al.*, 2016).

Using documentation of rainfall chronologies (newspaper archives, observatory records, personal records) Fenby and Gergis (2013) created a historical rainfall database of the period 1788-1860 and marked periods of wet and dry years in five sub-regions (New South Wales, southern Queensland, Victoria, Southern Australia, Tasmania). Gergis and Ashcroft (2013) verified the data provided by Fenby and Gergis (2013) with five station records and further combined the data with modern rainfall records to create a wet/drought index for eastern Australia. Gergis and Ashcroft (2013) showed that the ENSO-rainfall relationship is more pronounced in the inland region than at coastal areas of NSW. A yearly reconstruction of rainfall was derived from high-quality station data, and 12 tree ring records spreading over a broader region in Australia and spanning 206 years (1783-1988) in the SEA region (Gergis *et al.*, 2012). This dataset captures 33% of inter-annual and 72% of decadal variations in instrumental observations. The aforementioned studies have provided high temporal resolution datasets since European settlement, thus these datasets can be very useful to study both IPO and ENSO relationships with rainfall prior to the establishment of the BOM.

A recent study by Ho *et al.* (2015a) (Fig. 2.1c) provided a list of locations that have continuous paleo reconstructions for rainfall or streamflow until 2015. The authors later combined three available paleoclimate proxy records in Australia to estimate rainfall in the Murray Darling Basin (MDB) from 749 BCE to 1980 CE (Ho *et al.*, 2015b). A 210-year record,

reconstructed from tree rings in northwest Australia for the period 1802-2012 was developed to study the recent increase in summer rainfall in a long-term perspective (O'Donnell *et al.*, 2015).

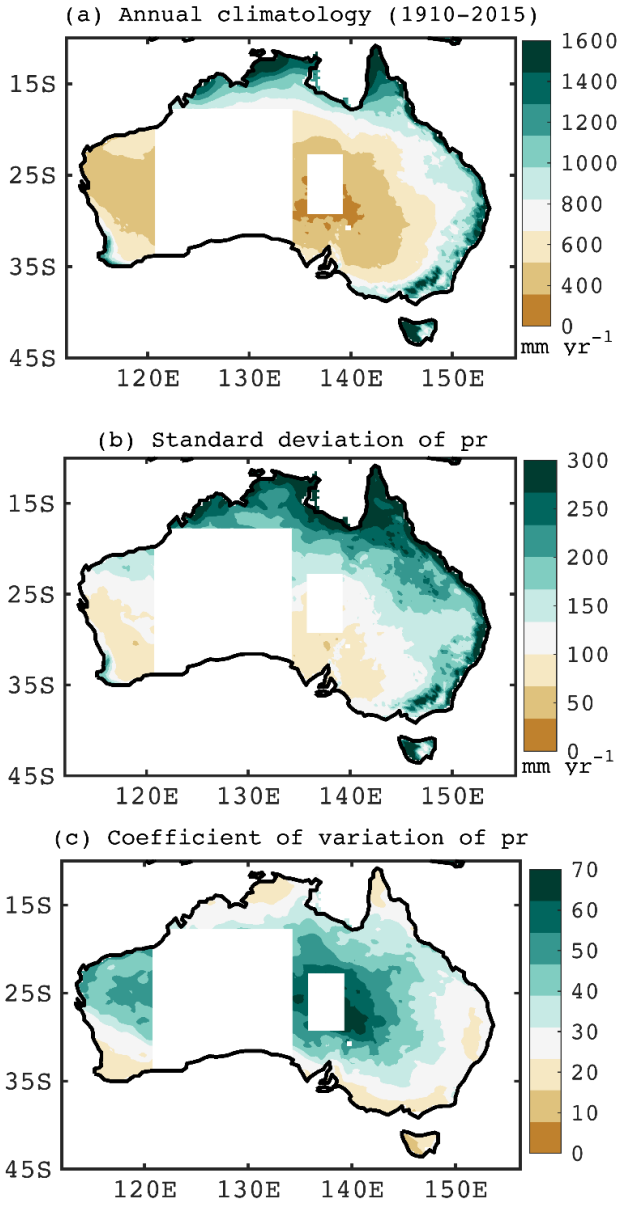

Figure 2.2 (a) Climatology (mm), (b) standard deviation (mm) (c) Coefficient of Variation (CV; standard deviation normalised by climatological mean) of annual mean rainfall. The period used is 1900-2015 in AWAP.

Further studies have provided a greater spatial extent and seasonal features of reconstructed rainfall. Work by Freund *et al.* (2017) developed warm and cool season rainfall reconstructions for eight Natural Resource Management (NRM) regions spanning the whole of

Australia. These reconstructions were developed based on 202 proxy records derived from corals, ice cores, tree rings and speleothems derived from throughout the Indo-Pacific region and spanning latitudinally from 20°N to 90°S. Using 176 tree-ring chronologies derived from Tasmania, New Zealand, Northern Territory, Western Australia and Indonesia, and one series of coral data from Queensland, Palmer *et al.* (2015) first introduced the gridded Australia and New Zealand Summer Drought Atlas for summer extending back to 1500 CE, and proposed that summer droughts in Eastern Australia display a long-term connection to positive phases of the IPO.

A similar connection of eastern Australian rainfall to the IPO was also proposed based on teleconnected responses with a highly resolved and precisely dated ice core from Law Dome spanning the last 1000 years (Vance *et al.*, 2015). This relationship has continued to be developed into catchment-specific reconstructions of inflow over the last millennium to better inform water resource management of the range of possible hydrological extremes beyond those known from instrumental data of the last century (Tozer *et al.*, 2018; Tozer *et al.*, 2016).

There are limitations to the perspectives that can currently be given on Australian rainfall by palaeoclimate evidence. In particular, there are a relatively small number of studies available for central, northern and western parts of Australia due to the lack of suitable high-resolution palaeoclimate archives in these areas. These studies also rely on assumptions that teleconnection patterns have remained stable so that the relationship between proxy records and observational data during the instrumental period continue to be representative during pre-instrumental times.

2.3 Rainfall characteristics, systems and large-scale drivers

Australia's climate is, on average, semi-arid with an annual average rainfall of 475 mm/year. Rainfall is also spatially variable: annual average rainfall (Fig. 2.2a) is comparatively high over west Tasmania, the coastal region of northwest Australia (NWA) and northeast Australia (NEA), the coastal region of eastern Australia including the inland Murray-Darling region of southeast Australia (SEA), and southwest of Western Australia (SWWA). These regions are shown in Fig. 2.3 Changes to rainfall over these regions will likely impact food production, and water and resource availability for industrial growth.

The standard deviation of observed annual rainfall is highest along the coastal regions of NWA, east Australia, west Tasmania, and SWWA and decreases gradually away from the

coast, indicating these regions are prone to large swings between periods of drought and flood (Fig. 2.2b). Note, the standard deviation is maximum where the annual rainfall is high, however, the standard deviation normalised by annual mean (coefficient of variation) is quite different (Fig. 2.2c). Rainfall variability by this measure is highest in the dry inland region, indicating irregular rainfall from year to year, with less variability in the coastal regions which typically have more consistent rainfall from year to year.

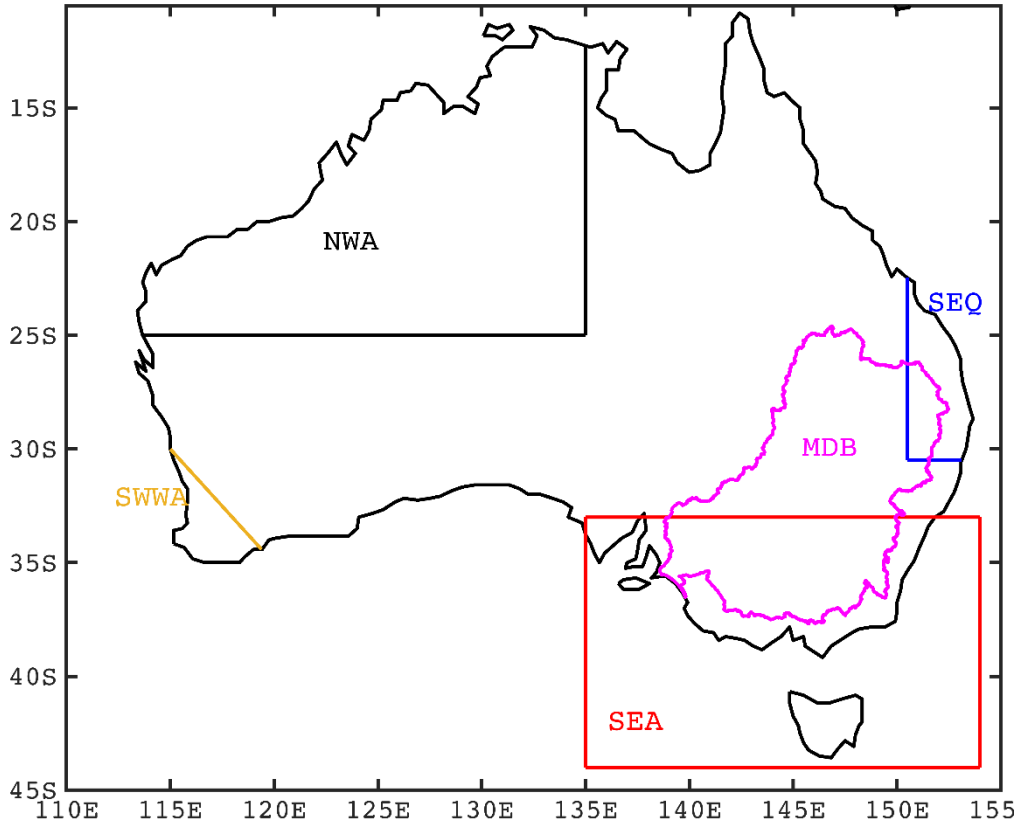

Figure 2.3 Outline of the regions that experience major rainfall trends in Australia. Northwest Australia (NWA; 10º-25ºS, 110º-135ºE), southeast Queensland (SEQ; 22˚-30.5˚S, east of 150.5˚E), southwest of Western Australia (SWWA; southwest of the line joining 30˚S, 115˚E and 35˚S, 120˚E), southeast Australia (SEA; 33˚ - 44˚S, 135 ˚ -154 ˚E).

Australia's rainfall is driven by various circulation systems (Fig. 2.4), such as the Australian-Indonesian Monsoon, fronts, tropical cyclones (TCs), East Coast Lows (ECLs) and various modes of large-scale climate variability such as the El Niño-Southern Oscillation (ENSO), the Interdecadal Pacific Oscillation (IPO), the Indian Ocean Dipole (IOD), the Southern Annular Mode (SAM), the Subtropical ridge (STR), and the Madden Julian Oscillation (MJO). The teleconnections between Australia's rainfall characteristics and these drivers have changed in the past and are likely to change in the future in response to internal

variability and anthropogenic emissions. Past changes in these rainfall systems and their projected changes in the future are summarised next.

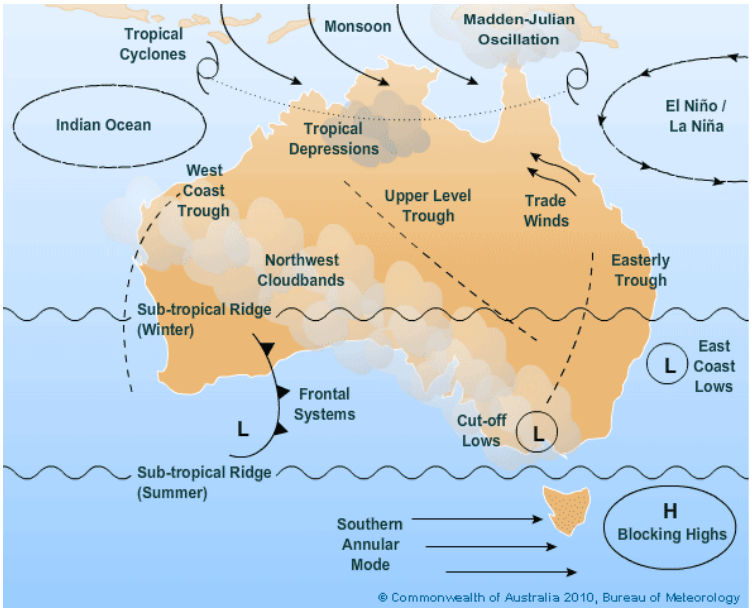

Figure 2.4 Schematic of Australia's major rainfall drivers. Reprinted with permission from Bureau of Meteorology, Copyright 2018 Commonwealth of Australia.

2.3.1 Rainfall systems: past and future changes

Here we discuss changes in the characteristics of the major rainfall systems that impact Australia's annual and seasonal rainfall such as the monsoon, TCs, ECLs, fronts. The northern part of the continent receives a substantial amount of rainfall from the austral summer monsoon (December – February) when northwesterly winds bring wet moist air to the continent and form convective clouds. Australia's monsoon region is the area from 120-150˚E and 10-20˚S (Brown *et al.*, 2016; Moise & Colman, 2010). Although monsoon area, rainfall, and intensity are projected to increase by 1.9%, 3.2%, and 1.3%, respectively on a global scale with each 1˚C of warming (Hsu *et al.*, 2013; Wang *et al.*, 2012), an average of 33 CMIP5 models project a 0.4% $^{\circ}C^{-1}$ change in Australian monsoon rainfall (Brown *et al.*, 2016). There is little consensus among CMIP3 and CMIP5 models when projecting future rainfall over tropical Australia (Moise *et al.*, 2012). According to Jourdain *et al.* (2013), the 12 'good' CMIP5 models (that produce Australian and Indian monsoon characteristics and the monsoon-ENSO relationship reasonably well) show a 5-20% increase in monsoon rainfall over the latter half of the 21st century when compared to pre-industrial times. Brown *et al.* (2016) categorised CMIP5 models into three sub-categories, 'DRY' models that project strong decreasing

monsoonal rainfall, 'MID' models that project a weak positive/negative trend, 'WET' models that project strong increasing monsoonal rainfall. 'DRY' models showed large cold sea surface temperature (SST) biases in the western equatorial Pacific, whereas such patterns were not evident in 'WET' models thus suggesting lower confidence in 'DRY' models. Thus changes in the monsoon remain uncertain. If the 'good' models (those models which show minimal SST biases in the equatorial Pacific) are to be believed, the monsoon is projected to increase by a small factor in the future.

TCs account for approximately 30% of the annual rainfall over NWA and 10% of the total annual rainfall over the northern continent (Lavender & Abbs, 2013). A number of studies have examined changes in the number and type of TCs making landfall in Australia, and there is much variability in their conclusions depending on the timescale examined (Clark *et al.*, 2018). Callaghan and Power (2011) created a database for cyclones that made landfall in eastern Australia from 1872/1873 to 2009/2010, showing a decrease of 62% in severe cyclones making landfall in eastern Australia since the early 1870s. The total number of TCs has decreased post-1985 due to the improvements in classification, resulting in the reclassification of TCs to weaker low-pressure tropical systems (Nicholls *et al.*, 1998). A very small but not significant positive trend in the number of the intense cyclones since 1969 is reported, although, the cause of the increase is not clear (Nicholls *et al.*, 1998). Overall, the number of TCs is estimated to decrease by 30% by the end of 21st century (Lavender & Walsh, 2011), though there is much uncertainty due to the coarse resolution of climate models.

ECLs are characterised by intense low-pressure systems that occur off the coast of eastern Australia. ECLs can occur throughout the year, though peak during the austral autumn and winter. On average Australia gets approximately 22 ECLs per year (Pepler *et al.*, 2015). ECLs contribute 23% of the total rainfall of the eastern seaboard and 40% of widespread heavy rainfall events (Pepler *et al.*, 2014). There is no change in the average number of observed ECLs between two periods, 1970-1987 and 1988-2005, however, high-resolution regional climate models project fewer ECLs with weaker intensity in the future (Ji *et al.*, 2015) and the decrease is greatest in winter (Evans *et al.*, 2015). The most intense ECLs are projected to decrease in winter but increase in summer (Evans *et al.*, 2015; Pepler *et al.*, 2016).

Southern Australia is impacted by extra-tropical systems known as fronts. The simplified definition of a frontal system is when two air masses of different densities and temperature collide and do not mix readily (Ahrens, 2012). The boundary of two air masses is

called a front and can be accompanied by rainfall. Front locations and type are classified based on the gradient of wet bulb temperature (Hewson, 1998) and the magnitude of speed and direction or speed of the front (Catto *et al.*, 2012b). A warm front is formed when poleward moving warm air mass strikes a cold air mass pushing it back, and the warm air rises above the cold air mass. A cold front is formed when a cold air mass strikes a warm air mass, forcing the warm air to rise.

Southern Australia is impacted by cold fronts, predominantly during spring and summer (Catto *et al.*, 2012b). Over west Australia, 24% of total rainfall is for accounted by warm fronts, although the frequency of warm fronts over Australia is very low (Catto *et al.*, 2012b). Recent trends in reanalysis data show an increase in the frequency of fronts in east Australia and decrease in southern Australia over the period 1989-2009 (Berry *et al.*, 2011a). This trend is projected to continue where a southward shift in the region of maximum front frequency from 20˚S-40˚S to 40˚S-60˚S is projected (Catto *et al.*, 2014).

2.3.2 Large-scale drivers: past and future changes

In this section, we discuss the major large-scale drivers of Australia's rainfall trends and their changes in the past and future projections. ENSO is the primary climatic factor contributing to Australia's interannual rainfall variability, with Nicholls *et al.* (1997) suggesting its influence leads to Australia's rainfall being more variable than expected compared to similar climates around the globe. During El Niño (La Niña) years, above average SST over central and east Pacific leads to below (above) normal rainfall over eastern and north-east Australia, which is significant particularly during winter and spring (Risbey *et al.*, 2009). A nonlinear relationship between ENSO and Australia's rainfall has been found, i.e. the magnitude of La Niña has a greater impact on Australia's rainfall than the magnitude of El Niño (King *et al.*, 2015; Power *et al.*, 2006). Although the mechanisms of this non-linearity are unclear, it is sensitive to the movement of the South Pacific Convergence Zone (SPCZ) (Cai *et al.*, 2010). King *et al.* (2015) argue that the non-linearity is explained by thermodynamical conditions than dynamical conditions in the southwest Pacific region; the moisture availability in the southwest Pacific region is strongly correlated with the negative phase of ENSO whereas the correlation is insignificant with the positive phase.

A weakening of the Walker Circulation is observed in climate models, as well as observations since the early twentieth century (Bellomo & Clement, 2015; Deser *et al.*, 2010). However, over the period 1980-2012 a strengthening of Walker circulation was observed (Luo

et al., 2012), which CMIP5 models do not replicate (Kociuba & Power, 2015). Although this could be due to a strong bout of internal variability, this raises possible concerns about the robustness of future projections of ENSO. Bayr *et al.* (2014) demonstrated using both CMIP3 and CMIP5 models that the Walker Circulation shows an anomalous eastward (westward) shift in response to global warming during an El Niño (La Niña) event. Also, in the future, the multimodel mean state is shifted more towards an El Niño-like state (Bayr *et al.*, 2014). On a year to year timescales, Cai *et al.* (2015) reported a projected increase in the frequency of swings from extreme La Niña conditions followed by an extreme El Niño event under the representative concentration pathway (RCP) 8.5 emission scenario. However, despite uncertainties in how ENSO may change in the future, Chung and Power (2017) and Perry *et al.* (2017) suggest that increases in greenhouse gas concentrations will lead to an increase in the spatial extent of ENSO rainfall teleconnections.

SST variability on interdecadal time scales (e.g. the IPO) strongly impacts Australian rainfall (Power *et al.*, 1999), with the positive phase of IPO associated with below normal monsoon rainfall and the negative phase associated with above normal monsoon rainfall (Latif *et al.*, 1997). During warmer tropical Pacific SSTs (i.e. during positive IPO phase), there is no significant relationship between ENSO and Australian climate, whereas, during the negative phase, ENSO and Australian climate are strongly correlated (Murphy & Timbal, 2008). This is potentially due to the asymmetry in El Niño and La Niña impacts noted above since there are generally La Niña events in negative IPO periods (Power *et al.*, 2006). Since the 1940s there have been two cold phases of IPO reported ~1945-1976 and ~1999-2014 and one warm phase from ~1977-1998 (Dong & Dai, 2015).

Another coupled atmospheric and ocean system, the IOD (Saji *et al.*, 1999) is characterised by periodic warming of SSTs over the eastern and western parts of the equatorial Indian Ocean. The IOD is active from June-November. The positive phase of the IOD is characterised by warmer SST patterns in the western Indian Ocean and cooler SST patterns in the eastern Indian Ocean, resulting in reduced rainfall over Australia (Ashok *et al.*, 2003). The IOD also modulates storm tracks over Australia, significantly impacting southern Australian agriculture (Ashok *et al.*, 2007). Phase-asymmetry also occurs in observed IOD trends; positive IOD (pIOD) events have increased markedly since 1950, but not negative IOD (nIOD) events. The number of pIOD events has increased from four in 30 years at the beginning of the twentieth century to 10 events in the recent past 30 years. In comparison, the number of nIOD events has

reduced to two from 10 events in the same period (Cai *et al.*, 2009a). The mean SST is projected to resemble a more pIOD-like state, although some change in frequency is expected in future in response to GHG warming (Cai *et al.*, 2013).

Australia's rainfall is further impacted by the teleconnection between ENSO and the IOD (Li *et al.*, 2016; Lim *et al.*, 2017). While the ENSO-southern Australian-rainfall relationship has weakened since 1980, the IOD-southern Australia-rainfall teleconnection has strengthened (Li *et al.*, 2016). The dynamics of these teleconnections is not well understood (McIntosh & Hendon, 2017) and requires further investigation.

The impacts of SAM on southern Australia's rainfall varies with season. SAM is characterised by a shift in the position of westerly winds between mid to high southern latitudes. During the positive phase of SAM, strong westerlies contract toward Antarctica, restricting the number of mid-latitude fronts reaching southern Australia and leading to below average rainfall (Risbey *et al.*, 2009). There has been a significant positive trend in the summertime SAM observed since the 1960s (Marshall, 2003; Montzka *et al.*, 2011). This trend is predominantly attributed to ozone depletion over the Antarctic and GHG increase (Arblaster & Meehl, 2006; Gillett & Fyfe, 2013). Although stratospheric ozone is projected to be restored to pre-industrial levels over the 21st century, an increase in GHGs will continue to change SAM trends in the future across all seasons (Arblaster *et al.*, 2014; Arblaster *et al.*, 2011). CMIP5 models project a significant positive trend in SAM over the 21st century under high emission scenarios (i.e. RCP8.5) leading to drier future conditions in southern Australia in winter (Lim *et al.*, 2016; Zheng *et al.*, 2013).

The STR is the area of high mean sea level pressure formed by the descending branch of the Hadley circulation (Timbal & Drosdowsky, 2013), which acts as a boundary to the mid-latitude fronts and storms. An intensified and southward shift in the STR results in below average rainfall, as storms are pushed polewards (Grose *et al.*, 2015). The position of the STR also varies annually: the STR is located around 29˚S in winter and at 40˚S in summer. There has been an increase in the intensity of the STR since 1970 (Timbal & Drosdowsky, 2013). Studies show a poleward expansion in Hadley circulation due to external forcings (Seidel *et al.*, 2008), however, the reason of the increased intensity in STR is not clear (Timbal & Drosdowsky, 2013). The STR is projected to intensify and shift poleward in the 21st century in both CMIP5 (Grose *et al.*, 2015) and CMIP3 (Kent *et al.*, 2013) model ensembles in response to increased greenhouse forcing.

One of the major sources of tropical intraseasonal variability is the MJO. The MJO is characterised by convective cells propagating from the Indian Ocean to the Pacific Ocean, which impacts northern Australia on timescales of 60-90 days and accounts for a large degree of intraseasonal rainfall variability (Wheeler *et al.*, 2009). The likelihood of an extreme weekly rainfall event in northern Australia is tripled in a wet phase of MJO relative to a dry phase (Wheeler & Hendon, 2004). Chang *et al.* (2015) showed that the MJO amplitude is projected to increase by 30% by the end of the 21st century relative to the period 1981-2000.

2.4 The significance of recent regional rainfall trends and their attribution

In this section, we review the literature on Australia's past rainfall trends and studies attributing trends to causes in three different regions (north Australia, southeast Australia, and west Australia). As highlighted in Fig. 2.2b, c, Australian rainfall has large spatial and temporal variability, which includes trends over the instrumental record. The leftmost panel in Fig. 2.5 shows rainfall trends over the period 1910-2015, the middle panel shows more recent trends between 1986 and 2015 in AWAP. On a longer time scale, annual rainfall over most parts of the continent shows a small increasing trend, with a notable exception over SWWA (Fig. 2.5a). Overall, there is a steeper trend in recent years, and rainfall over northwest Australia has increased and decreased in the east, southeast, and SWWA (Fig. 2.5b). The trend in rainfall in December-February (DJF), March-May (MAM), June-August (JJA), September-November (SON) for the period 1910-2015 are shown in Fig. 2.5 d, g, j, m, respectively, and similarly in Fig. 2.5 e, h, k, n for the period 1986-2015. On the longer time scale, the rainfall increase is most profound in DJF (Fig. 2.5d), with no significant trends in the other seasons, as indicated by a lack of stippling.

2.4.1 West Australia

In Western Australia, rainfall stations are mostly confined to coastal regions and are comparatively dense over SWWA, which makes it difficult to determine inland trends. The available gridded data set shows a significant positive annual rainfall trend in the inland (Fig. 2.5a).

SWWA receives almost 80% of its annual rainfall between April and October (Bates *et al.*, 2008). Past studies have indicated a gradual decrease in winter rainfall since the 1940s over SWWA and an abrupt decrease since 1970s (Hennessy *et al.*, 1999) and again around 2000 (Hope & Ganter, 2010). The rainfall decrease is largest in early (May to July) and late winter

(August to October) (Fig. 2.5j, k). This unusual persistent decline in rainfall initiated the formation of Indian Ocean Climate Initiative (IOCI, 2002) project in partnership between The Commonwealth Scientific and Industrial Research Organisation (CSIRO), BOM and several other government bodies to explore rainfall changes over SWWA.

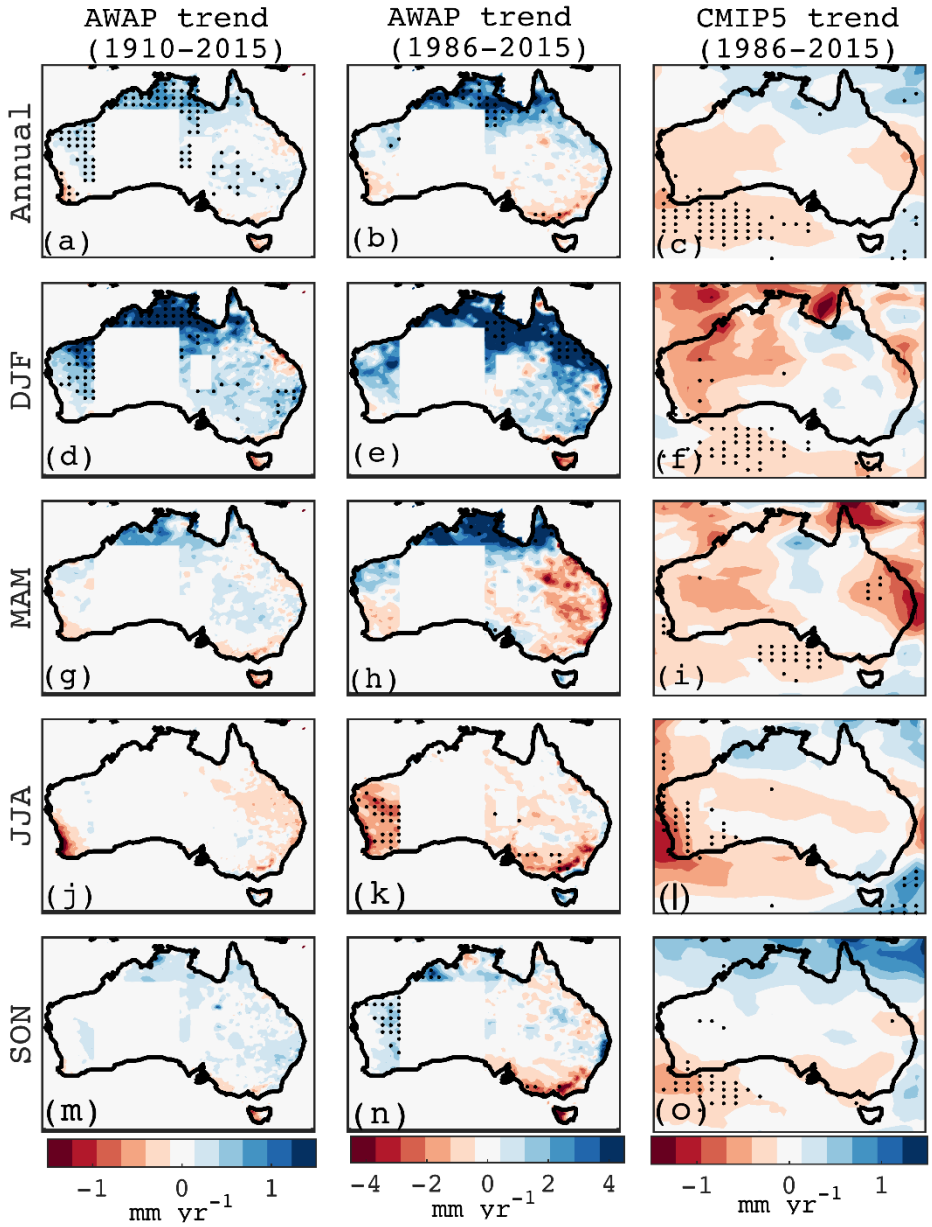

Figure 2.5 On the left column, trends (mm yr^{-1}) over the period 1910-2015 in (a) annual (d) December-February (DJF) (g) March-May (MAM) (j) June-August (JJA) and (m) September-November (SON) precipitation in AWAP. Middle column as in the left column, but for 30 years (1986-2015) trends in AWAP. Right column as in the middle column, but for the ensemble mean of 39 CMIP5 models (historical and RCP8.5). Note different magnitude of colorbar scales for each column. Stippling on the left and middle panel figures show significance at 95% level using Mann-Kendall non-parametric test, and the stippling on the rightmost panel shows regions where two-thirds of the CMIP5 models agree on the sign of the change.

Smith and Timbal (2012) suggested that the role of tropical oceans in the SWWA rainfall decline is minimal as compared to changes driven by atmospheric circulations. Various studies conclude that the rainfall decline is due to external forcings (Cai & Cowan, 2006; Cai *et al.*, 2011d; Delworth & Zeng, 2014; Timbal *et al.*, 2006a) which results in the poleward movement of westerly winds and associated long-term changes in MSLP (Allan & Haylock, 1993; Delworth & Zeng, 2014). As noted in section 2.3.1, southern Australia receives a substantial amount of rainfall from frontal systems, and the frequency of such frontal systems has decreased markedly since 1975 due to increased GHG emissions (Frederiksen & Frederiksen, 2007; Hope *et al.*, 2006; Raut *et al.*, 2014). Feng *et al.* (2010) showed that the SAM and SWWA rainfall relationship becomes insignificant if one extreme year – 1964 – is excluded from the analysis. However, Cai *et al.* (2011d) showed that the changes in the SAM are congruent with the rainfall decline in this region using satellite data. It has also been argued that the increased inland and decreased coastal rainfall is partially explained by land cover changes causing increasing moisture divergence over SWWA and increased moisture convergence and vertical velocity inland (Pitman *et al.*, 2004; Timbal & Arblaster, 2006b). Rainfall over SWWA has continued to be lower than the historical average over recent decades (Climate Change in Australia; CCIA 2015).

2.4.2 Southeast Australia

High rainfall variability is a key feature of southeast Australian climate (Murphy & Timbal, 2008; Nicholls *et al.*, 1997). SEA has experienced three major droughts after the instrumental period, the "Federation drought" (1895-1902), the "World War ll drought" (WWll, 1937-1945) and the "Millennium Drought" (1997–2009). The Federation drought prevailed over northern and east Australia while the "World War ll drought" extended over most parts of the continent, including east, central and north Australia. During the Federation drought, Australia was mainly affected by rainfall reduction in spring/summer. ENSO and the IPO were the main factors triggering the Federation drought (Verdon-Kidd & Kiem, 2009). Although the persistent El Niño shifted its phase to La Niña in 1898, it is thought that the positive IPO phase suppressed the prevailing La Niña condition (Verdon *et al.*, 2004). During the WWll drought, rainfall was below normal across all the seasons. El Niño changed its phase to La Niña, and the SAM changed its phase to negative. Hence, these factors are unlikely to explain the drought. The SST off the coast of NWA was cooler than average in 6 years out of 9 years and played a major role in the rainfall reduction (Verdon-Kidd & Kiem, 2009).

Recently SEA experienced its driest 13 years in the last 110 years from 1997-2009 (Timbal, 2009) followed by two very wet years 2011-2012. A significant decreasing trend is evident in the SEA in recent years during JJA and SON (Fig. 2.5k, n). In this context, the collaborative South Eastern Australian Climate Initiative (SEACI, 2010) was established in 2006 to provide knowledge about the climate variability of southeastern Australia. This initiative found that the rainfall decrease was strongest in autumn with a small decrease in winter and spring over the period from 1997 to 2009 and climate drivers including the SAM, ENSO, and the IOD are unlikely to explain the millennium drought (Murphy & Timbal, 2008). The SEACI scientists suggest that there is a strong correlation between rainfall over SEA and STR during all seasons except summer. They further showed that the trend is related to an anthropogenic expansion of Hadley cell at .5° latitude/decade rate, pushing rain-bearing systems further south. Climate models best captured the trend only when natural and anthropogenic forcings were included, although the simulated magnitude is smaller than observed. As much as 80% of rainfall is statistically associated with the strengthening of the STR (SEACI, 2010). During all three major droughts, the IOD phases were positive or neutral (Ummenhofer *et al.*, 2009). Thus SST pattern over the Indian Ocean plays a major role in rainfall variability over this region.

Paleoclimatic evidence suggested Eastern Australia had a higher degree of rainfall variability since 1000 CE than in the observed instrumental period, with more frequent wet and dry phases (Tozer *et al.*, 2016). The likelihood of a dry or wet period exceeding a decade in length was 10 times higher between 749 BCE and 1980 CE than what has been observed during the instrumental record (Hope *et al.*, 2015b). Similarly, it was found that megadroughts exceeding 5-years duration occurred in eastern Australia numerous times during the last millennium, including a 39-year long drought during an unprecedented century of aridity (Vance *et al.*, 2015). Similarly, the rate of recent declines in cool season rainfall in parts of southern Australia has been unusual though not unprecedented in the context of the last 400 years, while the spatial extent and duration of the Millennium Drought appears unprecedented over this multi-century reconstruction period (Freund *et al.*, 2017). These droughts challenge existing water storage strategies. Great variability, including the potential for prolonged droughts, should be taken into account in order to avoid a water crisis in the future.

Rainfall over Tasmania is spatially heterogeneous, modulated by mountains ranging from the west to central Tasmania. The interannual variability of rainfall over Tasmania is

largely influenced by three dominant factors, namely ENSO, SAM, and the Pacific-South American mode (PSA) (Hill *et al.*, 2009). Western Tasmania receives one of the highest totals (>2500 mm per year) of rainfall of any region in Australia. There has been a reduction in annual rainfall over Tasmania since 1975, much like other southern regions in Australia, which is largest in autumn (Nicholls, 2006). Meneghini *et al.* (2007) showed that SAM has a strong impact on the west of Tasmania, similar to SWWA. Tasmania exhibits an east-west pattern of annual rainfall due to its orographic conditions (Hill *et al.*, 2009). This dipole pattern is exacerbated due to the increasing trend in winter and spring rainfall in western Tasmania and decreasing rainfall during autumn over eastern Tasmania, and this is partly attributed to changes in SAM (Taschetto & England, 2009a).

2.4.3 Northern Australia (NA):

NA (north of 25˚S) receives more than 40% of Australia's total annual rainfall during the austral summer months. The last two decades (1995-2012) were anomalously wet compared to the previous two centuries (O'Donnell *et al.*, 2015). The NMR reconstructions identified that recent 30-year and 50-year increases in warm-season rainfall in tropical northern Australia were unusual in the multi-century context of the reconstructions (Freund *et al.*, 2017). There is a dipole pattern observed between northwest Australia and northeast Australia, where rainfall over NWA (west of 130˚E) has significantly increased since 1950, but annual rainfall trends have shown a decreasing trend east of 130˚E and especially along the mid and south coastal regions of Queensland (Taschetto & England, 2009a). An increased monsoonal flow is observed in this region since 1950 (Taschetto & England, 2009a) which some studies have argued has stemmed from an increase in aerosol emissions (Rotstayn *et al.*, 2012), specifically Asian aerosols (Rotstayn *et al.*, 2007). However, there are various other mechanisms proposed as a possible cause of the rainfall increase, such as warming over the tropical Atlantic (Lin & Li, 2012). A study using CMIP3 models showed that NA rainfall in models is poorly simulated due to a known model bias called the "Pacific Ocean cold tongue bias", which strengthens the ascending branch of the Walker circulation extending it too far into the west (Cai *et al.*, 2011b). The poor representation of convection might also be responsible for rainfall and circulation errors in climate models since simulations of CMIP5 models forced with observed SSTs show that rainfall is triggered early in atmospheric models (Ackerley *et al.*, 2015). Anthropogenic aerosols may play a major role in NWA summer rainfall increase (Rotstayn *et al.*, 2007; Rotstayn *et al.*, 2012) by strengthening monsoonal flow (Dey *et al.*, 2018). Anthropogenic

aerosols and GHG have opposing impacts, while aerosols induce a monsoon-like flow that transports moisture towards NWA, GHGs produce an anticyclonic flow situated over northern Australia, which results in weak trends in all forcing simulations in CMIP5 models (Dey *et al.*, 2018). However, there is still much uncertainty in the dominant causes of this substantial rainfall increase and our ability to model observed trends (Brown *et al.*, 2016; Clark *et al.*, 2018).

Rainfall in NA exhibits a significant increase over the 1910-2015 period, with a stronger increase in recent decades (1985-2015) (Fig. 2.5b). A number of studies examined a decrease in Southeast Queensland (SEQ; south of 22˚-36.5˚S) rainfall over a period 1950-2008 (Cai *et al.*, 2010; Li *et al.*, 2012). The trend in the SEQ has been attributed to the persistent warming in the Wharton Basin region of the Indian Ocean in the last 60 years (100˚-130˚E, 20˚-5˚S) (Li *et al.*, 2012). During a cold state in the Wharton Basin, cyclonic circulation and upward motion over NEA increases rainfall in this region and vice versa in a warm state. Cai *et al.* (2010) suggested an eastward shift of the Walker circulation associated with the break down in ENSO-Australia's rainfall relationship since 1980 as the possible mechanism of the region's rainfall decline. They also showed that none of the climate models analysed captures the rainfall decline with various forcings such as all forcings, GHG, ozone, aerosol emissions. This highlights a dominant role of internal variability in the observed rainfall decline.

2.4.4 Modeling of observed rainfall trends

GCMs often fail to simulate aspects of the observed magnitude and frequency of rainfall although they perform well while simulating temperature extremes (Randall *et al.*, 2007). This is in part due to their resolution, as GCMs cannot explicitly resolve convective systems, but rely on parameterisation schemes (Randall *et al.*, 2007). Over Australia, Alexander and Arblaster (2017) reported that mean and extreme temperature is simulated reasonably well, but there is large model spread among models while simulating mean and extreme rainfall.

The rightmost panel of Fig. 2.5 shows the rainfall trends between 1986 and 2015 in the ensemble mean of 39 CMIP5 models, combining historical (1986-2005) and RCP simulations (2006-2015). It is evident that the ensemble mean shows a weak positive trend in NWA and significant drying in SWWA, and parts of eastern Australia (Fig. 2.5c) however, the magnitude of these trends is smaller than observed. The NWA and east coast rainfall trends are not consistent across the models (with stippling indicating that two-thirds of the models agree on

the sign of the change). The summer increase in the north is very weak, and a decreasing trend is seen in the southwest, which is not observed (Fig. 2.5f). During autumn (Fig. 2.5i), models show a significant decrease in rainfall in coastal regions of eastern Australia, which is also seen in observed, but not significant. During winter, a significant decreasing trend in SWWA rainfall is seen both in the model ensemble (Fig. 2.5l) and observations (Fig. 2.5k). However, the winter rainfall decline in the SEA is not evident in the model ensemble (Fig. 2.5l). The trend in spring is weak compared to other seasons, yet there is a small decline in SWWA (Fig. 2.5o).

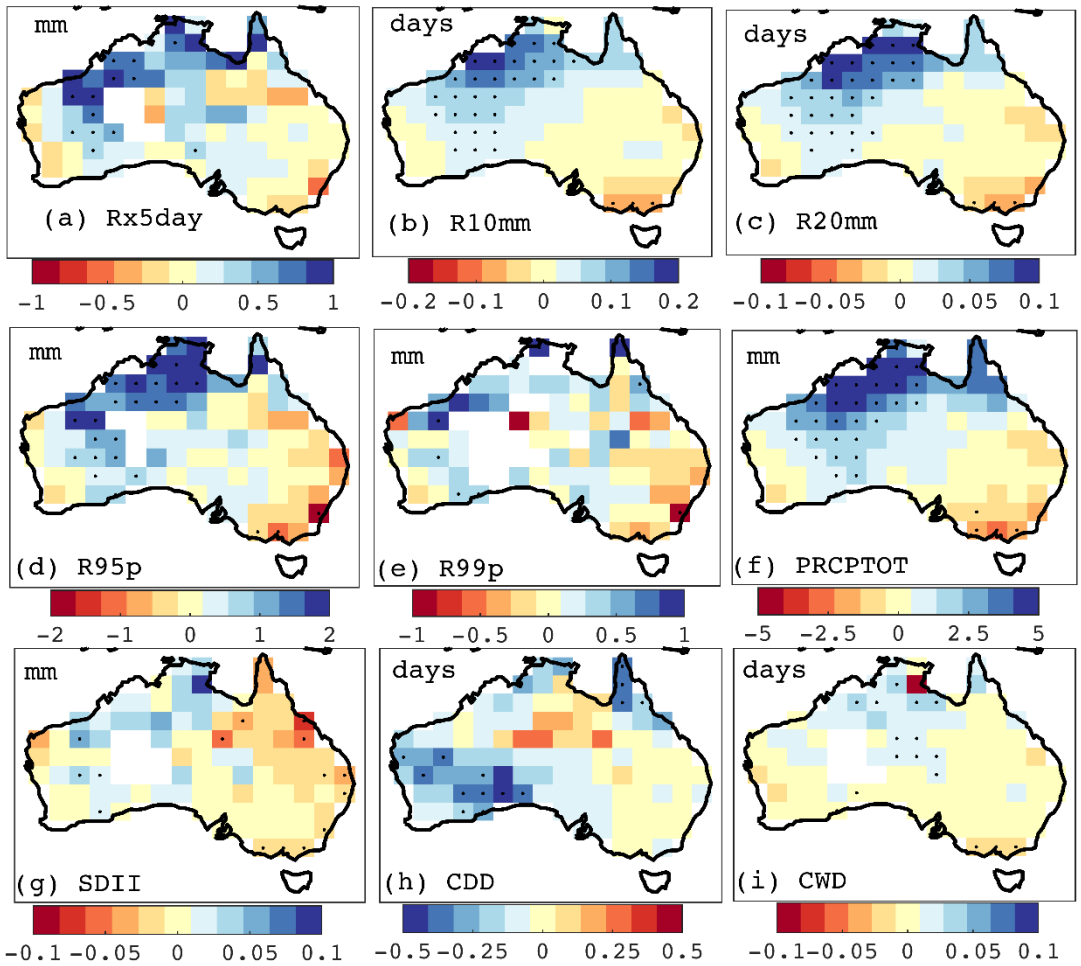

Figure 2.6 Trends in extreme precipitation indices for the GHCNDEX dataset (1951-2015) (a) maximum consecutive 5-day precipitation (Rx5day; mm), (b) heavy precipitation days (R10mm; days), (c) very heavy precipitation days (R20mm; days), (d) very wet days (R95p; mm), (e) extremely wet days (R99p; mm), (f) total wet day precipitation (PRCPTOT; mm), (g) simple daily intensity (SDII; mm), (h) consecutive dry days (CDD; days), (i) consecutive wet days (CWD; days). These datasets are downloaded on 27 July 2018 from https://www.climdex.org/gewocs.html.

2.5 Observed trends in rainfall extremes

An extreme is defined as the occurrence of a value of a weather or climate parameter above a threshold value or near the tails of the distribution (IPCC, 2012). Climate extremes may be driven by a combination of natural and/or anthropogenic forcings; thus changes in the background climate state can change the frequency, intensity, and mechanisms of extreme events. Rainfall extremes have very high interannual variability over Australia (Alexander & Arblaster, 2009). Since 1910, the percentage of area experiencing extreme heavy rainfall has increased while the percentage of area experiencing dry conditions has declined (Gallant & Karoly, 2010; Plummer *et al.*, 1999). Extreme indices (daily intensity, consecutive dry days, very heavy precipitation contribution) studied by Alexander and Arblaster (2009) and Alexander and Arblaster (2017) have generally increased over 1911-2010, with some statistically significant increases over Australia as a whole.

Contractor *et al.* (2018) shows an intensification in the entire rainfall distribution (light, moderate, and extreme rainfall) in daily observations in Australia over the 1958-2013 period. This implies an overall shift in the wet day rainfall distribution towards the heavier side. Also, there is an intensification of extreme rainfall events at all-time scales, e.g. daily (Contractor *et al.*, 2018), sub-daily (Westra *et al.*, 2014) and hourly extremes (Guerreiro *et al.*, 2018) in Australia.

On a regional scale, there are significant trends observed for shorter timescales (Jakob & Walland, 2016). While the rainfall frequency has increased in north Australia since 1958, there is a decline noted in southern parts of the continent (Contractor *et al.*, 2018). The spatial pattern of the rainfall frequency change is consistent with the spatial pattern of the mean rainfall trend in Australia. For example, the daily winter extreme rainfall in SWWA has become less frequent since 1965 (Li *et al.*, 2005). Groisman *et al.* (2005) reported a 43% $(100\ yr)^{-1}$ reduction in the frequency (not significant at 0.05 level) of very extreme events in SWWA over the period 1913-1998 whereas the frequency of extreme events has increased over the SEA by 52% $(100\ yr)^{-1}$ (significant at 0.05 level) from 1907-1998. However, there is large variability in this result depending on the time period considered, with Taschetto and England (2009) suggesting extreme rainfall events have become less frequent over the SEA and coastal Queensland, consistent with a decline in mean rainfall, over the 1970-2006 period. Overall, when considering trends over 90-100 years, extreme rainfall in the northwest has intensified and has become more frequent, whereas in SWWA extreme rainfall have become less frequent and less

intense, with non-significant trends elsewhere (Haylock & Nicholls, 2000; Nicholls *et al.*, 1999; Smith *et al.*, 2000; Suppiah & Hennessy, 1996).

Trends in short duration extremes differ from daily extremes spatially (Guerreiro *et al.*, 2018; Hardwick Jones *et al.*, 2010; Jakob *et al.*, 2011a, 2011b). For example, sub-hourly and hourly extreme events show a much faster increasing rate at a continental scale (Guerreiro *et al.*, 2018), compared to daily extremes which show small change over most parts of the continent (Hardwick Jones *et al.*, 2010). Wasko and Sharma (2015) found that rainfall within storms becomes less uniform at higher temperatures, implying intensified rainfall at peak stages and less intensified rainfall at other times during the storms. However, trends in these short duration events vary largely with seasons and geographical conditions and how extreme rainfall scales with warming is an ongoing research area (Bao *et al.*, 2017).

Fig. 2.6 shows trends in maximum consecutive 5-day precipitation (Rx5day), heavy precipitation days (R10mm), very heavy precipitation days (R20mm), very wet days (R95p), extremely wet days (R99p), simple daily intensity (SDII), consecutive dry days (CDD), consecutive wet days (CWD), annual total precipitation in wet days (PRCPTOT) over the time period 1951-2015 using GHCNDEX dataset (Donat *et al.*, 2013b) between 1951 and 2015 [source: https://www.climdex.org/gewocs.html]. There is a significant increase in Rx5day, PRCPTOT, R10mm, R20mm, R95p, CWD in NWA. A significant decrease in 'SDII' is evident in coastal eastern Australia. A significant decrease in CWD, PRCPTOT, R10mm, R20mm, SDII is found in three grid boxes in the SEA.

2.5.1 Attribution of Australian extreme rainfall events

Attribution of extreme events refers to the evaluation of plausible factors contributing to a change in the climate or event with accompanying statistical confidence (Hegerl *et al.*, 2010). A common approach of extreme event attribution studies is the 'Risk-based approach' (Shepherd, 2016) where models are run to generate two sets of simulations for 1) the factual world (accounts for real atmosphere, i.e. includes all the forcings), 2) a counter-factual world (hypothetical condition, including all forcings except anthropogenic emissions). Using this probabilistic method, the main question 'would the extreme event occur in the counterfactual world? If yes, what would be the magnitude?' can be answered quantitatively. The fraction of attributable risk (FAR) value provides an estimate of the contribution of human-induced changes or external forcings (e.g. ENSO) to an event.

$$FAR=1-P_1/P_0,$$

Where P_0 is the probability of extreme events when all forcings are included, and P_1 is the probability of the extreme event when all forcings except anthropogenic forcing are included.

A number of studies in Australia have applied this method to study the impact of anthropogenic emissions on extreme events. Lewis and Karoly (2015), for example, investigated causes of heavy March 2010-2012 rainfall over east Australia. A large part of the continent received much above average rainfall during 2010-2012 resulting in catastrophic floods in areas of Queensland, NSW, and Victoria. The majority of the studies attributed the extreme rainfall primarily to natural variability of the climate system, with one of the strongest La Niña events on record during 2010/2011, along with strong positive SAM (Hendon *et al.*, 2014; Trenberth, 2012), and another La Niña event in 2011/2012. FAR analysis showed limited evidence of anthropogenic forcing on the 2011-2012 extreme rainfall over SEA region (King *et al.*, 2013b; Lewis & Karoly, 2015) or the March 2012 extreme rainfall (Christidis *et al.*, 2013). A relatively modest contribution by long-term warming of the surrounding SSTs was found for the record spring and summer rainfall in eastern Australia in 2010 (Evans & Boyer-Souchet, 2012; Hendon *et al.*, 2014).

2.6 Projected future changes in mean and extreme rainfall

Climate models show a large inter-model spread in simulating future rainfall. These uncertainties arise from natural internal climate variability, model biases, including uncertainties from climate model parameters and future emissions projections (Hawkins & Sutton, 2009), the relative importance of which varies depending on the temporal and spatial scale of interest. Although the amount of rainfall averaged over Australia is projected to change very little in the future, some regional changes particularly continued drying in the southwest, are robust across projections. Australia is expected to receive intensified rainfall events, however, the frequency of rainfall events is projected to decrease (Pitman & Perkins, 2008). This is also evident in indices calculated from CMIP5 models which show that Australia is projected to experience increased 'consecutive dry days' and increased 'heavy precipitation' and 'maximum five-day precipitation' (Alexander & Arblaster, 2017; Sillmann *et al.*, 2013b).

Here we summarise future projections of rainfall in three regions in Australia for which there is sufficient literature.

2.6.1 Southwest West Australia

A further decrease of winter and spring rainfall in the SWWA region is robustly projected for the 21st century based on modelling studies across medium to high emission scenarios (Bates *et al.*, 2008; Hope *et al.*, 2015b; Timbal, 2004), due to fewer troughs and an increased number of high-pressure systems projected throughout the 21st century (Hope, 2006b). Due to the projected strong increase in temperature and evaporation, soil moisture is likely to reduce further increasing the severity and frequency of droughts in future (Hope *et al.*, 2015a). Overall, a 50% decrease in winter rainfall is projected in the RCP8.5 scenario by 2090. The annual maximum rainfall shows a positive change by 2090 relative to 1986-2005, however, there is low confidence in extreme rainfall projections in this region (Hope *et al.*, 2015b). A significant increase in consecutive dry days is projected for the period 2081-2100 under the RCP8.5 scenario (Alexander & Arblaster, 2017).

2.6.2 Southeast Australia

Mean rainfall over the SEA is projected to reduce further in the future, though with a large range depending on the scenario and the model used (Grose *et al.*, 2015; Grose *et al.*, 2017; Whetton *et al.*, 2016). GCMs project a range of -20 to 5% change in winter rainfall under RCP4.5 and -40 to 5% under RCP8.5, -15% to 10% and -15 to 25% change in summer rainfall under RCP 4.5 and RCP8.5 respectively (Timbal *et al.*, 2015). Short duration extreme rainfall events are projected to intensify while the intensity of longer-duration events is projected to increase till 2030 and decrease by 2070 (SEACI phase 2 report, 2012). The coastal region of Tasmania is projected to receive steadily increased rainfall, whereas the central and northwest region is projected to receive reduced rainfall (Grose *et al.*, 2010). Extreme rainfall events are projected to become more frequent across most regions of Tasmania except over the central plateau (White *et al.*, 2010). Overall, there is reasonable confidence in future winter rainfall decline in southern Australia, except Tasmania, which shows a little increase in rainfall (Hope *et al.*, 2015b).

2.6.3 Northern Australia

Future rainfall projections over NWA are uncertain. The multimodel mean of CMIP3 models shows a future reduction in mean summer rainfall due to the projected weakening of the Walker circulation (Cai *et al.*, 2011b). However, Brown *et al.* (2016) and Dey *et al.* (2018) found CMIP5 models show a small multimodel increase in NWA summer rainfall under the RCP8.5 scenario, although there is considerable model spread. Dey *et al.* (2018) suggested that

anthropogenic aerosols play a key role in the observed NWA summer rainfall increase, and given all RCP scenarios have declining aerosols, they contribute to the weak positive future trend. However, Brown *et al.* (2016) also note the importance of tropical Pacific SSTs to NWA rainfall projections. Overall, there is medium confidence in an increase in rainfall in the monsoon region (CCIA, chapter 7, 2015). The rainfall over Queensland is projected to change by -6% to 5% by 2030, and -19% to 14% by 2070 in CMIP3 models (Suppiah *et al.*, 2007). Overall, the trajectory of future NWA rainfall remains unclear (Brown *et al.*, 2016; Dey *et al.*, 2018; Jourdain *et al.*, 2013; Moise *et al.*, 2012).

2.7 Summary and future research scope

This paper has reviewed literature on past and projected changes in Australian rainfall in the pre-instrumental and instrumental period. The systems and large-scale drivers of Australia's rainfall are summarised in Table 2.1. A summary of mean and extreme rainfall in different Australian regions, possible underlying mechanisms, and future projections are given in Table 2.2.

Australia has a dense observational network, however, this is mostly confined to the coastal regions, and the inland regions are comparatively data-sparse. Paleoclimatic records of pre-instrumental rainfall are spatially limited to areas that preserve proxy archives, environments referencing eastern and northern Australia. Although not reviewed here, radars and various high-resolution satellite products are also available, and they are now becoming long enough to study means and extremes, although they have their own issues, e.g. inadequate sampling, errors in algorithm, biases stemming from the indirect relationship between observation and precipitation (Sun *et al.*, 2018). In addition, the Bureau of Meteorology high-resolution Regional Reanalysis for Australia (BARRA) is also becoming available in an ongoing project to provide high-resolution atmospheric and surface parameters at a 12km resolution and even higher resolutions for some sub-regions using model downscaling over the period 1990-2016 (Jakob *et al.*, 2017). As a result of the spatial and temporal limitations of valuable instrumental and pre-instrumental records, understanding long-term changes in rainfall in Australia remains a challenge.

Rainfall characteristics (such as TC, monsoon, fronts) and drivers (such as IOD, STR, SAM) are also expected to change along with the future mean total rainfall. We have already seen a detectable historical change in some of the drivers (see Table 2.1), however, changes in the characteristics are very small and not significant in most of the cases. Future changes in the

SAM will be impacted by the opposing influences of ozone recovery and GHGs (Arblaster *et al.*, 2014; Arblaster *et al.*, 2011; Wang *et al.*, 2014), with positive trends projected under high emission scenarios and negative trends under low GHG emission scenarios in austral summer. This example reveals the importance of the correct representation of atmospheric concentrations in models. In addition, there is a large inter-model spread in projecting large-scale climate drivers and the teleconnection with Australia's rainfall, which reduces confidence in future projections. This example reveals various feedbacks and complex atmospheric interactions with anthropogenic emissions should be accurately incorporated in GCMs to provide robust projections. The trend in rainfall small-scale characteristics such as TC and fronts are difficult to simulate given the coarse resolution of climate models. It is computationally expensive to run GCMs at a high enough resolution so that they can capture TCs as well as produce long-runs and multiple ensemble members. Thus there is remaining uncertainty in the future projections of these systems in GCMs. There are various improvements in models suggested by Camargo and Wing (2016) to reduce uncertainty in TC projections, including realistic SST patterns, correct representation of ENSO, improved convective parameterisation schemes to name a few.

Historical mean rainfall trends and future projections have been reviewed for three key agricultural regions of Australia. There is a significant increase in rainfall in the northwest and decreases in southwest, southeast and east Australia over the historical period since 1950. Models project a further drying trend in SWWA, SEA, and the coastal region of Queensland under increasing GHG emissions. Furthermore, the future trajectory of NWA rainfall is not clear as CMIP3 models show a very small decreasing trend due to the future weakening of Walker circulation (Cai *et al.*, 2011b), and CMIP5 models show a small increase over the period 2006-2099, although weaker than what is observed during 1950-2005 (Dey *et al.*, 2018). Aerosols have been suggested as an underlying mechanism in the persistent rainfall increase in this region. Further modelling studies using an improved representation of direct and indirect impacts of aerosols are required to provide more robust future projections.

As extreme heavy rainfall or drought events cause significant economic damage and potential loss of life, hydroclimatic extremes are of particular scientific and popular interest. Previous scientific studies focused on instrumental and pre-instrumental records of rainfall demonstrate substantial evidence that climate change is influencing the frequency and intensity of extreme events. The short length of observational datasets limits our ability to study very

extreme events (e.g. events with higher return periods) due to small sample sizes. Another limiting factor is the observational quality which makes it difficult to study extreme events using datasets from the early 20th century. For example, cyclone studies using early records are also questioned repeatedly due to the poor observation and classification techniques that existed before the introduction of satellite data.

In this review, extreme event attribution methods were discussed with particular reference to a recent case study: the 2010-2012 eastern Australia heavy rainfall event. FAR analysis showed limited evidence of climate change on this extreme rainfall event. FAR values only provide a quantification of the statistical likelihood of a class of events occurring with external forcings imposed compared to no external forcing. To take detection and attribution one step further, various drivers of extremes should be studied, such as changes in dynamical and thermodynamical components in response to external forcing. Various other issues of detection and attribution need to be addressed in the future, such as detection and attribution of more complex events (cyclone, droughts), changes in non-meteorological parameters (mortality, homes flooded due to an extreme event) and real-time attribution of extreme events (Haustein *et al.*, 2016).

Although there is little consensus among models in projected rainfall trends across Australia, overall CMIP5 models project a shift towards more extreme conditions in future, i.e. increasing the risk of prolonged droughts, frequent floods, and heat waves.

Table 2.1 Summary of past and projected trends of rainfall characteristics and large-scale drivers of Australia's rainfall based on reviewed literature.

Drivers	Past changes	Projected future changes
ENSO	The weakening of Walker Circulation since the beginning of 20th century (Deser *et al.*, 2010), strengthening over the period 1980-2012 however, the mechanism of the strengthening of the Walker Circulation is not clear (Luo *et al.*, 2012).	A further weakening of Walker Circulation is projected (low-confidence) (Collins *et al.*, 2010) along with frequent and intensified El Nino and La Nina events (Cai *et al.*, 2015). The occurrence of El Nino events is projected to almost double due to climate change (Santoso *et al.*, 2013).
IOD	The pIOD events have increased while negative events have decreased since 1950 with more frequent pIOD events. The Mechanism is not clear and needs to be studied further. Although, global warming could be one possible reason (Cai *et al.*, 2009b).	Increased pIOD events with an increase in frequency (Abram *et al.*, 2008; Cai *et al.*, 2013).
STR	Increase in the STR intensity since 1970 (Timbal & Drosdowsky, 2013). The reason is not clear as the trend in the intensity of Hadley Circulation needs to be studied further (Timbal & Drosdowsky, 2013).	Increase in the STR intensity and a poleward shift in CMIP3 (Kent *et al.*, 2013) and CMIP5 (Grose *et al.*, 2015) models.

MJO	Increase in MJO amplitude (Lee & Seo, 2011) and frequency (Jones & Carvalho, 2006).	MJO amplitude is projected to increase by 30% (Chang *et al.*, 2015).
Fronts	A small increase in frequency in fronts over the period 1989-2009. (Fig. 2 of Berry *et al.* (2011a)).	The southward shift in location. A small increase in front frequency and strength in RCP8.5 in southern Australia (see Fig. 3b &d of Catto *et al.* (2014).
Australian Monsoon	The historical trend is not clear. Some monsoon indices show a clear reduction post-1980 (Christensen *et al.*, 2013), however, Kajikawa *et al.* (2009) index shows an increase in monsoonal winds (Dey *et al.*, 2018). The changes in Australian Monsoon in response to greenhouse emissions need to be studied further.	There is a little consensus among models. Although, CMIP5 models show an increase of 0.4% K^{-1} in monsoon rainfall in RCP8.5 simulations (Brown *et al.*, 2016).
TC	There is a significant decline in total number of cyclones since 1969/1970. Also, there has been a decline in moderate and weak cyclones, but there is a weak, insignificant positive trend in the intense cyclone (Nicholls *et al.*, 1998).	The downscaled GCMs show that the number of cyclones is projected to decrease by the end of the 21st century. A decrease in TC occurrence by 50% and 30% are projected by Abbs (2012) and Lavender and Walsh (2011) respectively by the end of the 21st century relative to the current climate.
SAM	The significant positive trend since observational records began in the 1960s (Marshall, 2003), and possibly since	In future, ozone is projected to restore, however, the continuous rising levels of GHG will have opposing impacts

	the 1940s based on palaeoclimate evidence (Abram *et al.*, 2014). Ozone depletion over the Antarctic and increasing GHG in the atmosphere are the possible mechanisms (Thompson *et al.*, 2011).	on the SAM trend (Thompson *et al.*, 2011). A positive trend is projected in CMIP5 models by the end of the 21st century under RCP4.5 and RCP8.5 (Gillett & Fyfe, 2013).
East Coast Low (ECL)	No significant change (Ji *et al.*, 2015).	Fewer ECLs with weaker intensity (Ji *et al.*, 2015). The most intense ECLs are projected a small decrease in winter but an increase in summer (Pepler *et al.*, 2016).

Table 2.2 Summary of mean and extreme precipitation trends in North West Australia (NWA), Southeast Queensland, SEA, SWWA and Tasmania in past (since 1950) and projected changes based on reviewed literature.

Region	Historical mean trend	Historical extreme trend	Season	Possible mechanisms	Projected mean trend	Projected extreme trend
NWA	Rainfall significantly increased since 1950 (Li *et al.*, 2012; Li *et al.*, 2013).	Increase in Rx5day, R10mm, and R95p (Fig. 2.6a, b, c) (Dey *et al.*, 2018).	Summer	The reason is not clear. Increase in anthropogenic aerosols that strengthens monsoonal flow (Dey *et al.*, 2018; Rotstayn *et al.*, 2007; Rotstayn *et al.*, 2012), warming over the tropical Atlantic (Lin & Li, 2012), increase in the frequency of tropical cyclones (Clark *et al.*, 2018) are postulated as underlying mechanisms.	There is little consensus among models (Brown *et al.*, 2016). A small increase in RCP8.5 in CMIP5 models is projected but smaller than what is observed in the past (Dey *et al.*, 2018). However, CMIP3 models show a weak	The intensity of extreme events is projected to increase, whereas the change in frequency is not clear. Overall, there is low confidence in extreme projections (Dey *et al.*, 2018).

					decline in the future (Cai *et al.*, 2011b).	
Southeast Queensland	Decrease Since 1950 (Li *et al.*, 2012).	Fig. 2.6 does not show any significant trend. However, there is a decrease (but not significant) in intensity (Rx5day, R95p, R99p) and frequency (R10mm, R20mm) of extremes events which are only consistent with results from Taschetto and England (2009a).	Summer and autumn.	The reason is not clear. Warming in the Wharton Basin (Li *et al.*, 2013), break down in ENSO-Australia rainfall relationship post-1980 (Cai *et al.*, 2010), weakening of easterlies in the western Pacific reducing moisture transport (Taschetto & England, 2009a) are hypothesised mechanisms.	A -6% to 5% change in rainfall by 2030, and -19% to 14% by 2070 change is projected in CMIP3 models relative to 1990 (Suppiah *et al.*, 2007).	A significant increase in consecutive dry days, no significant trend in intensity and frequency of wet extremes (Alexander & Arblaster, 2017).
SEA	No significant long-term trend. Below	A significant decline in R10mm, R20mm, and R95p over the	Predominantly in autumn and a small	Increase in intensity and a southward shift in STR from an expansion of Hadley cell	Mean winter rainfall is projected to	Short duration (2-hr) extreme rainfall events

	average rainfall is observed since the beginning of the 1990s to 2009, followed by two years (2010-2012) of heavy rainfall; the rainfall has been below normal since then.	period 1951-2017, evident in Fig. 2.6. Similar trends were shown by Gallant *et al.* (2007).	decrease in winter and spring.	due to greenhouse gas emission (Timbal & Drosdowsky, 2013; Whan *et al.*, 2014).	decrease due to southward shift and strengthening of STR (Grose *et al.*, 2015).	are projected to intensify, but the intensity of long duration events will increase till 2030 but are projected to decrease by 2070 (SEACI, 2010).
SWWA	The gradual decrease since 1940 and an abrupt decrease since the 1970s and again around	A long-term decline in the frequency and intensity of extreme events is overserved (Charles *et al.*, 2010; Haylock & Nicholls, 2000), specifically	Winter	Not clear, a literature body reported that the decline is due to decreased numbers of synoptic systems due to external forcings (Hope *et al.*, 2006; Raut *et al.*, 2014). SAM is shown as another	Future rainfall is projected to decrease along with a dramatic decline in number of troughs (Hope *et*	A significant increase in consecutive dry days over the period 2081-2100 compared to 1986-2005

	2000 (Hope & Ganter, 2010).	during winter (Li *et al.*, 2005).		driver for this long-term drought (Cai *et al.*, 2011d).	*al.*, 2015b; Hope, 2006b).	(Alexander & Arblaster, 2017).
Tasmania	Rainfall has decreased since 1975. Exhibits east-west pattern of rainfall. Increasing rainfall trend in winter and spring in western Tasmania and decrease in the east in autumn (Taschetto &	There is no significant trend in extreme indices. Annual total wet-day precipitation, consecutive dry days, consecutive wet days have a significant decreasing trend over the period 1911-2010 (Alexander & Arblaster, 2017).	Increase in winter and spring in the west. The decrease in autumn is in the east.	East-west pattern due to orographic effects (Hill *et al.*, 2009). Increase in the rainfall in the west is attributed to a positive trend in SAM (Hill *et al.*, 2009; Meneghini *et al.*, 2007).	Rainfall over coastal regions increases steadily while decrease in central and northwest Tasmania (Grose *et al.*, 2010).	More frequent and intensified events in most areas except central plateau. The decline in the return period of extreme events will increase flood risk (White *et al.*, 2010).

	England, 2009a).					

Chapter 3

Investigating observed northwest Australian rainfall trends in Coupled Model Intercomparison Project phase 5 detection and attribution experiments

Abstract

Mean and extreme northwest Australian (NWA) summertime rainfall has increased significantly since 1950. While previous studies have explored a range of possible factors impacting NWA rainfall, the causes of this increase and possible future changes remain uncertain. This study explores the increasing NWA summertime rainfall trends in Coupled Model Intercomparison Project phase 5 (CMIP5) models. By using a suite of models that contributed realisations of the historical period with various forcings we explore the impact to this region of greenhouse gases and aerosol emissions since 1950 on mean rainfall and three extreme rainfall indices. The observed NWA rainfall trend is better captured in models when all forcings are included compared to simulations with only greenhouse gas forcing or with only natural forcing, although the models have a large spread. We hypothesise that anthropogenic aerosols played a major role in the observed rainfall trends, and the associated increase in monsoonal flow, and hence historicalNat and historicalGHG simulations tend not to capture observed rainfall trend. Throughout the 21st century, CMIP5 models simulate a stronger increase in mean summer precipitation and extreme indices of NWA rainfall in Representative Concentration Pathway (RCP) 8.5 simulations than in RCP2.6. The NWA region shows intensified extreme events with fewer heavy precipitation days, but the reliability of these projections in this region should be further tested with estimates of future anthropogenic aerosol changes.

Keywords: Australian rainfall, CMIP5 models, precipitation trends, precipitation extremes, Australian Summer Monsoon Index.

3.1 Introduction

Rainfall in Australia demonstrates a great degree of spatial and temporal heterogeneity (Nicholls *et al.*, 1997). One aspect of this heterogeneity is the observed increase in northwest Australia (NWA) summertime (December-February, DJF) rainfall over the period 1950 to present (Alexander & Arblaster, 2009; Groisman *et al.*, 1999; Taschetto & England, 2009a). NWA receives an annual rainfall of 600mm (long-term average over the period 1900-2011), 40% of it is received in DJF. The observed increase in NWA summer rainfall is in contrast to a decreasing autumn and winter rainfall trend observed in southeastern and southwest of Western Australia respectively (Groisman *et al.*, 1999). In this present study, we investigate the observed NWA rainfall trends in CMIP5 detection and attribution experiments.

3.1.1 Key rainfall drivers

Untangling the causes of the observed increase in rainfall is difficult as northern Australian rainfall is influenced by a complex suite of climate modes and systems including the El Nino – Southern Oscillation (ENSO), Indo-Australian monsoons, tropical cyclones (Dare *et al.*, 2012), the Indian Ocean Dipole (IOD; (Saji *et al.*, 1999)) and the Madden-Julian Oscillation (MJO; (Wheeler *et al.*, 2009)), the Interdecadal Pacific Oscillation (IPO;(Latif *et al.*, 1997)), and the Southern Annular Mode (Cai *et al.*, 2014a). The contributions of these modes of variability to northern Australian rainfall are spatially and temporally variable. For example, the effect of ENSO on NWA has been described as minor compared to on eastern Australia (Risbey *et al.*, 2009; Shi *et al.*, 2008).

Furthermore, IOD primarily impacts Australian rainfall during June-October (Risbey *et al.*, 2009) and is unlikely to explain the NWA summertime rainfall increase. The interdecadal variability of sea surface temperature (SST) (e.g. the IPO) is known to have a strong impact on Australian rainfall (Power *et al.*, 1999). The positive phase of the IPO is associated with below average monsoon rainfall, while the negative phase is associated with above-average monsoon rainfall (Latif *et al.*, 1997). During positive IPO phase (warmer tropical Pacific SSTs), the relationship between ENSO and Australia's climate is weak, whereas, during negative phase (cooler tropical Pacific SSTs), ENSO and Australia's climate are strongly correlated (Arblaster *et al.*, 2002; Murphy & Timbal, 2008). Since the 1940s there have been two cold IPO phases reported: 1945-1976 & 1999-2013, and one warm phase from 1977-1998 (Dong & Dai, 2015). Although, there is a fair amount of decadal variability, for example, a seasonal rainfall drop is seen during the 1980s, overall NWA rainfall has increased since 1950. Hence, it is unlikely that the IPO phase changes alone explain the trend in NWA rainfall.

Past studies have explored the possible causes of the observed NWA rainfall trends. The rainfall increase has been attributed variously to changes in monsoon flow induced by land surface changes (Wardle & Smith, 2004), overall increased monsoonal flow and low-level positive divergence (Taschetto & England, 2009b). Furthermore, rainfall can be triggered by convection due to solar heating and unstable boundary layer (Keenan & Carbone, 2008) and the intrusion of maritime moist air at low levels (Berry *et al.*, 2011b). Hence, changes in synoptic weather systems may relate to the increase in rainfall, although previous analysis suggests that changes in tropical cyclone rainfall cannot explain the increasing rainfall trend in recent past (Ng *et al.*, 2015).

3.1.2 Previous modelling work

Climate models have also been used to explore the causes of this observed trend. An increasing (decreasing) rainfall trend is seen in global climate model (GCM) simulations when anthropogenic aerosols are included (excluded) with the strongest increase over NWA (Rotstayn *et al.*, 2012). A similar pattern is observed in simulations, including only Asian aerosols (Rotstayn *et al.*, 2007). A study of northern Australia using Atmospheric Model Intercomparison Project (AMIP) simulations in Coupled Model Intercomparison Phase 5 (CMIP5) models shows evidence that a poor representation of convection is likely reason for errors in precipitation and circulation over NWA (Ackerley *et al.*, 2015), impacting the simulation of rainfall trends. A prior study by (Cai *et al.*, 2011b) showed a decrease in future NWA rainfall in a multi-model ensemble, which was attributed to a strong unrealistic ENSO-rainfall relationship. Overall, the cause of the observed trends remains unclear.

In addition to observed changes in mean summertime rainfall, the majority of tropical Australian stations experienced a positive trend in 99th and 95th percentile rainfall values during September-April over the 1910-1989 period (Suppiah & Hennessy, 1996). Extreme rainfall events can have a potentially severe impact on socio-economic and natural systems and require explicit consideration. This trend in extreme rainfall events has not yet been comprehensively studied, possibly due to the limited availability of data over this region. Alexander and Arblaster (2009) have shown that Australia is projected to experience much longer dry spells interrupted by increased heavy precipitation events in all future Representative Concentration Pathway (RCP) scenarios of the 21st Century. However, the multimodel mean of summer monsoon rainfall over Australia demonstrates very little change in future projection (Brown *et al.*, 2016).

In this current study, we address these research gaps in understanding the cause of trends in NWA mean and extreme rainfall, and possible future changes, using data available from CMIP5 models. We first evaluate a set of CMIP5 models against observations of NWA rainfall. Next, rainfall trends are calculated using data available through CMIP5 experiments over the period 1950-2005 provided with different forcings (including natural forcing only, greenhouse gas forcing only and anthropogenic aerosols only). In addition, we extend the scope of previous studies and explore both mean and extreme rainfall trends, including in future projections for the region, using extreme precipitation indices defined by the Expert Team on Climate Change Detection and Indices (ETCCDI) (Zhang *et al.*, 2011) in observation and models.

3.2 Data and methods

3.2.1 Observations

3.2.1.1 Precipitation and SST

We use monthly mean precipitation data from The Australian Water Availability Project (AWAP; (Jones *et al.*, 2009)) at 0.25º×0.25º horizontal resolution over the period 1901-2005. The NWA study region is defined as, 10º-25ºS, 110º-135ºE (the land area in the boxed region in Fig. 3.1a) (Lin & Li, 2012; Shi *et al.*, 2008), where the rainfall trend is positive and significant at the 95% level. We focus on the trend of summer (DJF) rainfall over NWA for the past 56 years (1950 – 2005) (Fig. 3.1b), which represents the period of maximum overlap between models and observations where an increasing trend has been observed. We also calculate rainfall trends from 26 high-quality weather station datasets (Table 3.2) to validate the trend in the AWAP product. HadISST (Rayner *et al.*, 2003) dataset is used to calculate trends in SST over the period 1950-2005.

3.2.1.2 Indices

The following precipitation-relevant ETCCDI indices are used and are applied on annual, not seasonal basis:

1. Heavy precipitation day (R10mm; unit: days/year) corresponds to a total number of days each year when daily precipitation exceeds 10 mm.
2. Maximum consecutive 5-day precipitation (Rx5day; unit: mm/year) indicates the maximum 5-day precipitation each year.
3. Very wet days (R95p; unit: mm/year) is the sum of precipitation on days when daily precipitation is above the 95th percentile of the daily rainfall distribution for each year.

We use extreme indices from the GHCNDEX (Donat *et al.*, 2013b) dataset, as it has the best spatial coverage over NWA. These datasets are freely available at http://www.climdex.org/gewocs.html at a resolution 2.5º×2.5º from 1951 to present. GHCNDEX is an updated, land-based gridded data set for temperature and precipitation indices calculated from the station based in-situ Global Historical Climatological Network – Daily (GHCN) (Menne *et al.*, 2012) data. Donat *et al.* (2013a) incorporated stations that only had observations for more than 40 years since 1950, minimizing the impact of varying station density. The overlapping time period (1951-2005) between GHCNDEX and CMIP5 models is used to analyse the past trends of these indices.

3.2.1.3 Australian Summer Monsoon Index (AUSMI)

There are several monsoon indices available for studying monsoon onset, strength and variability. Here, the trend of Australian monsoon variability is calculated using the AUSMI (Kajikawa *et al.*, 2009), which is a useful predictor for intraseasonal, interannual or interdecadal timescale variability (Kajikawa *et al.*, 2009; Rogers & Beringer, 2017). It is defined as the zonal wind at the 850hPa level averaged over 5˚S to 15˚S and 110˚E to 130˚E. Zonal wind data are taken from the 2.5˚×2.5˚ NCEP reanalysis data (Kalnay *et al.*, 1996) provided by the NOAA/OAR/ESRL PSD (http://www.esrl.noaa.gov/psd/).

3.2.2 Models

Eighteen CMIP5 models (Taylor *et al.*, 2012) were selected on the basis of availability of historical (1850-2005 experiment including anthropogenic and natural forcings), historicalNat (historical simulation but only includes natural forcing), historicalGHG (historical simulation but only includes greenhouse gas (GHG) forcing), RCP2.6 (low emission scenario) and RCP8.5 (high emission scenario) experiments. We required that models have monthly precipitation and zonal wind data available for all experiments. The Australian Community Climate and Earth-System Simulator (ACCESS) 1.3 model is included, although RCP2.6 simulations are not available. A maximum six realisations for those 18 models for historical simulations with various forcings and 17 models for RCPs were used for this study. In addition, in order to evaluate whether these precipitation and AUSMI trends lie outside of the natural climate variability, we have used pre-industrial control runs (piControl) of these 18 models to calculate 56-year and 94-year running trends in each model. The longest available period is used to calculate the running trends.

Note that aerosols interact with precipitation and cloud both in direct and indirect ways, making the impact of aerosols more ambiguous and difficult to quantify. Although there is an

improvement in the representation of aerosol-cloud feedback in CMIP5 when compared to CMIP3, the impact of aerosols on climate is highly uncertain (Wilcox *et al.*, 2015). Thus, we have investigated the impact of anthropogenic aerosols on NWA rainfall trend. There are nine CMIP5 models that have historicalMisc anthropogenic aerosol forcings only (described as historicalAA hereafter) simulations available. Table 3.1 summarises the forcing components of historicalAA in these models. Note that trends shown later in Figure 3.2-3.7 are calculated on their native grid, but for the spatial plots (Fig. 3.8-3.11), the models were regridded onto a common grid of 2.8125˚ latitude by 2.8125˚ longitude. Similarly, a subset of 14 CMIP5 models was used for which ETCCDI indices were available for all experimental designs, although only the first realisation of each model in each scenario is used to analyse extreme events. Out of these models, seven CMIP5 models (bold-faced in Table 3.3, Table 3.4, Table 3.5) have historicalAA simulations available for the indices and are used to further study the role of anthropogenic emissions on extreme trends over NWA.

The ETCCDI indices are pre-calculated for CMIP5 model simulations (Sillmann *et al.*, 2013a; Sillmann *et al.*, 2013b) and were downloaded from ftp://ftp.cccma.ec.gc.ca/data/climdex/CMIP5/. The model trends in ETCCDI indices are calculated on each model's native grid.

Table 3.1 Forcing agents included in historicalAA simulations in nine models. These nine models have simulations available for historical, historicalGHG, historicalNat, historicalMisc, RCP2.6, and RCP8.5 experiments.

Model name	rip number	forcings
CanESM2	r[1-5]i1p4	Direct+indirect effect including SA, SS, BC, OC, mineral dust (von Salzen *et al.*, 2013).
IPSL-CM5A-LR	r1i1p3	Dust, SS, BC, OC, SA are included (Dufresne *et al.*, 2013).
FGOALS-g2	r2i1p1	Aerosol direct effect only SA, BC, Ds, OC, SS (via conc.) (Bao *et al.*, 2013)

GISS-E2-H	r[1-5]i1p310	Anthropogenic tropospheric aerosol via emissions of SO_2, BC, OC, NH3(Miller *et al.*, 2014).
GISS-E2-R	r[1-5]i1p310	Anthropogenic tropospheric aerosol via emissions of SO_2, BC, OC, NH3 (Miller *et al.*, 2014).
CCSM4	r[1,4,6]i1p10	SS, Ds, SD, BC, MD, OC varying(Meehl *et al.*, 2012).
NorESM1-M	r1i1p1	Direct+indirect effect stratospheric SA by concentration, other aerosol components from emission. (Iversen *et al.*, 2013).
GFDL-CM3	r[1,3,5]i1p1	Direct+indirect, from emissions (Levy *et al.*, 2013).
GFDL-ESM2M	r1i1p5	SD, SS, BC, MD, OC by concentration (Dunne *et al.*, 2012).

3.3 Results

3.3.1 Precipitation

Figure 3.1a shows the spatial summer rainfall trend (stippling shows significance at the 95% level) from 1950 to 2005 with a significant increase over NWA. The observed summertime precipitation trend averaged over the boxed region in Figure 3.1a over the period of 1950 to 2005 is 2.13 mm/year, significant at 99% level (Fig. 3.1b). We also calculated the rainfall trend for each station contained within this region where data were available (Fig. 3.1c). The significant trends are shown by asterisk and insignificant trends are shown using circles with black outline. The color of the marker indicates the magnitude of the trend. The average rainfall trend calculated from station data is 2.18 mm/year, which is similar to the regional average result from the gridded AWAP dataset. Stations along the coast show a very small negative

trend, which are not significant. It is interesting to note that seven stations have trends greater than 4 mm/year, significant at 95% level (Table 3.2).

Table 3.2 Summer (DJF) precipitation trend (mm/year) calculated from station data. Boldface corresponds to trends significant at 95% level using Mann–Kendall nonparametric trend test

Station	Location	Data availability	Trend (mm/year)
KIMBERLEY RES.STATION	-15.65 128.71	1908-2010	1.20
MARGARET RIVER	-18.63 126.86	1914 – 2011	**2.98**
MOOLA BULLA	-18.19 127.50	1911 – 2013	**4.67**
MOUNT HOUSE STATION	-17.05 125.70	1924 – 2011	2.48
ROEBUCK PLAINS	-17.93 122.47	1904 – 2009	**4.20**
FOSSIL DOWNS	-18.14 125.78	1910 – 2015	**4.50**
ANNA PLAINS	-19.25 121.49	1909 – 2015	**4.12**
BIDYADANGA	-18.68 121.78	1892 – 2015	3.31
BONNEY DOWNS	-22.18 119.93	1908 – 2015	**3.65**
ROEBOURNE	-20.78 117.15	1888 – 2014	-0.83
EXMOUTH GULF	-22.38 114.11	1898 – 2013	-0.91
MARDIE	-21.19 115.98	1892 – 2015	0.41
MOUNT FLORANCE	-21.79 117.86	1887 – 2015	2.01
MOUNT AUGUSTUS	-24.31 116.91	1908 – 2012	-0.18
RHODES RIDGE	-23.10 119.37	1937 – 2011	**4.18**
DARWIN AIRPORT	-12.42 130.89	1902 – 2015	3.65
OENPELLI	-12.33 133.06	1911 – 2013	**4.30**

WARRUWI	-11.65 133.38	1917 – 2015	-1.56
VICTORIA RIVER DOWNS	-16.40 131.01	1886 – 2015	**5.31**
KATHERINE COUNCIL	-14.46 132.26	1891 – 2015	3.51
NEWCASTLE WATERS	-17.38 133.41	1890 – 2015	1.50
YUENDUMU	-22.26 131.80	1953 – 2015	1.77
RINGWOOD	-23.83 134.96	1955 – 2004	0.31
HAMILTON DOWNS	-23.51 133.27	1889 – 2015	0.87
ALICE SPRINGS AIRPORT	-23.80 133.89	1910 – 2015	-0.05
ALCOOTA	-22.82 134.45	1951 – 2008	1.30

Observed NWA DJF mean rainfall is compared with CMIP5 historical simulations across all realisations over the period 1950-2005 (Fig. 3.2). The figure indicates which models are wetter or drier compared to AWAP. It is evident that CCSM4, NorESM1-M, GFDL-ESM2M, CESM-CAM5, CNRM-CM5, FGOALS-g2, MIROC-ESM, MIROC-ESM-CHEM, and GFDL-CM3 are wetter than AWAP, whereas IPSL-CM5A-LR, HadGEM2-ES, GISS-E2-H, GISS-E2-R are dry models. The median values and spread in ACCESS1.3, bcc-csm1.1, BNU-ESM, Can-ESM2, MRI-CGCM3 are comparable to observed. IPSL-CM5A-LR and HadGEM2-ES have unrealistic negative median values, implying that the model tends to underestimate precipitation over NWA. A larger simulated spread of precipitation compared to AWAP indicates large inter-annual or internal variability of models. GFDL-ESM2M shows the largest spread among all the models implying large inter-annual variability in this model, as it has only one available realisation. IPSL-CM5A-LR, HadGEM2-ES, GISS-E2-H and GISS-E2-R all show a small spread of summertime precipitation compared to AWAP. These models have more than one simulation available, and the low spread of summer rainfall implies both inter-annual variability and inter-model spread are small in these models.

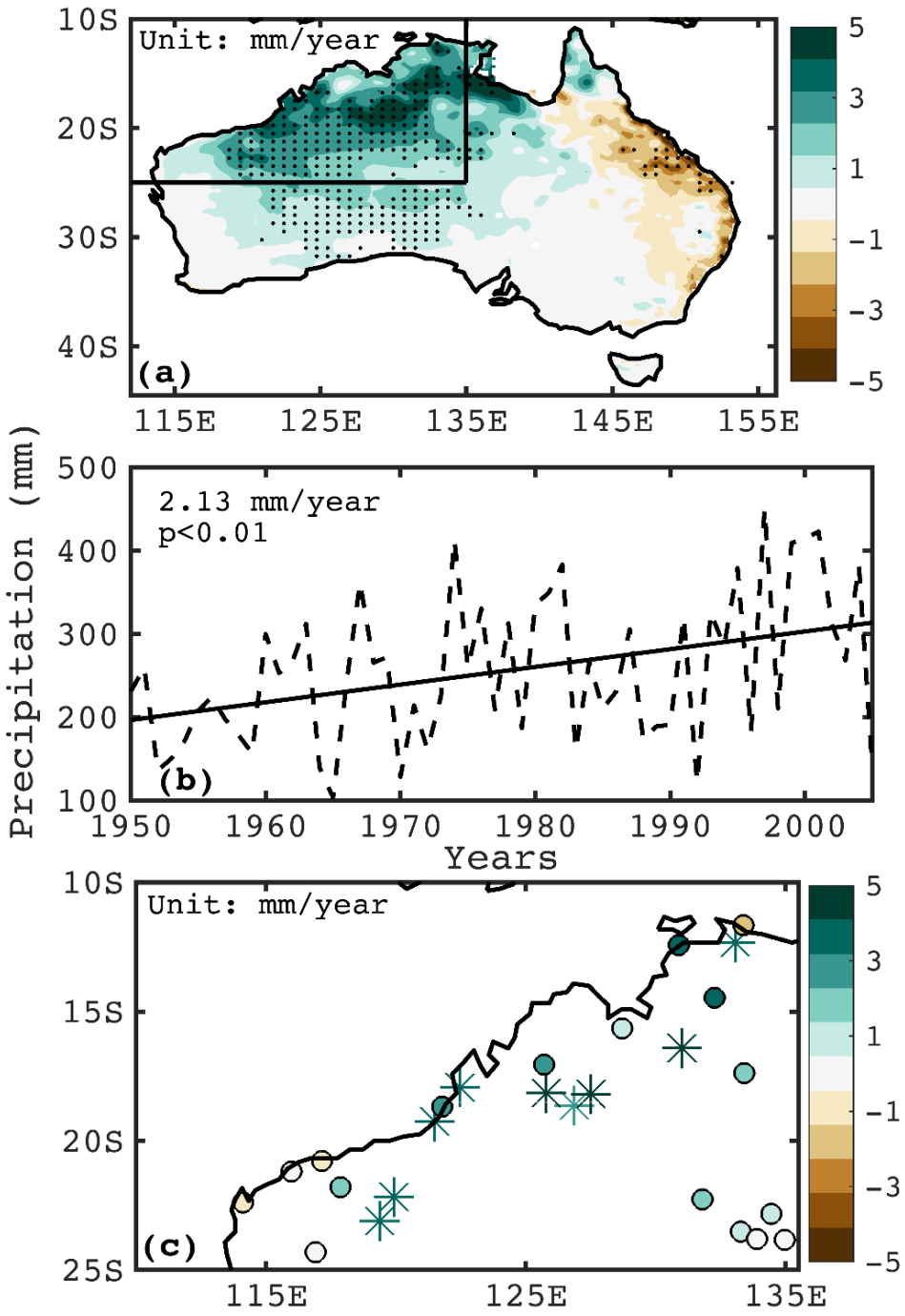

Figure 3.1 (a) Spatial trend (mm/year) of summer (DJF) precipitation over the period 1950–2005 from AWAP data set, stippling shows significant at 95% level. (b) Summer precipitation trend averaged over the boxed region (land only) in (a) over the time period 1950–2005 using AWAP (dotted line) and the black thick line is the line of best fit. (c) Rainfall trend (mm/year) calculated using station data set. Details of station location and rainfall trends are summarised in Table 3.2. Significant trends are shown by asterisk symbol and insignificant trends are shown by circles with black outline. The colour of the symbol indicates the magnitude of the trend. The significance was calculated using the Mann–Kendall nonparametric trend test.

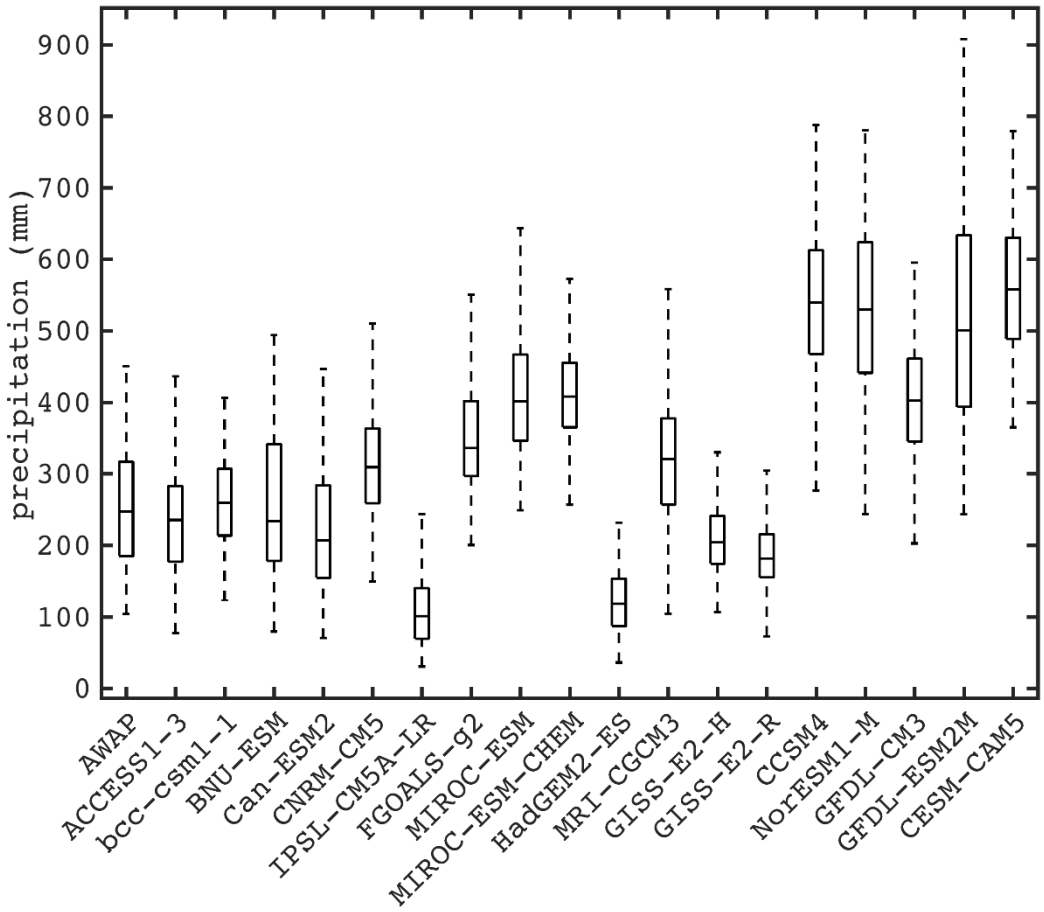

Figure 3.2 Box and whisker plots for summertime precipitation (mm) over the time period 1950–2005 of all realisations across 18 CMIP5 models in historical simulations and AWAP data set averaged over NWA. The box shows 25th–75th percentile of the data set. The whiskers extend to the extreme data point that is less than ±2.7σ.

Next, rainfall trends in the 18-model ensemble are compared to observed for the various scenarios. The NWA area-averaged summertime precipitation trend over 1950 – 2005 is first compared to AWAP for CMIP5 historical simulations with various forcings (Fig. 3.3a). The model trends significant at the 90% level are highlighted with grey crosses, showing varying significance. The grey boxes in the background show the 5th – 95th percentile of the 56-year running trends calculated from piControl runs. All three realisations of bcc-csm1-1 show negative trends, and there is only one realisation available for GFDL-ESM2M and BNU-ESM, which also show negative trends. Note GFDL-ESM2M has the largest spread in piControl trends similar to Figure 3.2. IPSL-CM5A-LR, MIROC-ESM, HadGEM2-ES, MRI-CGCM3, GISS-E2-R, CCSM4 have three or more realisations with positive rainfall trends. Out of these six models, three models are dry (IPSL-CM5A-LR, HadGEM2-ES, and GISS-E2-R; see Figure. 3.2), two models (MIROC-ESM, CCSM4) are wet. Overall, the magnitude of the trend

is underestimated in all historical realisations, relative to observed. The observed trend is higher than the range of trends in piControl simulations of all models. Also, there is a tendency for most of the significant model trends to sit outside the expected natural Variability.

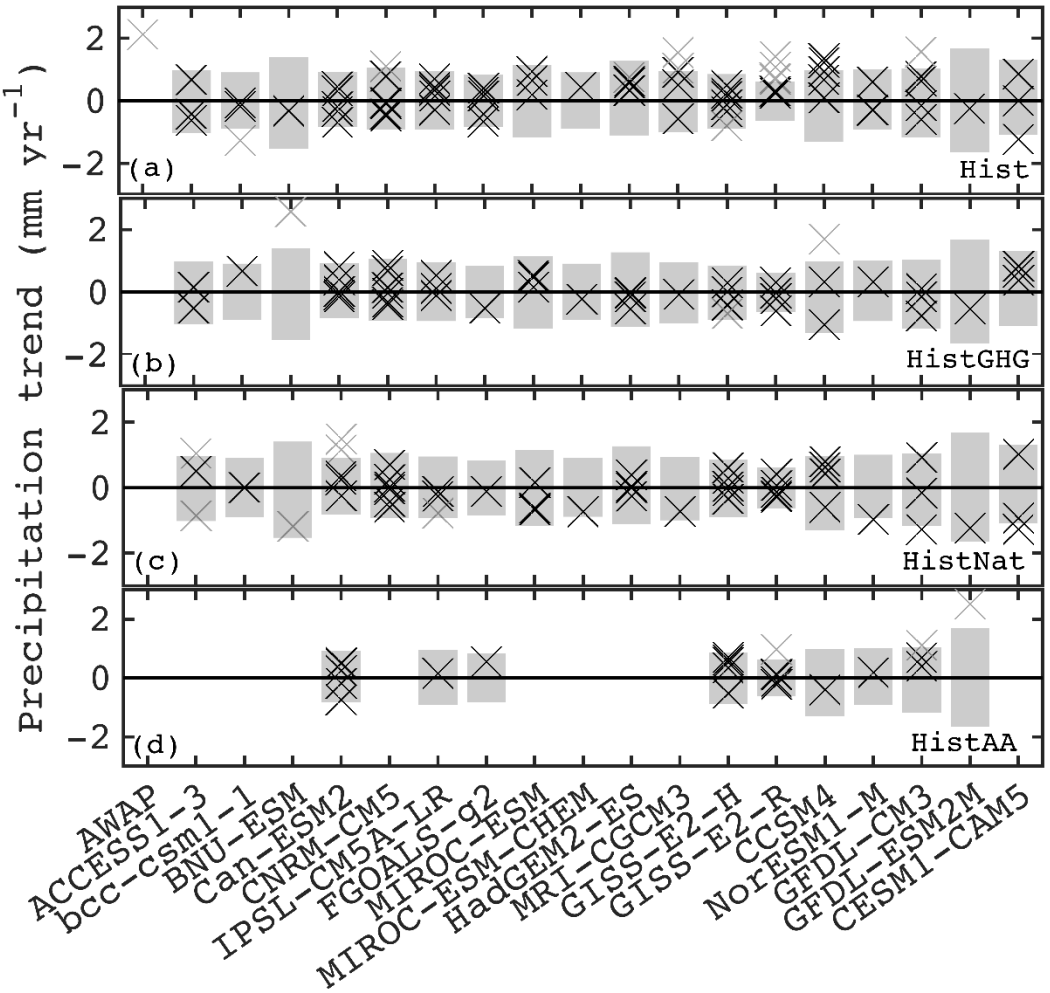

Figure 3.3 Summer precipitation trend (mm/year) in (a) AWAP and all realisations of 18 models in historical (hist) simulations averaged over NWA, (b) in historicalGHG (histGHG) simulations, (c) in historicalNat (histNat) simulations, (d) in historicalAA (histAA) simulation (only nine models are available). The time period used was 1950–2005. The grey boxes show 5th–9th percentile of the running 56-year trends in piControl runs. The AWAP trend is significant at 99% level. The model trends are tested at 90% level using the Mann–Kendall nonparametric significance test. The significant trends are highlighted by grey cross symbol.

Rainfall trends were also calculated for historicalGHG, historicalNat, and historicalAA simulations (shown in Fig. 3.3b, 3.3c, and 3.3d respectively). There is a tendency that models produce either very weak or negative trends when only GHG or only natural forcings are included, and few models show a significant rainfall trend in historicalGHG and historicalNat simulations. BNU-ESM has a significant positive trend of 2.57 mm/year in historicalGHG and significant negative trend in the historicalNat simulation. GFDL-ESM2M has a significant

positive trend of 2.5 mm/year in historicalAA simulation but shows negative trends for all three other simulations. However, the trend is better captured in historical simulations, though the magnitude is smaller compared to observed trend. MRI-CGCM3, GISS-E2-R, GFDL-CM3, bcc-csm1-1 in historical, BNU-ESM, and CCSM4 in historicalGHG, CanESM2 in historicalNat, GISS-E2-R, GFDL-CM3, GFDL-ESM2M in historicalAA simulations show significant trends that lie outside of the range in piControl trends.

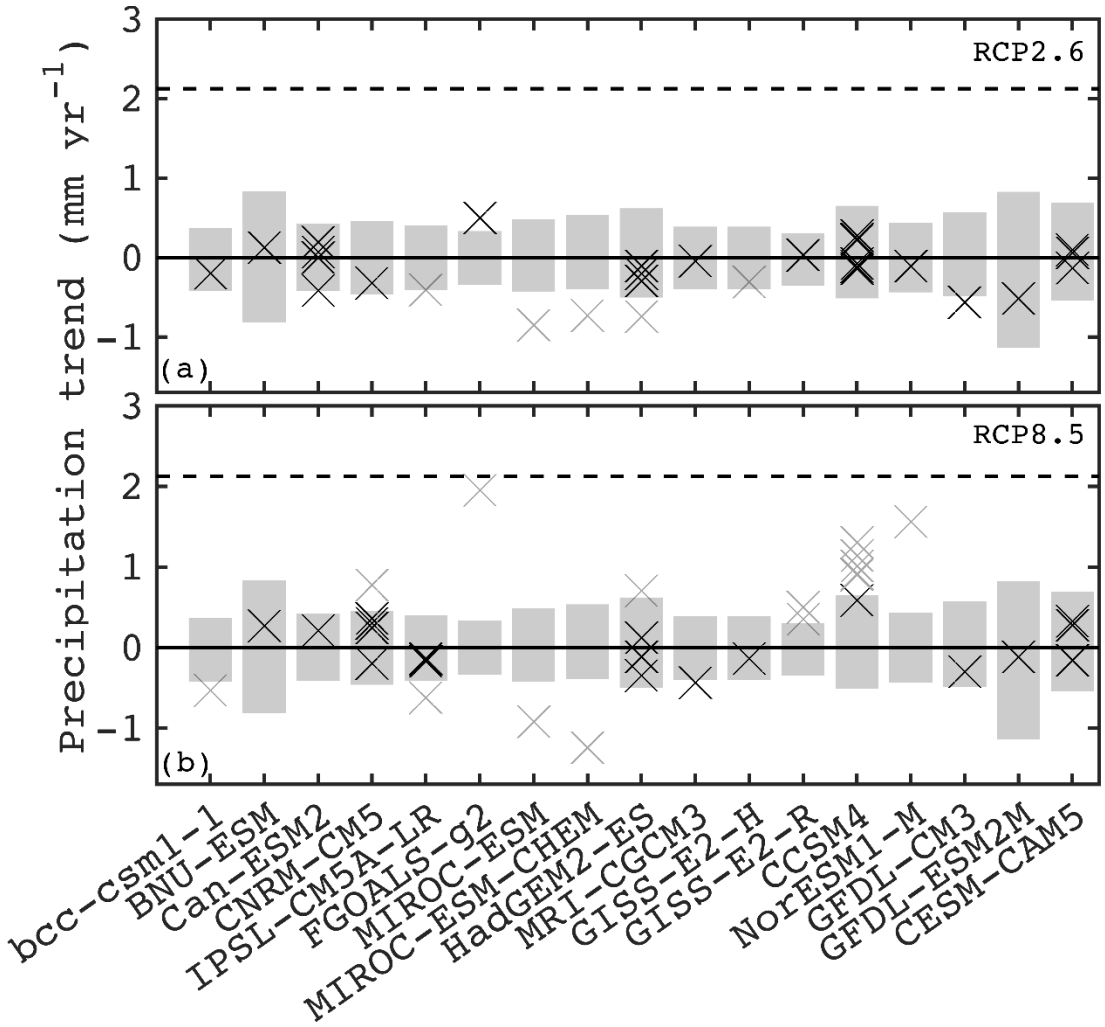

Figure 3.4 (a) Summer precipitation trend (mm/year) over the period 2006–2099 in RCP2.6 simulations of 17 CMIP5 models averaged over NWA. (b) Precipitation trend (mm/year) over the period 2006–2099 for RCP8.5 simulations averaged over NWA. The horizontal dotted line shows precipitation trend using AWAP data set from 1950 to 2005. The grey boxes show 5th–95th percentile of the running 94-year trends in piControl runs. Grey cross symbols show trends significant at 90% level using the Mann–Kendall nonparametric significance test.

Next, we calculated rainfall trends in two RCP scenarios over the period 2006-2099 in 17 models (Fig. 3.4). None of the models shows significant increasing precipitation trend in

RCP2.6. Five models (IPSL-CM5A-LR, MIROC-ESM, MIROC-ESM-CHEM, HadGEM2-ES, GISS-E2-H) show significant negative trends (Fig. 3.4a). The number of models showing significant positive rainfall trend is higher in RCP8.5 than RCP2.6 (Fig. 3.4b). FGOALS-g2 and NorESM1-M show significant large positive trends in RCP8.5. All realisations of GISS-E2-R and five realisations of CCSM4 show small but significant rainfall increase over NWA. Even in the RCP8.5 experiments, the trends produced for 2006-2099 are less than those observed in the AWAP data for 1950-2005. There are substantial differences in the trends produced by different models, but in general, the rainfall trends are notably smaller in RCP2.6 than RCP8.5 and smaller in both scenarios than the observed trend.

3.3.2 Australian monsoon index

The Australia Monsoon Index (AUSMI) is a measure of the strength of the monsoon circulation and is correlated (0.85) with precipitation over Australia (Yim *et al.*, 2014). NCEP reanalysis shows that the Australian monsoon, diagnosed from the AUSMI, has increased by 1.02 $m/s^{-1}year^{-1}$ since 1950 (Fig. 3.5a), but this trend is not determined to be statistically significant. We further investigate AUSMI changes in 18 models that were used to investigate precipitation trend with various forcings. Few realisations of the models tend to overestimate AUSMI trends in historical simulations (e.g. CNRM-CM5, MIROC-ESM, and GFDL-CM3), relative to observations, and CNRM-CM5 has a notably large spread. The maximum values of the trends in several realisations of these three models are significant at 90%. Overall, the AUSMI trend results are similar to results from precipitation trends in historical simulations. The models show similar AUSMI trends as those seen for precipitation, and there is a tendency for significant model AUSMI trends to lie outside the 5-95th percentile range.

Figure 3.5b,c show that the AUSMI trend is smaller or negative in historicalGHG and historicalNat experiment. Very few models show a significant trend in these simulations. Figure 3.5d shows trends in AUSMI in historicalAA simulation. Note, that trends are not significant in any of the simulations, however, GISS-E2-H, GISS-E2-R, and GFDL-CM3 have simulations that lie outside the range of natural variability. The AUSMI trend results in the RCP scenarios (Fig. 3.6) are similar to precipitation trends calculated in these future simulations (Fig. 3.4). None of the models shows a significant increasing trend in RCP2.6 simulations (Fig. 3.6a), and rather some show a significant decreasing trend (significant decreasing trends are highlighted by red). Overall, the AUSMI trend is more positive in RCP8.5 simulations than RCP2.6 and in some cases is significant. This is particularly evident in Can-ESM2, HadGEM2-ES, and CCSM4 (Fig. 3.6b).

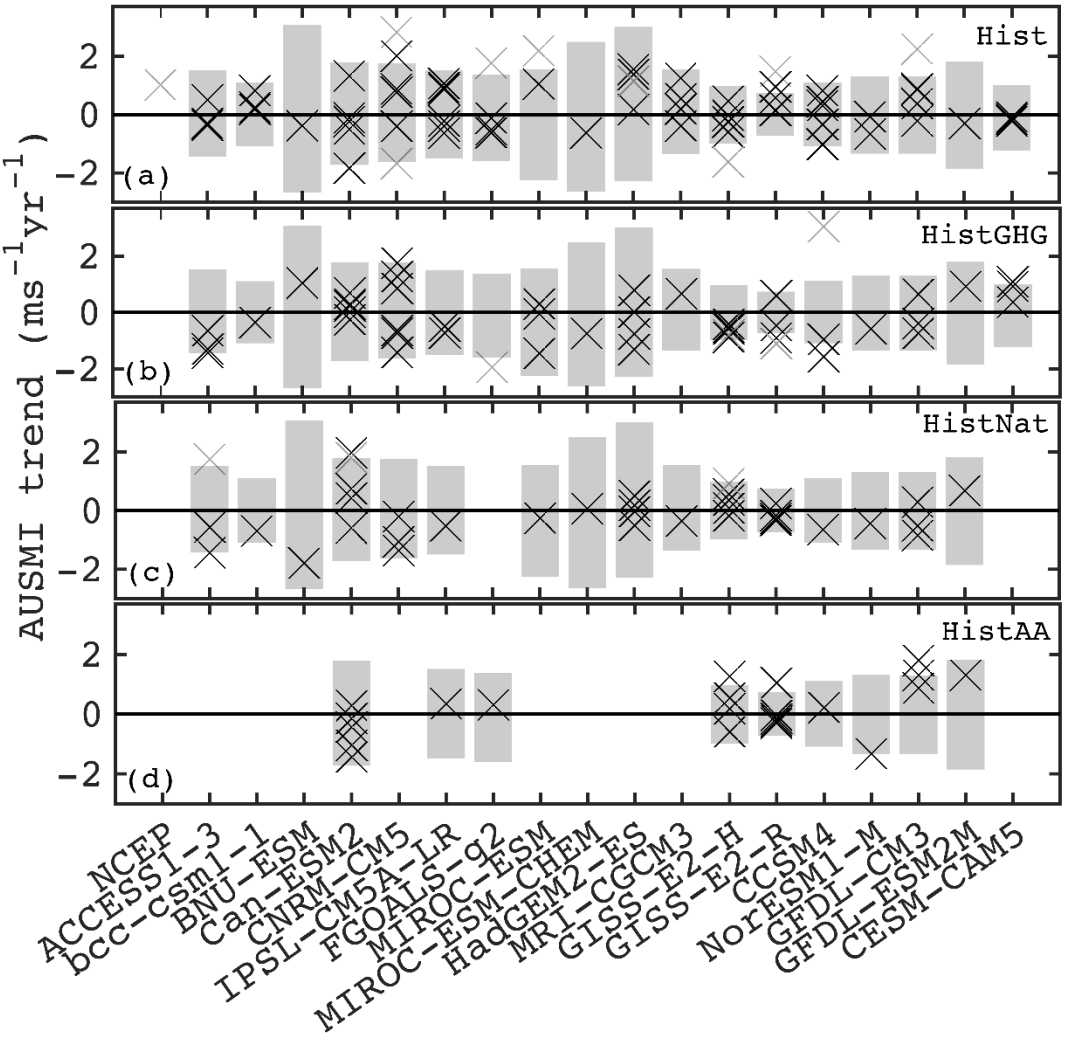

Figure 3.5 AUSMI trend (m s^{-1} $year^{-1}$) in (a) NCEP data set and all realisations of 18 models in historical simulations, (b) histGHG simulations, (c) histNat simulations, (d) histAA simulations (nine models). The time period used was 1950–2005. AUSMI is calculated during summer months (DJF). The grey boxes show 5th–95th percentile of the running 56-year trends in AUSMI in piControl runs. The trends of NCEP reanalysis and CMIP5 data sets are tested at 90% level using Mann–Kendall nonparametric significance test. The significant trends are highlighted by grey symbols. Note that CESM-CAM5 and fgoals-g2 do not have data available for histNat simulation.

Overall, the observed precipitation trend is not captured in historicalGHG and historicalNat simulations (except BNU-ESM in historicalGHG) which implies these trends maybe associated with a factor not included in these simulations. Therefore, we further investigated the role of anthropogenic aerosols using historicalAA simulations. Figure 3.7a and b summarise the spread of precipitation and AUSMI trends respectively, across all realisations in 9 models, including different forcings. The median value of precipitation trends in historical simulations is positive but smaller than observed trend. Multimodel median value of AUSMI

trends in historical simulations is small and negative. The median values of precipitation and AUSMI trends are negative in historicalGHG and historicalNat simulations. It is evident that median values of trends of precipitation and AUSMI in historicalAA are positive and higher than other past simulations. Furthermore, the multi-model median values are negative for RCP2.6, whereas RCP8.5 shows positive values for both precipitation and AUSMI trends. The spread in precipitation and AUSMI trends using all 18 models in historical, historicalGHG, historicalNat, RCP2.6 and RCP8.5 is similar (not shown here).

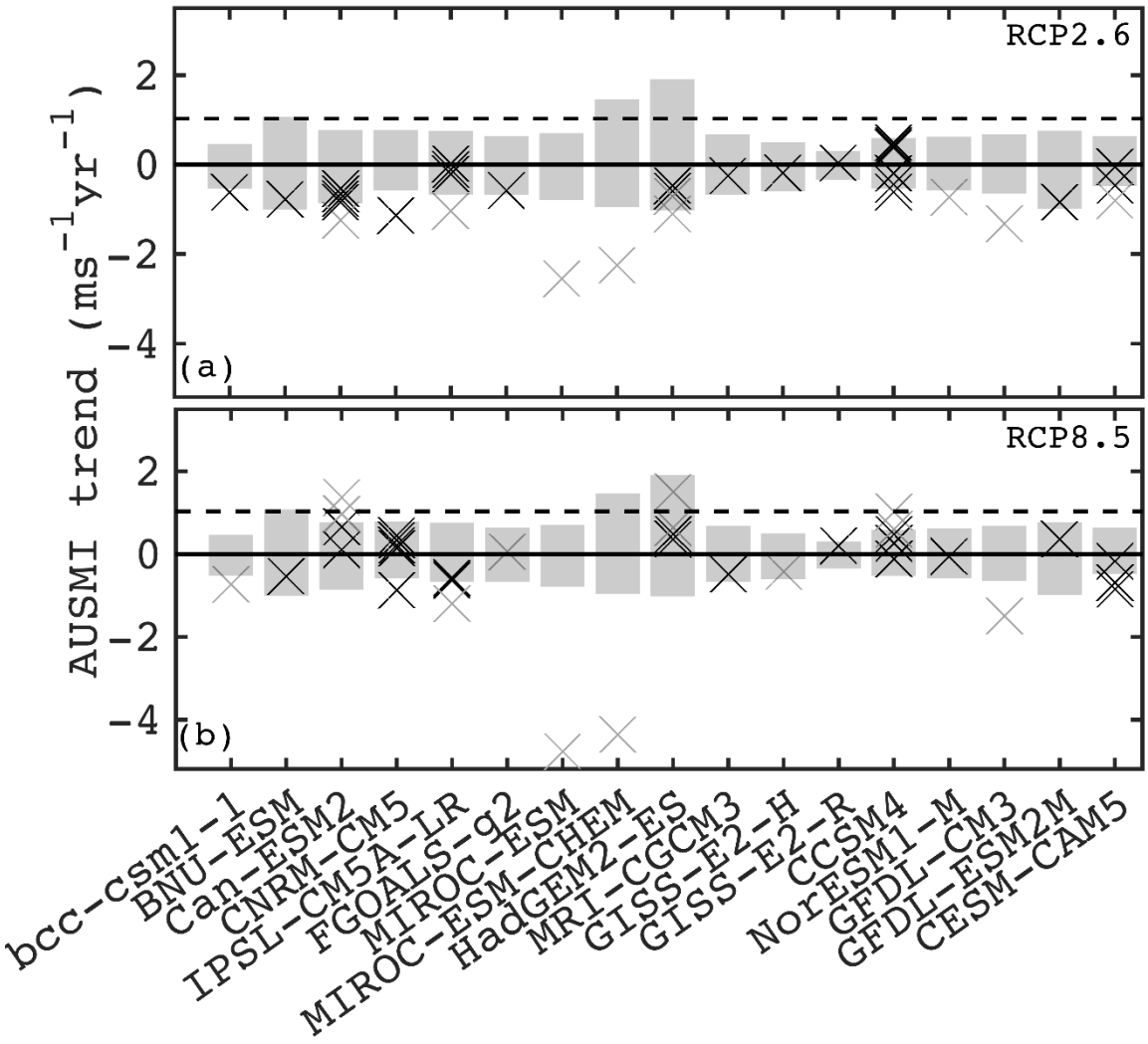

Figure 3.6 (a) AUSMI trend (m s^{-1} $year^{-1}$) over the period 2006–2099 in RCP2.6 simulations of 17 CMIP5 models. (b) AUSMI trend over the period 2006–2099 for RCP8.5 simulations. AUSMI is calculated during summer months (DJF). The horizontal dotted line shows AUSMI trend using NCEP data set from 1950–2005. The grey boxes show 5th–95th percentile of the running 94-year trends in AUSMI in piControl runs. Red cross symbols show trends significant at 90% level using Mann–Kendall nonparametric significance test.

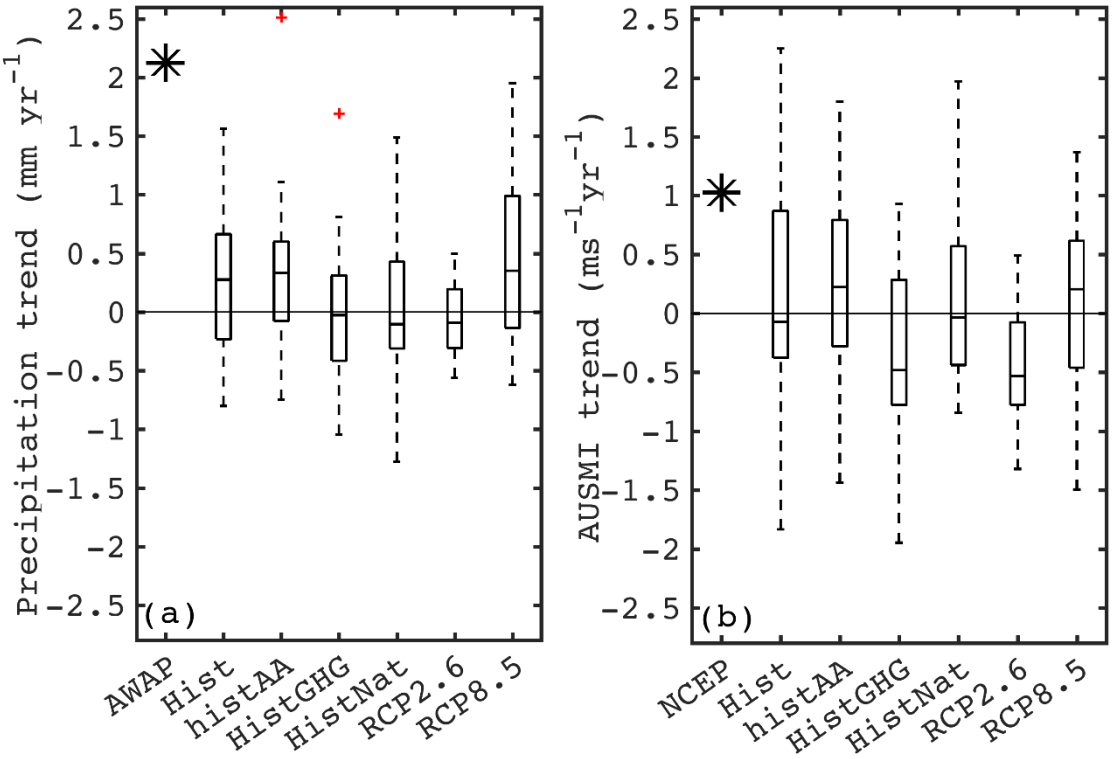

Figure 3.7 Box and whisker plots of the trends of (a) precipitation and (b) AUSMI in nine CMIP5 models across all realisations in various forcing scenarios. The plus symbols correspond to outliers. Black asterisks represent trends of precipitation and AUSMI in AWAP and NCEP data set, respectively. The time periods used in historical simulations and RCPs are 1950–2005 and 2006–2099, respectively. The box shows 25th–75th percentile of the data set. The whiskers extend to the extreme data point that is less than ±2.7σ. Values outside this range are marked as outliers.

3.3.3 Precipitation trends

Figure 3.7 suggests that aerosols play a key role in rainfall increase in NWA. Previous research shows that aerosols change the meridional temperature gradient over the Indian Ocean, increasing the monsoonal wind flow towards northern Australia (Rotstayn *et al.*, 2007). The spatial trend of precipitation in the multimodel ensemble is plotted using nine models (Fig. 3.8). Figure 3.8a shows a weak positive trend over NWA, which extends into eastern Australia. The historicalGHG ensemble mean shows mostly small negative trend over Australia except for east Australia where it shows significant increasing rainfall trend (Fig. 3.8b). There is a belt of very strong increasing precipitation trend extending from the equatorial Indian Ocean to the equatorial Pacific Ocean and a strong decreasing trend below this belt along the coast of north Australia, and in the Indian Ocean. The historicalAA ensemble mean shows higher positive precipitation trends over NWA comparative to historical and historicalGHG ensemble means, although the trends are not significant. In contrast to the historicalGHG ensemble mean there

is a belt of decreasing rainfall trend seen laying over equatorial Indian and the Pacific Oceans. There is a significant decreasing rainfall trend evident at 40˚S in historical (Fig. 3.8a), and historicalGHG (Fig. 3.8b) ensemble means, which is possibly related to the positive trend of SAM (Arblaster & Meehl, 2006). The authors further showed that the positive trend in SAM is mainly due to ozone depletion and increasing GHG.

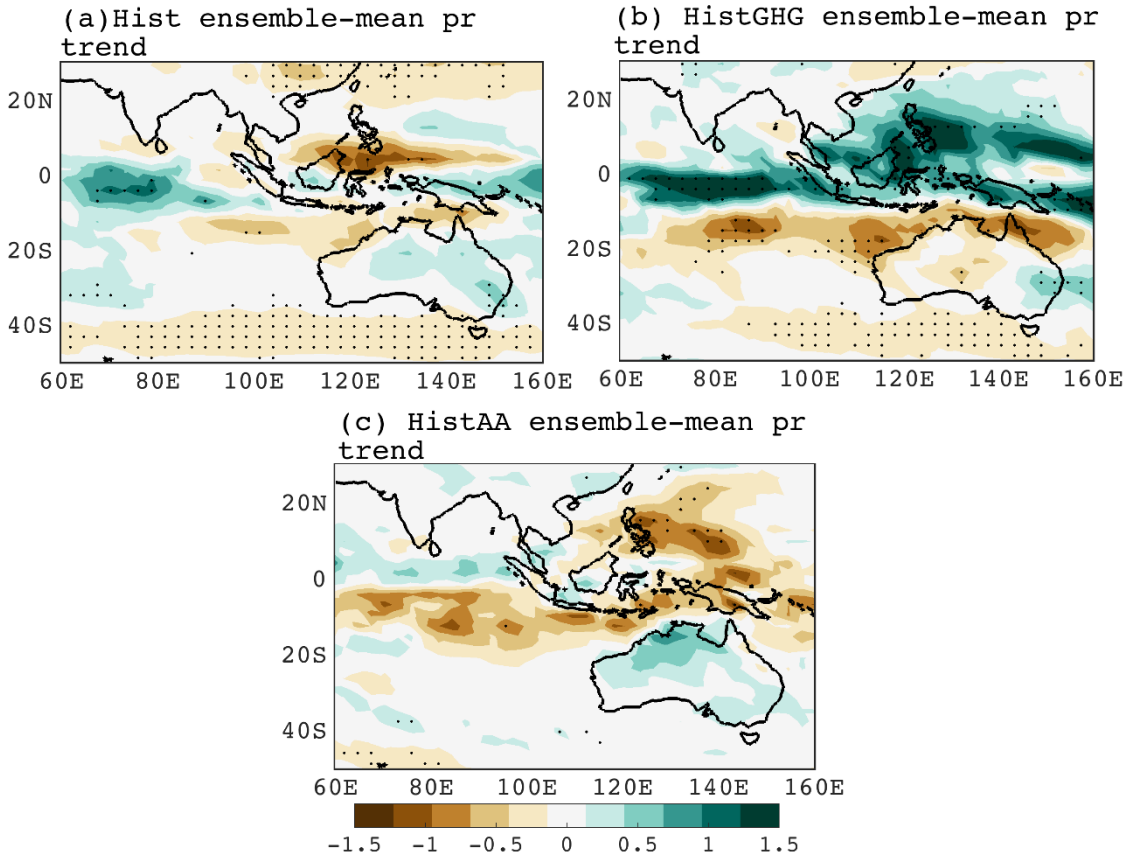

Figure 3.8 Spatial trend of summer (DJF) precipitation (mm/year) over the period 1950–2005 in (a) historical ensemble mean, (b) historicalGHG ensemble mean, (c) historicalAA ensemble mean. Stippling shows significant at 95% confidence level using Mann–Kendell nonparametric test.

3.3.4 Surface temperature trends

Skin temperature (Ts) shows the surface temperature over land and SST over the ocean region. The DJF trends of Ts in various experiments are plotted in Figure 3.9. The observed HadISST dataset (Fig. 3.9a) shows a positive IOD like pattern in the Indian Ocean as noted previously by (Cai *et al.*, 2009a) with a greater warming trend over the northwest Indian Ocean than the east Indian Ocean. This is consistent with previous research which shows that there has been an increased frequency of positive-IOD events post 1950 due to an increase in GHG (Cai *et al.*, 2014b). This SST pattern is captured in the historical ensemble mean, but the magnitude of

the trend difference between east and the west Indian Ocean is smaller compared to observed or in the historicalGHG ensemble mean. However, the historicalAA ensemble mean shows a basin-wide cooling pattern in the Indian Ocean region slowing down the warming in the Indian Ocean. Although, there is no negative IOD like pattern observed in histoticalAA simulations as pointed out by Rotstayn *et al.* (2007). One plausible reason of this could be the particular model used by Rotstayn *et al.* (2007) included large SST biases (Shi *et al.*, 2008). There is a higher cooling trend over tropical eastern Pacific (Fig. 3.9c) similar to La-Nina like pattern over Pacific.

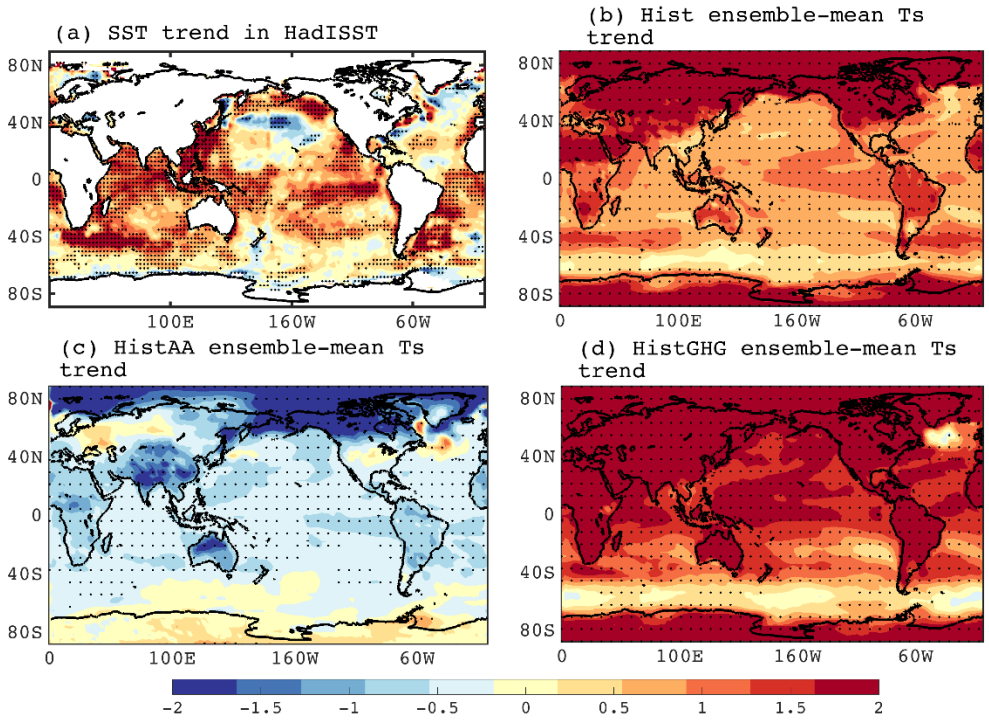

Figure 3.9 Spatial trend of summer (DJF) SST (K/century) over the period 1950–2005 in (a) HadISST and trend of Ts, in (b) historical ensemble mean, (c) historicalAA ensemble mean, (d) historicalGHG ensemble mean from 1950 to 2005. Stippling shows significant at 95% confidence level using Mann–Kendell nonparametric test.

3.3.5 Circulation trends

Trends of wind at 850 hPa in multimodel ensembles in various experiments are shown in Figure 3.10. In NCEP (Fig. 3.10a) there is a cyclonic circulation trend observed off the coast of NWA which is postulated as one of the plausible reasons for NWA rainfall increase, consistent with Shi *et al.* (2008). There is an anticyclonic flow observed over Indian Ocean basin and off the coast of NWA in the historical ensemble mean (Fig. 3.10b). In Figure 3.10c, there is an anticyclonic trend observed in the equatorial Indian Ocean. Note, an increased trend in westerlies evident in historicalAA simulations which strengthens monsoonal wind and is in

line with our hypothesis that anthropogenic aerosols strengthen monsoonal wind and hence increases NWA rainfall. We anticipate this increased monsoon-like flow is induced by cooler SST trend in tropical oceans and warmer SST in mid to high latitudes (Fig. 3.9c). There is an anticyclonic circulation trend in the historicalGHG ensemble mean (Fig. 3.10d) situated over northern Australia, satisfying the hypothesis that GHG produces a decreasing rainfall trend.

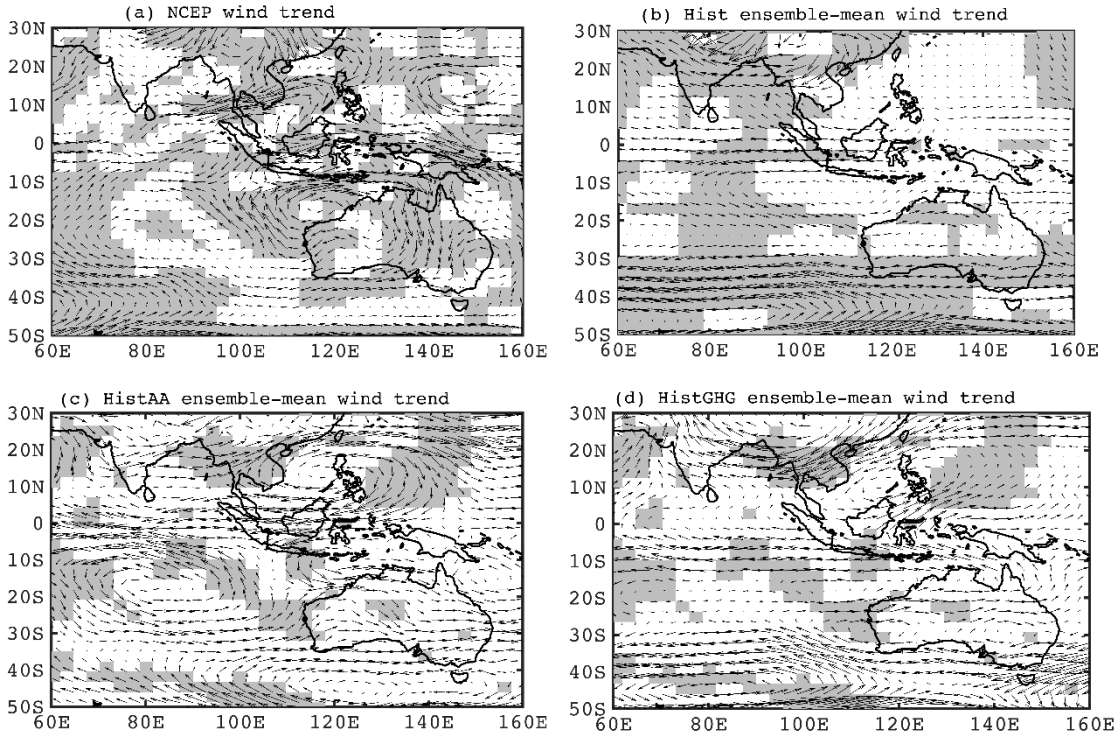

Figure 3.10 Spatial trend of summer (DJF) wind at 850 hPa (m s^{-1} $year^{-1}$) over the period 1950–2005 in (a) NCEP, (b) historical ensemble mean, (c) historicalAA ensemble mean, (d) historicalGHG ensemble mean. Shaded regions show areas where the trend in at least one component of wind (u or v) is significant at 95% confidence level using Mann–Kendall nonparametric significance test.

3.3.6 Extreme Indices

The GHCNDEX dataset shows that the number of days in NWA with precipitation >10mm ('Heavy precipitation days'; r10mm) increased by 0.08 days/year over the last 55 years (1951-2005). 'Maximum consecutive 5-day precipitation' (Rx5) increased by 0.47 mm/year over the same period. In addition, 'very wet days' (R95p) increased by 1.11 mm/year. These trends are significant at the 99% level.

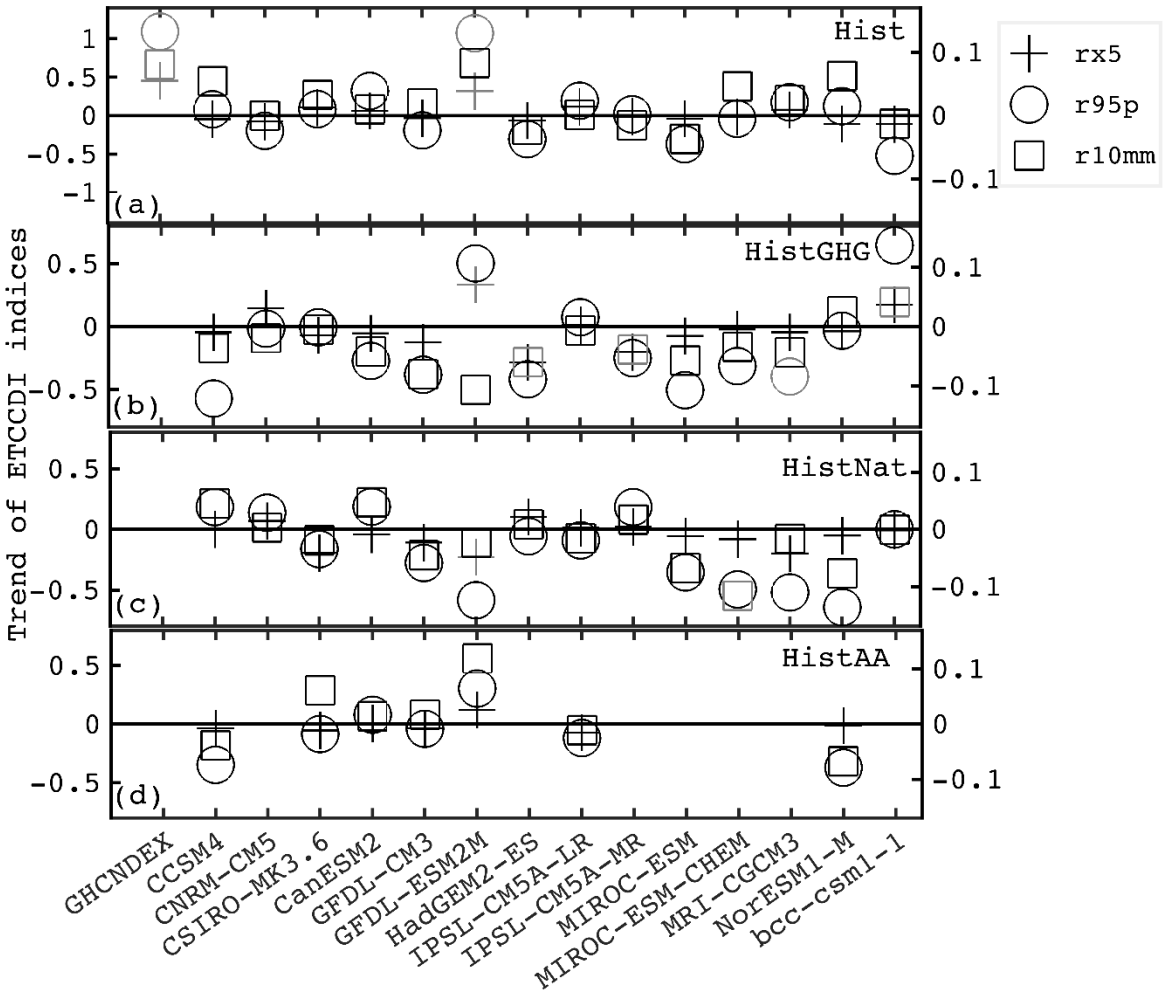

Figure 3.11 Annual trend of "maximum 5-day precipitation" (Rx5, plus, unit: mm/year), "very wet days" (R95p, circle, unit: mm/year), and "heavy precipitation day" (r10mm, square, unit: days/year, right y-axis) over the time period 2006–2099 for 14 CMIP5 models in (a) hist, (b) histGHG, (c) histNat, and (d) histAA (seven models) simulations averaged over NWA. The time period used is 1951–2005. GHCNDEX trends are significant at 99% level for all three indices. The model trends are tested at 90% level using Mann–Kendall nonparametric significance test. The significant trends are highlighted by grey symbols. Note that the axis for r10mm is on the right.

Observed GHCNDEX ETCDDI trends are compared with the trends of Rx5, R95p and R10mm in CMIP5 models (summarised in Table 3.3, Table 3.4 and Table 3.5 for each index respectively). ETCCDI trends are shown in Figure 3.11 for GHCNDEX and 14 CMIP5 models. CNRM-CM5, HadGEM2-ES, MIROC-ESM, bcc-csm1-1 demonstrate negative trends for all three indices in the historical scenario (Fig. 3.11a). Trends of R10mm, Rx5 and R95p are 0.068 days/year, 0.32 mm/year and 1.12 mm/year respectively in GFDL ESM2M historical scenario, which provides the closest match to observed. CanESM2, GFDL-ESM2M, IPSL-CM5A-LR, MRI-CGCM3 show positive trends for all three indices in historical simulation, although the trends are not significant (Fig. 3.11a). The slope of extreme indices in the historicalGHG (Fig.

3.11b), historicalNat (Fig. 3.11c), and historicalAA (Fig. 3.11d) simulations are comparatively smaller than in the historical, implying that the magnitude of the trend is best captured when all forcings are included. There are certain differences between the trends in historicalGHG and historicalNat for the various indices, for example, CCSM4 and IPSL-CM5A-MR show negative trends in historicalGHG and positive in historicalNat for all three indices and bcc-csm1-1 has very small trends for all three indices in historicalNat but positive in historicalGHG simulations. Note that none of the trends in the indices is significant in historicalAA, however, GFDL-ESM2M shows strong positive trends for all three indices that are comparable to the observed magnitude of the trend. Note that there is no indication of external forcing in trends in extreme indices as most of the model simulations show insignificant trends.

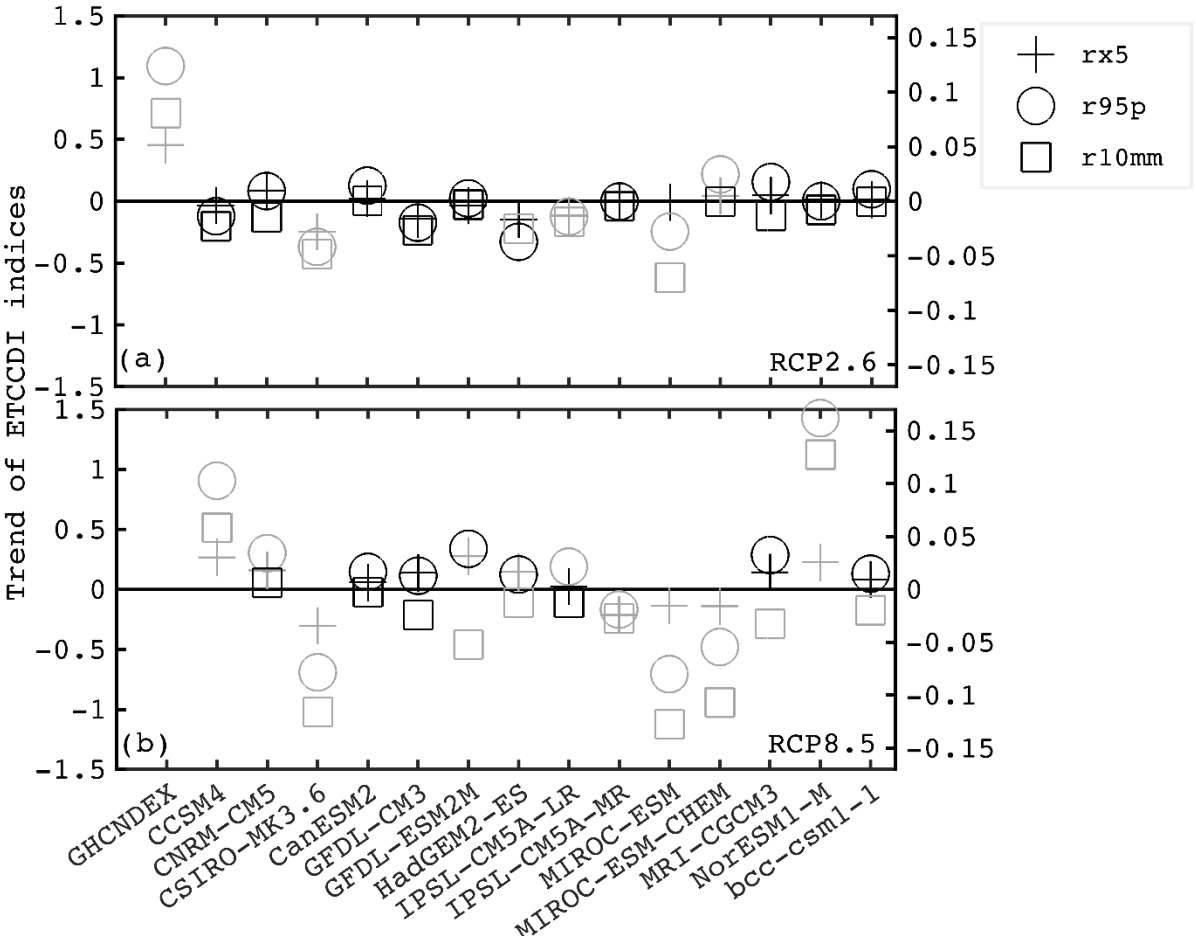

Figure 3.12 Annual trend of "maximum consecutive 5-day precipitation" (Rx5, plus, unit: mm/year), "very wet days" (R95p, circle, unit: mm/year), and "heavy precipitation day" (r10mm, square, unit: days/year, right y-axis) over the time period 2006–2099 for 14 CMIP5 models in (a) RCP2.6 and (b) RCP8.5 simulations. The time period used for GHCNDEX is 1951–2005. GHCNDEX trends are significant at 99% confidence level for all three indices. The model trends are tested at 90% level using Mann–Kendall nonparametric significance test. The significant trends are highlighted by grey symbols. Note that the axis for r10mm is on the right.

Notably, the trends of these indices are smaller in future projections, compared to the observed trends over the past 55 years (Fig. 3.12). Rx5 and R95p have larger trends in RCP8.5 than RCP2.6. MIROC-ESM, MIROC-ESM-CHEM, CSIRO-MK3.6 show significant decreasing trends for all three indices in RCP8.5 scenario (Fig. 3.12b). Note that these three models were categorised as "dry models" with decreasing monsoon precipitation trends and showed large equatorial Pacific SST biases by Brown *et al.* (2016). One interesting feature is eight models out of 14 show significant decreasing trends in R10mm.

Table 3.3 Annual trends of "maximum consecutive 5-day precipitation" (Rx5; unit: mm/year) ETCCDI index in CMIP5 models. The time period used for historical simulations with various forcings is 1951–2005. The time period used for trend calculation in RCP simulations is 2006–2099. Boldface signifies trends significant at 90% confidence level, *sign represents trends significant at 95% level. Boldface models have data set for histAA experiment. Annual trend of Rx5 in GHCNDEX is 0.47, significant at 99% confidence level.

	Hist	HistGHG	HistNat	HistAA	RCP2.6	RCP8.5
CCSM4	-0.09	-0.04	0.03	-0.04	-0.04	**0.3***
CNRM-CM5	-0.09	0.07	0.01		0.08	**0.15***
CSIRO-MK3.6	0.05	-0.07	-0.17	-0.05	**-0.23***	**-0.30***
CanESM2	0.07	-0.04	-0.01	0.007	0.01	0.07
GFDL-CM3	-0.02	-0.12	-0.10	-0.04	-0.14	0.12
GFDL-ESM2M	**0.32***	**0.33***	**-0.22**	0.12	-0.03	**0.27***
HadGEM2-ES	-0.06	-0.22	0.10		-0.17	**0.14**
IPSL-CM5A-LR	0.09	-0.007	0.05	-0.07	**-0.10***	0.03
IPSL-CM5A-MR	0.02	-0.16	0.0015		0.0008	**-0.21***
MIROC-ESM	-0.02	-0.08	-0.06		-0.02	**-0.14***
MIROC-ESM-CHEM	-0.02	-0.05	-0.08		**0.06**	**-0.14***
MRI-CGCM3	0.11	0.04	-0.28		0.05	0.13
NorESM1-M	-0.11	-0.03	-0.04	-0.01	0.01	**0.22***
bcc-csm1-1	-0.12	0.20	0.0042		-0.007	0.11

Table 3.4 Annual trends of "very wet days" (R95p; unit: mm/year) ETCCDI index in CMIP5 models over the period 1951–2005. The time period used for historical simulations with various forcings is 1951–2005. The time period used for trend calculation in RCP simulations is 2006–2099. Boldface signifies trends significant at 90% confidence level, * sign represents trends significant at 95% level. Boldface models have data set for histAA experiment. Annual trend of R95p in GHCNDEX is 1.11 mm/year, significant at 99% confidence level.

	Hist	HistGHG	HistNat	HistAA	RCP2.6	RCP8.5
CCSM4	-0.01	-0.55	0.20	-0.35	-0.14	**0.97***
CNRM-CM5	-0.31	-0.14	0.01		0.07	**0.29**
CSIRO-MK3.6	-0.03	0.02	-0.06	-0.08	**-0.36***	**-0.69***
CanESM2	0.29	-0.23	0.25	0.08	0.10	0.14
GFDL-CM3	-0.11	-0.35	-0.28	-0.04	-0.19	0.08
GFDL-ESM2M	**1.12***	0.52	-0.50	0.30	0.02	0.32
HadGEM2-ES	-0.25	-0.31	-0.06		-0.34	0.12
IPSL-CM5A-LR	0.15	0.03	-0.05	-0.12	**-0.11**	**0.21**
IPSL-CM5A-MR	0.04	-0.20	0.13		-0.01	**-0.17***
MIROC-ESM	-0.30	-0.45	-0.41		**-0.24***	**-0.72***
MIROC-ESM-CHEM	-0.08	-0.28	-0.54		**0.25**	**-0.51***
MRI-CGCM3	0.17	**-0.19**	-0.76		0.13	0.25
NorESM1-M	0.11	-0.03	-0.61	-0.37	-0.03	**1.44***
bcc-csm1-1	-0.38	0.69	0.02		0.04	0.18

Table 3.5 Annual trends of "heavy precipitation day" (R10mm; unit: days/year) ETCCDI index in CMIP5 models over the period 1951–2005. The time period used for historical simulations with various forcings is 1951–2005.The time period used for trend calculation in RCP simulations is 2006–2099. Boldface signifies trends significant at 90% confidence level, *sign represents trends significant at 95% level using Mann–Kendall nonparametric trend test. Boldface models have data set for histAA experiment. Annual trend of R10mm in GHCNDEX is 0.08 days/year, significant at 99% confidence level.

	Hist	HistGHG	HistNat	HistAA	RCP2.6	RCP8.5
CCSM4	0.04	-0.04	0.04	-0.04	-0.02	**0.06**

CNRM-CM5	-0.0037	-0.02	-0.0031		-0.01	0.006
CSIRO-MK3.6	0.02	-0.09	-0.01	0.06	**-0.05**	**-0.11**
CanESM2	0.0019	-0.03	0.05	0.014	-0.0002	-0.005
GFDL-CM3	0.03	-0.08	-0.04	0.017	-0.03	-0.02
GFDL-ESM2M	0.07	-0.09	0.004	0.12	-0.004	**-0.06**
HadGEM2-ES	-0.02	**-0.05**	0.01		**-0.03**	**-0.01**
IPSL-CM5A-LR	0.01	-0.02	-0.01	-0.01	**-0.02**	-0.01
IPSL-CM5A-MR	-0.01	**-0.03**	0.02		-0.01	**-0.02**
MIROC-ESM	-0.02	-0.06	-0.06		**-0.07**	**-0.13**
MIROC-ESM-CHEM	0.04	-0.03	**-0.11**		0.0001	**-0.11**
MRI-CGCM3	0.03	-0.03	-0.03		-0.01	**-0.03**
NorESM1-M	0.06	0.03	-0.09	-0.07	-0.01	**0.14**
Bcc-csm1-1	-0.01	**-0.01**	-0.003		-0.002	**-0.02**

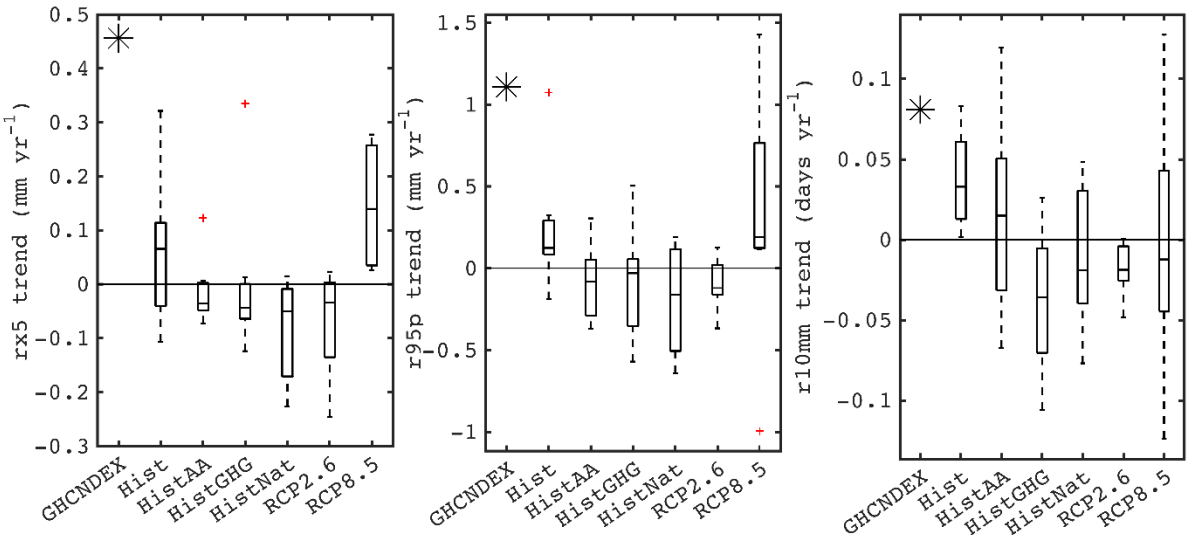

Figure 3.13 Box and whisker plots of annual trends of (a) "maximum consecutive 5-day precipitation" (Rx5, unit: mm/year), (b) "very wet days" (R95p, unit: mm/year), and (c) "heavy precipitation day" (r10mm, unit: days/year) in GHCNDEX and CMIP5 models in various forcing scenarios. The plus symbols correspond to outliers. The time periods used for historical simulations and RCPs are 1950–2005 and 2006–2099, respectively. The box shows 25th–75th percentile of the data set. The whiskers extend to the extreme data point that is less than ±2.7σ. Values outside this range are marked as outliers.

Figure 13 shows the multi-model spread of trends of ETCCDI indices in various forcings using seven CMIP5 models that have data available for all the experiments. Models show positive median values for all three indices in historical simulations. Similar to the spread of precipitation trends, multi-model median values are negative in historicalGHG and historicalNat for all three indices. It should be noted that median values of Rx5 and R95p are negative but the median value of R10mm is positive in historicalAA simulations. Median values of these three indices in RCP2.6 simulations are smaller compared to RCP8.5. In RCP8.5 simulations, multimodel median values are larger than the median values in historical simulation for Rx5 and R95p but negative with a very large spread for R10mm. Models project positive median values for Rx5 and R95p under RCP8.5 scenario but R10mm has negative median values in both RCP scenarios.

3.4 Discussion

These results provide further insight into the influences driving the observed increase in rainfall in summertime in NWA, although several causes remain possible.

It is well established that aerosols produce a net cooling and drying effect (Rotstayn *et al.*, 2007; Salzmann, 2016). Aerosols induce anomalous meridional circulation and weaken the ascending flow over southeast Asia and western Pacific region thus opposing the local Hadley cell (Bollasina *et al.*, 2011). Although there has been a robust increase of global precipitation of about 1.5-2% per Kelvin surface temperature increase in response to GHGs, and a robust precipitation decrease in response to aerosols, however, over Australia and east equatorial Indian Ocean the impacts of these two forcings are opposed (Salzmann, 2016). Previous studies have shown that GHG increases result in a positive IOD-like pattern, while aerosols induce a basin-wide cooling in the Indian Ocean and slow down the effect of GHG, (Dong & Zhou, 2014). The authors further showed that a negative IOD-like SST anomaly pattern is produced only when the direct aerosol effect is considered. The role of direct and indirect aerosol effects requires further exploration in the context of NWA rainfall increase.

First, we have shown that the precipitation trends in the historical simulations are weaker than observed across all CMIP5 models. Possible explanations of this could be - the observed changes represent a specific combination of a forced response and internal variability that is not reproduced in the available model simulations, bias in model sensitivity to forced change, natural variability in models is underestimated, and important mechanisms are not included or well represented in models. However, the trend in historical simulations (except

trend in BNU-ESM historicalGHG simulation) is more similar to observed than the trends produced in historicalGHG and historicalNat simulations. One possible explanation for this result could be the opposite impact of GHG and aerosol forcings on rainfall, as described by Rotstayn *et al.* (2012). This study concluded that the relatively smaller trend in historical simulations is due to the offsetting effect of different forcings, such that a GHG-induced decreased rainfall trend is compensated by the aerosol-induced increased trend. Using CSIRO MK3.6, they showed that aerosol-induced cyclonic circulation off the coast of NWA increases monsoonal flow, whereas simulations including only GHGs show anticyclonic circulation trends off the coast. The aerosol-induced cyclonic circulation results in positive convergence and vertical motion over NWA. It is thought that this type of circulation is associated with changes in Walker circulation or local Hadley circulation, although the precise underlying mechanisms of the opposite impacts of GHG and anthropogenic aerosols is not clear (Rotstayn *et al.*, 2012).

Previous research shows that increased monsoonal flow is a second key factor in the NWA rainfall increase (Taschetto & England, 2009a). This finding is consistent with our current results, where an increasing trend in AUSMI since 1950 is calculated, although this is not statistically significant. During the Austral monsoon, the AUSMI is positive, with strong westerly winds, while negative AUSMI occurs typically throughout the rest of the year. The time series in NCEP AUSMI over the last 56 years is also correlated with the NWA rainfall time series (R=0.68, at 0.01 significance level) in AWAP. The correlations in CMIP5 models (calculated for all available realisations and averaged for each model) range from -0.02 to 0.8, two-thirds of the models show correlations above 0.5 (all realisations of these models showed correlations significant at 0.05% confidence level). This suggests that the increase in rainfall in the region may be related to an increase in monsoon strength in CMIP5 models. Moreover, the observed trends in precipitation and AUSMI are not captured in historicalGHG and historicalNat simulations, which do not include anthropogenic aerosols.

Overall, we hypothesise that the rainfall increase over NWA can be related to increased monsoonal flow due to increased aerosol emissions in the last 56 years. The multi-model spread shows that historicalAA can capture precipitation and AUSMI trends better than historicalGHG and historicalNat simulations. The small trends in the historical scenario can be ascribed to counterbalancing of small or negative trends in historicalGHG and historicalNat and positive trends in historicalAA simulations, consistent with Rotstayn *et al.* (2012). However, it remains

possible that there are other factors impacting NWA rainfall, as even in single forcing or all forcings model ensemble means, the observed magnitude of the trend is not captured entirely.

In addition to mean summertime rainfall changes, ETCCDI extreme indices also have increasing trends in observations. The CMIP5 models analysed here showed mostly very small positive or negative trends for the three indices in response to various forcings. Multimodel median values for all three indices are positive in historical simulations. Therefore, it is possible that a fraction of the mean NWA summer rainfall in CMIP5 historical simulations is due to an increase in extreme events. Interestingly, median values of two out of three indices in historicalAA simulations are negative. This suggests that the higher order moments of the distribution of rainfall may change in complex ways due to external forcings (e.g. changes in extremes may not necessarily follow changes in mean). Christensen *et al.* (2013) studied changes in extreme indices relative to the present-day average and showed that seasonal average precipitation, simple precipitation daily intensity index, Rx5 are projected to increase with higher emission scenario.

We also explored mean and extreme rainfall changes in future projections in CMIP5. Both mean NWA precipitation and the AUSMI have lower trends in RCP scenarios for 2006-2099, relative to observed trends for 1950-2005, although trends of AUSMI and precipitation in RCP2.6 (R=0.61, significant at 99% confidence level) and RCP8.5 (R=0.62, significant at 99% confidence level) are well correlated. All RCPs are forced by decreasing time-evolving anthropogenic aerosols (Lamarque *et al.*, 2011), which may result in smaller precipitation trends in the future.

Moreover, trends of extreme indices are stronger in RCP8.5 than RCP2.6. Trends of Rx5 and R95p are positive, and trends of R10mm are negative in RCP8.5 simulations, implying that extreme events are likely to intensify with lesser frequency in warm future climate. However, there is a large spread in R10mm trends in RCP8.5 simulations. Hence, future trends should be studied further with aerosols forcings to provide robust conclusions. Cai *et al.* (2011b) suggested that the future reduction in the rainfall trend in this region is associated with weakening of Walker Circulation in warming condition, this suggests that further research is required to provide robust future rainfall projections over NWA.

The NWA mean precipitation is well correlated with a monsoonal increase in observations, as well as CMIP5 models in various past and future simulations. Hence, the physical processes underlying these trends require further investigation. For example, a physically realistic representation of ENSO system and the ENSO Australian rainfall is

essential for capturing rainfall characteristics in this region, and for quantifying the impact of aerosols. A previous study by Shi *et al.* (2008) using a low-resolution atmospheric model, CSIRO MK3, showed that modelled rainfall in the region is generated by a known "Pacific cold tongue bias", that pushes warm SST anomalies too far west into the western Pacific, with the ascending branch of Walker Circulation situated over NWA. Brown *et al.* (2016) segregated CMIP5 models into three terciles, 'DRY', 'MID', 'WET' models depending on the amount of future change of monsoon rainfall. They suggested that the 'DRY' models are less reliable as they demonstrate greater precipitation and SST biases across the equatorial Pacific, which is not evident in 'WET' models. Thus, reducing uncertainty in SST warming patterns due to model biases would lead to more reliable future projections.

3.5 Conclusions

This study has provided a comprehensive investigation of the observed increase in NWA rainfall in summer by using CMIP5 models run with various forcings of the historical period and 21st Century. Both station and gridded observational data showed a similar increasing trend in summertime rainfall in the region since 1950, which is consistent with previous results (Cai *et al.*, 2011b; Lin & Li, 2012; Shi *et al.*, 2008).

The observed NWA summertime rainfall is highly correlated with AUSMI, the monsoon strength index. This correlation in CMIP5 models was comparable, suggesting that strengthening of Australian monsoonal flow may have impacted NWA rainfall. None of the models used in our study accurately captured the magnitude of the observed precipitation trend in historical simulations, although the sign of the trend was captured by some realisations. In contrast, precipitation and AUSMI trends are very weak or negative across all historicalGHG and historicalNat realisations of models, which do not include anthropogenic aerosols in their experimental design. Multimodel median values of trends are positive in historicalAA and higher than historical simulations. Trends in the extreme indices of rainfall analysed here were also better captured in historical simulations than historicalGHG and historicalNat simulations.

The cause of observed rainfall trends in NWA is of particular scientific interest as understanding the processes behind this phenomenon is necessary for understanding likely future projections. In our study, the trends of precipitation in CMIP5 RCP scenarios are relatively smaller than historical simulations, with higher trends in RCP 8.5 than in RCP2.6. The intensity of extreme rainfall events is also projected to increase with reduced frequency in future climate. We propose that the increase in mean rainfall and monsoonal flow can be

explained by increased anthropogenic aerosols, which has an opposing climatic impact to GHGs. However, investigating the influence of model systematic biases in mean climate and variability, and the teleconnections on rainfall trends and projections will lead to better understanding of future climate projections.

Chapter 4

The timing and drivers of extreme rainfall events in Australia

Abstract

Australia experiences some of the world's most variable rainfall. The various large-scale-climate drivers modulating Australia's rainfall are part of the cause of this high variability. Previous studies have mostly focused on understanding rainfall variability in terms of frequency and intensity. However, understanding the timing of when extreme rainfall occurs is crucial for seasonal prediction, although it largely remains unexplored. Here we investigate the timing of extreme rainfall in Australia and the spatial variability of this timing. Also, this study examines how some of the large-scale drivers, such as the El Niño-Southern Oscillation (ENSO) and the Interdecadal Pacific Oscillation (IPO) determine the timing and inter-annual variability of the timing of extreme rainfall in Australia. Our results show that there is a clear spatial north-south delineation in the season when extreme rainfall occurs in Australia, shown by a contour diagonally extending roughly from Exmouth region in the west to Newcastle/Sydney region in the east of Australia. North of this contour, extreme rainfall (maximum 5-day consecutive rainfall) usually occurs in summer (December-February), with the smallest interannual variability in the timing of extreme rainfall in this region. In the south, extreme rainfall usually occurs in autumn/winter months; however, the timing is highly variable. In southeast Australia, extreme rainfall can fall at any time of the year, which makes seasonal prediction extremely challenging for this region.

Both observation and reanalysis dataset show that the area where extreme rainfall occurs in summer extends further south during negative IPO years. We also find that IPO and ENSO phases, and the interaction between them, play significant roles in both determining the timing of extreme rainfall and constraining the interannual variability, especially in SEA. Studying the relationship between rainfall and large-scale drivers is critical for improving the seasonal prediction of extreme rainfall.

4.1 Introduction

4.1.1 Australia's climatological context

Australia extends across the tropics to the mid-latitudes, which leads to high variability in rainfall associated with tropical and mid-latitude climate influences, and interactions between the tropics and mid-latitudes (Narsey *et al.*, 2017; Wright, 1997). Various large-scale drivers such as the El Niño-Southern Oscillation (ENSO), the Interdecadal Pacific Oscillation (IPO), the Southern Annular Mode (SAM), the Indian Ocean Dipole (IOD), the Madden-Julian Oscillation (MJO), and blocking high play major roles in modulating rainfall in Australia (Dey *et al.*, 2019). These drivers peak in different seasons, thus different regions in Australia receive the majority of total annual rainfall in different seasons, depending on the dominant driver.

Australia can be broadly divided into two rainfall regimes: approximately, the north of 25˚S receives rainfall mainly during summer months (October-April), while the south of the country receives rainfall in cooler months (April to November) (Risbey *et al.*, 2009). The dominant large-scale drivers modulating rainfall in the north are ENSO, MJO, and the Inter Tropical Convergence Zone (ITCZ) (Dey *et al.*, 2019). These drivers influence rainfall characteristics in the north, such as monsoonal bursts (Moise *et al.*, 2019), tropical cyclones (Lavender & Abbs, 2013), and local convection due to the diurnal cycle (Rauniyar & Walsh, 2011), causing the majority of the rain to fall in summer. The cooler months are usually dry in the north of Australia. Rainfall in southern Australia is modulated by large-scale drivers such as ENSO, SAM, IOD, and IPO. In this region, rainfall is mainly brought by fronts, cut off lows, and east coast lows embedded within westerlies (Catto *et al.*, 2012a; Pepler *et al.*, 2014; Pepler *et al.*, 2019). Although these systems can occur at any time of the year, they are more common in winter.

4.1.2 Timing of extreme rainfall

When studying extremes, most of the studies focus on the intensity of extreme rainfall events (Contractor *et al.*, 2018; Gallant *et al.*, 2007; Haylock & Nicholls, 2000). However, an increasing number of studies show that focusing on just the intensity and frequency of extreme events does not show the entire picture of extreme rainfall characteristics (Du *et al.*, 2019; Pendergrass & Knutti, 2018). Extreme events such as the maximum consecutive 5-day precipitation (Rx5) (Zhang *et al.*, 2011) can lead to devastating floods or can also bring relief from drought and greatly contribute to the water storage. Half of the stations analysed globally

show that more than 50% of the total annual rainfall falls in the 12 wettest days in the year, while this number is even smaller for many stations in Australia (Pendergrass & Knutti, 2018). This highlights the importance of extreme events contributing to total rainfall. Therefore, it is essential to know when these systems usually occur in different regions in Australia. A persistent decline in winter rainfall has been seen in the south of Australia since the 1970s (Dey *et al.*, 2019; Hope *et al.*, 2010; Pepler *et al.*, 2019; Timbal, 2004). The most productive agricultural land in Australia, known as the wheat-sheep zone, is situated in the inland of the southwest of Western Australia (SWWA) and in the east, it extends from the southeast of South Australia to southeast Queensland (Fig. 4.1). These regions receive majority of its annual rainfall in winter, supporting the wheat yield in May-October. However, a decline in total annual and winter rainfall has led to a shift in the wheat and sheep production zone by 70km in the south (Chen *et al.*, 2019). Thus, a temporal shift in the season/month in which maximum rainfall is received climatologically in a region can greatly impact flood management, crop production, and future planning; however, it remains unexplored.

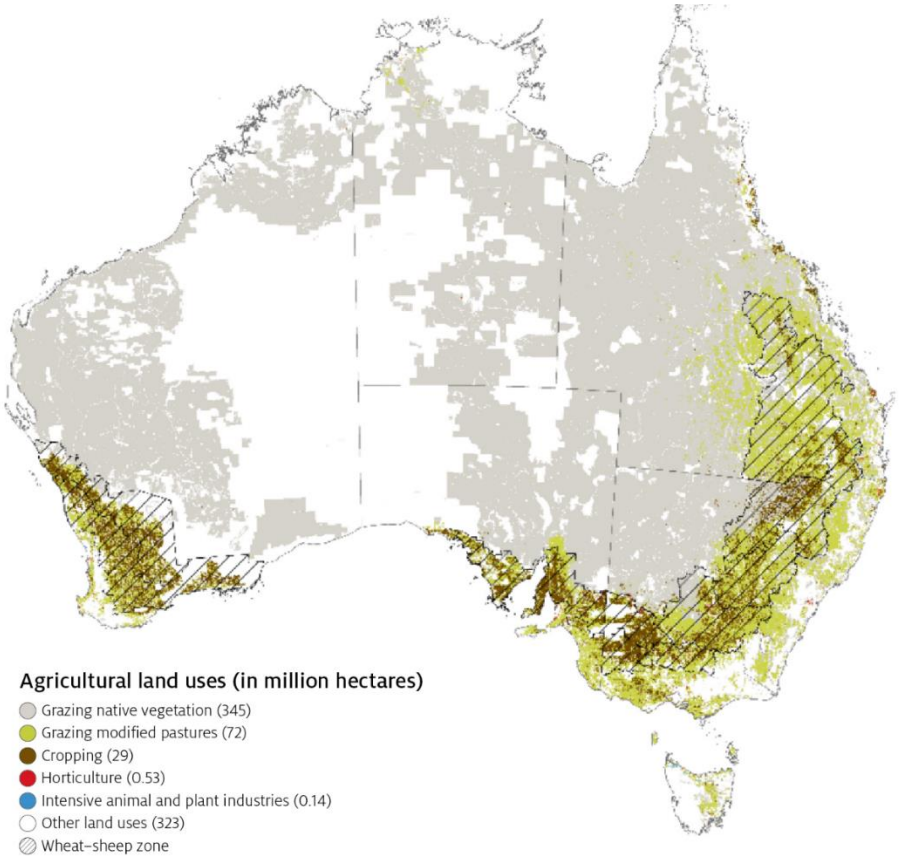

Figure 4.1 Agriculture production zones, Figure 2 from Jackson et al (2018).
Source: Wheat-sheep zone – Agricultural and Grazing Industries Survey, 2016, ABARES; Land use of Australia, 2010–11, ABARES

With global warming, the timing of the maximum 1-day precipitation (Rx1) has shifted to later months in the year Marelle *et al.* (2018). A continent-wide shift in the timing of floods has been reported in Europe due to climate change (Blöschl *et al.*, 2017). To our knowledge, Marelle *et al.* (2018) is the first study that investigates historical and future changes in the timing of extreme rainfall at a global scale. However, the study does not find any robust historical change in the seasonality of the timing in extreme rainfall in Australia. Thus, the study by Marelle *et al.* (2018) does not include future projections of the seasonality in the extreme rainfall timing in Australia. This could imply that the anthropogenic signal is too small compared to the natural variability. A rigorous study is required to understand the natural variability in the timing of extreme rainfall in Australia before attempting to find changes due to anthropogenic forcings. This chapter builds on Marelle *et al.* (2018) by investigating when extremes usually occur in a calendar year in Australia (exception is made for studying the impact of ENSO, where July to June is considered; more information is provided in the data and method section), and the year to year variability in the timing of extreme rainfall.

ENSO is one of the largest sources of rainfall variability in Australia. During El Niño (La Niña) years, above average sea surface temperature (SST) over central and east Pacific leads to decreased (increased) convection thus causes below (above) normal rainfall over eastern and north-east Australia. The ENSO-Australia rainfall relationship is strongest in spring and summer months in east Australia (Cai *et al.*, 2011a; Power *et al.*, 1999; Risbey *et al.*, 2009). During El Niño (EN) years, Australia receives below normal rainfall, while the opposite is true for La Niña (LN) years. The ENSO-Australia rainfall relationship undergoes significant decadal variability due to a weak ENSO-like decadal-scale phenomenon, the Interdecadal Pacific Oscillation (IPO). Both IPO and ENSO affect global as well as regional weather patterns, causing regional variations in rainfall and other meteorological parameters. So far, in the observational record (i.e. post-1910), we have experienced two positive IPO (pIPO; ~1925-1944 ~1977-1998) phases and two negative IPO (nIPO; ~1945–1976 and ~1999–2014) phases (Henley, 2017). The IPO plays a crucial role in modulating Australia's rainfall at a longer time scale where a negative phase is associated with stronger ENSO-Australian rainfall relationship, and the rainfall predictive models perform well while during a positive phase, the association weakens, and the rainfall predictive models perform poorly (Power *et al.*, 1999; Zhao *et al.*, 2016).

Similar to mean rainfall, extreme rainfall is significantly modulated by IPO and ENSO, specifically in east Australia (King *et al.*, 2013). Following King *et al.* (2013), we explore the relationship between extreme rainfall timing and IPO-ENSO interaction. This is done by studying extreme rainfall timing in four different combinations of IPO and ENSO phases - when both ENSO and IPO are in warm phase (EN-pIPO), years when both ENSO and IPO are in cold phase (LN-nIPO), years when ENSO is in warm, but IPO is in cold (EN-nIPO) phase, and years when ENSO is in cold, but IPO is in warm (LN-pIPO) phase. These relationships can be useful for improving the seasonal prediction of extreme rainfall.

4.2 Data and Methods

4.2.1 Definition of the timing of extremes

In this study, we consider Rx5 as the metric for precipitation extremes because as mentioned above, this index is a proxy for extreme rainfall in addition to contributing substantially to seasonal and annual rainfall totals. On the other hand, looking at the maximum 1-day rainfall (Rx1) provides similar results, although somewhat noisier compared to Rx5.

To define the timing of extreme rainfall, we note the first date of the Rx5 index and calculate the month in which it occurs (called extreme rainfall month hereafter) at each grid point and for each year. The months are numbered from 1-12, January is the 1st month and December is the 12th month. Also, we note the day of the year (nth day; starting from January the 1st). The data are circular in nature, (the difference between the 1st and 12th month, i.e. December and January, is not 11, as they are adjacent months). Thus, instead of using regular statistics, a circular algorithm can be used for these kinds of data (Fisher, 1953). The data analysis is performed using a readily available package in MATLAB (Berens, 2009). Next, the circular mean, median, and standard deviation are calculated over the period of interest and transformed to a linear scale. Similarly, the circular standard deviation (unit: days) in the timing of Rx5 is calculated using the first day of the Rx5 occurrence in a year (i.e. nth day of the year). We used the Kuiper test (analogous to K-S test) for testing if two distributions are significantly different.

Circular variance is a crucial statistic in directional/circular statistics, as it is a measure of the spread in the dataset. The value of the circular variance ranges between 0 to 1, where, 0 implies no spread around the mean direction, and values close to 1 imply high spread in the data (See Berens (2009) for further information and formulas). The calculation of circular

standard deviation, which measures the angular deviation, is analogous to the linear standard deviation. As the circular variance is shown with the circular histogram plot, the metric is not transformed to a linear scale, whereas, the values of circular standard deviation is transformed to linear scale to represent the deviation from the mean extreme rainfall month in days.

4.2.2 ENSO and IPO Index calculations

To characterise ENSO phases, we use the monthly nino3.4 index data; freely available from https://www.esrl.noaa.gov/psd/gcos_wgsp/Timeseries/Data/nino34.long.anom.data. As nino3.4 reaches its peak during December-April and changes its phase by June, we consider July-June as the ENSO year, instead of using a calendar year (Fowler *et al.*, 2008; Kahru *et al.*, 2004). The monthly nino3.4 index is averaged over the ENSO year. Next, El Niño and La Niña years are classified when the nino3.4 index, averaged over the ENSO years is >0.25 and <-0.25 respectively. The threshold is chosen to maintain enough data points in each phase of ENSO as well as to filter out weaker/neutral ENSO years. To understand the relationship between extremes and ENSO, Rx5 is calculated over ENSO years and compared with the nino3.4 index. Next, we calculate the monthly IPO index by calculating the second Principle Component of the low-pass filtered near-global SST, using HadISST data (Rayner *et al.*, 2003), following Power *et al.* (1999). The years when the IPO index averaged over a calendar year is >0 is classified as pIPO years and when it is <0, the year is classified as nIPO year. To explore the interaction between IPO and ESO, the ENSO year is used to calculate nino3.4, IPO and Rx5. The same thresholds mentioned above are used to distinguish between IPO and ENSO phases.

4.2.3 Observed and reanalysis datasets

We use the daily Australian Water Availability Project (AWAP; Jones et al.2009) data at 0.25° × 0.25° horizontal resolution over the period 1911-2016. The AWAP dataset is widely used for studying rainfall in Australia (Alexander & Arblaster, 2017; Dey *et al.*, 2019; King *et al.*, 2013; Moise *et al.*, 2019), also, previous research shows that AWAP can replicate extreme rainfall characteristics when compared against station data (King *et al.*, 2013a). However, due to scarce station density in some regions, areas of central Australia are often masked to avoid regions where there is low confidence in the dataset. In this study, we mask two boxes in white, following Chung and Power (2017).

We only have reliable data with enough spatial coverage of rainfall for the last two positive and two negative IPO phases, which makes it challenging to study the relationship between the

IPO and Australia's rainfall. Further segregating ENSO years into positive and negative phases in each IPO phase results in fewer data points. Thus, in this study, we use the Twentieth Century Reanalysis (20CR) dataset at ~1.875x1.875° resolution (Compo *et al.*, 2011) to compare against AWAP to strengthen our conclusions. The reanalysis product provides 56 ensemble members over the period 1851-2011, which allows enough samples to study the relationship between Australia's rainfall and ENSO and IPO. Previous research shows that 20CR captures the observed relationship between extreme rainfall intensity with ENSO and IPO reasonably well (King *et al.*, 2013). The 20CR assimilates observed sea surface temperature and sea ice distributions, using ensemble Kalman filter method with an ensemble of forecasts from global numerical weather prediction model as a "first guess" to generate 56 ensemble members of the atmosphere. We record the first day of Rx5 in each year to calculate extreme rainfall month for each simulation. Next, the circular mean was calculated across 56 ensemble members to obtain the timing of extreme rainfall and standard deviation in 20CR dataset. For calculating the histograms in 20CR, we combine all 161 years of each realisation, resulting in 9016 years of data (56x161).

A black contour is overlaid on each plot showing the median month of extreme rainfall (Fig. 4.2-4.7 & 4.9). This contour separates the area of summer (December – February) extreme rainfall from regions where extreme rainfall occurs in other months (i.e. March-November). To plot this contour, we have used the spatial data of the median month of extreme rainfall. Grid points where extreme rainfall occurs in summer were assigned the value 1, and the rest of the grid points are assigned a value 0. This leaves the dataset with only two values, either 1 or 0. Next, a low pass filter is applied to remove small-scale noise. Lastly, this information is used to plot the contour, which is imposed on the figures. This method is applied in AWAP and 20CR data throughout the study.

4.3 Results and Discussion

4.3.1 Timing of extreme rainfall

The median of extreme rainfall month over the period 1911-2016 in AWAP data is shown in Fig. 4.2a. The timing of extreme rainfall has a distinct diagonal north-south pattern. In the north, extreme rainfall usually occurs in February and in the south of Australia, extreme rainfall occurs in late autumn/early winter. The black contour clearly distinguishes the areas of summer extreme rainfall from the areas where extreme rainfall occurs in other months. The majority of

winter extreme rainfall is seen in the inland areas of southeast Australia (SEA) and SWWA. Whereas, the timing of extreme rainfall in the coastal region of SEA and nearby alpine regions is spatially noisy, which makes it challenging to study rainfall in these regions. Note, the area where extreme rainfall occurs in winter closely matches the wheat and sheep belt of Australia (Fig 4.1). This highlights that a shift in the timing of rainfall events could potentially have large impacts on these regions.

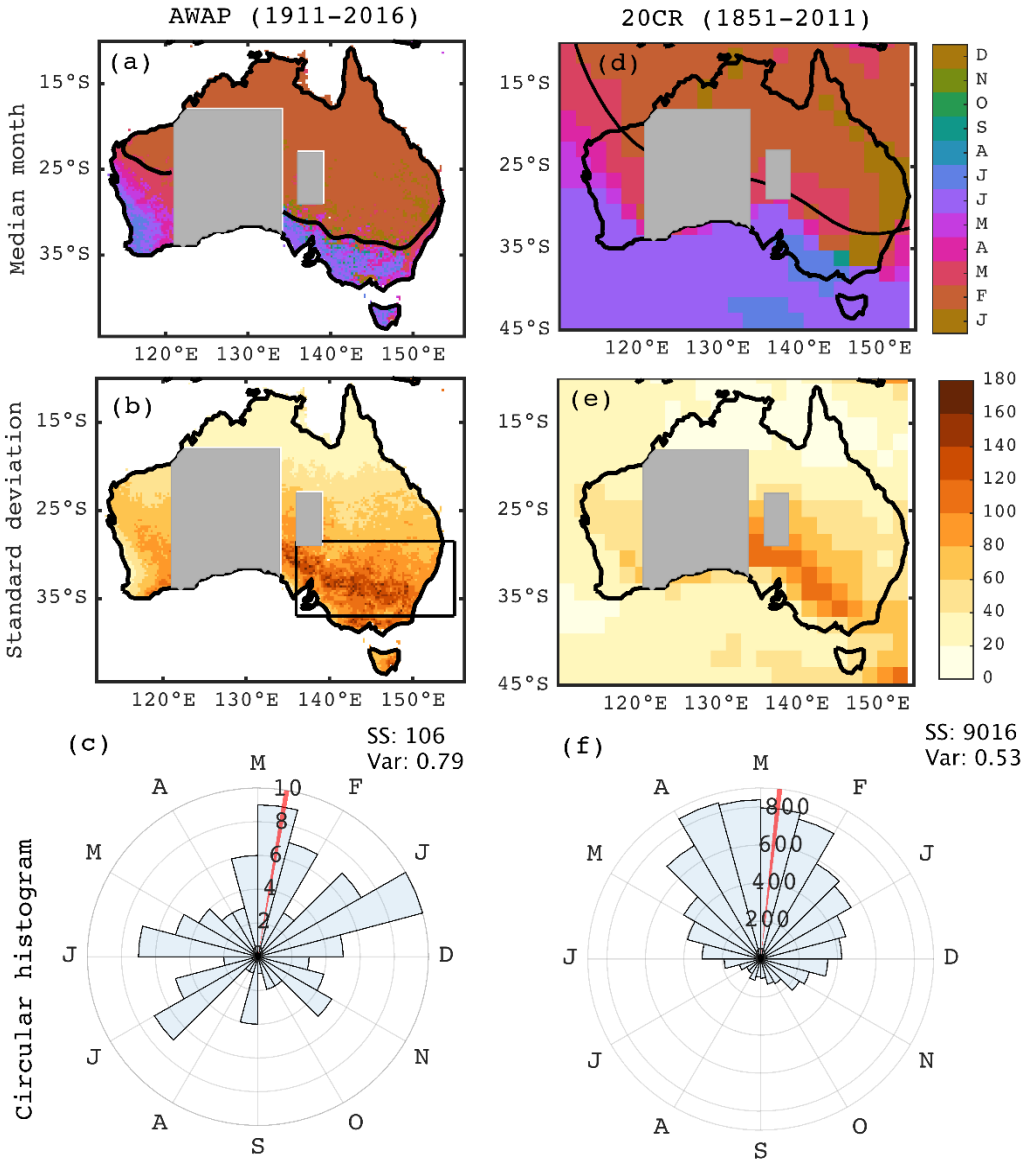

Figure 4.2 The median of extreme rainfall month in (a) AWAP and (d) 20CR ensemble mean. The standard deviation (unit: days) in the timing of extreme rainfall in (b) AWAP and (e) 20CR ensemble mean. The circular histogram of the extreme rainfall month, averaged over South-East Australia (SEA; the box highlighted in (b) in (c) AWAP and (f) C20C composite using 56 ensemble members. The red line shows the median month of the area averaged extreme rainfall month in SEA. The numbers inside the circle shows the frequency of extremes. The sample size (SS) and variance in the dataset is shown in the right-hand side of the histograms. The time period used in AWAP and 20CR datasets are 1911-2016, and 1851-2011, respectively.

The smallest inter-annual variability in the timing of extreme rainfall is north of 20°S and SWWA, ranging from 20 to 40 days. This implies that the timing of extreme rainfall is consistent in these regions. The variability increases southward with high values in the areas where the extreme rainfall timing transitions from summer to winter months. The maximum standard deviation is seen in SEA; the values are as high as 160-180 days – indicating that extremes can occur at any time throughout the year. The region highlighted by the black box (hereafter called the SEA box) is where the maximum variability is seen. This region will be used in this study to calculate histograms. One of the reasons behind not extending the SEA box (shown in Fig. 4.2a) to the coast is because we intend to study the area where summer extremes merge with winter rainfall. The circular histogram of extreme rainfall month, area-averaged over SEA (Fig. 4.2c) reinforces the high variability in the timing of extreme rainfall in this region, with a variance of 0.79. The climatological median month of the timing of extreme rainfall is between February and March, shown by the red line.

The timing of extreme rainfall in the 20CR ensemble mean is tested next to investigate the applicability of this dataset for further analyses. The 20CR ensemble mean captures a north and south pattern in the timing of extreme rainfall, similar to observed (Fig. 4.2d). The black contour shows a similar diagonal division in the timing of extreme rainfall in Australia, although, it is situated slightly northward compared to AWAP. In the 20CR ensemble mean, the area of summer extremes is followed by autumn extremes in central Australia and winter extremes in the further south (Victoria, and SWWA). The variability in the timing of extreme rainfall in the 20CR ensemble mean (Fig. 4.2e) shows a similar pattern as observed, with minimum standard deviation in the north and increasing southward (Fig. 4.2e). However, the variability overall in SEA is smaller compared to observed, and the region of maximum standard deviation is located further south. This is because the median of extreme rainfall in 20CR does not precisely match the observed pattern. Note, as the standard deviation is calculated using the ensemble mean across 56 ensemble members, this could explain the smaller than observed variability in the timing of extreme in 20CR.

The circular histogram, averaged over SEA, shows that the median month of extreme rainfall is located between February and March, similar to observed. The variance in the data is 0.53, smaller compared to the AWAP but as explained above is likely related to our use of the ensemble mean. Note, the reanalysis data have much coarser resolution than AWAP. We repeated the analysis using AWAP data interpolated onto 20CR grids. However, the variability

is still higher in AWAP compared to 20CR. Thus, the coarse spatial resolution cannot explain the lower than observed variability in the reanalysis data. Overall, the 20CR data capture the observed spatial pattern of the timing of extreme rainfall and standard deviation and thus we use it for the purposes of further analysis in this study. This is consistent with Ashcroft *et al.* (2014), where the authors show that 20CR is able to capture the inter-annual variability of rainfall in SEA.

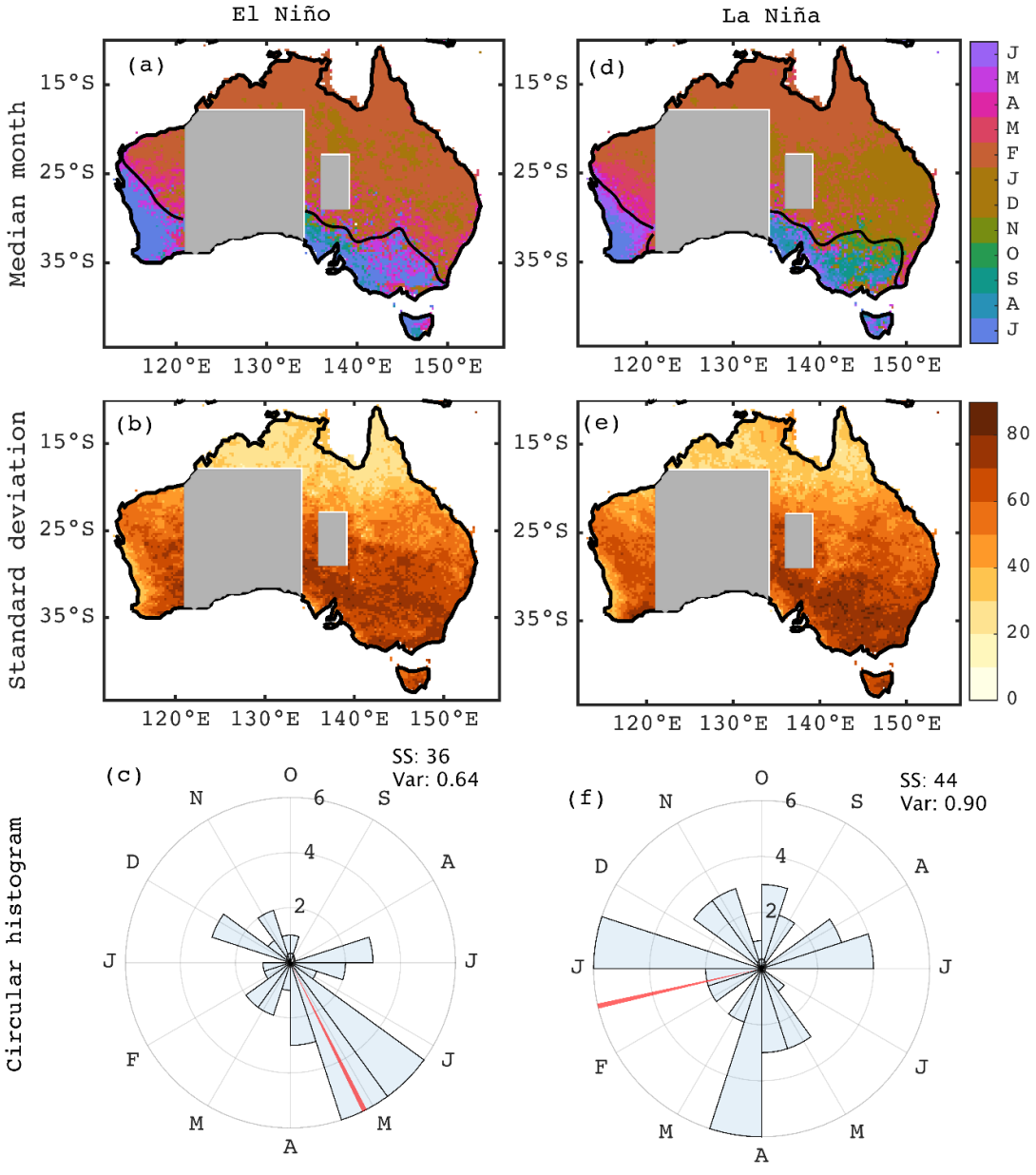

Figure 4.3 a-c The median of extreme rainfall month, standard deviation in the timing of extreme rainfall, and the circular histogram of extreme rainfall month averaged over SEA in El Niño years. d-f, same as a-c, but for La Niña years in AWAP dataset.

4.3.2 The role of ENSO

It is well established that ENSO is the largest source of inter-annual variability of Australia's mean and extreme rainfall (Risbey *et al.*, 2009). Both El Niño and La Niña years show similar diagonally separated north and south pattern of summer and winter dominated extreme rainfall (Fig. 4.3). In La Niña years (Fig. 4.3d), large parts of east Australia show extremes in the early summer months (December/January). The major distinction in extreme rainfall month is seen in SEA, where, in La Niña years, extremes occur in spring/late winter, and in El Niño years (Fig. 4.3a), extremes occur mostly in autumn/early winter. This implies that depending on the phase of ENSO, the timing of extreme rainfall in SEA can vary by six months. Cai *et al.* (2011c) showed that there is no direct pathway for ENSO to impact rainfall in SEA; instead, ENSO affects rainfall through its interaction with IOD. The IOD impacts Australia's rainfall, especially the southern latitudes in winter and peaks in spring (Risbey *et al.*, 2009). Previous research shows that the occurrence of IOD and ENSO are inter-dependent, i.e. a negative IOD (positive IOD) tends to coincide with La Niña (El Niño) events (Jourdain *et al.*, 2016; Wang *et al.*, 2019). La Niña years are usually (not always) preceded by neutral or negative IOD events (Meyers *et al.*, 2007; Risbey *et al.*, 2009). The correlation between ENSO and IOD is ~0.6, which leads to above-average spring rainfall (Risbey *et al.*, 2009). Thus, the strong covariance between ENSO and IOD in spring could explain the spring extreme rainfall in SEA in La Niña years.

Studying the timing of extreme rainfall based on ENSO phases constrains the variability in SEA to 90 days, i.e. a season length (Fig. 4.3b), whereas the variability in all years was up to 180 days. This indicates that understanding the relationship between large-scale drivers and the timing of extreme rainfall can narrow down the variability in SEA, thus, has huge implications on improving seasonal prediction of extreme rainfall. The area of high standard deviation is larger and concentrated in SEA in La Niña years compared to El Niño years, (Fig. 4.3b, e). Whereas, the region of maximum variability in El Niño years is spatially inhomogeneous in SEA. The distribution of extreme rainfall months, averaged over SEA, during La Niña events (Fig. 4.3f) is spread throughout the year (higher frequency in summer months), with the median month being January. Whereas, the median direction of extreme rainfall events during El Niño years is in late autumn (between April and March) (Fig. 4.3c). These two distributions are statistically significant at the 5% level, and the median directions are significantly different. As seen in the figure, the extreme rainfall month is spread

throughout the year in La Niña years, the variance during La Niña years is 0.9, whereas the variance during El Niño years is 0.64. Thus, it is challenging to predict the timing of extreme rainfall during La Niña years. The possible reason for high variability in La Niña years could be the covariance between ENSO and other large-scale drivers, such as IOD. As discussed above, negative IOD events often co-occur with La Niña years, resulting in above-average spring rainfall.

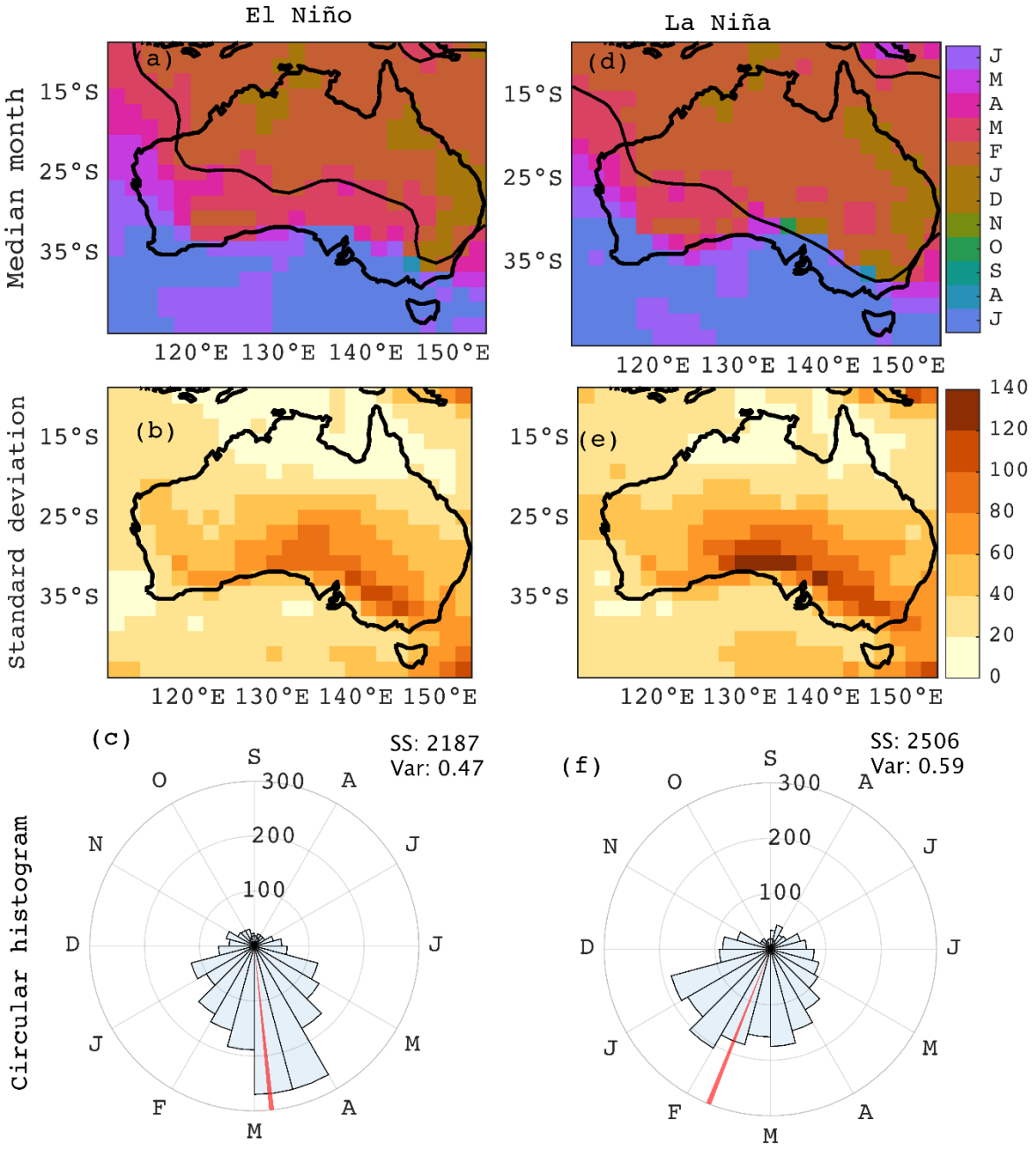

Figure 4.4 Same as Fig. 4.3, but using 20CR ensemble mean using 56 ensemble member mean (a,b,d,e), and composites (c,f). Time period used is 1851-2011.

The median month of extreme rainfall in the 20CR ensemble broadly matches the observed pattern (Fig. 4.4). The black contour extends further southward in La Niña compared to El Niño years (Fig. 4.4a,d), however, this is not observed in AWAP. During La Niña years, larger areas show extreme rainfall in summer months in central and eastern Australia compared to El Niño years. The primary distinction observed in extreme rainfall month between El Niño and La Niña years in SEA is that extreme rainfall occurs in spring/late winter in La Niña years and autumn/early winter in El Niño years, which is not captured in 20CR. This could potentially imply that the large-scale interactions between ENSO and IOD and its impact on the timing of extreme rainfall are not accurately represented in the reanalysis dataset.

Note, variability in the 20CR ensemble mean is greater than a season in SEA, i.e. higher than observed in AWAP. The standard deviation in La Niña years is high compared to El Niño years, similar to observed (Fig. 4.4b, e). The circular histogram shows the distribution of area-averaged extreme rainfall month in El Niño and La Niña years in 20CR composites. The median month of extreme rainfall is in February in La Niña years, whereas in El Niño years the median is shifted to later in the year. The two distributions are significantly different at the 0.0001 level. The standard deviation during El Niño and La Niña years are 0.55 and 0.64, respectively. Higher variability in La Niña compared to El Niño years is seen in 49 realisations out of 56. Overall, both in AWAP observations and 20CR, the robust features evident are: 1. the variability is higher in La Niña years compared to El Niño years, and 2. La Niña years increase the area of summer extreme rainfall in Australia.

4.3.3 The role of IPO

The large variability in SEA is in part associated with the complex interactions between large-scale drivers and decadal variability (Ashcroft *et al.*, 2019). During nIPO years, the region of summer extreme rainfall is extended southward in SEA, and simultaneously, the area of winter extreme rainfall is pushed further southward (black contour in Fig. 4.5d). A similar result was reported by Speer *et al.* (2011) where the authors found a significant poleward shift in the subtropical ridge in nIPO years, allowing enhanced tropical interactions and increased rainfall in east Australia. However, during pIPO years, the area of summer extreme rainfall remains restricted to the north compared nIPO years (Fig. 4.5a). Investigating the interannual variability according to IPO phases limits the standard deviation values within a season (90 days), much smaller compared to all years (Fig. 4.5b, d). As the area where summer and winter extreme

rainfall merge, shifts southward in nIPO years, the patch of high standard deviation is located further south compared to pIPO years.

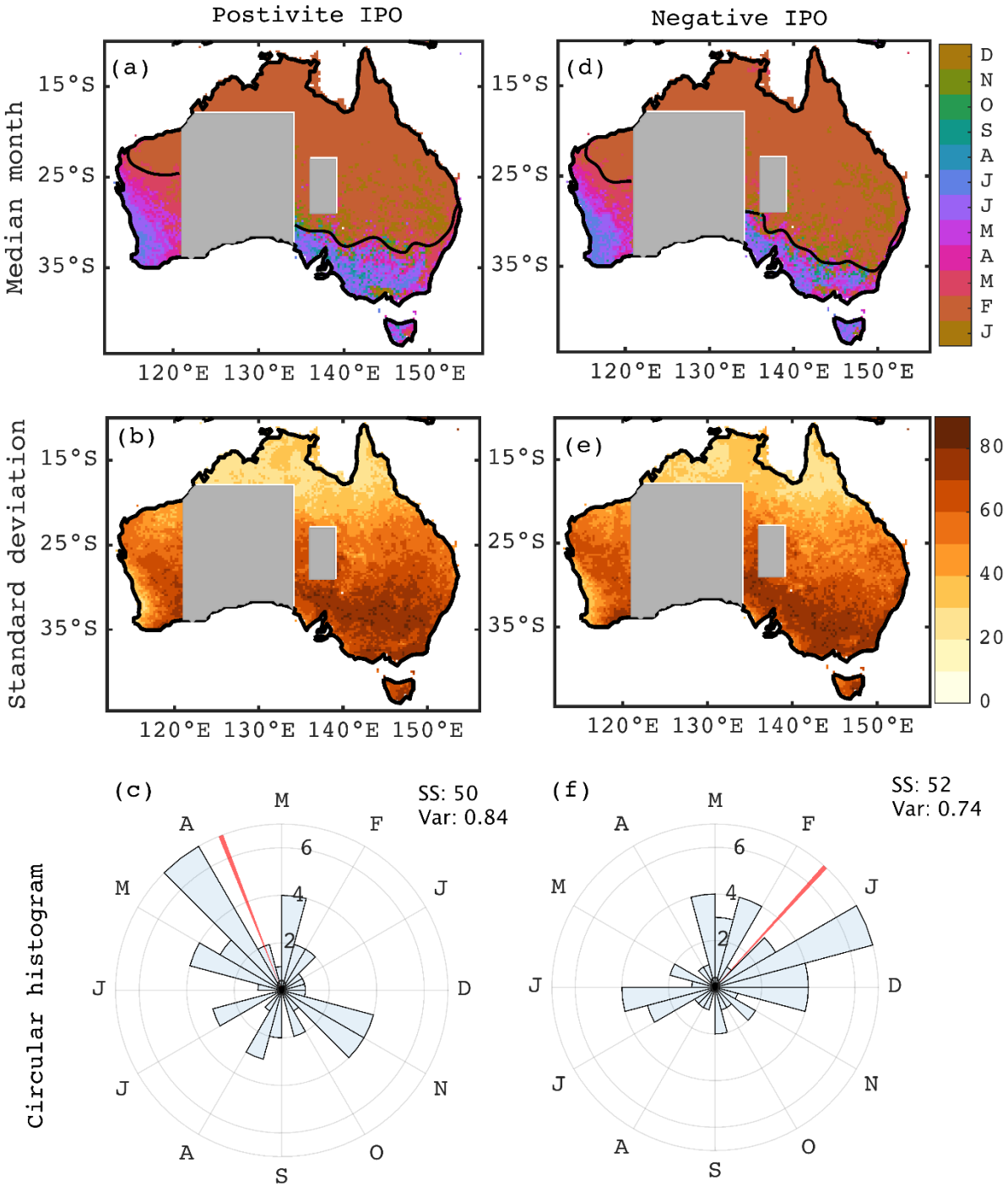

Figure 4.5 a-c median of extreme rainfall month, standard deviation in the timing of extreme rainfall, and the circular histogram averaged over SEA in positive IPO years (pIPO). d-f, same as a-c for negative IPO years (nIPO) in AWAP dataset.

Circular histograms averaged over SEA show that during nIPO years, extreme rainfall occurs mostly between November and March (Fig. 4.5f). On the other hand, during pIPO years (Fig. 4.5e), extreme rainfall usually occurs in autumn months, with fewer events in summer. The distributions of extreme rainfall month during positive and negative IPO events in SEA are significantly different at the 90% confidence interval. Note, the variability in the timing of extreme rainfall is higher during pIPO (0.84) compared to nIPO events (0.74). This is consistent with Lim *et al.* (2017), where the authors show that during pIPO phases, the relationship between Australia's rainfall and large-scale drivers (ENSO and IOD) is weak; thus predictability of rainfall in SEA is very low. Also, the ENSO-SAM relationship is stronger during the nIPO phase, and the opposite is true for the pIPO phase (Fogt & Bromwich, 2006; Fogt *et al.*, 2011). Therefore, high variability during pIPO compared to nIPO is potentially a result of strong relationship between the large-scale drivers and Australia's rainfall in nIPO years.

The 20CR ensemble mean (Fig. 4.6a, d) shows a larger area of summer extremes in east Australia during nIPO, compared to pIPO years. Also, the black contour separating areas of extremes in summer and other seasons is shifted southward in nIPO years, similar to observed in AWAP. Micevski *et al.* (2006) found a similar north-south shift in east Australia in the flood risk zones associated with a switch in IPO phases. The implications are: increased flood risk in the south of Queensland, NSW, and north of Victoria in nIPO years and increased drought risk in these regions in pIPO years (Kiem & Franks, 2004; Kiem *et al.*, 2003; Micevski *et al.*, 2006). The shift in flood and drought risk zones related to IPO phases is due to a decadal shift in regional convergence zone which is generated as a result of interaction between the South Pacific Convergence Zone and the ITCZ (Micevski *et al.*, 2006).

The variability in the timing of extreme rainfall overall shows a similar spatial pattern to observed; however, the values are higher than a season (Fig. 4.6b, e). In SEA, a slightly higher standard deviation is seen during nIPO compared to pIPO years, which is the opposite of what is observed. Similar to the spatial plots, the histogram averaged over SEA show higher variability in nIPO events (0.56) compared to pIPO events (0.47), which is again the opposite of what is observed. Repeating the analysis in each ensemble member shows that 42 out of 56 ensemble members show higher variability in nIPO years than pIPO. During nIPO years, the median extreme rainfall month, shown by the red line, is located between February and March, whereas it shifts later in the year during pIPO events. The two distributions are significantly

different, and the median directions are significantly different as well. Overall, the reanalysis dataset captures the major distinctions observed between nIPO and pIPO years, although, does not constrain the variability within a season.

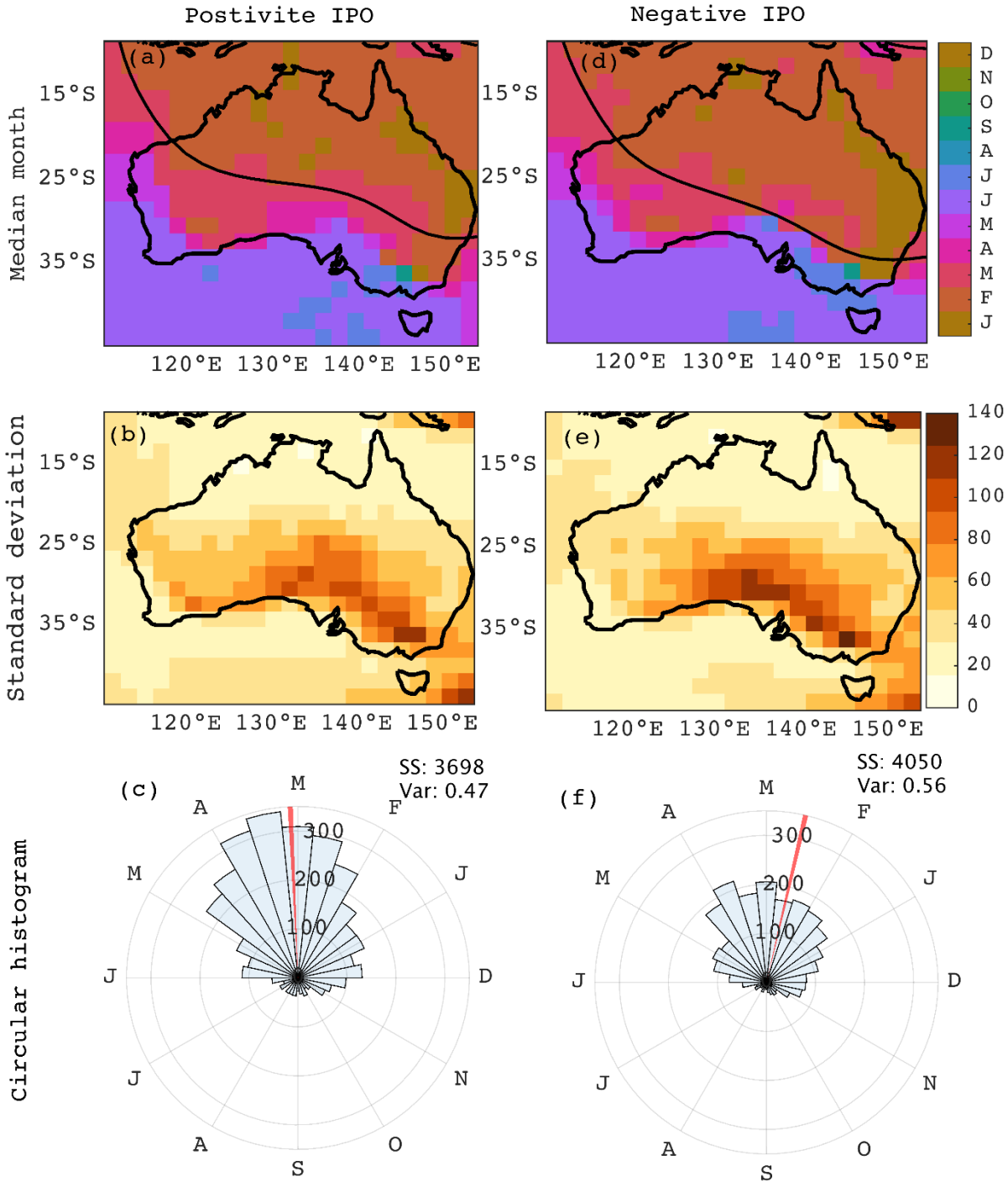

Figure 4.6 Same as Fig. 4.5, but for the 20CR ensemble mean (a,b,d,e), and composites (c,f).

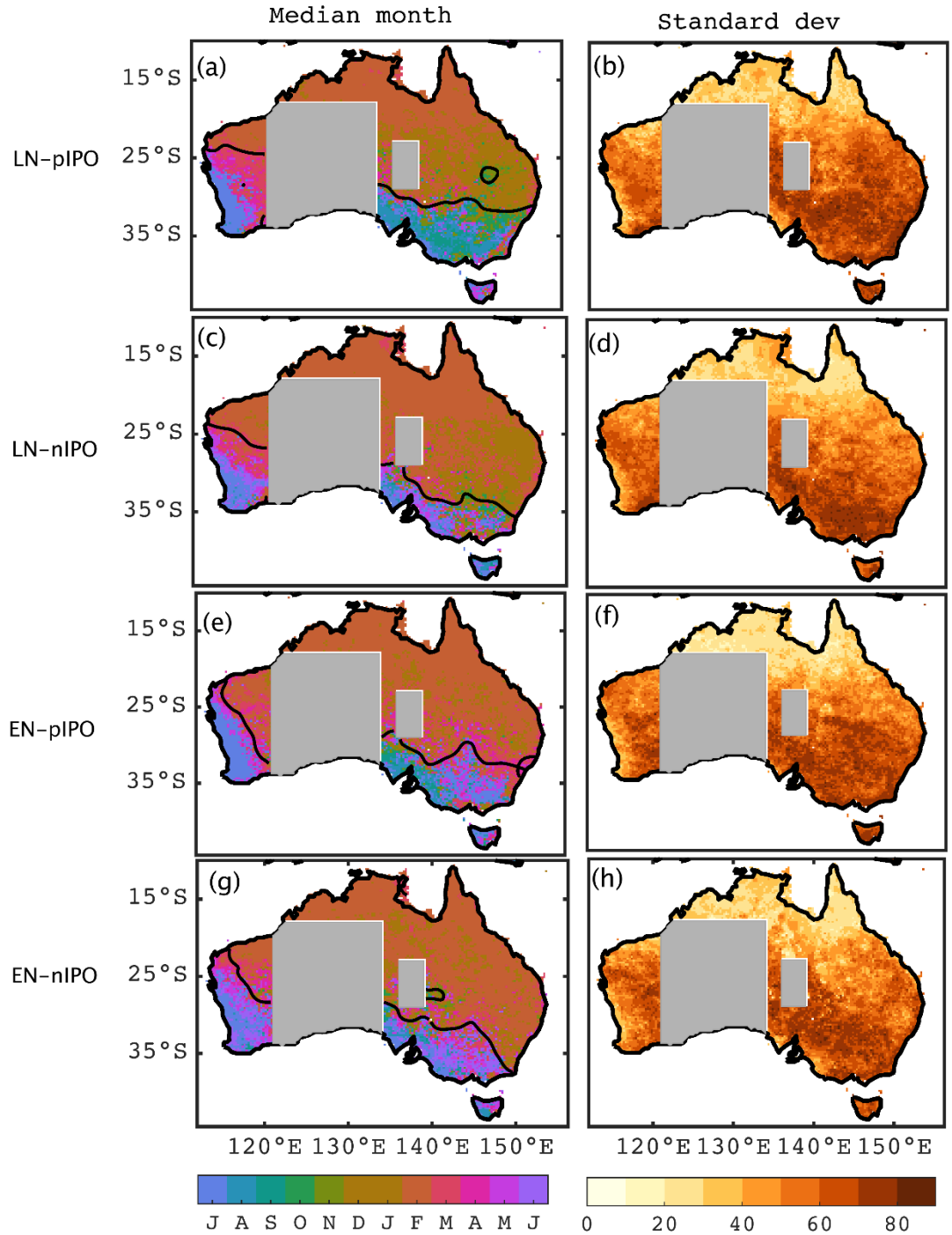

Figure 4.7 The interaction between ENSO and IPO phases. The median of extreme rainfall month and standard deviation in a,b) La Niña-positive IPO, c,d) La Niña-negative IPO, e,f) El Niño- positive IPO, g,h) El Niño- negative IPO years.

4.3.4 The role of the interaction between ENSO and IPO

So far, previous research has studied the role of the interaction between ENSO and IPO on Australia's annual rainfall as well as extreme rainfall frequency and intensity (Ashcroft *et al.*,

2019; King *et al.*, 2013; Power *et al.*, 1999; Speer *et al.*, 2011). Here we repeat our analysis using ENSO years (July-June) to investigate the impact of the interaction between ENSO and the IPO on the timing of extreme rainfall (Fig. 4.7). During LN-pIPO years (Fig. 4.7a), the area of summer extreme rainfall is situated northward compared to the climatological median (Fig. 1a), and a large part of SEA receives extreme rainfall in spring months, similar to all La Niña years composite. During LN-nIPO (Fig. 4.7c), the summer extremes branch reaches further south of the country and also results in summer extreme rainfall in parts of Victoria. During La Niña years, in both phases of IPO, the south of Queensland receives extreme rainfall in early summer months (December/January). Figure 4.7e, g show that El Niño years further segregated according to IPO phases, do not show a large distinction in the spatial plots of the median of extreme rainfall month.

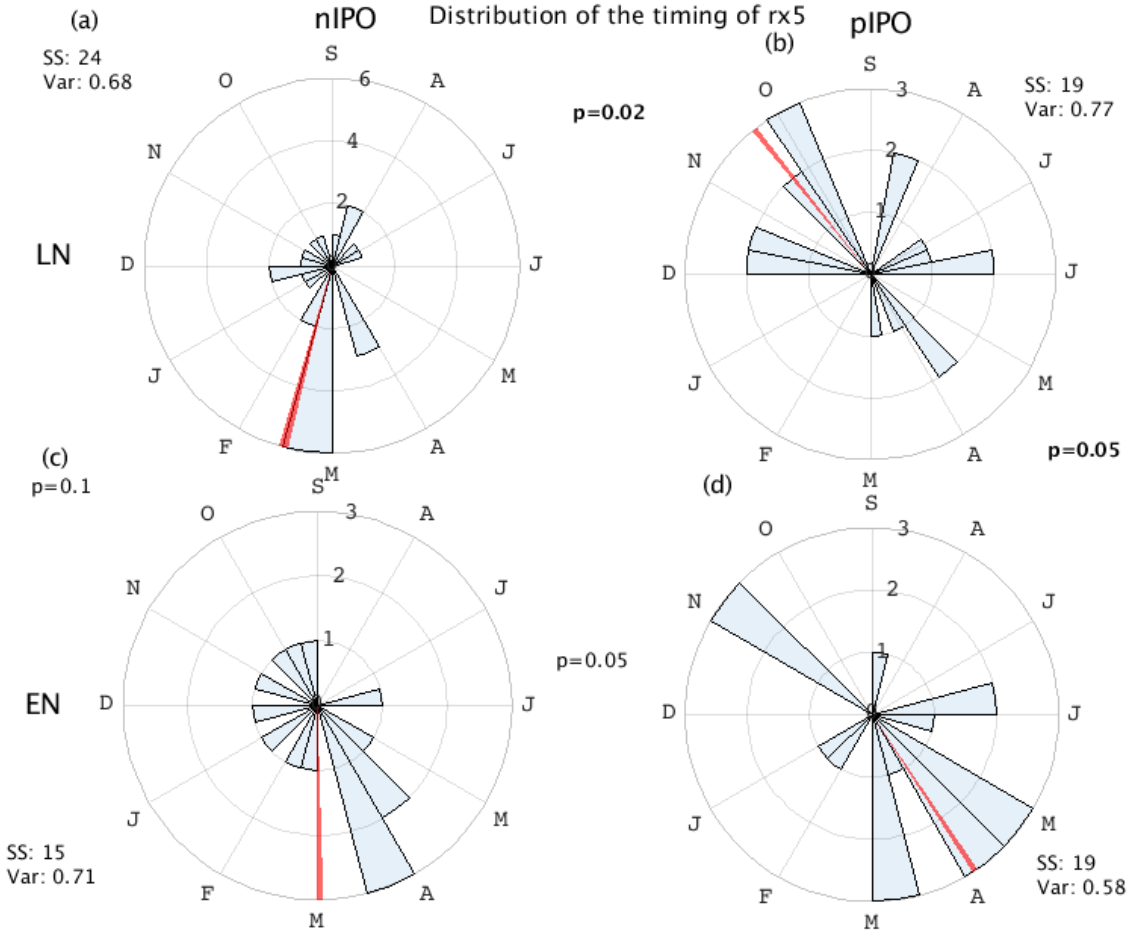

Figure 4.8 Circular histogram of the extreme rainfall month averaged over SEA in AWAP dataset, over the period 1911-2016 in (a) La Niña-negative IPO, (b) La Niña-positive IPO, (c) El Niño-negative IPO, (d) El Niño-positive IPO years.

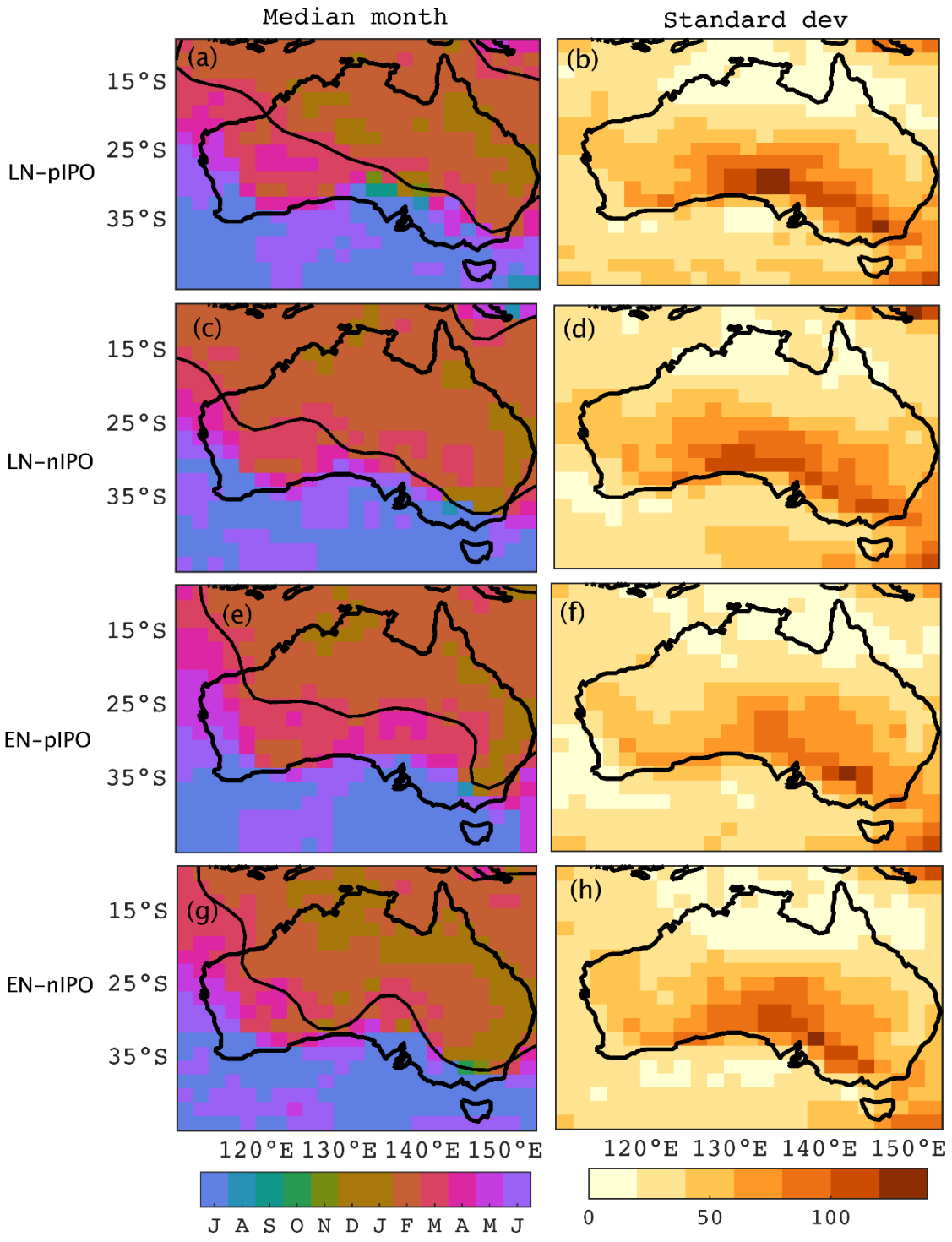

Figure 4.9 Same as Fig. 4.7, but for the 20CR ensemble mean using 56 ensemble members mean over the time period 1851-2011.

The major difference found between EN-pIPO and EN-nIPO years is, larger areas show extremes in summer months, including in SEA in the nIPO phase. Hence, the robust features seen from this plot combined with previous plots are, firstly, in the nIPO phase, the area of summer extreme rainfall is pushed southward compared to pIPO in both phases of ENSO (most evident in La Niña years). Secondly, the major difference is seen between LN-pIPO and LN-nIPO years, where extreme rainfall in SEA in LN-pIPO occurs usually occurs in late winter/spring months. In contrast, winter/spring extremes this region is replaced by summer extreme rainfall in LN-nIPO years. The timing of extreme rainfall in SEA shows little difference between EN-pIPO (Fig. 4.7e) and EN-nIPO (Fig. 4.7g) years, where both show autumn/early winter rainfall in SEA. Overall, the largest effect of IPO is seen during La Niña years, where a shift of up to six months in the timing of extreme rainfall is seen in SEA depending on the phase of IPO, however, little change is seen during El Niño years.

The area-averaged circular distribution of the extreme rainfall month (Fig. 4.8) is in line with the spatial plots. In LN-nIPO years (Fig. 4.8a), the median of extreme rainfall month is summer, whereas, in LN-pIPO years (Fig. 4.8b), the median extreme rainfall month is spring. These two distributions are significantly different with significantly different median directions. The possible reasons of the shift in the timing of extreme rainfall could be a larger area of summer extremes in nIPO years (as shown in Fig. 4.5), and a weak relationship between ENSO-Australia's rainfall in pIPO years. Relatively smaller difference is seen in El Niño years between two IPO phases. The median month of extreme rainfall during EN-nIPO (Fig. 4.8c) years is March while the extreme month is shifted to later in the year in EN-pIPO years (Fig. 4.8d). These two distributions are significantly different at the 5% level. Looking particularly at the nIPO phase, distributions in EN-nIPO and LN-nIPO years are only different at the 90% significance level. The maximum standard deviation is seen in LN-pIPO years, and the least is seen in EN-pIPO.

As there is a small sample size in each of the four combinations of IPO and ENSO phases using AWAP data, the reanalysis data are useful to draw conclusions using a much larger sample size. The analyses were repeated in the reanalysis dataset (Fig. 4.9,4.10). The reanalysis data captures most of the important features that are observed in AWAP. For example, a larger area of summer extreme rainfall and the southward extension of the area of summer extremes during nIPO years is seen in both El Niño and La Niña years. However, another major feature seen in the observed dataset is the seasonal difference in the timing of extreme rainfall between

LN-pIPO and LN-nIPO years in SEA. This feature is not seen in reanalysis data. This indicates that it is likely that the reanalysis data do not capture the decadal variability in large-scale drivers and its teleconnections with Australia's rainfall. Although King *et al.* (2015) showed that 20CR data captured the ENSO-extreme rainfall intensity relationship reasonably well, further efforts are required to understand the inter-annual and decadal variability in the teleconnections of large-scale drivers and Australian rainfall using reanalysis data. The spatial plots show that the highest and least standard deviation in SEA is seen in LN-pIPO and LN-nIPO years, respectively (Fig. 4.9), similar to observed (Fig. 4.8). This is also evident in the next figure of the circular histogram of extreme rainfall month in the reanalysis composite (Fig. 4.10).

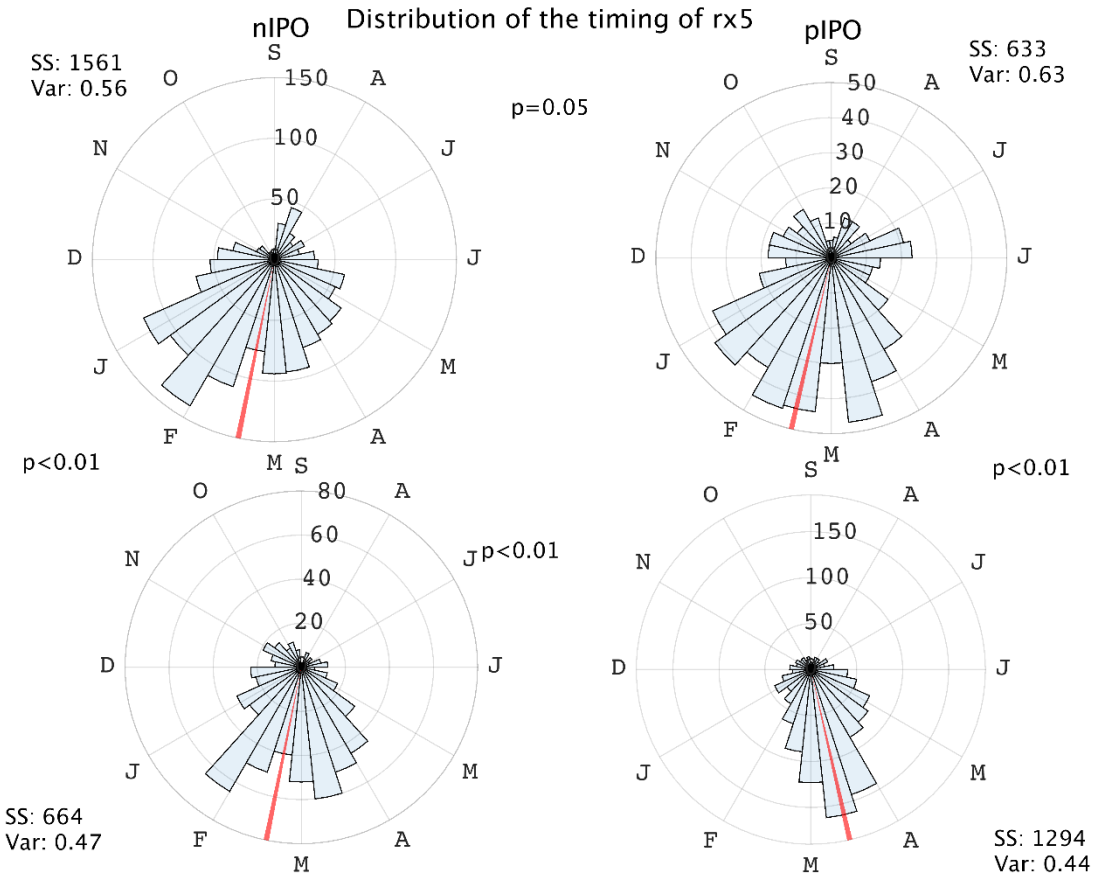

Figure 4.10 Same as Fig. 4.8, but for the 20CR composite using 56 ensemble members over the time period 1851-2011.

4.4 Conclusions

Our results indicate that the timing of extreme rainfall has a clear spatial diagonal distinction in Australia. Extremes in the north usually occur in summer months, while the south of the

country tends to receive extreme rainfall during autumn/winter. The variability in the timing of extreme rainfall is least in the north and increases southward, with maximum variability in SEA. The area where extreme rainfall occurs in winter is extremely important for crop production and livestock industries, also known as the wheat-sheep zone of Australia (Jackson *et al.*, 2018). Our results showed that depending on the phase of large-scale drivers, the timing of extreme rainfall in these regions can shift by up to six months, which could have large implications on agriculture sector in Australia. Thus, predicting seasonal rainfall is of specific interest for both sustaining agricultural industry as well as for flood risk management and preparedness (White *et al.*, 2015). The current forecasting system used by the Bureau of Meteorology seasonal rainfall in Australia, ACCESS1-S shows reasonable skill in predicting median rainfall, however, extreme rainfall predictions require improvement (Hudson *et al.*, 2017). Our study aims to understand the pattern in the timing of extreme rainfall in Australia and the variability associated with the large-scale Pacific drivers. Identifying relationships have implications in improving seasonal predictions. Also, future studies could use this study as the basis to understand if there is any shift in the timing of extreme rainfall due to anthropogenic forces. Below we conclude the major findings of this paper as follows.

4.4.1 Impact of ENSO

Both AWAP and the reanalysis data show that La Niña years result in large areas of extreme rainfall in the summer months in Australia. The major distinction is seen in SEA, where during La Niña years, extreme rainfall occurs during spring months, possibly because of its strong covariance with IOD. However, this feature is not captured by the reanalysis analysed. Thus, it is possible that the reanalysis data do not accurately capture the interaction between ENSO and IOD and their teleconnections with rainfall in SEA, however, this needs to be tested further. The variability in the timing of extreme rainfall during La Niña events is higher compared to El Niño events, both in the observed as well as the reanalysis dataset. This is plausibly due to two factors, 1. A strong relationship between La Niña and Australia's rainfall and 2. High covariance between ENSO and other large-scale drivers. In other words, La Niña years are often associated with neutral/negative IOD (in spring) and positive SAM events (in summer). Also, extreme rainfall in the south of Australia can occur due to weather systems embedded within the westerlies in the south of Australia in winter. All these factors increase the likelihood of above-average rainfall in any season of the year. Thus, Rx5 can occur at any time of the year. Whereas the relationship between El Niño and Australia's rainfall is relatively weak,

therefore, the likelihood of extreme rainfall in summer and spring is low, which shrinks the window of extreme rainfall to occur only in cool months.

4.4.2 Impacts of IPO

A robust southward extension of the area of summer extreme rainfall is seen in nIPO years compared to pIPO years in SEA in both observed and reanalysis datasets. Similarly, the area of maximum standard deviation moves south and north according to the movement of summer extreme rainfall branch. Overall, higher variability is seen in pIPO years compared to nIPO events. This is possibly because; during nIPO phase, large-scale drivers are strongly related to Australia's rainfall, whereas, the relationships weaken during pIPO phase. However, the reanalysis dataset does not capture the high variability during pIPO; instead, it shows slightly higher variability during nIPO years.

4.4.3 The role of interaction between ENSO and IPO

Our results show that both IPO and ENSO influence the timing of extreme rainfall in southeast Australia, making the timing of extreme rainfall highly variable in this region. A clear southward extension of summer extreme rainfall is seen in nIPO years in both phases of ENSO in AWAP as well as the 20CR dataset. No major difference is seen between EN-nIPO and EN-pIPO years, although, major distinction is seen between LN-pIPO and LN-nIPO. This is also consistent with King *et al.* (2013), where there is a significant difference in extreme rainfall intensities between LN-pIPO and LN-nIPO. However, not much difference is seen between EN-nIPO and EN-pIPO years. Thus, it is possible that the intensity of extreme rainfall is dependent on which months it occurs in, as, usually depending on which month it occurs, it is modulated by different large-scale drivers. Further studies are required to understand if there is a consistent relationship between the month in which extreme rainfall occurs and extreme rainfall intensity. These types of studies, in combination with results presented in this article would help make a distinction between years with extremely damaging rainfall events and years with moderate extremes.

Overall, both ENSO and IPO constrain the variability significantly in Australia, especially in SEA. The maximum and minimum variability in the timing of extreme rainfall is seen during LN-pIPO and EN-pIPO years, respectively. The observed relationships between large scale drivers and extreme rainfall timing should be tested using ACCESS-S1, although to our knowledge, this has not been studied yet. The results presented in this paper indicate that

other large-scale drivers such as IOD and SAM potentially play key roles in modulating the timing of extreme rainfall in Australia. Furthermore, these large-scale drivers and their relationship with Australia's rainfall also undergo significant decadal variability, which adds to the complexity. Overall improving our understanding of the relationship between large-scale drivers and Australia's rainfall is crucial for improving seasonal prediction of extreme rainfall.

Chapter 5

Understanding extreme rainfall scaling rates in Australia in historical climate and future projections

Abstract

Understanding the relationship between extreme rainfall and temperature is of particular interest due to recent observed temperature increases. In theory, extreme rainfall is expected to increase at a rate similar to the Clausius-Clapeyron (C-C) rate, which is ~7%˚C^{-1}. Using observed surface or air temperature to calculate scaling rates show a weak positive relationship (increasing rainfall with increasing temperatures) in south Australia, whereas, a strong negative relationship (decreasing rainfall with increasing temperatures) is seen in the north. A set of CMIP5 models that produce scaling rates similar to observed using surface and air temperature are next analysed. Using dew point temperature (DPT), which demonstrates more consistent scaling rates across different climatic zones, we find a super C-C scaling rate in the tropical north (>20%C^{-1}) and south Australia (10-15%C^{-1}). To understand this regional variability in scaling rates, we further investigate the role of thermodynamic and dynamic factors. Our results show that the dynamic factors in the tropical north and the thermodynamic factors in the south play dominant roles in the super C-C rates. Further, we show using DPT that the scaling rates in extreme rainfall and the thermodynamic and dynamic factors examined (specific humidity, wind convergence and moisture flux convergence) are higher in future model simulations compared to the current period. Thus, scaling rates are non-stationary.

We further investigate the applicability of scaling rates in extrapolating extremes into the future by comparing extreme rainfall projections calculated using scaling rates and projections calculated by subtracting extremes in current climate from the future. Future projection of extremes using scaling rates is almost eight times higher than the changes calculated using the traditional approach. This study indicates the challenges associated with using scaling rates for studying extreme rainfall projections. Future studies should consider the non-stationary and non-linear aspects of extreme rainfall-DPT relationships to make

assessments of extreme rainfall projections. Overall significant knowledge gap still exists around scaling rates and the applicability for future extreme rainfall remains questionable.

Keywords: Extreme rainfall, temperature, Clausius-Clapeyron, climate change, scaling rates

5.1 Introduction

5.1.1 Temperature-extreme rainfall relationship

According to the Clausius-Clapeyron (C-C) relationship, the water vapour holding capacity of the Earth's atmosphere increases by 7% per degree increase in temperature (Trenberth *et al.*, 2003). Consistent with the C-C relationship, studies have shown that global atmospheric water vapour has increased at a rate of 7.3% per degree increase in global surface temperature (O'Gorman & Muller, 2010). However, the increase in mean rainfall with temperature is much smaller than the rate of increase in water vapour content in the atmosphere, approximately $2\%C^{-1}$ (Held & Soden, 2006). This lower rate of precipitation increase relative to the moisture availability is due to the energy balance constraint of the atmosphere (Pendergrass & Hartmann, 2014; Stephens & Ellis, 2008). However, in both observations and models, extreme rainfall increases at an equal or higher rate than the increase in mean rainfall, or even water vapour content (O'Gorman & Schneider, 2009; Pall *et al.*, 2007). Such significant increases in extreme rainfall with temperature could have severe socio-economic implications.

The purpose of studying the relationship between extreme rainfall and the temperature is that the available Global Climate Models (GCMs) show robust projections for temperatures compared to the precipitation, and confidence in extreme rainfall projections in climate models are low (Alexander & Arblaster, 2009). Thus, understanding the relationship between extreme rainfall and temperature could help in quantifying future changes in extreme rainfall using temperature projections (Wasko *et al.*, 2018), assuming one can explore climate change signal using scaling rates.

Although extreme rainfall intensity increases with temperature at the global scale (Allen & Ingram, 2002; Liu *et al.*, 2009), the relationship between extreme rainfall and temperature varies regionally and is not well known. The relationship is likely non-linear and complex (Hardwick Jones *et al.*, 2010). Several studies have studied the relationship between extreme rainfall and surface temperature at global (Allan & Soden, 2008; Wang G. *et al.*, 2017), as well

as at regional scales (Drobinski *et al.*, 2016; Jones *et al.*, 2009; Utsumi *et al.*, 2011). Previous studies found a non-linear hook shape relationship almost everywhere globally, where extreme rainfall increases with temperature but decreases after a threshold point (Drobinski *et al.*, 2016; Drobinski *et al.*, 2018; Wang X. *et al.*, 2017) – the decrease is strongest in the tropics (Utsumi *et al.*, 2011).

There have been many previous attempts to explain the non-linear temperature-extreme rainfall relationship. Some of the mechanisms proposed so far in different regions are seasonal variation and precipitation type (Berg *et al.*, 2009; Berg *et al.*, 2013), a decrease in precipitation event duration in Japan (Utsumi *et al.*, 2011), a stable and anticyclonic condition leading to reduced convection and higher sunlight, thus higher surface temperature (Wang G. *et al.*, 2017). Other factors that affect scaling rates but are beyond the scope of our study are time and spatial averaging, precipitation efficiency and vertical updrafts, and orographic lifting (Drobinski *et al.*, 2016).

5.1.2 Purpose of this study

Australia is one such location where scaling rates and the methods used are debated. Consistent with global studies, strong negative scaling rates are found in the northern part of Australia and weakly positive in southern parts (Bao *et al.*, 2017; Hardwick Jones *et al.*, 2010). Bao *et al.* (2017) suggest that the negative scaling is due to local cooling where north Australia experiences a considerable drop in temperature during extreme events. However, Barbero *et al.* (2018) suggest that the local cooling is a result of the statistical property of the autocorrelated nature of temperature data. Overall, most of the studies agree that extreme rainfall is usually associated with cooler surface temperatures (Barbero *et al.*, 2018). However, the colder surface temperature is not the first-order driver of negative scaling in Australia (Barbero *et al.*, 2018).

An increasing body of literature suggests that the dominant mechanism is the lack of moisture availability at higher temperatures (Ali *et al.*, 2018; Barbero *et al.*, 2018; Bui *et al.*, 2019; Hardwick Jones *et al.*, 2010; Lenderink *et al.*, 2018; Roderick *et al.*, 2019; Wasko *et al.*, 2018; Zhang *et al.*, 2019). The C-C relationship holds when relative humidity is constant, however, relative humidity is not constant in reality. Thus, the extreme rainfall does not scale according to the C-C equation (Hardwick Jones *et al.*, 2010). Therefore, using dew point

temperature (DPT), which takes into account the moisture availability, provides more consistent results across different climate zones (Barbero *et al.*, 2018; Wasko *et al.*, 2018).

Although there are studies investigating various methods of calculating scaling rates, few have examined the mechanisms behind the regional variations in scaling rates. A decomposition into thermodynamic and dynamic factors reveals that while thermodynamic factors lead to spatially homogeneous scaling rates and dominate the sign of the scaling globally, it is dynamical factors that cause the regional variations (Pfahl *et al.*, 2017). The variability is highest in the tropics where extreme rainfall increases at a much faster rate compared to the global rates (Sugiyama *et al.*, 2010). While Australia experiences a high degree of variability due to its location extended from tropics to the mid-latitudes, the reasons behind variations in extreme rainfall scaling rates remain unclear.

This research aims to understand the regional variations in historical scaling rates in Australia and the role of thermodynamic and dynamic factors, including in future model simulations. There is a fundamental knowledge gap in this field, where the relationship between climate variability and scaling rates is not clear. Although, the rationale for studying scaling rates in many studies was presented as to robustly project extreme rainfall (Ali *et al.*, 2018; Ali & Mishra, 2017; Bao *et al.*, 2017; Mukherjee *et al.*, 2018). There has not been any study yet testing whether applying these scaling rates can be used to extrapolate extreme rainfall into the future. Next, this study explores the drawbacks of using this method to extrapolate extreme rainfall into the future.

5.2 Methods

5.2.1 Data

We use daily mean rainfall and temperature data from the Australian Water Availability Project (AWAP) over the period 1986-2015 at 0.25º×0.25º horizontal resolution (Jones *et al.*, 2009). Although the minimum rainfall recorded in the station dataset is 0.1mm/day, the gridded dataset can have much smaller values due to interpolation and spatial smoothening. Thus, it is crucial to remove days with insignificant precipitation values to avoid spurious trends. In this study, we only use the days in both AWAP and models when rainfall exceeded 0.1mm. As there are very few stations available in the central and western part of Australia, we mask these regions in AWAP following the approach of Chung and Power (2017).

We use daily datasets from 18 of the Coupled Model Intercomparison Project phase 5 (CMIP5) models (only one realisation is used for each model) standard historical simulation (with time-evolving natural and anthropogenic forcings) that have rainfall, surface air temperature, surface specific humidity, surface relative humidity, surface winds, and air temperature datasets available for this study (Taylor *et al.*, 2012). The models used here are listed in Table 5.1. As the historical simulation ended in 2005, the historical and RCP8.5 (high emission scenario) datasets are concatenated to carry out a continuous analysis for the period 1986-2015 in models to represent the current climate. All the models are regridded to a common 1.5˚x1.5˚ grid over the land region (the original resolution of each model is listed in Table 5.1). All calculations are performed in each model simulation and averaged across models to get the multi-model mean value. We divide Australia into three regions for the analysis, north of 30˚S; hereafter called as north Australia (NA), north of 17˚S; hereafter called as tropical north Australia (TNA), and south of 30˚S; hereafter called as south Australia (SA). The reasons for choosing these regions are further discussed in the result section.

Table 5.1 List of the 18 CMIP5 models used for this study (Taylor *et al.*, 2012).

Model names	Model resolution
ACCESS1.0	1.25×1.875
BNU-ESM	2.7906×2.8125
CNRM-CM5	1.4008×1.40625
CSIRO-MK3.6.0	1.8653×1.875
CanESM2	2.7906×2.8125
GFDL-CM3	2×2.5
GFDL-ESM2G	2.0225×2
GFDL-ESM2M	2.0225×2.5
HadGEM2-CC	1.25×1.875
IPSL-CM5A-LR	1.8947×3.75
IPSL-CM5A-MR	1.2676×2.5
IPSL-CM5B-LR	1.8947×3.75
MIROC-ESM	2.7906×2.8125
MIROC-ESM-CHEM	2.7906×2.8125
MIROC5	1.4008×1.40625
MRI-CGCM3	1.12148×1.125

BCC-CSM1.1	2.7906×2.8125
INM-CM4	1.5×2

5.2.2 Scaling methods

We calculate scaling rates in extreme rainfall in observations and models by applying several steps:

1. We rank the daily precipitation data by daily temperature (rainfall amounts associated with highest to lowest temperature) at every grid point using a 30 years dataset (1986-2015) in observations and models.
2. We segregate the rainfall and temperature datasets into 12 bins allowing adequate data to fit a linear regression (Hardwick Jones *et al.*, 2010). The number of data points in each bin is the same, and we only consider bins that have at least 100 data points to make sure we have enough data points in each bin to carry out statistical calculations.
3. Next, the 99^{th} percentiles of precipitation amount were calculated in each bin. The median temperature of each bin (called the 'bin temperature') is calculated.
4. The 99th percentile precipitation depths (PD) are calculated for each bin. The PD is the sum of rainfall of all the events >=99th percentile).
5. Finally, to calculate the scaling rate, linear regression is fitted to the logarithm of extreme precipitation depths and the bin temperature following Hardwick Jones *et al.* (2010).

Also, binning rainfall data over a period using daily ascending (descending) temperature values would line up the rainfall values from winter to summer (summer to winter), making this method sensitive to seasonality. Thus, we calculate the scaling factors in four different seasons in Australia, DJF (December – February), MAM (March-May), JJA (June-August), and SON (September – November) to understand the seasonal variability of scaling rates. We use a longer time period, 1911-2015 for calculating scaling rates in each season, as using 1986-2015, many regions did not satisfy the criteria of containing enough data points (at least 100 data points) in each bin to calculate the 99th percentile.

The DPT at 2 m is calculated using the formula following Zhang *et al.* (2019)

$DPT=\frac{257.14\times X}{18.678-X}$; Where $X=\log\frac{RH}{100}+\frac{18.678\times T}{257.14+T}$

Where RH is relative humidity (%), and T represents surface temperature (˚C).

To explore the research questions, a similar binning method is applied to a broader set of variables, specific humidity, wind convergence and moisture flux convergence (MFC) in model datasets. Similar to rainfall scaling, only rain days (days with rainfall ≥0.1 mm) are considered for calculating scaling rates of other variables. The MFC is calculated following Banacos and Schultz (2005) using the formula:

$$MFC=\underbrace{-u\frac{\partial q}{\partial x}-v\frac{\partial q}{\partial y}}_{(1)}\underbrace{-q(\frac{\partial u}{\partial x}+\frac{\partial v}{\partial x})}_{(2)}$$

Where the first term on the right hand of the equation represents moisture advection and the second term is moisture convergence, and q is specific humidity of the near-surface atmosphere.

Similarly, wind convergence is calculated as

$$\text{Wind convergence}=-(\frac{\partial u}{\partial x}+\frac{\partial v}{\partial x})$$

Where u and v are surface zonal and meridional wind components (m/s), respectively.

The scaling rates in specific humidity, MFC and wind convergence are calculated by applying linear regression to the logarithm of the percentile depth of the variable. Note, using simply the 99th percentile of the variable in each bin instead of using the logarithm of percentile depth result in same slopes.

5.2.3 Future extremes storylines

To calculate the scaling rates in future simulations, we calculate scaling rates in rainfall as well as other variables in the period 2061-2090 in CMIP5 model simulations. Next, we create four storylines of future change in annual maximum 1-day precipitation (Rx1) (Zhang *et al.*, 2011).

(a) ***The RCP8.5 – hist storyline***: Percentage changes in mean Rx1 between historical (1986-2015) and RCP8.5 (2061-2090) simulations in all models.

In the next three scenarios, Rx1 is extrapolated ($Rx1_{extrap}$) using the following formula:

$Rx1_{extrap}=Rx1_{hist}\times (1+ \text{scaling factor})^{\Delta DPT}$---------- (1)

Where $Rx1_{hist}$ is the mean Rx1 calculated in each CMIP5 model over the period 1986-2015. ΔDPT is the change in DPT between the periods 1986 – 2015 and 2061-2090; the scaling factor varies in different scenarios.

(b) ***The C-C scaling storyline***: The percentage change between $Rx1_{extrap}$ and $Rx1_{hist}$ using 7% future increase according to C-C relationship. For example, using this storyline equation (1) would look like:

$Rx1_{extrap}=Rx1_{hist}\times (1+ 0.07)^{\Delta DPT}$

(c) ***The historical scaling storyline***: The percentage change in $Rx1_{extrap}$ and $Rx1_{hist}$ using scaling rates calculated over the period 1986-2015.

(d) ***The RCP8.5 scaling storyline***: The percentage change in $Rx1_{extrap}$ and $Rx1_{hist}$ using scaling rates calculated over the period 2061-2090.

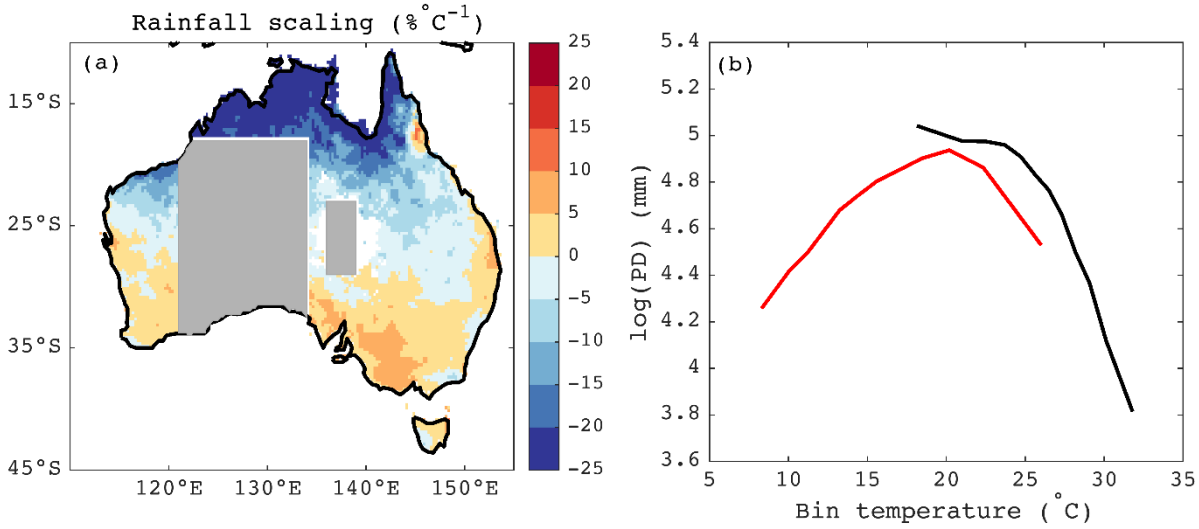

Figure 5.1 (a) Scaling (%˚C^{-1}) of the 99th percentile of rainfall using daily mean surface temperature and (b) the logarithm of the percentile depth of the 99th percentile of rainfall in each bin in north Australia (black curve) and south Australia (red curve) plotted against the bin temperature (the median temperature of each bin). The AWAP data is used over the period 1986-2015.

5.3 Results

5.3.1 Observed and modelled scaling rates in extreme rainfall

The scaling rates of the 99th percentile of rainfall with temperature shows a strong north-south spatial pattern in AWAP data (Fig. 5.1a). The scaling rates in the north are below –21%˚C^{-1}, and in southern latitudes are 2-4 %˚C^{-1}. Due to the north-south pattern, we compare the variation in the PD across temperature bins in NA and SA (Fig 5.1b). The PD in NA shows a sharp decline with an increase in temperature resulting in a strong negative scaling, in SA the PD shows a hook shape. The temperature after which the PD starts to decrease is known as the break-point temperature, which is observed in many previous studies (Berg *et al.*, 2009; Drobinski *et al.*, 2018). The break-point temperature is 18.3˚C for NA and 20.1˚C for SA (Fig 5.1b). Scaling rates calculated using surface temperature show large deviations from expected C-C scaling rate.

As reported by previous studies that binning method is sensitive to seasonality (Ali *et al.*, 2018; Zhang *et al.*, 2017), next, we investigate the scaling rates in four seasons in Australia, shown in the left panel of Figure 5.2. The middle panel shows the PD vs bin temperature plots in NA and SA. The panel on the right shows the correlation between seasonal Rx1 and the corresponding surface temperature calculated over the period 1911-2015. Note, using 1986-2015 for Figure 5.2 does not change overall spatial scaling patterns. The scaling rates are mostly negative in summer in Australia, except in a few regions in the south (Fig. 5.2a). The PD decreases monotonically in both regions (Fig. 5.2b). During MAM, and SON strong negative scaling rates are observed in the north, and sub C-C scaling rates are observed in the south (Fig. 5.2d, j). During JJA, there were not enough data points in each bin in the NA as it is the dry season (Fig. 5.2g). The scaling rate in the SA shows positive values in most regions that are comparable to the C-C relationship. This is because, in winter, the temperatures are below the usual break-point temperature (i.e. below 20˚C) in both the regions. The correlation maps between Rx1 and the corresponding surface temperature show clear similarity with the maps of scaling rates in all seasons (Fig. 5.2c,f,i,l). This similarity indicates that extreme rainfall coincides with relatively cooler temperatures across all seasons, especially in warmer months (December - May). Besides, strong north-south scaling pattern is evident in all seasons, except for summer when negative scaling is seen almost everywhere in Australia. Thus, negative scaling in the north cannot be attributed to the sensitivity to the seasonality of this method.

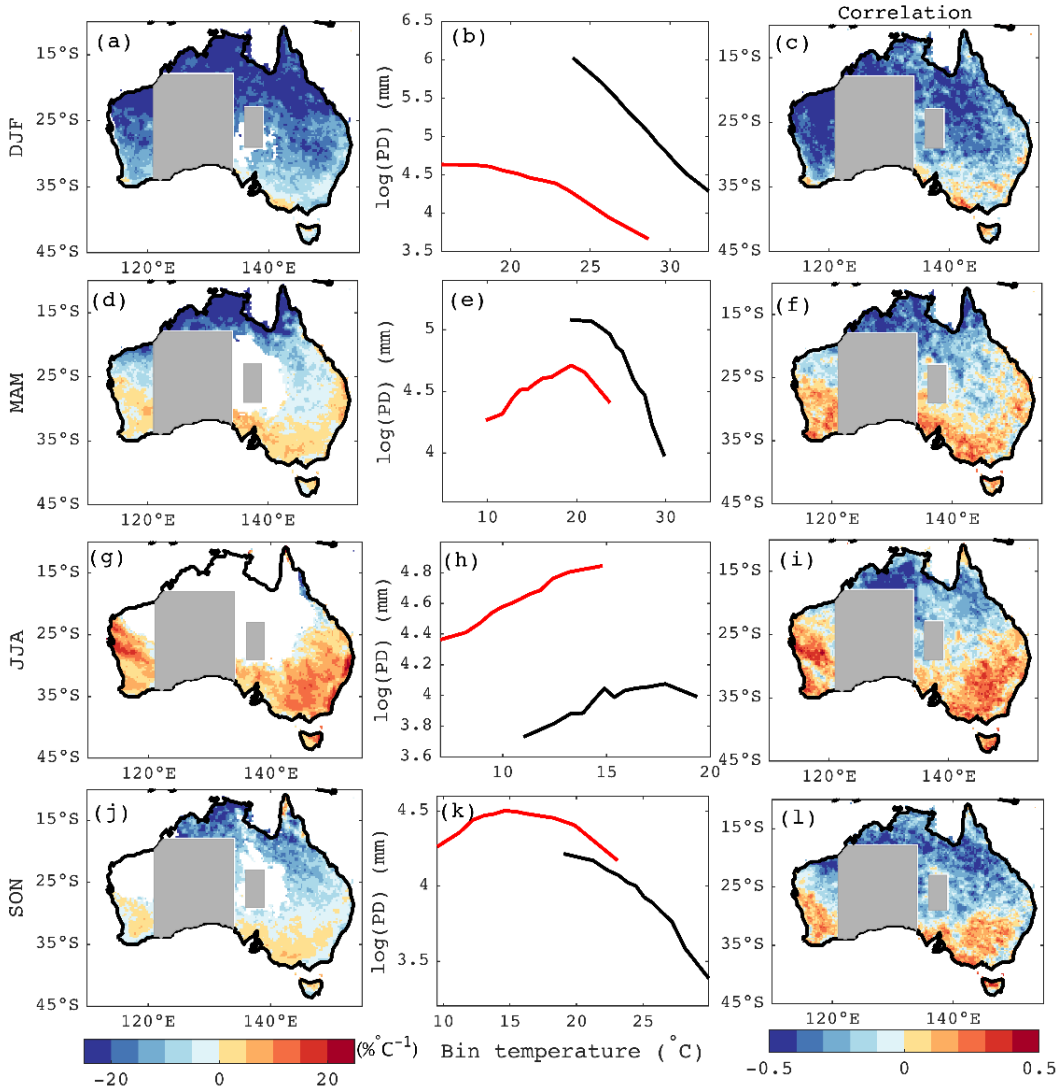

Figure 5.2 The panel on the left shows the scaling rates (%˚C^{-1}), the middle panel shows the logarithm of the percentile depth vs surface temperature plot averaged in north (black curve) and south Australia (red curve). The right panel shows the correlation between seasonal Rx1 and the corresponding temperature on the day. The plots are shown for December-February (a-c), March-May (d-f), June-August (g-i), and September-November (j-l). The AWAP data is used over the period 1911-2015.

Next, we investigate if the CMIP5 models produce consistent results with observed scaling rates in order to use them further for examining future projections. The scaling using surface temperature in the multi-model ensemble mean using CMIP5 models shows a similar north-south polarity in scaling rates (Fig. 5.3a). The PD of the extreme rainfall in NA shows a strong decline after the break-point temperature in most of the models; however, the spread in PD values across models in NA is slightly higher than SA (Fig. 5.3b). Overall, the models capture the hook shape in both the regions and the break-point temperatures are 22.9 ˚C and 20.5 ˚C in NA and SA respectively in the multi-model mean. Next, we use air temperature to

bin the extreme rainfall to test if the scaling rates more closely match observations. Although using air temperature reduces the magnitude of the negative scaling rate – the sign of scaling remains similar (Fig. 5.3c). The PD vs air temperature plot shows a strong hook shape in both regions (Fig. 5.3d). Thus, surface cooling due to extreme rainfall event does not explain the strong negative scaling in the north. This reaffirms that local cooling due to extreme rainfall event might place some of the extreme events to the cooler bins but is not the fundamental mechanism of the negative scaling rates in the north. Although, surface cooling might lead to a regional variation in the scaling rates. For example, strong positive scaling rates in the northeast is observed, whereas the northwest still shows negative values. Also, the models analysed here replicate the scaling rates using surface and air temperatures reasonably well, thus increasing confidence in models.

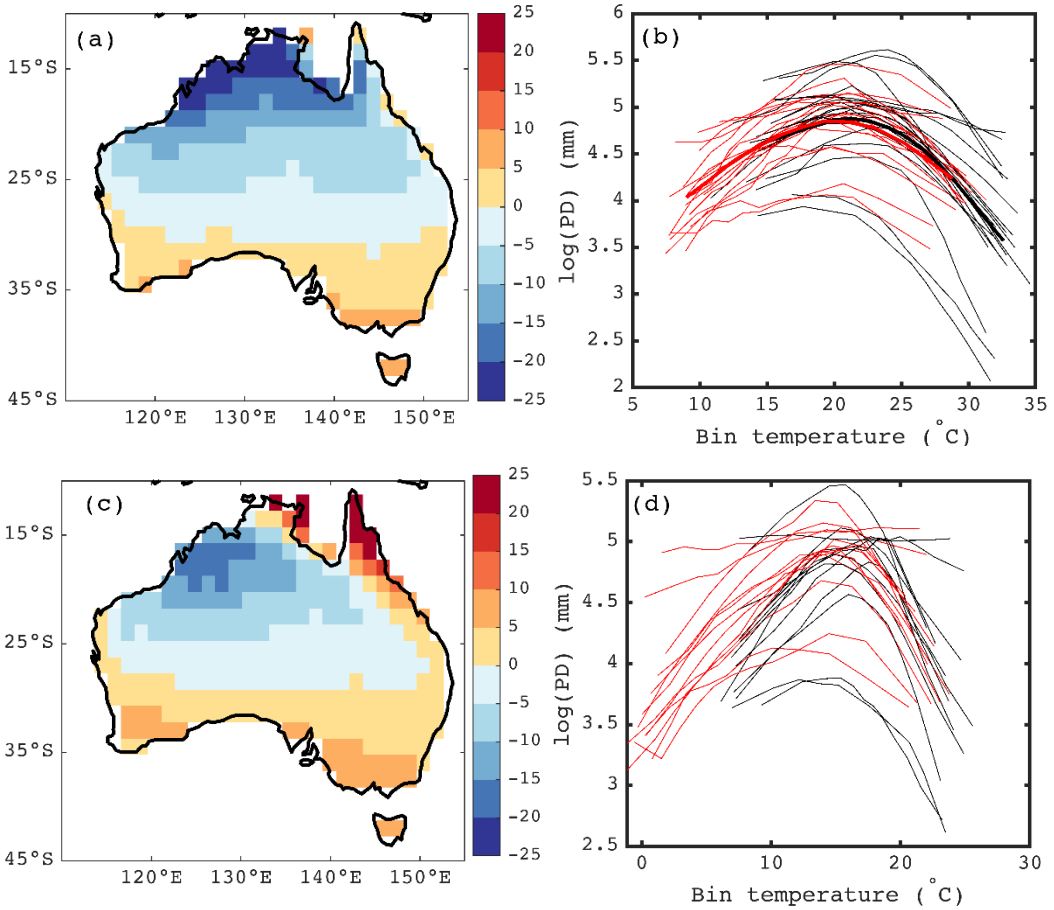

Figure 5.3 The left panel shows the scaling rates (%˚C^{-1}) of the 99th percentile rainfall using (a) surface temperature and (c) air temperature (at 850 hPa) in CMIP5 ensemble mean. The right panel shows the logarithm of the percentile depth of the 99th percentile of rainfall in north Australia (black curve) and south Australia (red curve) in each bin vs (b) surface temperature (d) air temperature in 18 CMIP5 models and ensemble mean (thick lines).

Previous research shows that DPT produces scaling rates that are more comparable to C-C rate than the surface and air temperature in previous studies (Ali & Mishra, 2017; Barbero *et al.*, 2018; Bui *et al.*, 2019; Lenderink *et al.*, 2017; Roderick *et al.*, 2019; Wasko *et al.*, 2018). Many studies have reported scaling rates using DPT in observations in Australia, for example, Figure 1 of Ali *et al.* (2018), and Figure 2 of (Bui *et al.*, 2019) show observed scaling rates using DPT. We use these figures to compare scaling rates in CMIP5 model historical simulations. The extreme scaling rates using DPT in the CMIP5 model ensemble mean shows positive scaling rates in Australia (Fig. 5.4), consistent with previous observational studies. The scaling rates in the TNA exceeds 20% $^{\circ}C^{-1}$, and in SA ranges between 10-15%$^{\circ}C^{-1,}$ indicating a super C-C scaling rate in both regions. Using station datasets previous studies show a scaling rate close to 10%$^{\circ}C^{-1}$ near Darwin (Wasko *et al.*, 2018), and the majority of the stations in the tropics show scaling rate >10%$^{\circ}C^{-1}$ (see Fig. 3 of Zhang *et al.* (2019)). Due to the super C-C relationship in the TNA and SA regions in CMIP5 models, we investigate the scaling rates in these regions in depth.

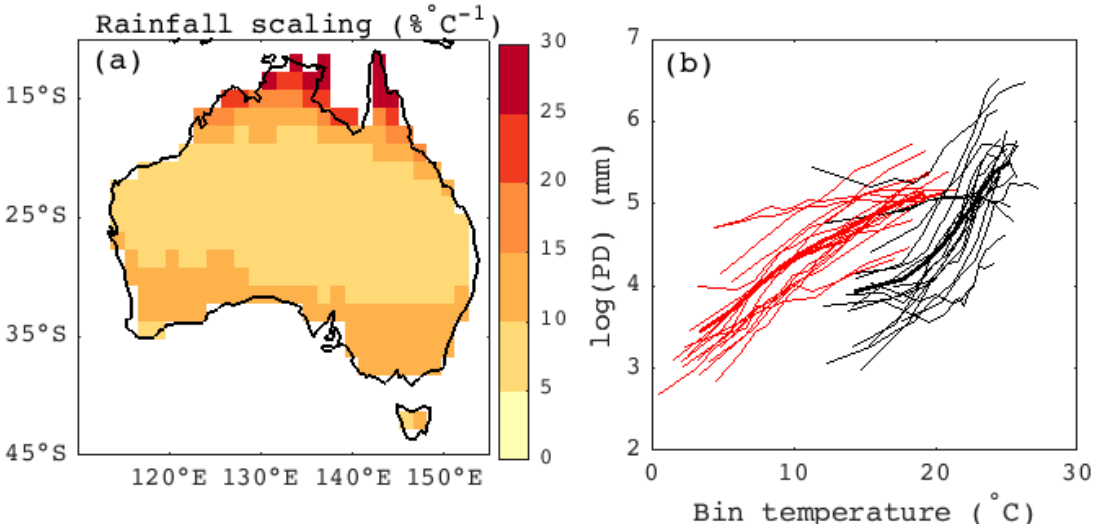

Figure 5.4 The scaling rates (%$^{\circ}C^{-1}$) of the 99th percentile rainfall using dew point temperature in CMIP5 ensemble mean. (b) The logarithm of the percentile depth of 99th percentile of rainfall vs bin temperature (the median dew point temperature of each bin) in tropical north Australia (black curve) and south Australia (red curve) in each bin in 18 CMIP5 models and ensemble mean (thick lines).

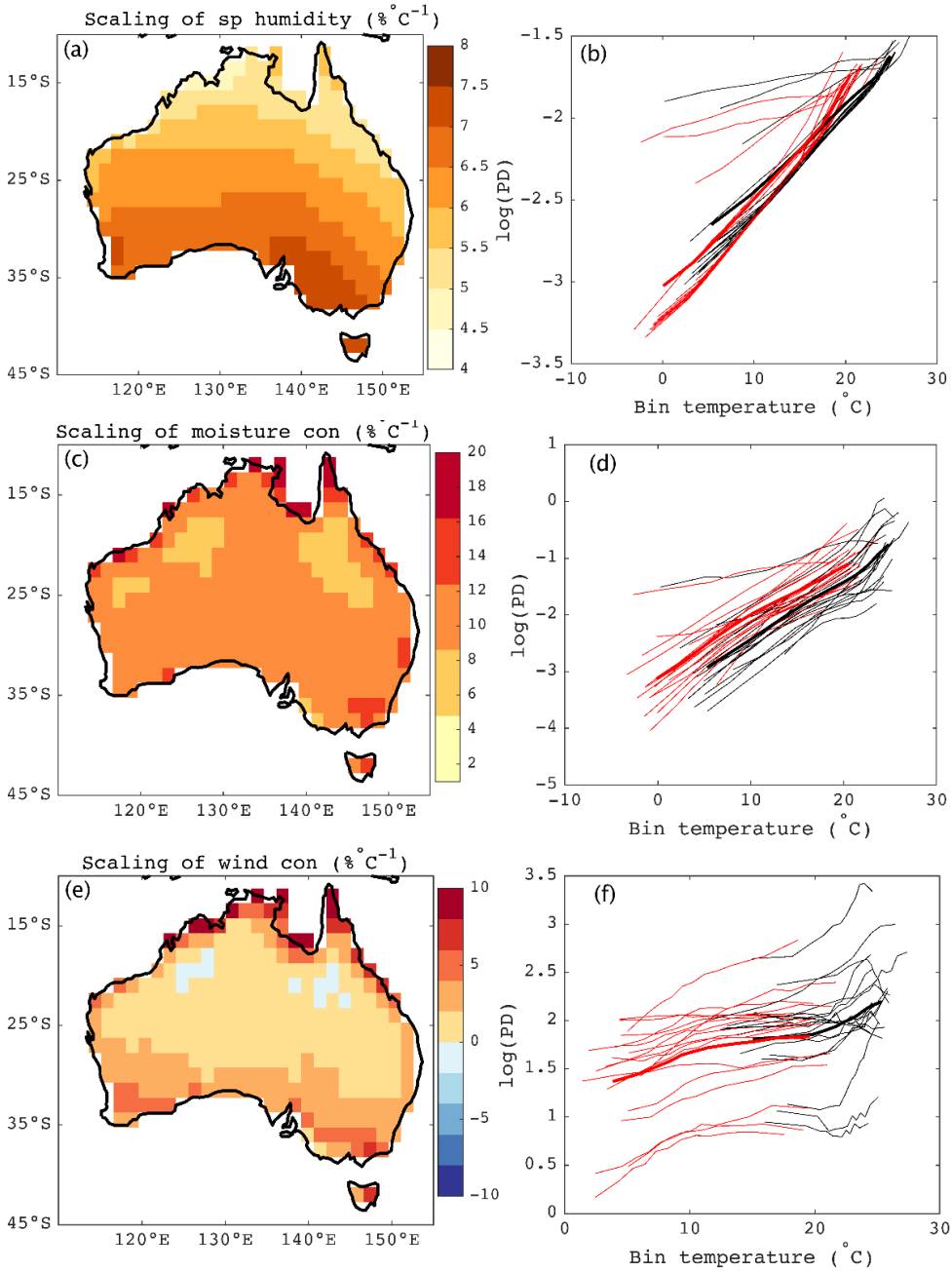

Figure 5.5 The scaling rates (%˚C^{-1}) of the 99th percentile of (a) specific humidity, (c) wind convergence, and (e) moisture convergence in the CMIP5 ensemble mean using 18 CMIP5 models over the period 1986-2015. The logarithm of the percentile depth of (b) specific humidity, (d) wind convergence and (e) moisture convergence in northern Australia (black curves) and southern Australia (red curves) in each bin, the thick black and red curves show the percentile depth vs temperature variation in CMIP5 model ensemble mean in north Australia and south Australia respectively.

5.3.2 Scaling rates in thermodynamic and dynamic factors of extreme rainfall in models

To understand the regional variation in scaling rates, specifically super C-C scaling rates evident in the TNA and SA in climate models, we looked at the driving factors of extremes.

We examine three main factors: thermodynamics (moisture availability), dynamics (wind convergence), a combination of thermodynamics and dynamics (the moisture flux convergence). We use DPT to study the role of dynamic and thermodynamic parameters in extreme rainfall scaling rates. The source of moisture for moderate and heavy rainfall events is usually moisture transported from elsewhere instead of regional evaporation (Trenberth *et al.*, 2003). Thus, low-level moisture flux convergence fuels extreme rainfall events. The MFC, which is a combination of dynamics and thermodynamics, plays a crucial role in forming extreme rainfall bearing systems (Holman & Vavrus, 2012).

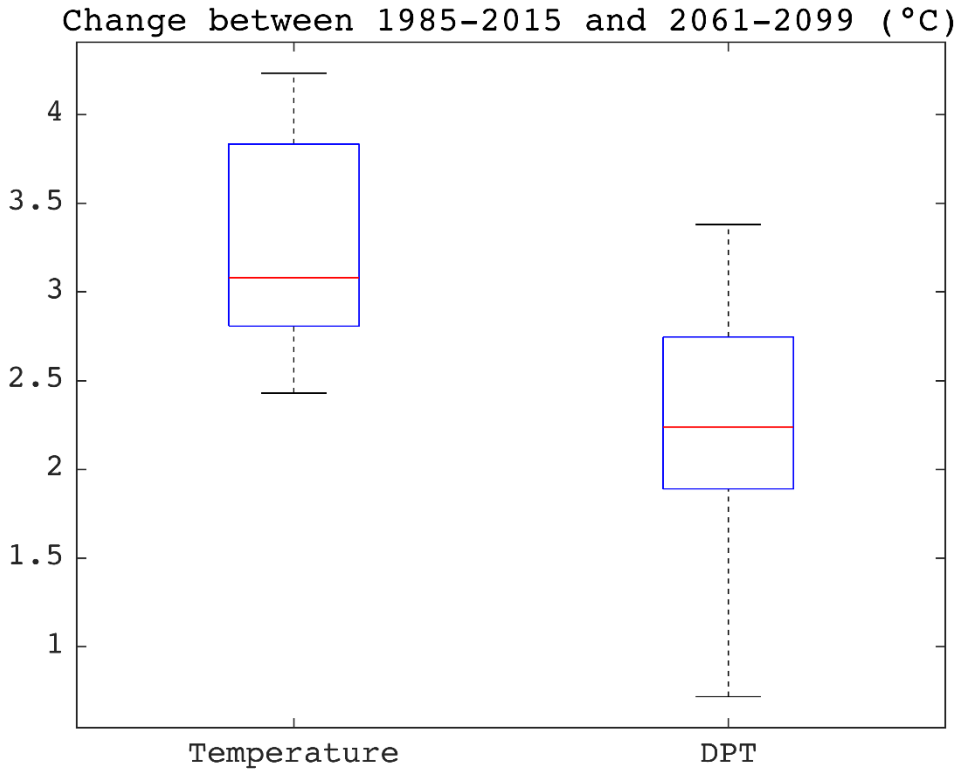

Figure 5.6 The change in temperature (˚C) and dew point temperature (˚C) between the periods 1986-2015 and 2061-2090 in CMIP5 models, area averaged over Australia. The box shows the 25-75th percentile, and the whiskers show the 5-95th percentile spread across models.

We first study the scaling rate of surface specific humidity with DPT. The scaling rates of specific humidity are positive all over the continent (Fig. 5.5a), strongest in the SEA and Tasmania (>8%˚C^{-1}). However, the scaling rates decline northward, reducing to 4%˚C^{-1} in the TNA. The PD vs DPT plot shows that it increases steeply; however, at the high temperature bins, the increase becomes even steeper (Fig. 5.5b). The spatial pattern of scaling rates of MFC is positive everywhere (Fig. 5.5c), the values are higher in the coastal regions of Australia –

highest in the tropical north and the SEA – where a strong scaling rate in specific humidity at the surface is observed (Fig. 5.5a). The values in most of the regions range from 9 to 12%˚C^{-1}, and in the north, it is >16%˚C^{-1}. The PD of MFC in both regions show a steady increase (Fig. 5.5d).

Next, the scaling rates in the dynamical component of the MFC – i.e. surface wind convergence is shown in the bottom panel of Figure 5.5. High wind convergence is required for the formation of extreme rainfall events as strong convergence helps to form rain bearing systems given the right atmospheric conditions. The scaling rates in surface wind convergence exceed 10%˚C^{-1} per degree in the TNA, where CMIP5 models produce super C-C scaling rates. The values are small in the central regions but increases in the southern parts of Australia, however, the scaling rate in the south is lower than the TNA. The PD vs bin temperature plot shows that although the models show similar slopes, there is a large range of wind convergence values across models indicating a higher degree of uncertainty among models in both regions (Fig. 5.5f). Again, this shows although models produce consistent results for thermodynamic factors, there are significant discrepancies simulating dynamics of the atmosphere, especially in the tropics (Sugiyama *et al.*, 2010).

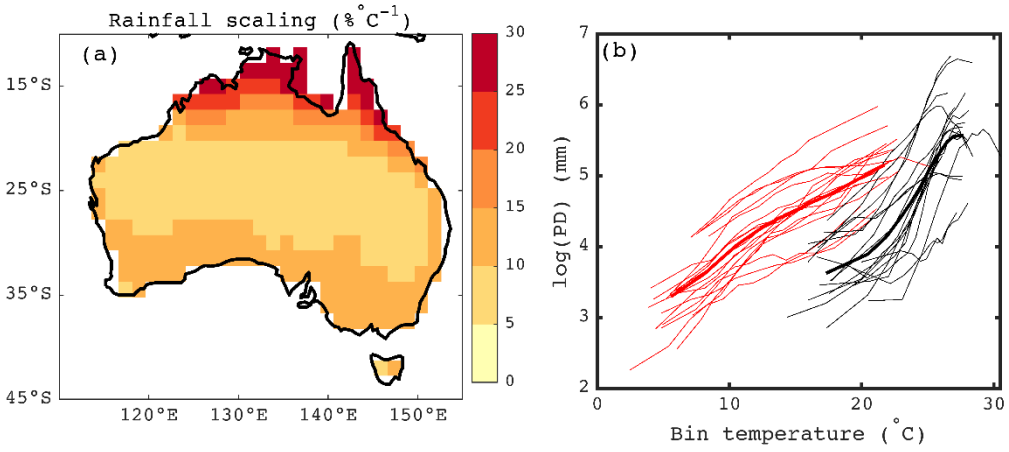

Figure 5.7 Same as Fig. 5.4, but for the time period 2061-2090 using RCP8.5 simulations.

5.3.3 Future scaling rates and extremes scenarios

As stated earlier, the overarching purpose of studying scaling rates is to provide robust projections of rainfall extremes. To provide robust projections for extreme rainfall using DPT, the first question that needs to be answered is - do climate models project DPT robustly? This is difficult to address, as gridded DPT data is not freely available in Australia, which makes it

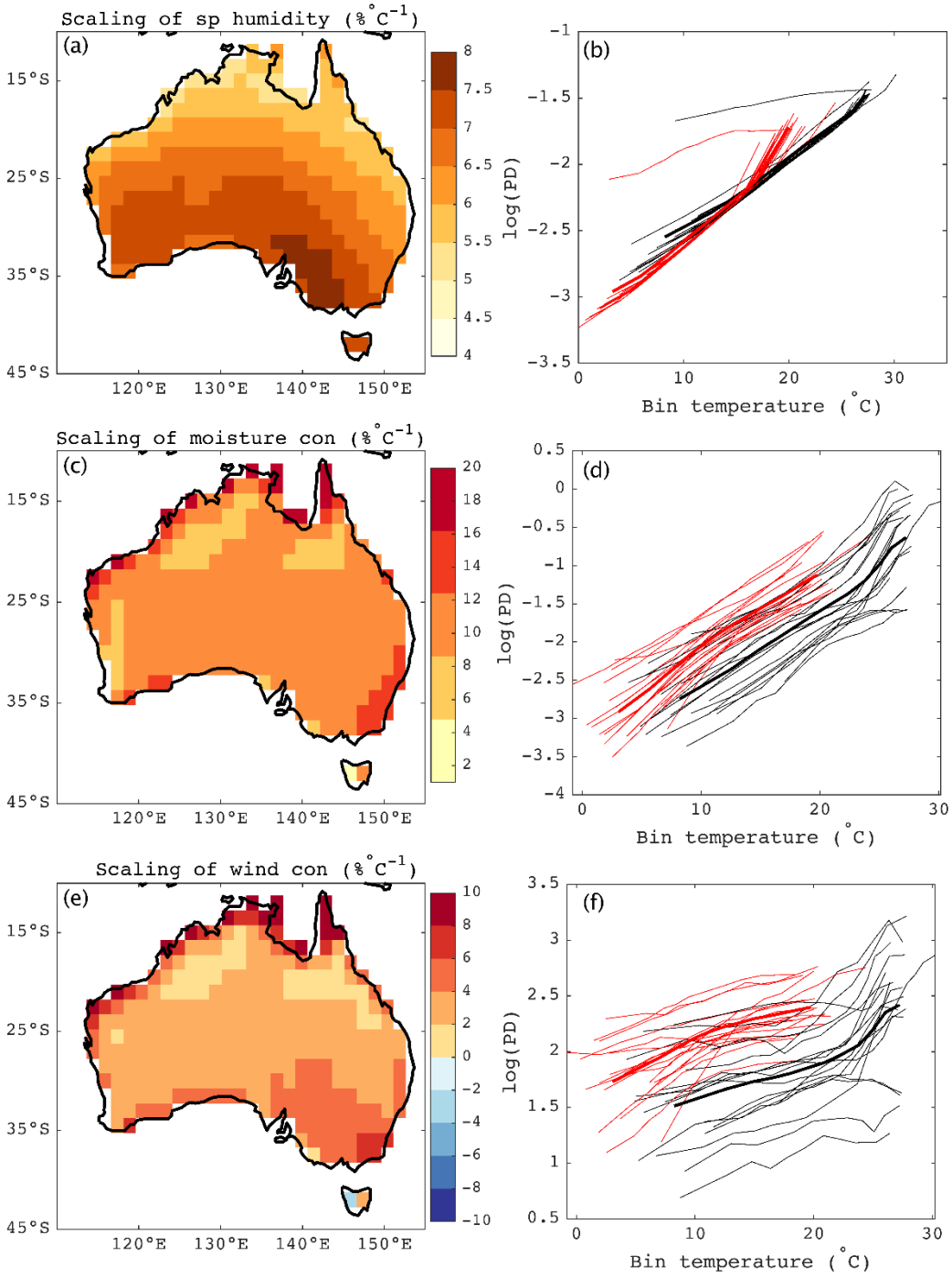

Figure 5.8 Same as Fig. 5.6, but over the period 2061-2090 in RCP8.5 simulations.

challenging to compare model historical simulations with observations. However, previous studies have already shown a robust historic as well as future increase in temperature (Lenderink & Attema, 2015; Lucas, 2010). Figure 5.6 shows changes in daily mean temperature and DPT between two periods 1985-2016 and 2061-2090 in models. All models show increases in both temperature as well as DPT in future, however, the model spread is 20% higher in DPT compared to the temperature. Overall, the figure shows a good agreement among the models in projecting DPT. The future scaling rate of extreme rainfall with DPT over the

period 2061-2090 using CMIP5 model ensemble mean shows a spatial pattern similar to the historical rates (Fig 5.7). The scaling rates, averaged over Australia, increase by almost 26.5% compared to the scaling rates calculated using the period 1986-2015. The scaling rates are positive everywhere and stronger than the historical scaling rates, > 25% C^{-1} in the TNA (Fig. 5.7a). The PD vs DPT plot shows a steeper slope for the TNA and SA (Fig. 5.7b). The increase in scaling rates in future period implies a non-stationarity in the relationship between extreme rainfall and DPT.

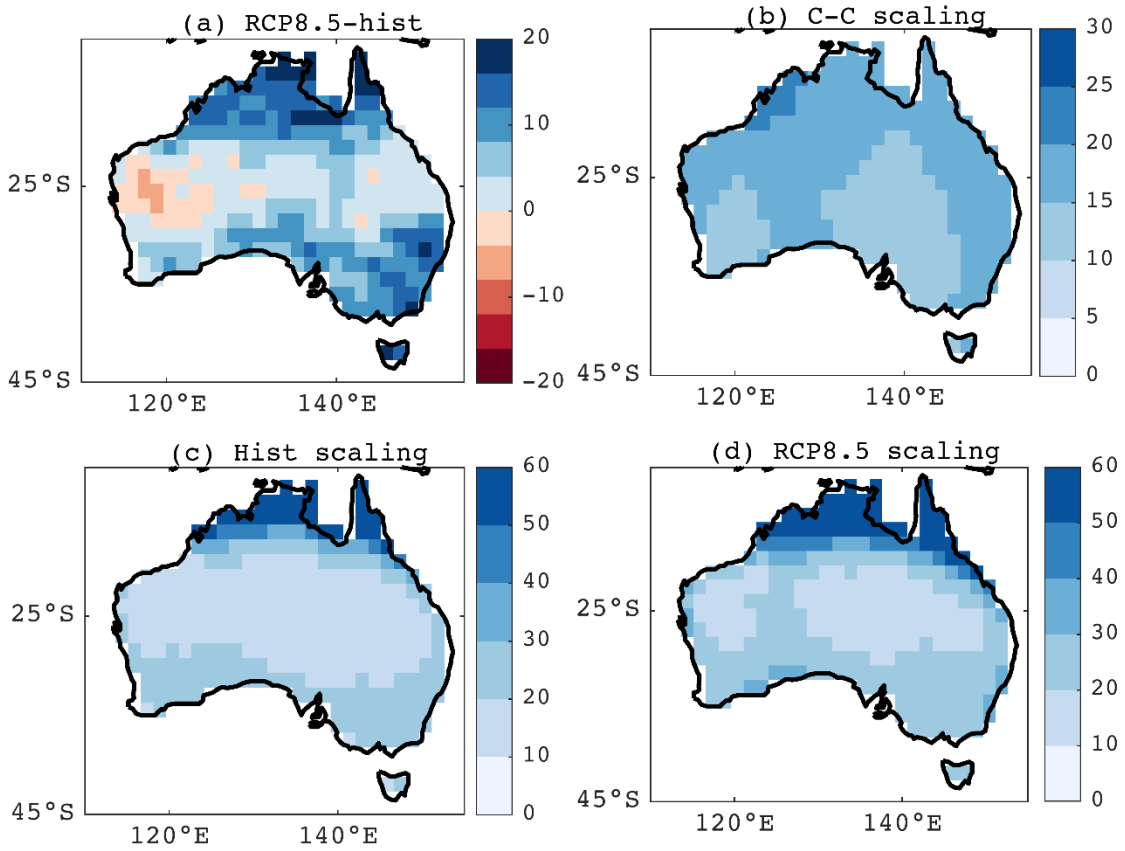

Figure 5.9 Ensemble mean of the percentage change in Rx1 in Australia in (a) the RCP8.5 – hist storyline (b) The C-C scaling storyline (c) the historical scaling storyline (d) the RCP8.5 scaling storyline. Refer to the method section for more details on the storylines.

The scaling rates in specific humidity, moisture convergence and wind convergence in future simulations show increase in the future period, although the spatial patterns remain similar to the historical scaling rates (Fig. 5.8). Similarly, the PD versus DPT graphs show similar patterns to the historical plots, although the slopes are steeper for the future period.

Next, we investigate the changes in extreme rainfall intensity in four storylines (defined in section 5.2.3) to understand the potential change in extreme rainfall intensity with DPT change.

Figure 5.9 shows the percentage change in Rx1, and Figure 5.10 shows the area-averaged change in Rx1 intensity in CMIP5 models to provide an estimate of the model spread. ***The RCP8.5 – hist storyline*** shows a continent-wide increase in the intensity of Rx1 in Australia, except for parts in West Australia (Fig. 5.9a), which is in line with the expectation that extremes are projected to increase. The spatial pattern in the percentage change in Rx1 is similar to the scaling rates in Fig 5.4. A higher increase in Rx1 is projected in the north and southeast Australia which is where we see higher scaling rates. The multi-model median shows a 5.7% change in Rx1 intensity between the two periods analysed, although multi-model median shows an increase of 2.2˚C in DPT. More than 75% of the models show a future increase in Rx1 in Australia (Fig. 5.10); however, there is considerable regional variation.

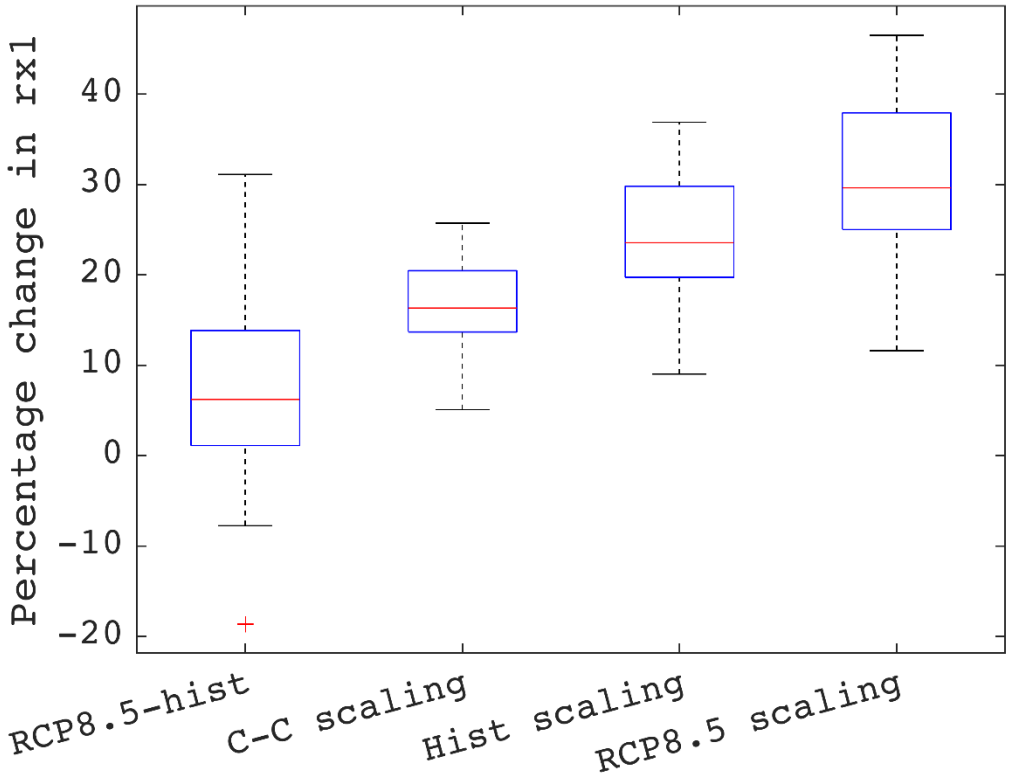

Figure 5.10 Box and whisker plot of area averaged percentage change in Rx1 in 18 CMIP5 models in Australia in (a) The RCP8.5 – hist storyline (b) The C-C scaling storyline (c) the historical scaling storyline (d) the RCP8.5 scaling storyline. Refer to the method section for more details on the storylines.

For the next three storylines considered, the changes are only positive as we assume an increase in Rx1 by different scaling factors. ***The C-C scaling storyline*** shows a 5-25% change with a median change of 16% in Australia; the increase is again maximum in the NA (Fig. 5.9b). The spatial changes in Rx1 in ***the historical scaling storyline*** and ***the RCP8.5 scaling***

storyline are mostly dominated by the scaling rate pattern. The range of changes in intensities in ***the historical scaling storyline*** and ***the RCP8.5 scaling storyline*** is 16-49% and 21-66% respectively. The multi-model median changes in Rx1 are 33% and 44% using historical and RCP8.5 scaling rates, respectively. These values are much higher than the future changes in extreme rainfall by using the traditional approach. These extremely high values of extreme rainfall change do not follow the historical change in extreme rainfall in Australia, where we have not seen any drastic increase in extreme rainfall since the 1950s, except for northwest Australia (Dey *et al.*, 2019). In addition, the interpolation of future extreme rainfall assumes one directional change in extremes, thus it cannot capture the regional variations in extreme rainfall changes. Overall, the applicability of scaling rates to project extreme rainfall remains questionable.

5.4 Discussion and concluding remarks

Several studies have examined the relationship between extreme rainfall and surface temperature in various regions, including Australia, where a negative scaling rate has been calculated in the north and a weakly positive scaling rate in the south. Previous studies suggest that the scaling rates can be used as an alternative method to robustly project extreme rainfall. In this study, we first aim to understand the regional variations in extreme scaling rates and the role of dynamic and thermodynamic factors. Next, we calculate the scaling rates in future simulations. Finally, an attempt has been made to answer the question, "can scaling rates be used to robustly project extreme rainfall?"

There are many arguments in this area of research. The most pronounce argument is which variable is suitable for studying scaling rates? Although a few regions globally show scaling rates that are comparable to the C-C rates using surface and air temperature, majority of the regions globally show negative scaling rates (Ali *et al.*, 2018; Pfahl *et al.*, 2017). Many studies suggest that the surface temperature is not an ideal parameter for studying scaling rates (Bui *et al.*, 2019; Wasko *et al.*, 2018; Wasko & Nathan, 2019). In addition, Ali and Mishra (2017) showed that surface temperature fluctuations play only a small role in strong negative scaling rate by affecting the binning method. Although, in Australia, the scaling rates using air temperatures improve but maintain a negative in the north and weakly positive in the south pattern in observations (Bui *et al.*, 2019) as well as in model simulations. Using observed DPT to calculate scaling rates show consistent values across the globe, although many regions show higher than C-C scaling rate (Ali *et al.*, 2018). Our results show consistent results using a set

of 18 CMIP5 models, where using surface temperature result in strong negative scaling rate in most regions in Australia, using DPT temperature result in comparable results to observed (see Figure 2 of Roderick *et al.* (2019)). Thus, the CMIP5 models show remarkable agreement across models as well as with observations. Overall, DPT provides consistent result across regions in Australia, where a positive relationship between DPT and extreme rainfall is resulted using both observed and climate model datasets.

Many regions have experienced a much higher scaling rate values than C-C rate (super C-C scaling). Using globally averaged temperature to calculate extreme rainfall scaling produces a 95%/K increase in the top 10% of rainfall intensity (Liu *et al.*, 2009). A super C-C scaling relationship has been found, especially in hourly and sub-daily data in some parts, for example –in the Netherlands (Lenderink *et al.*, 2017; Lenderink & van Meijgaard, 2008), Australia (Guerreiro *et al.*, 2018; Wasko *et al.*, 2018), North America (Mishra *et al.*, 2012; Shaw *et al.*, 2011), and India (Ali & Mishra, 2017). Almost 33% of stations globally show super C-C scaling rates for daily extremes (Ali *et al.*, 2018). Another study showed that 18 out of 34 stations in Australia and surrounding territories show scaling rates above $9\%^{\circ}C^{-1}$ (see Figure 5.3 of Bui *et al.* (2019)). Thus, observations already indicate super C-C extreme scaling rates in various regions (Lenderink *et al.*, 2018) strongest in the tropics (O'Gorman, 2012; Pall *et al.*, 2007). The CMIP5 models show a super C-C scaling rate in SA and TNA, which is further investigated in this study.

There are only a few studies exploring the mechanisms behind the super C-C relationship or the regional variations in scaling rates in Australia. To understand the causes of these regional variations of scaling rates, we investigate the roles of thermodynamic and dynamic factors. This analysis reveals that the available surface moisture changes at a higher rate with DPT in SA relative to NA. However, the circulation change with DPT is most sensitive in the TNA. This could imply that the super C-C scaling rate in extreme rainfall in the TNA is partly explained by the greater changes in circulation (dynamics), whereas in the SA – surface level moisture plays a more significant role (thermodynamics). This is consistent with other studies - Catto *et al.* (2012a) showed that the large-scale circulation plays a more important role than the thermodynamics in the rainfall trends in the NA. Similar results were found by Clark *et al.* (2018). The authors showed that the observed rainfall increase in NA is mainly due to an increase in the frequency of organised convective systems – rather than an

increase in rainfall intensity associated with those events – suggesting a crucial role of dynamics over thermodynamics in this region.

The models overall perform well in simulating historical scaling rates and produce consistent spatial patterns with previous observational studies. However, the values of scaling rates using climate models are slightly higher than the observed values shown in previous studies using station dataset (Ali *et al.*, 2018; Roderick *et al.*, 2019). The spread across the models in simulating extreme rainfall-temperature relationship is higher in the TNA compared to the SA. The spread is even larger in both regions in simulating the dynamic driver (i.e. wind convergence), showing a higher intermodel discrepancy. This is not unexpected as models suffer from various biases related to dynamics both in tropics (such as double ITCZ) (Hwang & Frierson, 2013) and extra-tropics (such as biases in simulating westerlies) (Swart & Fyfe, 2012).

So far, the studies investigating physical mechanisms behind extreme rainfall scaling rate has pointed out vertical wind velocity, atmospheric water vapour, and temperature lapse rate as important dynamical and thermodynamical factors (O'Gorman, 2012; Pfahl *et al.*, 2017; Sugiyama *et al.*, 2010). Here we show that surface parameters also play key roles in extreme rainfall and can partly explain the regional variations in Australia. Understanding the roles of various drivers in extreme rainfall and therefore connecting results with historically observed changes in the drivers and extreme rainfall can improve our confidence in the scaling method as well as climate models. Thus, future studies should focus on the surface as well as the upper atmosphere instabilities to explain regional variations in other regions.

There are several important limitations to scaling studies, and including the methodologies employed in our current study, that should be noted. Most of the available studies deal with station datasets (Guerreiro *et al.*, 2018; Jones *et al.*, 2009; Wasko *et al.*, 2018; Wasko & Nathan, 2019). However, station data are not directly comparable with gridded data or climate models. The number of studies looking at historical scaling rates using DPT is scarce due to the limited availability of DPT measurements (Lenderink *et al.*, 2018). Besides, to our knowledge, there is no study available using the observational gridded dataset, as, although the gridded rainfall products in Australia perform well in estimating rainfall extremes (King *et al.*, 2013a), gridded DPT data are not freely available.

The binning method is sensitive to the annual seasonal cycle (Ali *et al.*, 2018; Zhang *et al.*, 2017). The scaling rates calculated in four different seasons in Australia showed a similar north-south pattern across all seasons– strongest in summer. This is because dry conditions are related to warm conditions as more sunshine, fewer clouds lead to warm surface temperatures (Trenberth & Shea, 2005). The scaling rates are positive in the SA in winter. A fundamental explanation is high temperatures in summer leads to a higher moisture holding capacity in the atmosphere thus require a higher level of moisture for the air to be saturated whereas in winter the moisture-holding capacity reduces which makes it easier to rain (Berg *et al.*, 2009). Ali *et al.* (2018) showed that after removing the seasonal cycle, globally, 33% stations show super scaling rate compared to the 22% without removing seasonality. Thus, with and without removing seasonality, using this method produce high scaling rates in several regions globally.

Overall, our study provides important insights into changes in rainfall extremes with DPT in Australia. The future simulations examined here show higher extreme rainfall scaling rates than historical simulations – exceeding 25 %˚C^{-1} in the TNA. Future simulations show a robust increase in DPT. The scaling rates in both thermodynamic and dynamic factors also exceed the historical scaling rates. This indicates that the changes with DPT in extreme rainfall and its underlying drivers are non-stationary. Moreover, the non-stationarity, in fact, the increase in scaling rates plausibly could be attributed to climate change as both dynamic and thermodynamic factors show a similar shift in scaling rates. Thus, extreme rainfall cannot be simply extrapolated using scaling rate over a fixed time, the uncertainty associated with its non-stationary nature should be considered.

Finally, we investigate the applicability of scaling rates by creating three storylines, where the extreme rainfall increases with a 7% scaling rate, with historic scaling rate, and using scaling rate calculated in RCP8.5 simulation. These three scenarios were compared with the traditional approach of studying future change in extreme rainfall by calculating the difference between future and historical simulations. The multi-model median shows an increase of 5.7% in Rx1 between future and historical scenario using the traditional approach. Whereas, a simple extrapolation into future, using a 7% scaling rate, historical scaling rate and future scaling rate, increases by 16%, 33%, and 44% in Rx1 shown in multi-model median values respectively in Australia. A simple approach to test the applicability of scaling rates is to check if historical changes in extreme rainfall have been consistent with the observed scaling rates.

Darwin has experienced a 19.7% increase in mean Rx1 intensity between the two periods 1950-1980 and 1981-2014 (see Table 1 of Roderick *et al.* (2019)), although the scaling rate calculated is 9.4% (Barbero *et al.*, 2018). Similarly, scaling rate in the south of Australia is >7%, however, there is no robust evidence of increase in extreme rainfall in this region, instead, a persistent decline in rainfall is observed (Hope *et al.*, 2010; Murphy & Timbal, 2008). Thus, the historical change in extreme rainfall does not follow observed scaling rates, which raises concerns about its applicability to project extreme rainfall. Below we summarise the challenges in applying scaling rates and suggest future research directions.

1. The relationship between extreme rainfall and surface temperature is non-linear, the non-linearity still exists when studying the relationship between extreme rainfall and DPT. Thus, fitting a linear regression to calculate scaling rate is not appropriate.
2. By definition, the binning method suffers from a strong seasonal signature, which affects this method. As the temperatures in the low bin come from the winter season and the temperatures in the upper bins come from hot summer days, thus there is a strong seasonal signature which cannot be avoided completely.
3. The scaling rates are calculated using temperature/DPT and rainfall at a daily scale, however, it is still not clear how scaling rates can be used to draw conclusions on changes in extreme rainfall because of climate change. Thus, future studies should investigate how scaling rates can be used to provide climate scale information and if there is any relationship at all.
4. This study finds that scaling rates are non-stationary. Further investigation is required to make robust conclusions on the possible mechanisms of the non-stationarity nature and how it can be incorporated into extreme rainfall projections.

Chapter 6

Evidence of a continent-wide shift of episodic rainfall in Australia

Highlights

1. Rainfall in Australia has become more temporally episodic, with an increase in the frequency of short-duration (1-2 day) events and a decrease in long-duration (> 2 days) events in the south of Australia.
2. North of the country has experienced an increase in the frequency of long-duration persistent events (> 6 days).
3. Trends determined using rainfall event-based approach are more spatially coherent than analysis of other characteristics of rainfall.

Abstract

Extreme daily rainfall has intensified and become more frequent globally. However, in Australia, long-term changes in the characteristics of extreme rainfall are not well understood. Commonly used indices that examine the characteristics of rainfall rarely show statistically significant long-term historical changes in mean and extreme rainfall events. Here we use a rainfall event-based approach to study observed changes in intensity and frequency of rainfall events in Australia. This approach defines rain events as *n* consecutive days of rain to account for varying event duration. The intensity of a rainfall event is defined as the average of the daily accumulation of rainfall over the event duration. We find that short-duration rainfall events (1-2 day) have become more frequent and have intensified in large parts of Australia since the beginning of the 20th century. The frequency of longer duration rainfall events (3-4 day and 5-6 day) show substantial and statistically significant reductions in the south of Australia and increases in some parts of northern Australia. The frequency of rainfall events lasting > 6 days has increased in the north and decreased in the south. The robust increase in short-duration episodic rainfall events across Australia and decrease in the frequency of extended episodic events imply rainfall has become more sporadic in Australia. Changes in rainfall intensities are less consistent compared to changes in frequency across the continent. We find an increase in intensity in the 1-2 and 3-4 day events, but the trends in the intensity of those events lasting > 4 days are mostly not significant. Overall, changes in the characteristics

of rainfall events of duration *n* days provide more spatially coherent results than those presented previously.

Keywords: Persistent rainfall, rainfall events, extremes, long-term trends, frequency, intensity

6.1 Introduction

Trends in both the intensity and frequency of extreme daily rainfall have increased globally both in wet and dry regions (Donat *et al.*, 2019). Previous research shows that the rate of increase in heavy rainfall events is much higher than both the rate of evaporation and the rate of total rainfall (Trenberth *et al.*, 2003), which establishes the concept that "when it rains, it rains more" (Contractor *et al.*, 2018). Many regions have observed an increase in the intensity and frequency of extreme events at the expense of a decrease in the frequency of light to moderate events (Goswami *et al.*, 2006; Miao *et al.*, 2016). Overall, Australia follows a similar pattern to the global trends, where a "when it rains, it rains more" pattern has been reported (Contractor *et al.*, 2018). Several regions in Australia have exhibited long-term changes in mean rainfall. For example, a significant increase in north-west Australia (NWA) (Ackerley *et al.*, 2015; Dey *et al.*, 2018), a decrease in the southwest of Western Australia (SWWA) and a recent decrease has emerged in southeast Australia (SEA) in the last 30 years (Hope *et al.*, 2010; Pepler *et al.*, 2019). However, changes in extreme rainfall characteristics rarely show significant long-term trends (Alexander & Arblaster, 2017).

Australia experiences one of the highest variable rainfall in the world (Nicholls *et al.*, 1997). Part of the reason being many large-scale climate drivers, such as the El Niño Southern Oscillation (ENSO), the Southern Annular Mode (SAM), the Indian Ocean Dipole (IOD), the Subtropical Ridge (STR), and the Madden Julian Oscillation (MJO) modulating rainfall in Australia (Dey *et al.*, 2019; Risbey *et al.*, 2009). These large-scale drivers undergo significant inter-annual and interdecadal variabilities, further increasing rainfall variability in Australia (Fogt & Bromwich, 2006; King *et al.*, 2013; Power *et al.*, 1999). Thus, detecting long-term trends in mean and especially extreme rainfall in Australia is challenging.

Few studies examine changes in the characteristics of the entire rainfall distribution (Contractor *et al.*, 2018), as most focus on extreme heavy rainfall due to potential socio-economic impacts. However, assessments of extreme rainfall can be very sensitive to the way the extremes are defined (Pendergrass, 2018). Many studies use a threshold or percentile-based approach to study changes in frequency and intensity of extreme rainfall events

(Anagnostopoulou & Tolika, 2012; Contractor *et al.*, 2018; Easterling *et al.*, 2000). These methods have notable limitations; for example, a fixed threshold-based approach is complex when applied to a broad region. This is because, a single threshold for extreme rainfall does not apply to Australia as a whole as the climatological rainfall varies significantly (Nicholls *et al.*, 1997). Furthermore, the thresholds applied are dependent on expert judgement which involves some level of subjectivity (Beguería, 2005). While percentile-based thresholds based on wet days (days when rainfall is greater than a minimum threshold) take into account geographical variations in rainfall, these thresholds are sensitive to the changes in the fraction of wet days thus should be carefully interpreted (Schär *et al.*, 2016).

Another approach to examining rainfall extremes is to calculate the maximum rainfall accumulations over a fixed, but arbitrary, number of consecutive days in a given period such as a month, season or year. In studies to date, the selection of the number of days over which a rainfall accumulation is calculated is also arbitrary (for example, Rx5: maximum consecutive 5-day rainfall event for a given month, season or year) (Zhang *et al.*, 2011). Indices like Rx5 can be drawn from either multiple short-duration rainfall events or a single long persistent event, and may not necessarily cover the full duration if the rainfall event lasts longer than five days (Du *et al.*, 2019).

Climate scientists are often asked *how* rainfall is changing. The scientific community has largely focused on exploring sub-daily to single day rainfall which have yielded some interesting findings, particularly with respect to extremes (Alexander & Arblaster, 2017; Guerreiro *et al.*, 2018; Wasko & Sharma, 2015). However, changes to the nature of the sequencing of rainfall have not yet been examined. This is, the episodic nature of rainfall and how this might have changed. The indices used in studies to date, like Rx5 described earlier, provide a useful snapshot of changes to characteristics of daily rainfall but a comparison between single day totals and five day totals doesn't provide a comprehensive picture of the nature of rainfall change. It is particularly important to examine the episodic nature of rainfall as it can provide information that is useful for understanding the processes by which rainfall is changing. Further, examining changes to the characteristics of rainfall events can provide targeted information about trends that are relevant for socio-economic impacts. For example, if a large amount of rain falls over a short period of time e.g. order of days, the risk of flooding dramatically increases (Rahman *et al.*, 2002). Conversely, if the same amount of rain falls over

a considerably longer period e.g. order of weeks, it may increase soil moisture which can provide relief from an existing drought (Michailidi *et al.*, 2018).

Examining rainfall events using existing indices shows an incomplete picture of event characteristics. Du *et al.* (2019) defined a persistent extreme event as maximum consecutive days of rainfall (*n*) with the condition that the rainfall accumulation for each day exceeds the average daily rainfall accumulation (RxEvent). They showed that globally the increase in RxEvent is 49% higher than the increase in Rx1. Thus, studying extremes using the approaches to date still has some limitations; in this case, underestimating changes in extreme rainfall events.

Here, we apply a methodology similar to the approaches of Du *et al.* (2019) to examine episodic rainfall events, where an event is defined as *n* consecutive days of precipitation. By taking this approach, we will comprehensively explore the question of how the characteristics of rainfall are changing in Australia. This will include an assessment of changes for the entire precipitation distribution, including extremes.

6.2 Methods

We use the daily Australian Water Availability Project (AWAP; Jones et al.2009) data at 0.25° × 0.25° horizontal resolution over the period 1911-2016. AWAP dataset is constructed using quality-controlled station dataset from the Australian Data Archive for Meteorology (ADAM). The number of stations used in AWAP data since 1900 varies significantly, with maximum number of stations in 1970s and decreasing since then (see Figure 1b of Dey *et al.* (2019)). In addition, AWAP data suffers from high degree of spatially inhomogeneous station density. As there are very few stations in central-west Australia, which can produce spurious trends, we apply a mask to these regions following Chung and Power (2017). Interpolation and smoothing techniques can introduce unrealistically small rainfall values at grid points where there is no data (Hutchinson, 1998; Jones *et al.*, 2009), thus most studies use a threshold to avoid spurious trends, especially for frequency indices (Alexander & Arblaster, 2017; Clark *et al.*, 2018; Gallant *et al.*, 2007). Here we use 1 mm as a threshold. Note, the least rainfall value recorded by Lavery *et al.* (1992) station dataset is 0.1 mm. Overall, previous research shows that AWAP data estimates daily rainfall well when compared against robust station datasets (Jones *et al.*, 2009; King *et al.*, 2013), thus can be applied to study rainfall characteristics.

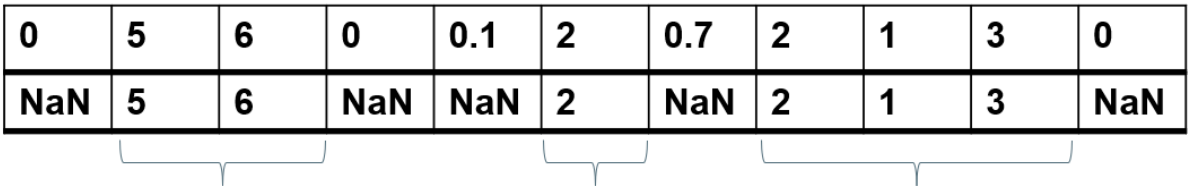

Figure 6.1 Schematic explaining the method to identify rainfall events. The first row is an example of rainfall time series. The second row shows the transformed timeseries after ignoring the non-rain days (<1 mm rainfall). Each rainfall event is preceded and followed by a non-rainy day. In this schematic, we find a 3 day, a single day and a 2 day events.

We apply a rainfall event-based approach rather than using either exceedance or particular threshold-based rainfall analysis. Here, a rainfall event is defined as any sequence of *n* consecutive days with rainfall ≥ 1 mm. Each event must be separated by at least one non-rainy day (< 1 mm). A schematic explaining the rainfall event identification method is shown in Figure 6.1. For simplicity, we stratify rainfall events into four categories based on the event duration: a 1-2 day event (maximum two days of consecutive rainfall), a 3-4 day event (consecutive rainfall of 3 or 4 days), a 5-6 day event (consecutive rainfall of 5 or 6 days) and > 6 days events (consecutive rainfall for more than 6 days). Next, we calculate the climatology of percentage contribution of each event type to annual total rainfall over the period 1911-2016.

Changes to aspects of the frequency and intensity of the above event categories are then examined. Rainfall event intensity (mm/day) is defined as the total rainfall (over n days) divided by the event duration, where the event duration is defined as the number of consecutive days of rain (n) for event type. The trends in the median and maximum rainfall event intensities were examined for each event category in a given year and/or season. Table 6.1 summarises the event indices calculated to study the frequency and intensity of rainfall events of each category.

Table 6.1 Table summarising the indices calculated to study the frequency and intensities of rainfall events in each event category.

Frequency indices of rainfall events	
1-2 day	Light (0-25th), moderate (25-75th), heavy (>95th)
3-4 day	Light (0-25th), moderate (25-75th), heavy (>95th)
5-6 day	Moderate (<50th), heavy (>50th)

>6 day	Moderate (<50th), heavy (>50th)
Intensity indices of rainfall events	
1-2 day	Median, maximum
3-4 day	Median, maximum
5-6 day	Median, maximum
>6 day	Median, maximum

We calculate the 25th, 75th, and 95th percentiles of the rainfall event intensity. For 1-2 day and 3-4 day events, annual frequency of light (number of events with rainfall event intensity <25th percentile), moderate (number of events with rainfall event intensity between 25^{th} and 75th percentiles), heavy or extreme events (number of events with rainfall event intensity>95th percentile) are calculated. As 5-6 day events and > 6-days events are rare throughout much of Australia with the exception of tropical north and west of Tasmania, these events are not further stratified into the light, moderate and heavy categories as there are too few events to robustly examine a trend. Instead, for events lasting > 4 days, we examine the changes in the number of events above or below the median rainfall event intensity, defined as heavy and moderate events respectively. Note, the percentiles calculated in this study are quite extreme relative to all day percentiles, as they are conditioned on rainfall events, making them more similar to wet day percentiles. The significance of the trends in rainfall event intensity and frequency are calculated using Mann-Kendall non-parametric test.

The frequency and intensity metrics were computed at the grid-scale and were then area-averaged for three different regions where a significant historical change in annual rainfall has been observed (Fig. s6.1). The regions are NWA (10˚–25˚S, 110˚–135˚E), SEA (33˚–44˚S, 135˚–154˚E) and SWWA (southwest of the line joining 30˚S, 115˚E, and 35˚S, 120˚E). We calculate time-series of event frequency over 1911–2016 and 1950–2016. The rationale for choosing these regions and time periods is to test the applicability of our method of studying rainfall characteristics against known historic trends. Note, Figure s6.1 marks the regions discussed in this study.

For each event type (i.e. 1-2 day event, 3-4 day event etc.) we only examine regions where the event has occurred at least once in a year for at least 30 years to make sure we have enough data to calculate trends and mask out the regions otherwise. Thus, a small region is masked for 5-6 day events in central Australia in addition to the regular masking, whereas for

> 6 days events, a much larger region is masked as they are scarce in those regions. The seasonal figures presented here have larger masked regions due to two reasons: 1. we only shade the areas that show significant trends and 2. very few regions experienced extended duration events at least once in more than 30 years when looking at particular seasons. For similar reasons, we only show significant trends for frequency and intensity plots when further segregated into light, moderate, and heavy events.

To further examine the metrics described above, the same analysis was also performed using a high-quality station network of daily rainfall dataset in Australia (Lavery *et al.*, 1992). There were originally 191 stations which were reduced to 152 stations after further quality control (King *et al.*, 2013a). Further, Viney and Bates (2004) found that rainfall accumulations were tagged against the wrong days due to not taking measurements over the weekend, which resulted in too many extreme events on Mondays and too few on Sundays. King *et al.* (2013a) found the 'Sunday-Monday' problem at 30 sites among the 152 high-quality stations. The above issues might result in spurious trends. Thus following King *et al.* (2013a) we remove the stations that have a Sunday-Monday problem, which leaves us with 112 stations. The trend in each station is calculated over the period from 1911 to the latest available period (the latest available period among stations ranges from 2004-2018). Figure s6.2 shows the finishing years of each station. Note, we have also performed the analysis using 0.5 mm as a threshold for AWAP and station datasets, and our results remained unchanged.

6.3 Results

6.3.1 Frequency analysis

6.3.1.1 Frequency analysis in gridded data

Climatological patterns in the north and east coast of Australia, SWWA and west Tasmania show the highest rainfall accumulations (Fig. s6.3(a)). The climatological number of rain days (days when rainfall is >1mm) have a very similar spatial pattern to the climatological annual average rainfall (Fig. s6.3(b)), similar to results found by Contractor *et al.* (2018). Figure 6.2a shows a climatology of event frequency in Australia where events of all durations are included, providing an overview of whether rainfall is likely to fall from few or many events. Here, an event is a discrete period of *n* consecutive days of rain. The highest frequency of rain events of any duration occurs in the south of Victoria on the southern slopes of the Great Dividing Range and the east of Tasmania, showing that rainfall events are most frequent and episodic here. This pattern is distinct from annual average rainfall in Tasmania (Fig. s6.3(a)), where the largest

annual rainfall totals are observed in west Tasmania, rather than the east. The frequency of rainfall events is lowest in central and central-west Australia, highlighting that rainfall accumulations here are the result of very few individual rainfall events. The average duration of rainfall events is greatest in the tropical north of Australia, the west of Tasmania, and in the coast of SWWA (Fig. 6.2b) and decreases sharply in the centre of the country. The spatial map of the average event duration is similar to the climatological annual average rainfall in Australia.

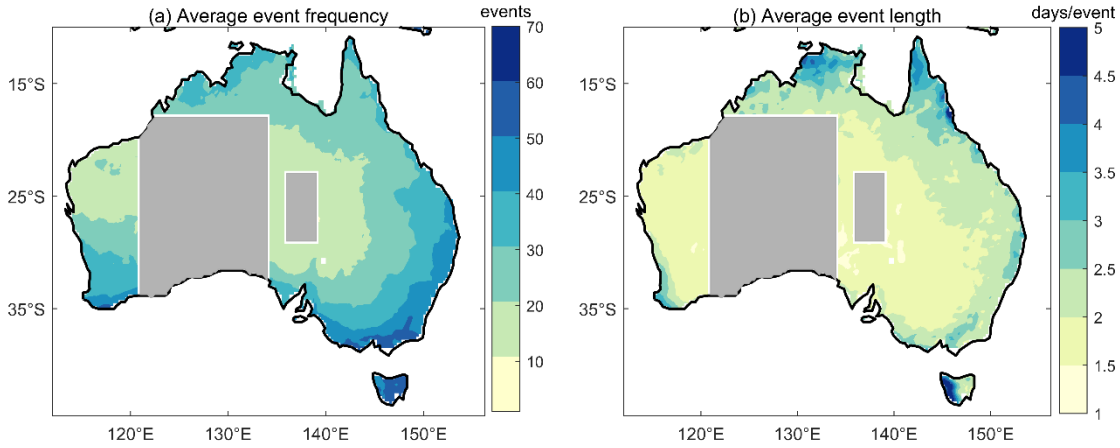

Figure 6.2 (a) The climatological annual average frequency of rainfall events irrespective of the event duration, (b) the climatological annual average event duration (days/event). The climatologies are calculated using AWAP data over the period 1911-2016. The grey region shows the masked area following Chung & Power (2017).

Figure 6.3 shows a climatology of the percentage contribution of rainfall from each event category to annual total rainfall, defined in the methods Section. A reduction or increase in those events with the highest percentage contribution potentially affects the total rainfall of the region. The percentage of rainfall from 1-2 day events is the smallest in the west of Tasmania and coastal regions of east Australia and increases rapidly inland (Fig. 6.3a). More than 50% of total rainfall is received from these short-duration events in the inland regions of New South Wales (NSW), South Australia (SA), and Western Australia (WA). The maximum contribution from 3-4 day events occurs between the latitude bands of 20˚S to 30˚S and in the east of Tasmania (Fig. 6.3b). The maximum contribution from 5-6 day events is typically in latitudes between 15˚S to 30˚S, with a maximum in the northwest of WA (Fig. 6.3c). Almost 60-80% of the total annual rainfall comes from > 6 day events in parts of tropical north of Australia, which reflects the monsoon. In west Tasmania, the high number of > 6 day events reflects persistent onshore, moist westerlies encountering orography (Fig. 6.3d). The coastal

SWWA receives 30-40% of its annual rainfall from > 6 days rainfall events. The major synoptic signature of rainfall in this region is a series of fronts and troughs, suggesting that 6 day events are more likely to be a rapid sequencing of rain-bearing systems rather than a single event (Hope *et al.*, 2006; Wright, 1974). The rest of the continent receives rainfall from a combination of the other three categories and the short-duration (1-2 day) events dominate in the inland regions.

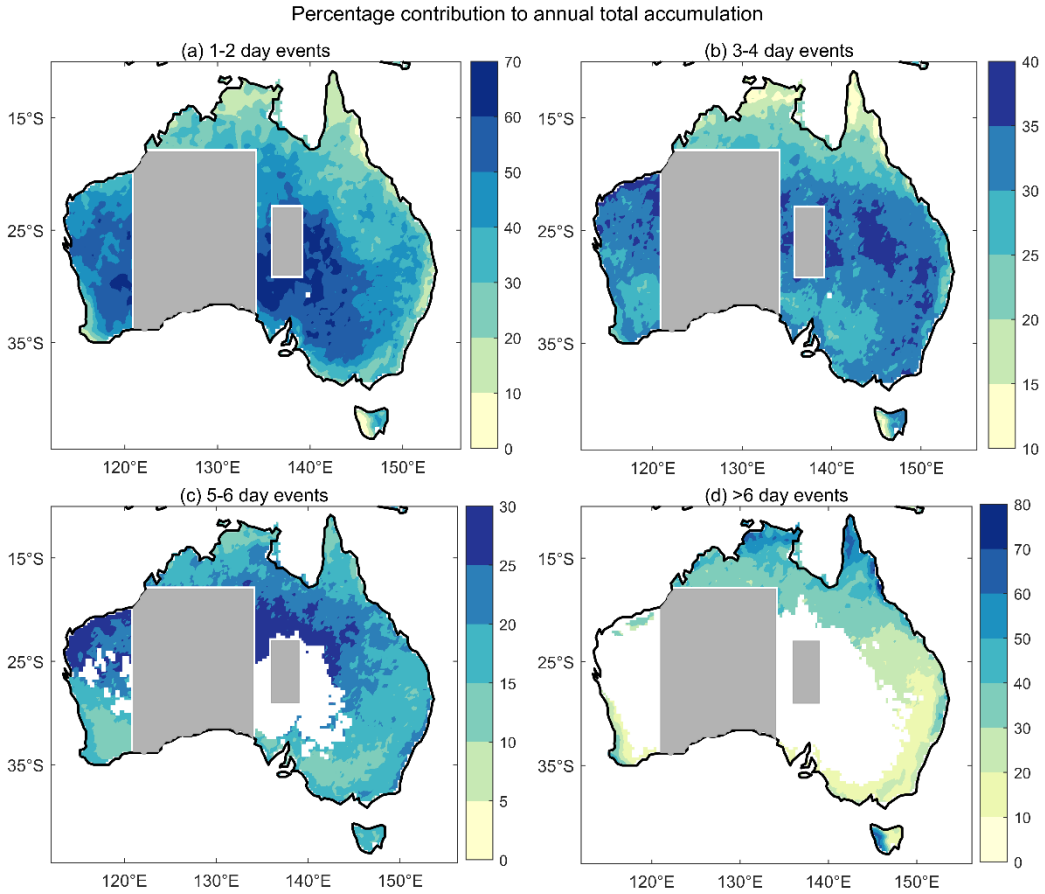

Figure 6.3 The climatological percentage contribution to the annual total rainfall from (a) 1-2 day events, (b) 3-4 day events (c) 5-6 day events (d) >6 day events. The AWAP data over the period 1911-2016 is used to calculate the climatologies. The white regions are where data points were not available for at least 30 years for each event category.

The trend analysis (Fig. 6.4a) shows increases in the frequency of rainfall events almost everywhere in the country except for the tropical north. This differs from trends in the number of rain days (Fig. s6.3(c)), which shows a significant increase in the north and decrease in the south. These trends indicate a plausible shift in the event category. The trend analysis in event duration shows that typical event duration has decreased in the south and increased in the north of the country (Fig. 6.4b). The strong increase in event duration in the tropical north could help

to explain the weak decreasing trends in event frequency here (Fig 6.4a). The above results show that outside the tropics (below approximately 20°S) there has been a tendency toward an increase in the frequency of rain events and a decrease in the event duration, which suggests a trend towards more short and episodic rainfall events.

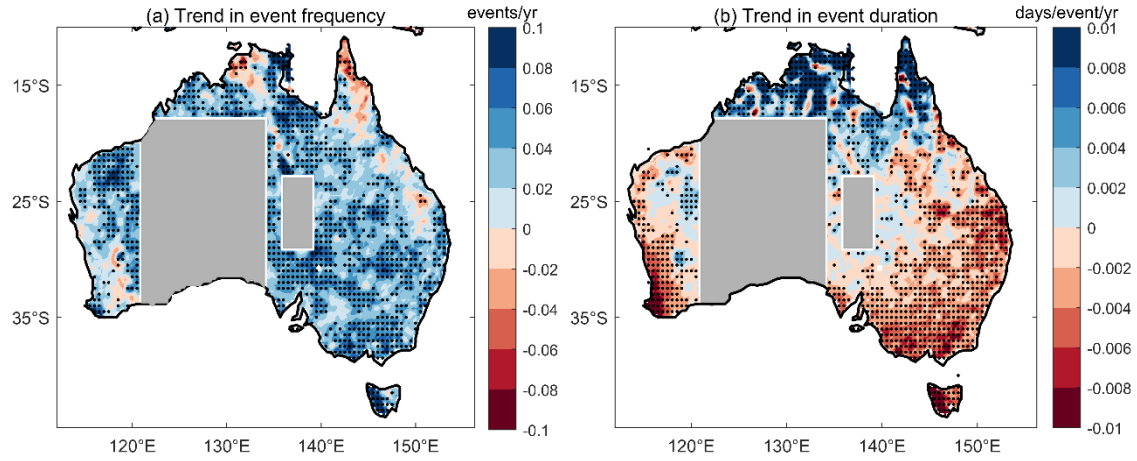

Figure 6.4 The trends calculated using linear regression in (a) event frequency (events/year) and (d) event duration (days/event/year) using AWAP data over the period 1911-2016. The stippling shows significance at 95% level using Mann-Kendall non-parametric test.

There is a significant increase in the frequency of 1-2 day events around most of Australia except for the tropical north (Fig. 6.5a). The frequency of 3-4 day events shows an increase in the north; however, there are areas of significant decreases in tropical Australia (Fig. 6.5b) – similar to Figure 6.5a. There is a decrease in the frequency of 3-4 day events across south-east Australia. This includes coherent areas where these reductions are statistically significant, namely in parts of southeast Queensland (QLD) and southern NSW and northern Victoria, north and west of the Great Dividing Range. The SWWA shows an area of significant decreasing trends in 3-4 day events. Some significant increases in 3-4 day events are observed in northwest Australia and west Tasmania. The increase of 3-4 day events in west Tasmania is significant. This is at odds with the observed decrease in rainfall in this region, specifically in winter and autumn (Rehman *et al.*, 2019).

The largest regional differences in trends occur for the longest duration rainfall events. Those rainfall events lasting 5-6 days (Fig. 6.5c) or > 6 days (Fig. 6.5d) show broadly similar patterns (except for tropical north Australia and west Tasmania), with increase in the north and decrease in the south of the country. The largest decreases occur in SEA and SWWA. The reductions in long-duration rain events in the south are strong and significant and contrast to

the significant increases in 1-2 day events that were previously described. In tropical north Australia, increases in the 5-6 day events are spatially incoherent and statistically insignificant, whereas the frequency of events > 6 days increases sharply. The increase in persistent long events in the north, in combination with increases in rain days and event duration, implies a shift toward more extended persistent rainfall events in this region. Note, significant increases in the frequency of 1-2, 3-4, and 5-6 day events are evident in the northwest of WA (Fig. s6.1). There has been a significant decrease in the frequency of > 6 day events in west Tasmania and a strong increase in 3-4 day events as mentioned in the previous paragraph.

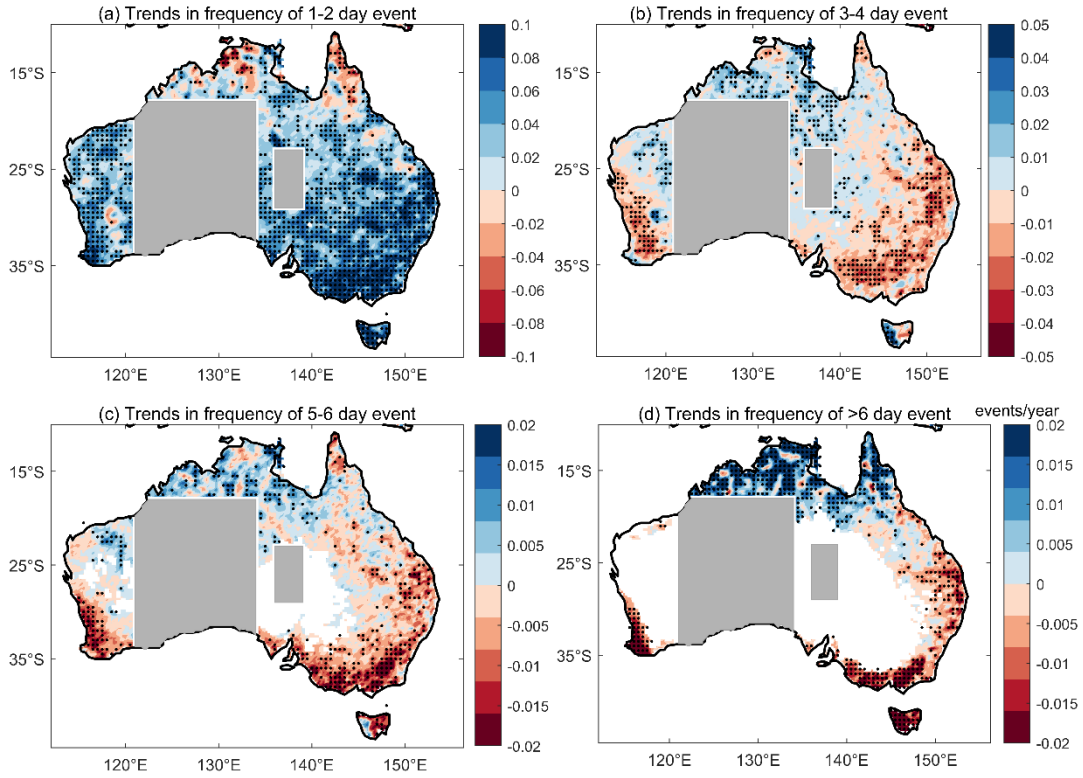

Figure 6.5 Trends in frequency (events/year) of (a) 1-2 day events, (b) 3-4 day events (c) 5-6 day events (d) >6 day events, calculated over the period 1911-2016. The white regions are where data points were not available for at least 30 years for each event category.

6.3.1.2 Frequency analysis in station dataset

The trends in the gridded datasets are compared against a high-quality station dataset (Fig. 6.6) to ensure they are robust. The number of stations varies for each of the event type assessed because, as is described in the methods section, the stations must satisfy a completeness criterion where at least 30 years of data is available for that event type. All stations were eligible to be used for the 1-2 day and 3-4 day events, 87 stations were used for the 5-6 day events, and

only 35 stations were used for the > 6 day events. The spatial variation in the trends observed in the station dataset is broadly similar to the gridded dataset. The significant trends are shown in dark color triangles, and insignificant trends are shown in light color circles. Out of 112 stations, 28 stations show a significant increase in the frequency of short-duration 1-2 day events, and only two stations show a significant negative trend. The 3-4 day events show 16 stations with a significant negative trend, and only seven stations show a significant positive trend. The stations showing negative trends are mostly concentrated in SWWA and coastal SEA. For the 5-6 day events, 7 stations show significant negative trends and no station shows a significant positive trend. The extended events (> 6 days event) have become significantly less frequent at 3 stations in south of Australia whereas a significant increase in frequency is observed at two sites in northern Australia. Overall, the number of stations showing a significant decrease in the frequency of extended events in southern Australia, especially in SWWA and Victoria increases as the event duration increases.

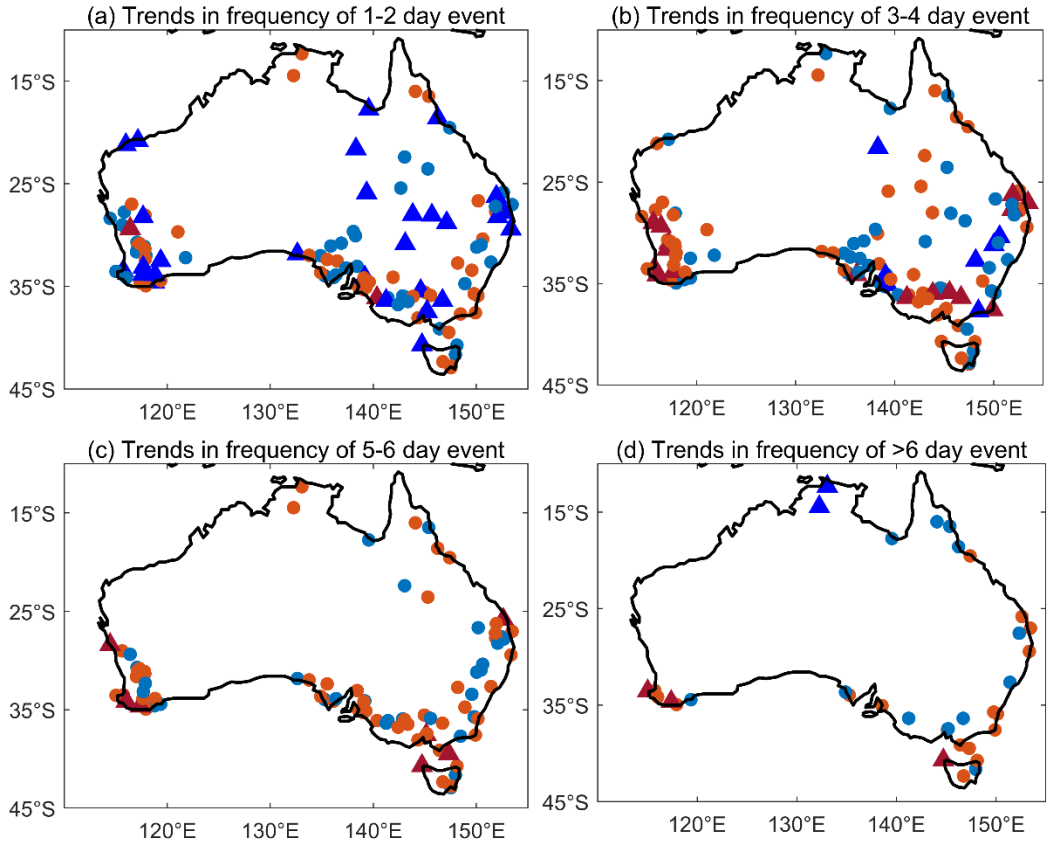

Figure 6.6 Similar as Fig. 6.5, but for station dataset. Only stations with more than 30 data points were plotted for each event type. Blue shades show positive trend and red shades show negative trends. The station datasets in dark colour triangle show significant trends at 95% level, and insignificant trends are shown in light colour circles. The trends are calculated from 1911 to the latest available period at each station. The finishing date for each station is shown in Fig. s2.

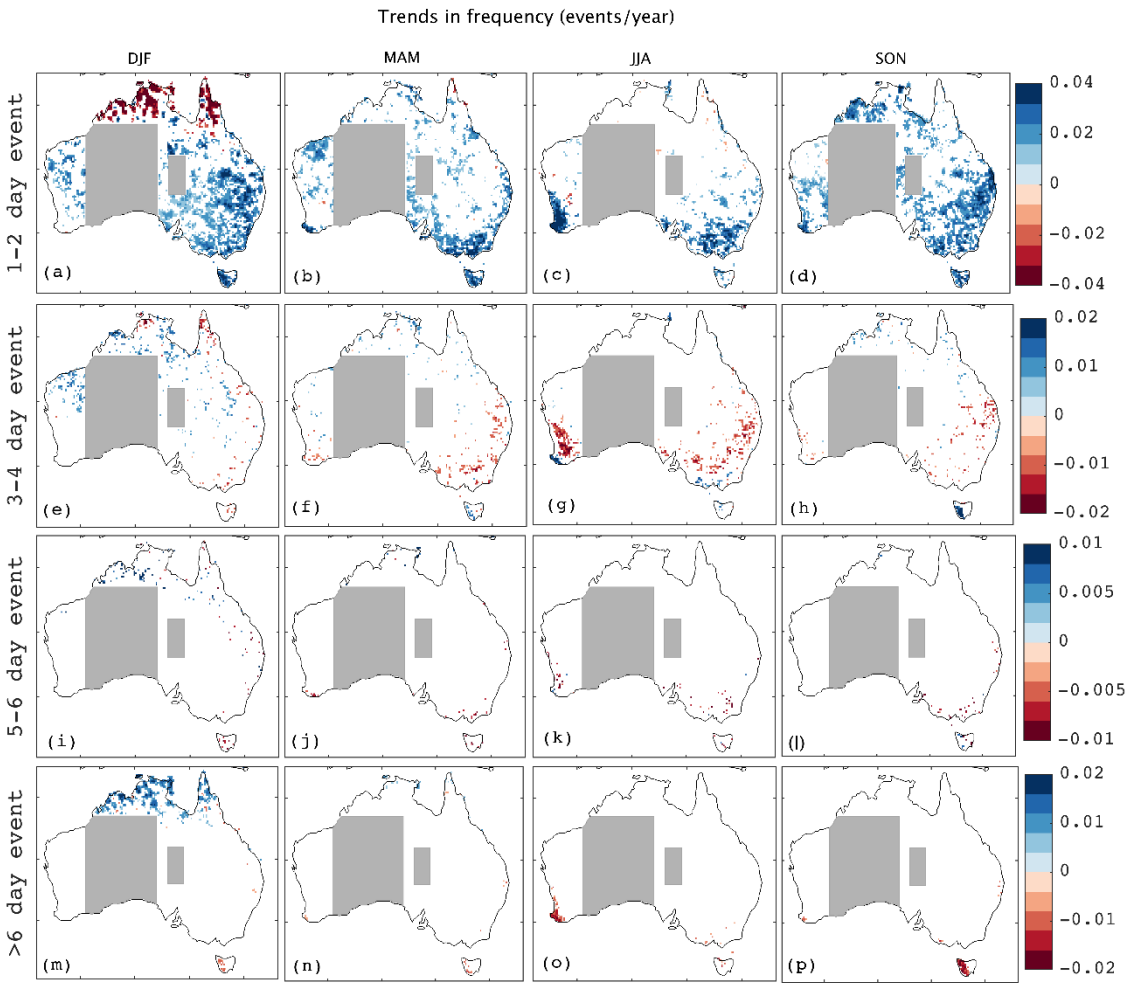

Figure 6.7 Trends in frequency (events/year) of (a-d) 1-2 day events, (e-h) 3-4 day events (i-l) 5-6 day events (m-p) and >6 day events (m-p), in December-February (DJF), March-May (MAM), June-August (JJA), and September-November (SON), calculated over the period 1911-2016. The white regions are where either the events occurred in less than 30 years over the period or the trends are not significant at the 95% level.

6.3.1.3 Frequency analysis in different seasons

Some of the trends in annual rainfall observed in Australia are a result of changes in seasonal rainfall. For example, NWA has experienced an increase in summer (DJF) rainfall since 1950 (Alexander & Arblaster, 2017; Dey *et al.*, 2018; Nicholls & Collins, 2006). The rainfall in agriculturally-sensitive regions in Australia, mainly SEA and SWWA, has decreased since, most significant in winter and spring (Dey *et al.*, 2019; Gallant *et al.*, 2007; Hennessy *et al.*, 1999). To further elucidate the trends observed in Figure 6.5, we investigate whether the annual trends emanate from any particular season(s). We show the trends in the four event categories for each season in Figure 6.7. Here we only shade the regions where trends are significant at

the 95% level. Highlighting if trends stem from particular times of the year can reveal information about the association between rainfall events and the rain-bearing systems that make up the events. The increase in the frequency of 1-2 day events over most of Australia is evident across all seasons. The decrease in the north of the country is only evident in tropical north Australia in December-February (DJF) which is consistent with our hypothesis that with increasing event duration, there are not sufficient non-rain days in-between for the events to be classified as short-duration events.

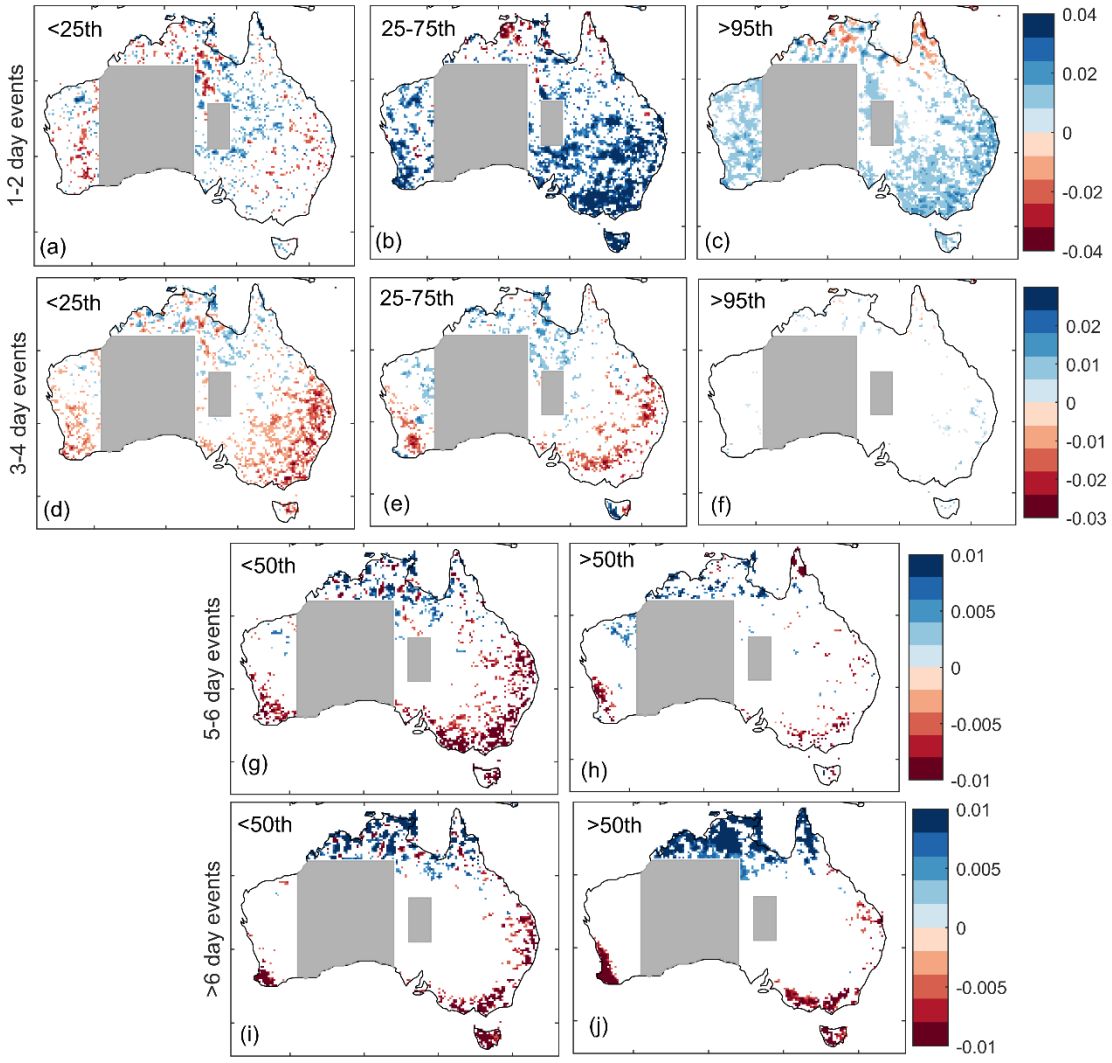

Figure 6.8 The trends in the frequency (events/year) of 1-2 day events (first panel) further segregated into (a) light <25th percentile, (b) moderate (25th-75th percentile), and extreme events (>95th percentile). The second panel shows the trends for 3-4 day events (d-f). The third and fourth panel show the trends in the frequency of events >50th and <50th percentile in 5-6 day and >6 day events respectively. Only significant trends at the 95% confidence level are shaded.

There is a decrease in 3-4 day events in the tropical north and increases in the northwest WA during the austral summer. In March-May (MAM), a decrease in these events is evident in the Murray Darling Basin (MDB) and SWWA, and there is an increase in west Tasmania. The negative trends over the MDB and inner region of SWWA are stronger in winter than other seasons, and a strong increase is seen in the coast of SWWA in winter. Note these regions have already experienced a strong decline in rainfall in winter months in past decades (Dey *et al.*, 2019; Gallant *et al.*, 2007; Nicholls, 2006). During September-November (SON), there is a significant increase in 3-4 day events in west of Tasmania.

No spatially consistent trends are observed for 5-6 day events. For > 6 day events there is a substantial increase in frequency in northern Australia in DJF. There is a significant decrease in these events in SWWA in JJA and a concurrent significant increase in 3-4 day events here. Similarly, in SON, there are concurrent statistically significant decreases in > 6 day events and increases in 3-4 day events in west Tasmania. These provide further evidence of a shift in the event category from extended persistent events (event duration >6 days) to events of shorter-duration events (3-4 days) in these regions.

6.3.1.4 Frequency analysis with event intensities

Understanding the frequency of rainfall events of different intensities provides information on the changes in rainfall event distribution from light to heavy events. The percentile values calculated to define frequency indices (see Table 6.1) are shown in Figure s6.4 for each event type. Figure 6.8 shows the trends in frequency of different rainfall event intensities. There is no coherent trend in short-duration, light events (Fig. 6.8a). In contrast, Figure 6.8b and 6.8c show strong, spatially coherent increases in 1-2 day moderate and heavy rain events with the exception of tropical northern Australia. The light 3-4 day events have significant decreasing trends everywhere in the south, and increasing trends in the north (Fig. 6.8d). The moderate events have a similar decreasing trend in the south of Australia but no significant trend in the coast of SEA (Fig. 6.8e). There is an increase in moderate events in the west of Tasmania. The trends in 5-6 day and >6 day events in both moderate and heavy events show a decrease in the south (Fig. 6.8 g-j). In north Australia, the trends in 5-6 day events are not coherent but become strong and coherent for moderate as well as heavy >6 days events.

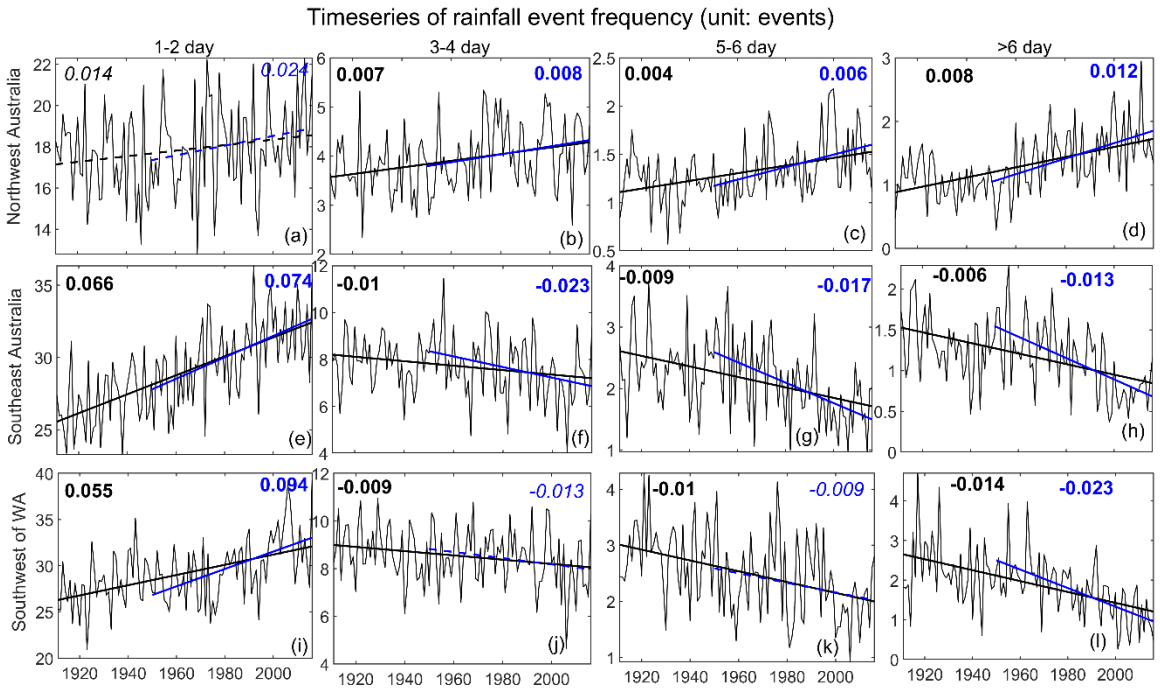

Figure 6.9 The area-averaged time series (unit: events) of 1-2 day (a,e,i) , 3-4 day (b,f,j), 5-6 day (c,g,k), and >6 day events (d,h,i) in northwest Australia (a-d), southeast Australia (e-h), and in southwest of Western Australia (i-l). The black line shows the trend over 1911-2016 in NWA, SEA, and SWWA. The blue line shows the trends over the period 1950-2016. The slopes are calculated using linear regression. The trends significant (insignificant) at the 95% confidence level are shown in solid (dash) line and bold (italic) fonts.

6.3.1.5 Area-averaged trends in event frequency

The area-averaged time series of the frequency of the four types of events in NWA, SWWA, and SEA (Fig. s6.1) are shown in Figure 6.9. The black line shows the long-term trend over the period 1911-2016, and the blue line shows the medium-term trend over 1950-2016. The insignificant trends are shown in dotted lines and the slope values are shown in italic fonts. Here we describe the major features of the timeseries of each region:

- In NWA, the trends in short duration 1-2 day events are not significant, similar to the spatial plot in Fig 6.5, where inhomogeneous trends are seen in this region. The longer events (>2 days) have increased in both periods analysed with faster rate in the medium-term period than the trends using the long-term period. The > 6 day events, which brings 60-80% of total rainfall in this region, have become more frequent with steeper increase in the medium-term.

- The frequency of 1-2 day events in SEA has significantly increased over both periods. The events lasting longer than two days (3-4 day, 5-6 day, > 6 days) have significantly declined in both periods, with a faster decline in the medium term.
- In SWWA, the frequency of 1-2 day events has increased significantly in both periods. The frequency of 3-4 day and 5-6 day events show decrease in the long term however, the trends become insignificant in the medium term. The >6 day events which brings 30-40% of total annual rainfall in this region, shows a persistent and strong decrease in long-term and medium-term.

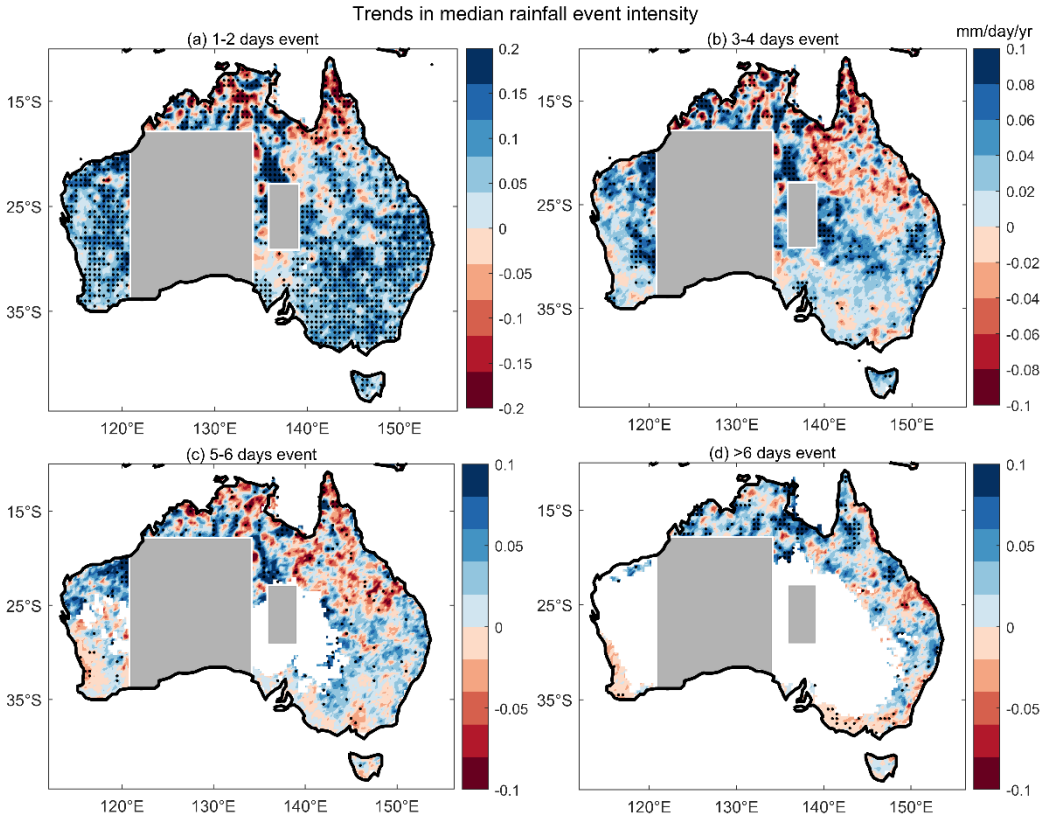

Figure 6.10 The trends in the median of rainfall event intensity (mm/day/year) in (a) 1-2 day events, (b) 3-4 day events, (c) 5-6 day events, and (d) >6 day events. The stippling represents areas where the trend is significant at the 95% confidence level.

6.3.2 Intensity analysis

6.3.2.1 Intensity analysis in gridded data and seasonal maps

In this section, we examine whether the intensity of rainfall events (defined in the methods section) in each event category has changed in the observational record. Figure 6.10 shows the median of the intensity of rainfall events. The intensity of 1-2 day events (Fig. 6.10a) shows a significant increase in most regions, whereas there is no robust or spatially coherent trend in

the tropical north where both significant decreasing and increasing trends are present. The trends in the median intensity of 3-4 day events show a similar pattern as for the shorter-duration events, a significant increase for latitudes below approximately 25°S, and inhomogeneous trends in the north. The trends in intensities of 5-6 day events and > 6 days event are not spatially coherent. There are significant increases in the median intensities of 1-2 day, 3-4 day, and 5-6 day events in the northwest of WA. Overall, the trends in intensity are less spatially homogeneous than the trends in frequency.

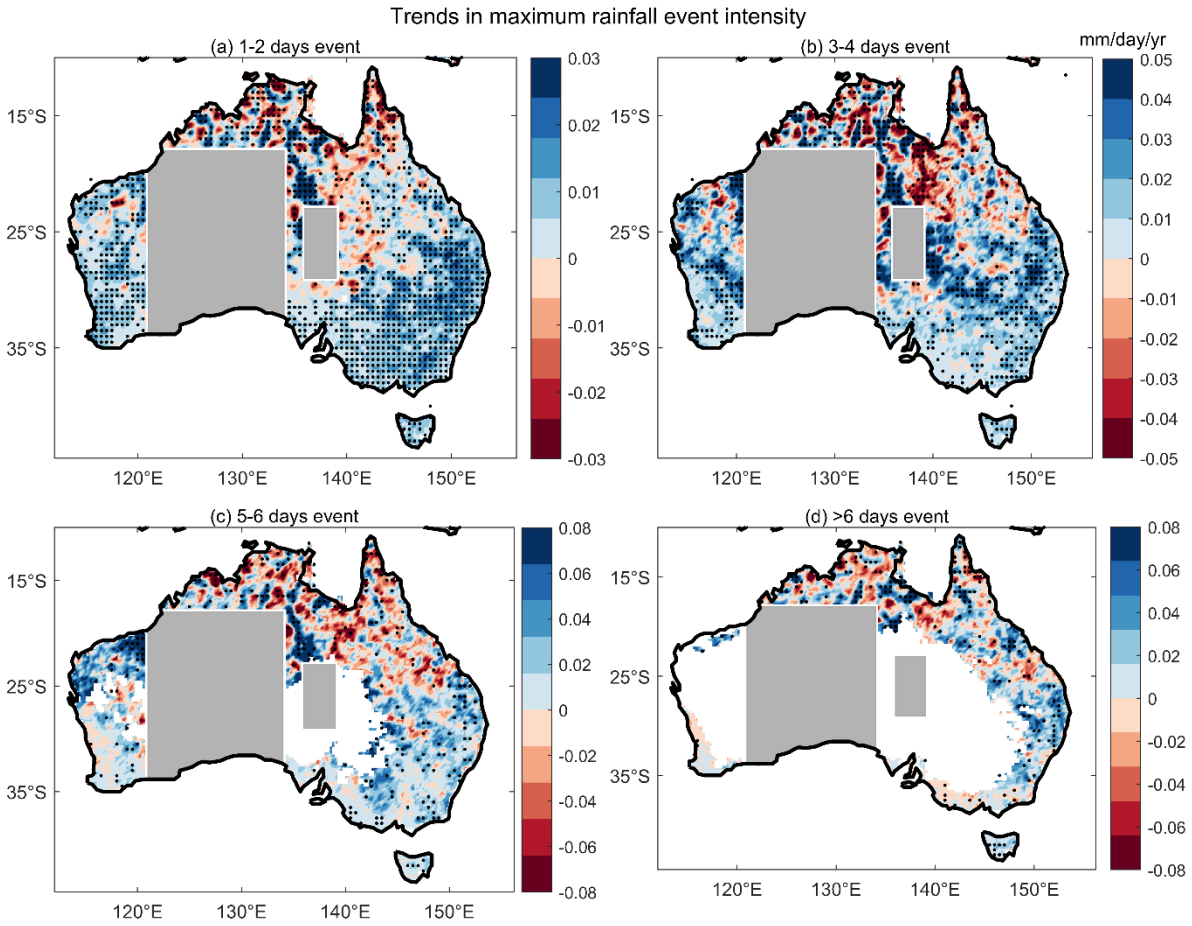

Figure 6.11 Same as Fig. 6.10, for annual maximum of rainfall event intensity.

Figure 6.11 shows the trends in the maximum intensity of rainfall events of the four categories, which is indicative of extreme rainfall. The maximum intensity of 1-2 day events has a strong increasing trend across most of the country similar to the trend in the median intensity of 1-2 day rainfall events. There is no spatially coherent or significant trend observed in the maximum intensity of rainfall events > 2 days. Figure 6.12 shows the maximum intensity of rainfall events in different seasons, where only significant trends are shaded. The sign of the

trends is similar to the trends in frequency, there is an increase in the maximum intensity of 1-2 day events during all seasons across much of the continent (Fig. 6.12 a-d). The maximum intensity of 3-4 day events has some spatially noisy areas showing positive trends in DJF (Fig. 6.12e) but no significant trends in other seasons. Similarly, there are no significant trends in intensity in longer events, showing that there is no evident change in intensity in extended events in any of the seasons.

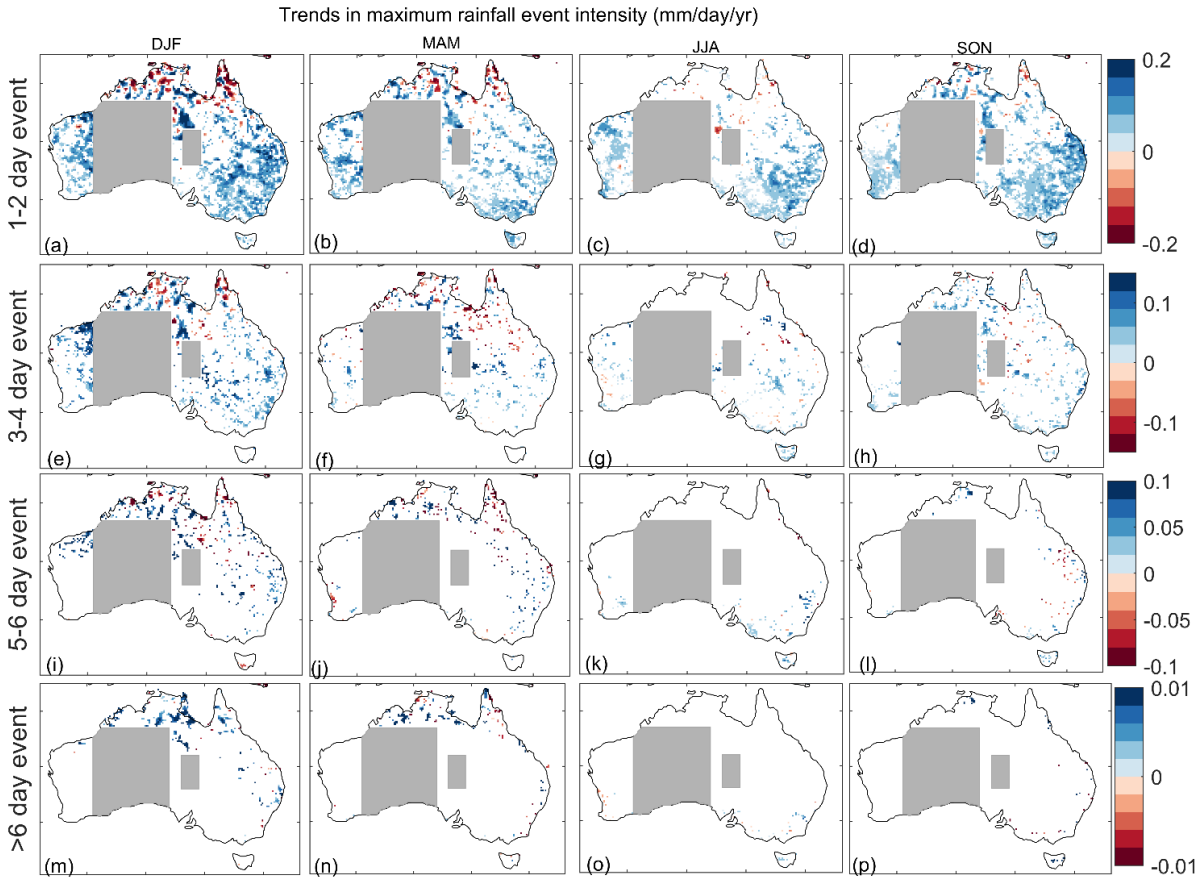

Figure 6.12 Same as Fig. 6.7 but for the maximum of rainfall event intensity. Only significant trends at the 95% level are shaded.

6.3.2.2 Intensity analysis in station dataset

Similar to section 6.3.1.2, the trends in maximum rainfall event intensity in gridded dataset are compared with high-quality station dataset (Fig. 6.13). Out of 112 stations, 11 stations show significant increase in 1-2 day events, whereas only one station in SEA shows significant negative trend. Trends in 3-4 day events are spatially inhomogeneous, with six stations showing significant negative trend and six stations showing significant positive trend scattered across Australia. For 5-6 day events, two stations show a significant increase (located on the coast of

east Australia) and three stations show a significant decrease (located in SEA and SWWA). Extended events which last >6 days show a significant decrease at three stations with no significant increase in maximum rainfall event intensity at any station. Overall, the number of stations showing significant trends in rainfall event intensity is smaller compared to the frequency of rainfall events in any of the event categories. This re-establishes that the changes in frequency are stronger and thus more detectable compared to changes in intensity.

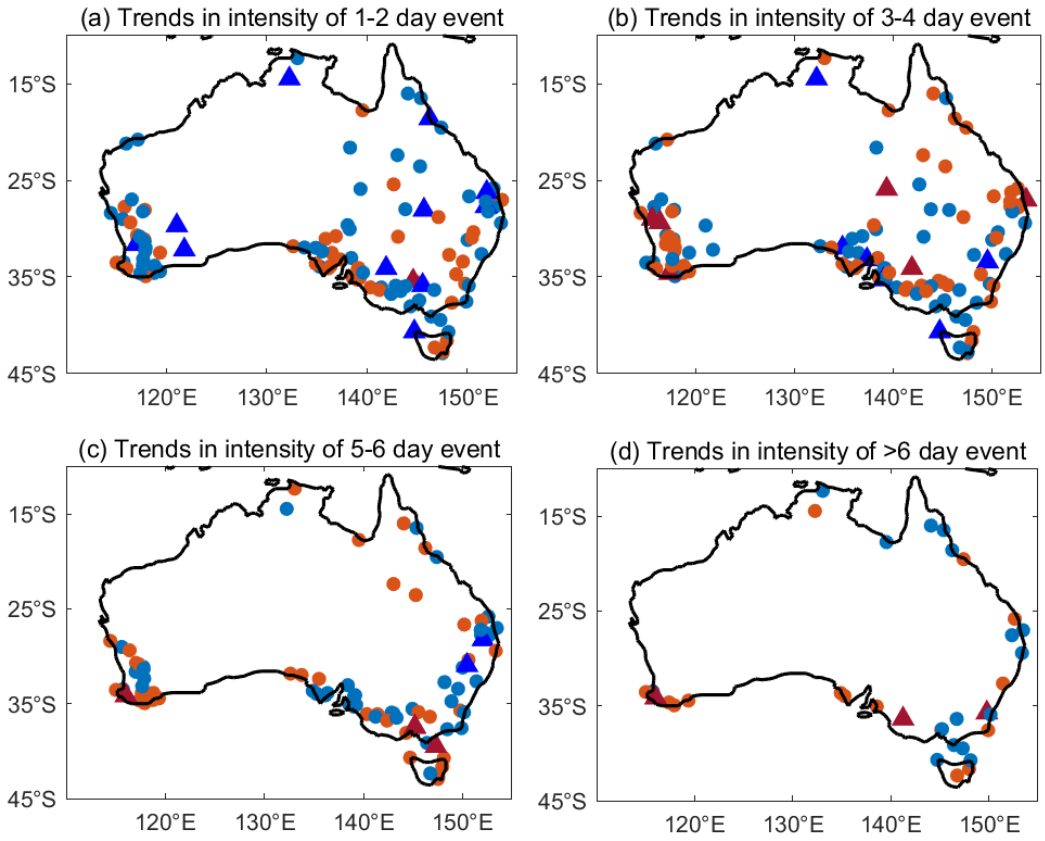

Figure 6.13 Same as Fig. 6.6, for annual maximum of rainfall event intensity.

6.3.2.3 Area-averaged trends in event intensity

Figure 6.14 and 6.15 show the area-averaged time series of the median and maximum intensities respectively of the four types of events, averaged over NWA, SEA and SWWA. No region shows a decrease in the median intensity in any event category (Fig. 6.14). Instead, 16 trends calculated out of the 24 trends (two trends are calculated at each region) show increases that are statistically significant at the 0.05 level. The trends in area average maximum rainfall event intensity are all positive in NWA, showing that extreme rainfall in each event category has intensified in this region. The maximum of 1-2 day events is significantly positive in all

three regions in different periods, which reiterates that short duration extreme events have intensified in Australia. In SEA, the trends in events of >2 days are not significant in long as well as medium term. Some notable features are peaks in both median and maximum intensities of 3-4 day and 5-6 day rainfall events from 2010-2012 in SEA. During 2010-2012 large parts of Australia received much above average rainfall and resulted in widespread floods in areas of NSW, Victoria and QLD (King *et al.*, 2013b). Although there are no significant trends in 3-4 day and 5-6 day events in SWWA, there is a significant decrease in >6 day events evident in the long-term period. Overall, except for >6 day events in SWWA, none of the event types show a significant decrease in maximum rainfall event intensity.

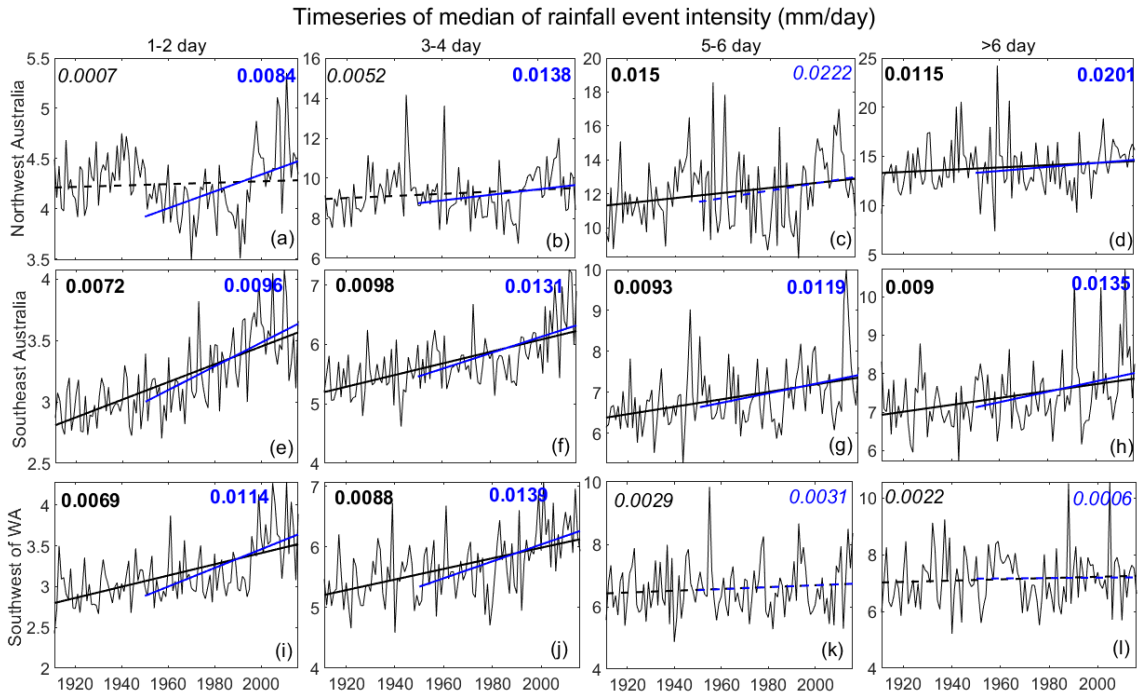

Figure 6.14 Same as Fig. 6.9, but for the median rainfall event intensity.

6.4 Discussion

Previous studies show that only a few regions in Australia demonstrate significant long-term trends in mean and extreme rainfall (Alexander & Arblaster, 2009; Alexander & Arblaster, 2017; Dey *et al.*, 2019). As discussed in the introduction, the available indices to study mean and extreme rainfall do not capture all aspects of changes in rainfall characteristics. At present, we lack understanding of how rainfall duration has changed in the past. Even without a change in total rainfall, a change in how the rain falls (e.g. heavy rainfall in a single day or a multi-day event with light rain) has implications for those dependent on rainfall (e.g. agricultural sector)

and on understanding future changes in rainfall. The rainfall event-based approach employed here shows a near continent-wide increase in frequency and intensity of short-duration events and a decrease in the frequency of extended events with the exception of the tropical north, where extended events have become more frequent. This is the first time that the wide-reaching extent of a long-term significant trend toward more episodic (i.e. 1-2 day) and fewer persistent (i.e. > 2 days) rainfall events has been identified. The trends in the intensity of rainfall events are positive for all event categories which is consistent with the finding "when it rains, it rains more" (Contractor *et al.*, 2018). The method employed here provides valuable information on the types of events contributing to the changes in annual and seasonal mean rainfall. Further, this method provides information relevant to understanding the mechanisms causing the change.

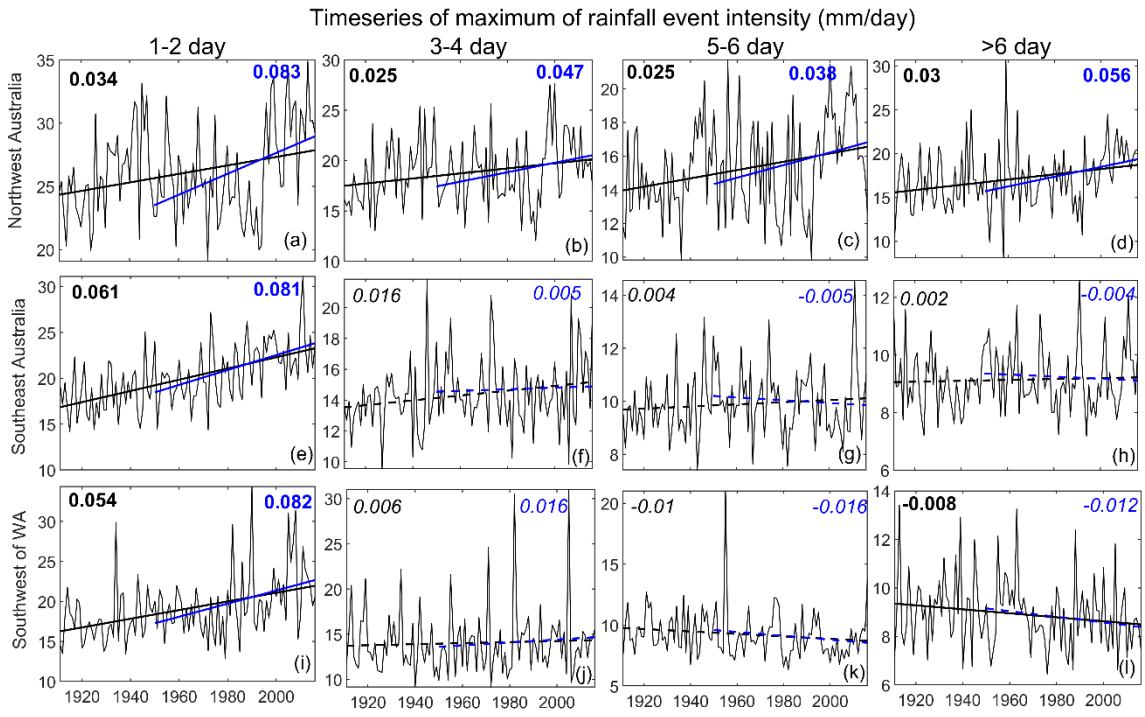

Figure 6.15 Same as Fig. 6.9 but for annual maximum rainfall event intensities.

Tropical north Australia receives most of its annual rainfall via monsoon during summer (DJF) (Berry & Reeder, 2016; Moise *et al.*, 2019). Monsoon rainfall is characterised by bursts (periods of monsoonal activity), and breaks (relatively dry phase). Typically, monsoonal bursts in north Australia persist for 6.7 days (Moise *et al.*, 2019). Our results show, in the north of Australia, while the short-duration rainfall events show mixed trends, the extended persistent events (> 6 days) have become more frequent and longer in duration. These

results suggest there has been a change to the monsoon burst regime in tropical northwest Australia. Clark *et al.* (2018) showed the observed increase in NWA is due to an increase in frequency of organised rainfall bearing synoptic systems rather than an increase in rainfall amounts from those events. This is consistent with our results where we do not find any spatially coherent significant change in intensity in any of the event categories in tropical north Australia.

A recent study showed that a set of CMIP5 models with the correct representation of the Madden-Julian Oscillation projected fewer monsoonal bursts in future with increased rainfall intensity and a small increase in bursts duration in RCP8.5 (Moise *et al.,* 2019). The authors further proposed that the decrease in the number of bursts is consistent with global warming and thermodynamic response – where, in a warmer world, fewer but more intense events are expected. However, our study and previous studies, show evidence of increases in the frequency and intensity of extreme events globally as well as in Australia (Alexander & Arblaster, 2017; Trenberth *et al.*, 2003). In addition, the future change in monsoon burst seems incongruent with the historical increasing trend in rainfall in north Australia. Thus, the future decrease in number of bursts could also potentially be a result of increase in the duration of the bursts and should be investigated further.

In the northwest of WA, annual rainfall has increased; however, there are fewer studies available in this region. Our analysis shows an increase in frequency and intensity of rainfall events of duration up to 6 days. One of the significant drivers of rainfall in this region is the Northwest Cloud Bands (NWCB) (Reid *et al.*, 2019; Wright, 1997). These bands extend from the northwest to the southeast of the country and generally last on average 1-6 day with the maximum duration found is 12 days (Reid *et al.*, 2019). Recent research shows that there has been an increase in the number of NWCB days, and this increase is the most dominant in summer (Reid *et al.*, 2019). Also, an increase in the number of tropical cyclones has been reported in this region which could partially explain the increase in rainfall events of duration up to 6 days (Clark *et al.*, 2018; Lavender & Abbs, 2013).

A significant proportion of total annual rainfall in SWWA and SEA comes from mid-latitude fronts, or low-pressure systems associated with mid-latitude westerlies (Catto *et al.*, 2014; Risbey *et al.*, 2009). Past studies describe a decrease in rainfall in southern Australia due to a southward shift in the descending branch of Hadley circulation and strengthening of the subtropical ridge which constrains the fronts from reaching Australia's mainland (Hope *et al.*,

2006; Pepler *et al.*, 2019). The SWWA receives the majority of its annual rainfall from extended persistent events (> 2 days) as shown in Figure 6.3. SWWA is one of the few regions in Australia where a long-term significant decline in rainfall has been observed (Hope & Ganter, 2010). Our results show that although the frequency and intensity of the 1-2 day events have increased continuously since 1911, the extended duration events (5-6 day, and >6 day) show a long-term decrease in frequency. These trends are significant annually as well as in winter. A persistent decrease in rainfall in SEA is reported by previous research, mainly attributed to reduced frequency of fronts, and cutoff lows (Risbey *et al.*, 2013; Timbal *et al.*, 2015). Frequency of all event categories except for 1-2 day events have decreased in this region. Overall, our results indicate that the reduction in rainfall in southern Australia is the result of a reduction in the frequency of multi-day events, which is also reflected in a shift toward more episodic rainfall (i.e. more 1-2 day events). This could be a result of changes to a number of synoptic features that are associated with changes to regional circulation patterns. Hope *et al.* (2006) showed that the decreased frequency of troughs associated with heavy rainfall explains half of the rainfall decline in SWWA. The authors also suggested that the decrease in the intensity from these events also has a significant impact on the rainfall reduction in this region. A consistent long-term reduction in maximum rainfall event intensity in our analysis is seen for >6 day events.

Rainfall in Tasmania is highly spatially variable due to its orography; the west of Tasmania receives more than 80% rainfall from rainfall events of duration > 6 days. Climatologically, west Tasmania is one of the wettest places in Australia (Dey *et al.*, 2019; Taschetto & England, 2009a). There has been a strong decrease in events > 6 days and an increase in 3-4 day events in spring which again points to a reduction in persistent rainfall events. Like the west, the east of Tasmania also shows a reduction in all persistent events. However, in east Tasmania there is an increase in 1-2 day events much like SEA. The trends in west Tasmania are more similar to SWWA.

There is growing evidence that short-duration rainfall events, for example, sub-daily (Westra *et al.*, 2014) and sub-hourly (Guerreiro *et al.*, 2018) rainfall have intensified in Australia. The increase in these short-duration rainfall events is higher than the expected 7%/˚C increase in Australia and other regions (Guerreiro *et al.*, 2018; Lenderink *et al.*, 2017). Our results are consistent and show even for rainfall events at a daily scale where maximum rainfall intensity of short-duration rainfall events (1-2 day) increases across all seasons in most regions.

The persistent increase in the frequency and intensity of 1-2 day events could be a thermodynamic response to global warming where an increase in the moisture-holding capacity of the atmosphere makes it easier to rain with favourable atmospheric conditions and/or a change in circulation (Allan & Soden, 2008; Chou *et al.*, 2012). Some previous research shows that there is a direct link between increased water vapour and more frequent extreme rainfall events that is consistent across different seasons (Ye *et al.*, 2015). However, the thermodynamic response of rainfall to warming is complex, and further research is required to understand the role of both thermodynamics and dynamics in the shift towards episodic rainfall in Australia.

6.5 Conclusions

There is a spatially coherent increase in short-duration (1-2 day) rainfall events in Australia which is consistent across all seasons. Events of longer duration (> 2 days) have increased in the north and decreased in the south of Australia. Thus, in the south, there is evidence of a change toward more episodic rainfall at the expense of persistent, multi-day rainfall events. In the north, rainfall duration is getting longer, where rainfall events lasting > 6 days have become more frequent. Our rainfall event-based approach shows evidence of continent-wide long-term changes in the rainfall characteristics that have not been identified using other approaches.

The trends we observe using our rainfall event-based approach provide valuable information about how seasonal and annual rainfall is changing on the daily time scale. Further, the approach used here (or similar approaches) can be used to help elucidate the physical mechanisms behind these trends. Future work should connect these trends with weather systems to further reveal whether the events examined here are the result of single or multiple weather systems and how those systems are changing.

Chapter 7

Conclusions and future work

7.1 Summary

This thesis makes an addition to the field of Australian rainfall research by improving our understanding of how the mean and extreme rainfall has changed. First, the thesis investigated the role of anthropogenic forces in rainfall changes. Next, the role of large-scale natural drivers was investigated by studying the timing of extreme rainfall. Third, this thesis pointed out the issues with traditional approaches to explore historical and future extreme events. Lastly, this research came up with a novel and improved method to study mean and rainfall characteristics, which can be used in future studies globally.

Our current state of understanding of rainfall change in Australia was first reviewed in the context of new datasets. The major changes in rainfall detected were a long-term increase in rainfall in northwest Australia (NWA), a persistent decline in the southwest of Western Australia (SWWA), and a decrease in southeast Australia (SEA). However, the trends in SEA become insignificant when analysed at a longer time-scale (1910-2015). Previous studies show that in addition to large-scale drivers, anthropogenic forcings play a significant role in modulating rainfall in Australia. For example, the sub-tropical ridge has been shifted southward, pushing the rain-bearing systems away from Australia, thus reducing rainfall in southern latitudes (Grose *et al.*, 2015). The observed rainfall decline in SWWA is largely attributed to ozone depletion and greenhouse gas increase (Arblaster *et al.*, 2014; Arblaster *et al.*, 2011).

On the other hand, there are only a few attributional studies investigating the role of anthropogenic forcings on the significant rainfall increase in NWA, which is strongest in summer. The rainfall increase was evident in both gridded and observational datasets. This thesis investigated the underlying mechanisms of rainfall increase in this region using the Coupled Model Intercomparison Project phase 5 (CMIP5) historical all-forcing simulations. While the majority of the models showed a positive trend in rainfall, none of the models captured the observed magnitude of the rainfall increase. The reason behind models

underestimating trends in rainfall was further investigated using single forcing detection and attribution experiments. While historical anthropogenic aerosol only (historicalAA) simulations showed an increase in rainfall by strengthening monsoonal flow, historical greenhouse gas only (historicalGHG) simulations showed a decline in rainfall due to a divergent wind trend situated over north Australia. Thus, aerosols and greenhouse gases have offsetting impacts in climate models, which led to an overall underestimation of rainfall trends in historical simulations in north Australia. Thus, correct representation of these anthropogenic drivers and their interactions with Australian rainfall is crucial for understanding the rainfall increase in NWA. For extreme rainfall, both observation and model datasets agreed on an increase in NWA since 1950. Although changes in CMIP5 model simulations were again much smaller compared to observed, the majority of the models showed an increase in mean and extreme rainfall intensity in future simulations. The increase in the Representative Concentration Pathway (RCP) 8.5 simulations were higher than in lower emission RCP2.6 simulations. The results presented here are complimentary to a more recent study by Moise *et al.* (2019), which shows that a set of CMIP5 models with correct Madden-Julian Oscillation (MJO) representation projects an increase in monsoon rainfall. Overall, for reliable rainfall projections in this region, it is essential to use models that incorporate both direct and indirect effects of aerosols along with correct representation of large-scale natural drivers.

Large-scale drivers play a major role in modulating intensity, frequency and the timing of extreme rainfall in Australia. North of Australia receives the majority of its annual rainfall due to monsoonal activities in December-February (DJF). The south of Australia receives rainfall due to several weather signatures, such as fronts, east coast lows (ECL), and cut-off lows, predominantly in winter (June-August). This thesis examined the general timing of extreme rainfall occurring in a year and the relationship between the timing of extreme rainfall (maximum consecutive 5-day rainfall (Rx5)) and large-scale drivers. A clear north-south delineation in extreme rainfall timing was found in Australia. In the north, extreme rainfall occurs in summer months, whereas, extreme rainfall in the south occurs in autumn/winter. The standard deviation in the timing of extreme rainfall is lowest in the north, implying that the extreme rainfall usually occurs around the same time of the year in this region. The standard deviation increased southward, with the maximum year to year variability observed in SEA almost +/-180 days. This implies that extreme rainfall in this region can occur at any time of the year. Thus, predicting the timing of extreme rainfall is highly challenging in SEA.

As summarised in chapter 2, there are many large-scale drivers impacting Australia's rainfall. However, so far, only the relationships between these large-scale drivers and mean and extreme rainfall intensity and/or frequency have been studied. This thesis examines the relationship between the timing of extreme rainfall with large-scale Pacific drivers (the Interdecadal Pacific Oscillation (IPO), and the El-Nino Southern Oscillation (ENSO). The results showed that there is a strong influence of ENSO and IPO in modulating the timing of extreme rainfall. As the observational record is small, ensemble runs of the Twentieth Century Reanalysis (20CR) reanalysis were used to study the relationship between extreme rainfall timing and large-scale drivers in Australia. Depending on the phase of IPO, the area where extreme rainfall occurs in summer moves southward (during negative IPO phase) and northward (during positive IPO phase) compared to usual. This feature was seen in both observed and reanalysis datasets. During La Niña years, extreme rainfall in SEA is received in spring months, whereas during El Niño years, extremes occurs in late autumn/winter months. The results indicated that interaction between ENSO and IOD could explain this shift in the timing of extreme rainfall in SEA. In addition, the timing of extreme rainfall varies significantly with the interaction between IPO and ENSO. Both observed and reanalysis datasets showed larger areas of extreme rainfall in summer during negative IPO (nIPO) and La Niña years compared to positive IPO (pIPO) and El Niño years. The results presented in this chapter showed that depending on phases of the IPO and ENSO, the timing of extreme rainfall in Australia, specifically SEA, shifted significantly.

As stated above, the high variability of rainfall in Australia makes it challenging to study and attribute longer-term changes in rainfall. Different methods, varying datasets and discrepancies in definitions lead to inconsistent results, specifically for extreme rainfall. So far, only a few regions show significant long-term changes in rainfall using existing methods; the areas showing significant trends in extreme rainfall is even fewer. The CMIP5 and CMIP3 models have been widely used to understand historical changes in rainfall in order to provide robust rainfall projections. However, most of the crucial trends that are found in observed dataset are not replicated in models, for example, CMIP5 models cannot capture the strength of the historical increase in rainfall in NWA, and show very little consistency in future rainfall projections. Similarly, the majority of the models cannot capture the strength of the recent decline in rainfall in SEA. Although future simulations show a decline in rainfall in SEA, the model agreement is rather weak. The SWWA is the only region in Australia where models

robustly capture a significant reduction in rainfall and project a further decrease in rainfall with more than two-thirds of the models in agreement. Overall, providing robust rainfall projections remains challenging. On the other hand, numerous studies have reported an unequivocal increase in temperature historically, as well as a robust increase in the future. Thus, a new research pathway of extrapolating extreme rainfall using the relationship between temperature and extreme rainfall was investigated in this thesis.

According to the Clausius-Clapeyron (C-C) relationship, a 7% increase in extreme rainfall is expected per degree warming of the atmosphere. However, strong variability in scaling rates is observed due to the complex interplay between thermodynamic and dynamic drivers. It is already established that using dew point temperature (DPT) instead of dry-bulb temperature for scaling rate calculation provides more consistent results; thus, in this study scaling rates are calculated using DPT. Tropical north and south of Australia showed scaling rates higher than the C-C scaling rate. A further attempt was made to understand the underlying mechanisms of the super C-C relationship in some regions of Australia by studying the thermodynamic and dynamic drivers of extreme rainfall. The results showed that changes in thermodynamic drivers (specific humidity) with temperature led to the super C-C scaling rate in the south of Australia, whereas changes in the dynamic drivers (wind convergence) played a more significant role in the tropics. The scaling rates calculated using the RCP8.5 simulation over the period 2061-2090 were higher than scaling rates calculated in historical simulations over the period 1986-2015. This indicated that scaling rates are non-stationary. Thus, historical scaling rates cannot simply be used to extrapolate extreme rainfall into the future. Finally, comparing the methods of projecting extreme rainfall showed that the changes using the traditional approach were much smaller compared to the expected 7% C-C scaling rate. Thus, if scaling rates are to be believed, the traditional approach can significantly underestimate future changes in extreme rainfall. However, scaling rates are non-stationary and non-linear, which has not been taken into account in any previously published study. Thus, the applicability of using it to extrapolate extremes into the future remains questionable.

Finally, this research developed a new approach to study rainfall characteristics as existing approaches rarely showed any robust long-term changes in rainfall in Australia. A novel rainfall event-based approach was applied to detect long-term changes in rainfall characteristics in Australia. A rainfall event was defined as the number consecutive days of rain days. Using this approach, for the first time continent-wide significant changes were

observed, which has not been found in previous studies. First, a near continent-wide increase in the frequency of rainfall events is seen over 1911-2016. In contrast, the average rainfall event duration showed a clear increase north of 20°S and a decrease south of 20°S, suggesting a shift towards episodic rainfall in Australia below 20°S. A more in-depth analysis of rainfall events segregated according to event duration showed that short-duration rainfall events, such as 1-2 day events, have become more frequent and intensified almost everywhere in Australia, evident in all seasons. The extended duration events (>2 days) showed a clear reduction in frequency in long-term drought-stricken regions in Australia. For rainfall event intensity, short-duration events (1-2 day) have intensified; however, trends in longer duration events were not significant. Overall, trends in frequency were more spatially coherent compared to changes in intensity. This novel method opens a new pathway to study changes in rainfall characteristics while providing indications on the type of rainfall event responsible for causing an overall variation in rainfall.

7.2 Knowledge gaps and future research directions

There are still significant knowledge gaps in the field of mean and extreme rainfall. The knowledge gaps and future applications of this research are discussed below:

In NWA, the direction of future rainfall changes remains uncertain. The primary large-scale drivers crucial for rainfall in NWA is summarised in this thesis. Both indirect and direct effects of aerosols are known to modulate regional rainfall (Huang *et al.*, 2007). As shown in this research, aerosols play a crucial role in increasing the monsoonal flow and thus increases rainfall in this region. Therefore, future studies are required to explicitly understand the role of indirect and direct effects of aerosols in rainfall changes in this region using new generation CMIP6 simulations. The aerosols chemistry model intercomparison project (AerChemMIP) simulations (Collins *et al.*, 2017) will allow more scope for examining these impacts than previous generations of climate models.

As pointed out in this research, the variability in the timing of extreme rainfall is maximum in the south of Australia. This is the most crucial region in Australia from agriculture and demographic perspective, also known as the wheat belt of Australia (Nawi, 2009). Understanding the timing of extreme rainfall has implications for improving seasonal prediction of mean and extreme rainfall. For example, this study showed that large-scale drivers, such as phases of ENSO and IPO partly determine in which month extreme rainfall

occurs in Australia. Although chapter 4 only investigated the role of IPO and ENSO, the results presented in the chapter provided indications that IOD and SAM also potentially play key roles in modulating the timing of extreme rainfall. In future, the relationship of IOD and SAM with the timing of extreme rainfall should be tested explicitly, and specifically the interaction between these large-scale drivers and decadal variability. In addition, future research should investigate whether Australia's current seasonal prediction system, the Australian Community Climate and Earth-System Simulator-S1 (ACCESS-S1) can capture the large-scale interactions between the timing of extreme rainfall and the Pacific variability, that was reported in this research.

There are still some fundamental questions that remain uncertain using scaling rates to project extreme rainfall. For example, there is a lack of understanding around how scaling rate, defined as a relationship between temperature and extreme rainfall at a daily time scale, calculated over a period, can be used to conclude changes in extreme rainfall at the climate scale (e.g. changes in future compared to historical time period). In addition, chapter 5 showed that scaling rates are non-linear and non-stationary, which makes it challenging to use them to infer extreme rainfall projections. Overall, future research focusing on rainfall projections using scaling rates should consider the non-linear and non-stationary aspects of scaling rates. The applicability of scaling rates for extreme rainfall projection remains questionable.

This thesis introduced a new approach to study rainfall characteristics by using rainfall events, which resulted in the detection of significant long-term changes in rainfall characteristics. In future, I aim to study the mechanisms behind the near-continent-wide increase in intensity and frequency of short-duration rainfall events in Australia. This method can be used elsewhere and globally, to understand robust changes in rainfall characteristics. This new approach opens various new avenues for future rainfall studies. For example, further modelling studies are required to investigate if climate models can capture the shift toward short-duration episodic rainfall in Australia. Upon verifying the historical trends in climate models, this method can be used for robust rainfall projections.

There is a need to update the existing approaches to study rainfall characteristics, such as the Expert Team on Climate Change Detection and Indices (ETCCDI; Zhang et al., 2011) indices. As pointed out in this research, the majority of studies investigate the intensity and frequency of extreme rainfall, and thus uses indices such as maximum 1-day rainfall (Rx1), and Rx5. This thesis briefly summarises the major issues with some of the existing indices in

chapter 6, thus revisiting the indices to understand what it means for Australia's rainfall should be studied in future. For example, understand the contribution of Rx5 and Rx1 to total rainfall and if it has changed historically, is crucial before applying these indices in future research. In addition, there is a need to understand how rainfall has changed beyond just the intensity and frequency, for example, duration and the timing of extreme rainfall.

It goes without saying that improving and constraining rainfall projections is crucial; however, projections of more nuanced information on rainfall characteristics are required. For example, the wheat-sheep belt of Australia has shifted further south (Chen *et al.*, 2019) as a result of a persistent decrease in winter rainfall in this region. This reiterates the importance of understanding fine-scale information such as a future shift in seasonal rainfall at a regional scale. More endeavour is required in breaking down rainfall projections using regional modelling, and improved downscaling techniques. In addition, further effort is needed to untangle the reasons behind our low confidence in historical as well as future changes in rainfall. A collective effort using various sources of observation datasets to calculate updated and improved indices is required.

Appendices

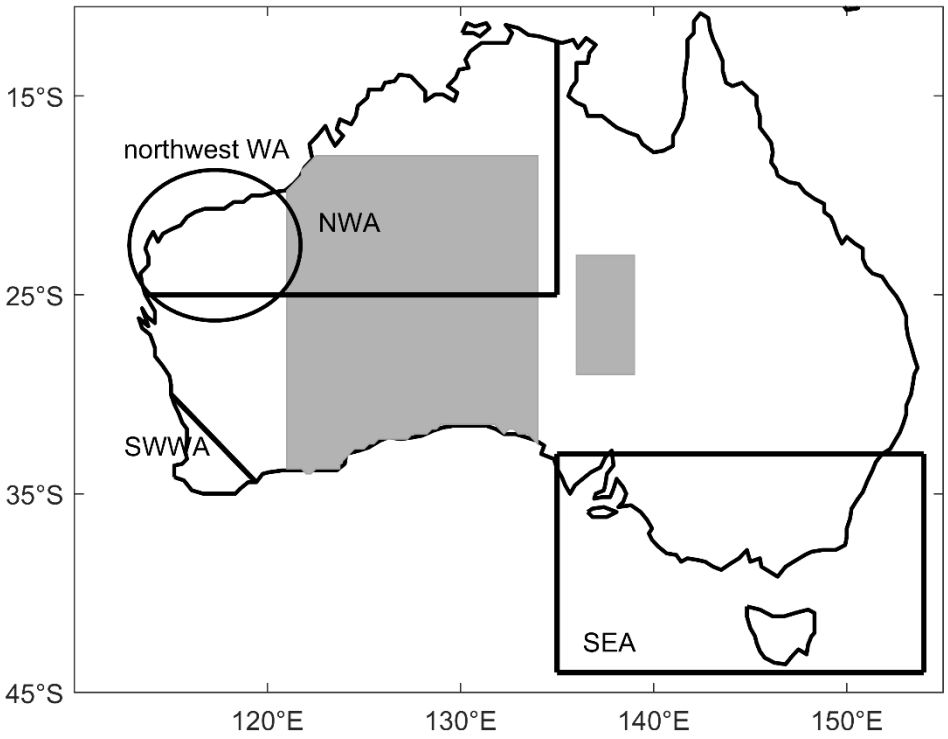

Figure s6.1. The figure highlights the regions that are frequently discussed in the text, northwest Australia (NWA; 10˚–25˚S, 110˚–135˚E), southeast Australia (SEA; 33˚–44˚S, 135˚–154˚E) and southwest of Western Australia (SWWA; southwest of the line joining 30˚S, 115˚E, and 35˚S, 120˚E), and northwest of Western Australia.

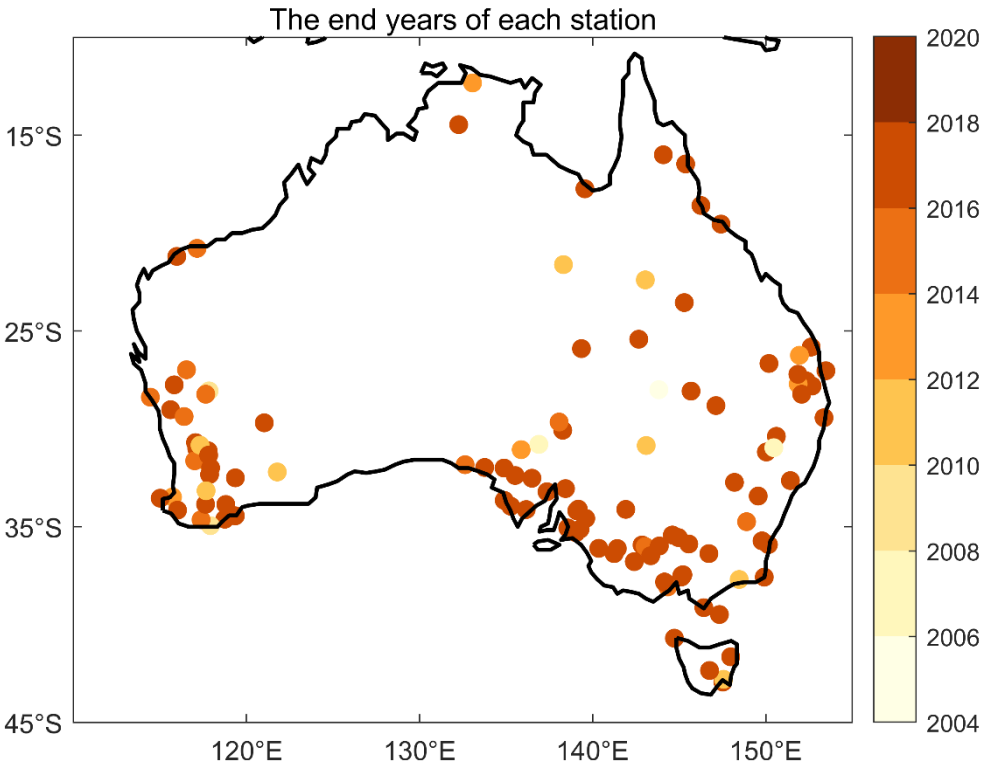

Figure s6.2. The finishing year (the latest year when dataset is available) at each station. The trends in Fig. 6 and Fig. 13 are calculated over the period 1911-latest available year of dataset, shown here.

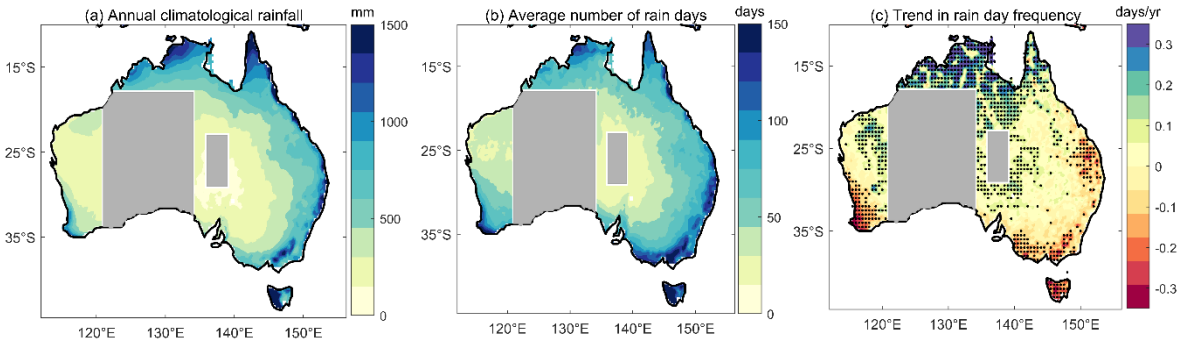

Figure s6.3. (a) Climatological annual total rainfall (mm), (b) the climatological average of rain days (c) the trends in the annual number of rain days (days/year). The AWAP daily rainfall data is used over the period 1911-2016. The stipplings show areas where trends are significant at the 95% confidence level. Significance is calculated using Mann-Kendall non-parametric test.

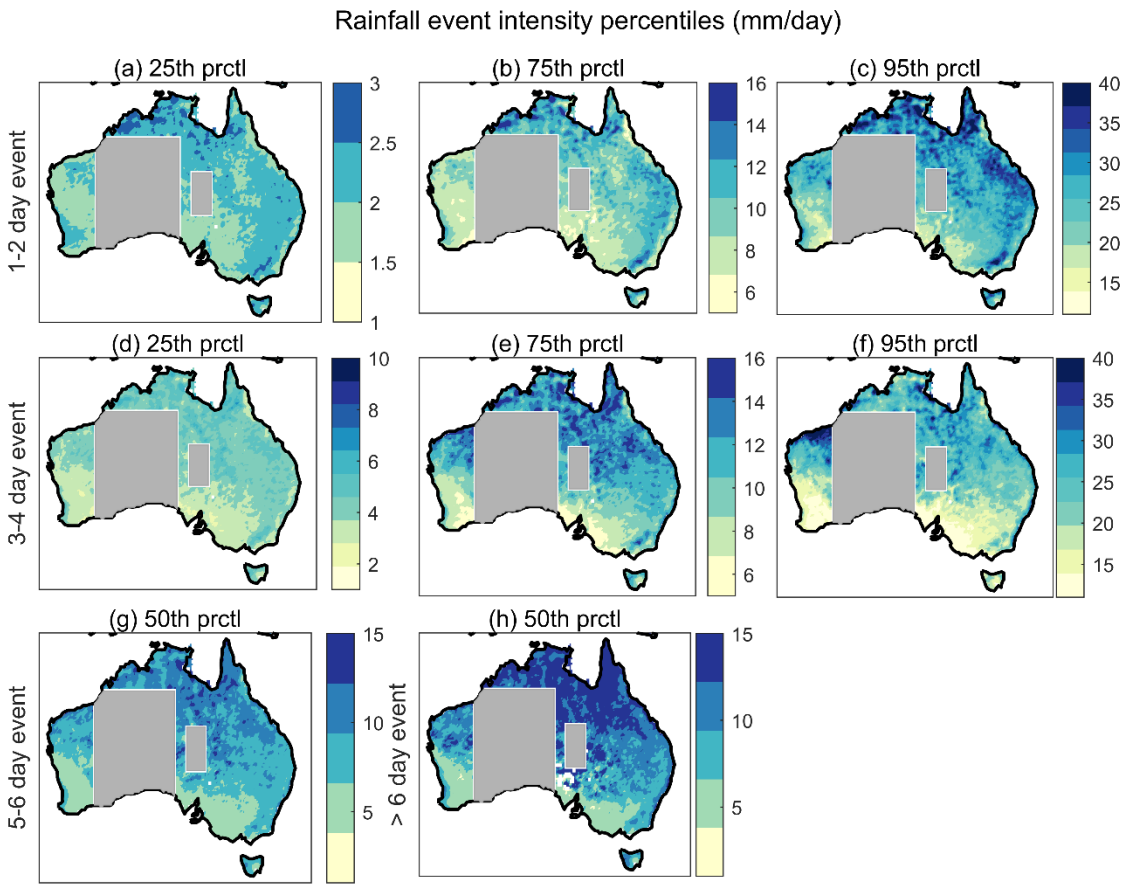

Figure s6.4. The (a) 25th (b) 75th (c) 95th percentile of rainfall event intensity (mm/day) for 1-2 day events, (d-f) 3-4 day events, and the 50th percentile of rainfall event intensity of (g) 5-6 day events and (h) >6 day events.

Bibliography

Abbs, D. (2012). The impact of climate change on the climatology of tropical cyclones in the Australian region. Retrieved September, 5, 2014 from https://research.csiro.au/climate/wp-content/uploads/sites/54/2016/03/11_WP11-CAF-climchange-tropcyclones.pdf.

Abram, N. J., Gagan, M. K., Cole, J. E., Hantoro, W. S., & Mudelsee, M. (2008). Recent intensification of tropical climate variability in the Indian Ocean. *Nature Geoscience*, 1(12), 849

Abram, N. J., Mulvaney, R., Vimeux, F., Phipps, S. J., Turner, J., & England, M. H. (2014). Evolution of the Southern Annular Mode during the past millennium. *Nature Climate Change*, 4(7), 564. Ackerley, D., Berry, G., Jakob, C., Reeder, M. J., & Schwendike, J. (2015). Summertime precipitation over northern Australia in AMIP simulations from CMIP5. *Quarterly Journal of the Royal Meteorological Society*, 141(690), 1753-1768.

Ahrens, C. D. (2012). Meteorology today: an introduction to weather, climate, and the environment: Cengage Learning.

Alexander, L. V., & Arblaster, J. M. (2009). Assessing trends in observed and modelled climate extremes over Australia in relation to future projections. *International Journal of Climatology*, 29(3), 417-435.

Alexander, L. V., & Arblaster, J. M. (2017). Historical and projected trends in temperature and precipitation extremes in Australia in observations and CMIP5. *Weather and Climate Extremes*, 15, 34-56.

Alexander, L. V., Zhang, X., Peterson, T. C., Caesar, J., Gleason, B., Klein Tank, A. M. G., . . . Vazquez-Aguirre, J. L. (2006). Global observed changes in daily climate extremes of temperature and precipitation. *Journal of Geophysical Research: Atmospheres*, 111, D05109

Ali, H., Fowler, H. J., & Mishra, V. (2018). Global observational evidence of strong linkage between dew point temperature and precipitation extremes. *Geophysical Research Letters*, 45(22), 12,320-12,330.

Ali, H., & Mishra, V. (2017). Contrasting response of rainfall extremes to increase in surface air and dewpoint temperatures at urban locations in India. *Scientific reports*, 7(1), 1228.

Allan, R. J., & Haylock, M. R. (1993). Circulation features associated with the winter rainfall decrease in southwestern Australia. *Journal of Climate*, 6(7), 1356-1367.

Allan, R. P., & Soden, B. J. (2008). Atmospheric warming and the amplification of precipitation extremes. *Science*, 321(5895), 1481-1484.

Allen, M. R., & Ingram, W. J. (2002). Constraints on future changes in climate and the hydrologic cycle. *Nature*, 419(6903), 228-232.

Anagnostopoulou, C., & Tolika, K. (2012). Extreme precipitation in Europe: statistical threshold selection based on climatological criteria. *Theoretical and Applied Climatology*, 107(3), 479-489.

Andrys, J., Kala, J., & Lyons, T. J. (2017). Regional climate projections of mean and extreme climate for the southwest of Western Australia (1970–1999 compared to 2030–2059). *Climate Dynamics*, 48(5-6), 1723-1747.

Arblaster, J., Gillett, N., Calvo, N., Forster, P., Polvani, L., Son, S., . . . Wu, Y. (2014). *Stratospheric ozone changes and climate* (P. A. N. Ayité-Lô Nohende Ajavon, John A. Pyle, A.R. Ravishankara Ed. Vol. 55). Geneva Switzerland: World Meteorological Organization.

Arblaster, J., Meehl, G., & Karoly, D. (2011). Future climate change in the Southern Hemisphere: Competing effects of ozone and greenhouse gases. *Geophysical Research Letters,* 38(2) , L02701.

Arblaster, J., Meehl, G., & Moore, A. (2002). Interdecadal modulation of Australian rainfall. *Climate Dynamics,* 18(6), 519-531.

Arblaster, J. M., & Meehl, G. A. (2006). Contributions of external forcings to southern annular mode trends. *Journal of Climate,* 19(12), 2896-2905.

Ashcroft, L., Karoly, D. J., & Dowdy, A. J. (2019). Historical extreme rainfall events in southeastern Australia. *Weather and Climate Extremes,* 25, 100210.

Ashcroft, L., Karoly, D. J., & Gergis, J. (2014). Southeastern Australian climate variability 1860–2009: a multivariate analysis. *International Journal of Climatology,* 34(6), 1928-1944.

Ashok, K., Guan, Z., & Yamagata, T. (2003). Influence of the Indian Ocean Dipole on the Australian winter rainfall. *Geophysical Research Letters,* 30(15), 1821.

Ashok, K., Nakamura, H., & Yamagata, T. (2007). Impacts of ENSO and Indian Ocean dipole events on the Southern Hemisphere storm-track activity during austral winter. *Journal of Climate,* 20(13), 3147-3163.

Australian Bureau of Statistics. (2019). Australian Demographic Statistics Retrieved 20/06/2020 http://www.abs.gov.au/ausstats/abs@.nsf/mf/3101.0

Avila, F. B., Dong, S., Menang, K. P., Rajczak, J., Renom, M., Donat, M. G., & Alexander, L. V. (2015). Systematic investigation of gridding-related scaling effects on annual statistics of daily temperature and precipitation maxima: A case study for south-east Australia. *Weather and Climate Extremes,* 9, 6-16.

Banacos, P. C., & Schultz, D. M. (2005). The use of moisture flux convergence in forecasting convective initiation: Historical and operational perspectives. *Weather and Forecasting,* 20(3), 351-366.

Bao, J., Sherwood, S. C., Alexander, L. V., & Evans, J. P. (2017). Future increases in extreme precipitation exceed observed scaling rates. *Nature Climate Change,* 7(2), 128.

Barbero, R., Westra, S., Lenderink, G., & Fowler, H. (2018). Temperature-extreme precipitation scaling: a two-way causality? *International Journal of Climatology,* 38, e1274-e1279.

Bates, B. C., Hope, P., Ryan, B., Smith, I., & Charles, S. (2008). Key findings from the Indian Ocean Climate Initiative and their impact on policy development in Australia. *Climatic Change,* 89(3-4), 339-354.

Bayr, T., Dommenget, D., Martin, T., & Power, S. B. (2014). The eastward shift of the Walker Circulation in response to global warming and its relationship to ENSO variability. *Climate Dynamics,* 43(9), 2747-2763.

Beguería, S. (2005). Uncertainties in partial duration series modelling of extremes related to the choice of the threshold value. *Journal of Hydrology,* 303(1), 215-230.

Bellomo, K., & Clement, A. C. (2015). Evidence for weakening of the Walker circulation from cloud observations. *Geophysical Research Letters,* 42(18), 7758-7766.

Berens, P. (2009). CircStat: a MATLAB toolbox for circular statistics. *Journal of Statistical Software,* 31(10), 1-21.

Berg, P., Haerter, J. O., Thejll, P., Piani, C., Hagemann, S., & Christensen, J. H. (2009). Seasonal characteristics of the relationship between daily precipitation intensity and surface temperature,114, D18102.

Berg, P., Moseley, C., & Haerter, J. O. (2013). Strong increase in convective precipitation in response to higher temperatures. *Nature Geoscience,* 6, 181.

https://www.nature.com/articles/ngeo1731#supplementary-information
Berry, G., Jakob, C., & Reeder, M. (2011a). Recent global trends in atmospheric fronts. *Geophysical Research Letters,* 38(21), L21812.
Berry, G., Reeder, M. J., & Jakob, C. (2011b). Physical Mechanisms Regulating Summertime Rainfall over Northwestern Australia. *Journal of Climate,* 24(14), 3705-3717.
Berry, G. J., & Reeder, M. J. (2016). The Dynamics of Australian Monsoon Bursts. *Journal of the Atmospheric Sciences,* 73(1), 55-69.
Blöschl, G., Hall, J., Parajka, J., Perdigão, R. A., Merz, B., Arheimer, B., . . . Borga, M. (2017). Changing climate shifts timing of European floods. *science,* 357(6351), 588-590.
Bollasina, M. A., Ming, Y., & Ramaswamy, V. (2011). Anthropogenic aerosols and the weakening of the South Asian summer monsoon. *science,* 334(6055), 502-505.
Brown, J. R., Moise, A. F., Colman, R., & Zhang, H. (2016). Will a Warmer World Mean a Wetter or Drier Australian Monsoon? *Journal of Climate,* 29(12), 4577-4596.
Bui, A., Johnson, F., & Wasko, C. (2019). The relationship of atmospheric air temperature and dew point temperature to extreme rainfall. *Environmental Research Letters,* 14(7), 074025.
Cai, W., & Cowan, T. (2006). SAM and regional rainfall in IPCC AR4 models: Can anthropogenic forcing account for southwest Western Australian winter rainfall reduction? *Geophysical Research Letters,* 33(24),L24708.
Cai, W., Cowan, T., & Sullivan, A. (2009a). Recent unprecedented skewness towards positive Indian Ocean Dipole occurrences and its impact on Australian rainfall. *Geophysical Research Letters,* 36(11),L11705.
Cai, W., Cowan, T., Sullivan, A., Ribbe, J., & Shi, G. (2011b). Are Anthropogenic Aerosols Responsible for the Northwest Australia Summer Rainfall Increase? A CMIP3 Perspective and Implications. *Journal of Climate,* 24(10), 2556-2564.
Cai, W., Purich, A., Cowan, T., van Rensch, P., & Weller, E. (2014a). Did climate change–induced rainfall trends contribute to the Australian Millennium Drought? *Journal of Climate,* 27(9), 3145-3168.
Cai, W., Santoso, A., Wang, G., Weller, E., Wu, L., Ashok, K., . . . Yamagata, T. (2014b). Increased frequency of extreme Indian Ocean Dipole events due to greenhouse warming. *Nature,* 510(7504), 254-258.
Cai, W., Sullivan, A., & Cowan, T. (2009b). Climate change contributes to more frequent consecutive positive Indian Ocean Dipole events. *Geophysical Research Letters,* 36(23),L23704.
Cai, W., Sullivan, A., & Cowan, T. (2011a). Interactions of ENSO, the IOD, and the SAM in CMIP3 models. *Journal of Climate,* 24(6), 1688-1704.
Cai, W., Van Rensch, P., Borlace, S., & Cowan, T. (2011d). Does the Southern Annular Mode contribute to the persistence of the multidecade-long drought over southwest Western Australia? *Geophysical Research Letters,* 38(14),L14712.
Cai, W., Van Rensch, P., Cowan, T., & Hendon, H. H. (2011c). Teleconnection pathways of ENSO and the IOD and the mechanisms for impacts on Australian rainfall. *Journal of Climate,* 24(15), 3910-3923.
Cai, W., Van Rensch, P., Cowan, T., & Sullivan, A. (2010). Asymmetry in ENSO teleconnection with regional rainfall, its multidecadal variability, and impact. *Journal of Climate,* 23(18), 4944-4955.
Cai, W., Wang, G., Santoso, A., McPhaden, M. J., Wu, L., Jin, F.-F., . . . Guilyardi, E. (2015). Increased frequency of extreme La Niña events under greenhouse warming. *Nature Climate Change,* 5(2), 132-137.

Cai, W., Zheng, X.-T., Weller, E., Collins, M., Cowan, T., Lengaigne, M., . . . Yamagata, T. (2013). Projected response of the Indian Ocean Dipole to greenhouse warming. *Nature Geoscience,* 6(12), 999.

Callaghan, J., & Power, S. B. (2011). Variability and decline in the number of severe tropical cyclones making land-fall over eastern Australia since the late nineteenth century. *Climate Dynamics,* 37(3-4), 647-662.

Camargo, S. J., & Wing, A. A. (2016). Tropical cyclones in climate models. *Wiley Interdisciplinary Reviews: Climate Change,* 7(2), 211-237.

Catto, J., Jakob, C., Berry, G., & Nicholls, N. (2012b). Relating global precipitation to atmospheric fronts. *Geophysical Research Letters,* 39(10),L10805.

Catto, J., Nicholls, N., Jakob, C., & Shelton, K. (2014). Atmospheric fronts in current and future climates. *Geophysical Research Letters,* 41(21), 7642-7650.

Catto, J. L., Jakob, C., & Nicholls, N. (2012a). The influence of changes in synoptic regimes on north Australian wet season rainfall trends. *Journal of Geophysical Research: Atmospheres,* 117(D10), D10102.

Chang, C. W. J., Tseng, W. L., Hsu, H. H., Keenlyside, N., & Tsuang, B. J. (2015). The Madden-Julian Oscillation in a warmer world. *Geophysical Research Letters,* 42(14), 6034-6042.

Charles, S., Silberstein, R., Teng, J., Fu, G., Hodgson, G., Gabrovsek, C., . . . Kirono, D. (2010). Climate analyses for South-West Western Australia: A report to the Australian Government from the CSIRO South-West Western Australia Sustainable Yields Project.

Chen, C., Fletcher, A., Ota, N., Lawes, R., & Oliver, Y. (2019). The spatial response of water-limited wheat yield to historical climate change across Western Australia since 1900. Paper presented at the Proceedings 19th Australian Agronomy Conference. Wagga Wagga, Australia.

Chou, C., Chen, C.-A., Tan, P.-H., & Chen, K. T. (2012). Mechanisms for Global Warming Impacts on Precipitation Frequency and Intensity. *Journal of Climate,* 25(9), 3291-3306.

Christensen, J.H., K. Krishna Kumar, E. Aldrian, S.-I. An, I.F.A. Cavalcanti, M. de Castro, . . . T. Zhou, 2013: Climate Phenomena and their Relevance for Future Regional Climate Change. In: Climate Change 2013: The Physical Science Basis. Contribution of Working Group I to the Fifth Assessment Report of the Intergovernmental Panel on Climate Change [Stocker, T.F., D. Qin, G.-K. Plattner, M. Tignor, S.K. Allen, J. Boschung, A. Nauels, Y. Xia, V. Bex and P.M. Midgley (eds.)]. Cambridge University Press, Cambridge, United Kingdom and New York, NY, USA Christidis, N., Stott, P. A., Karoly, D. J., & Ciavarella, A. (2013). An attribution study of the heavy rainfall over eastern Australia in March 2012. *Bulletin of the American Meteorological Society,* 94(9), S58.

Chung, C., & Power, S. (2017). The non-linear impact of El Niño, La Niña and the Southern Oscillation on seasonal and regional Australian precipitation. *Journal of Southern Hemisphere Earth Systems Science,* 67(1), 25-45.

Clark, S., Reeder, M., & Jakob, C. (2018). Rainfall regimes over northwestern Australia. *Quarterly Journal of the Royal Meteorological Society,* 144(711), 458-467.

Collins, M., An, S.-I., Cai, W., Ganachaud, A., Guilyardi, E., Jin, F.-F., . . . Wittenberg, A. (2010). The impact of global warming on the tropical Pacific Ocean and El Niño. *Nature Geoscience,* 3(6), 391.

Collins, W. J., Lamarque, J.-F., Schulz, M., Boucher, O., Eyring, V., Hegglin, M. I., . . . Shindell, D. (2017). AerChemMIP: quantifying the effects of chemistry and aerosols in CMIP6 , *Geoscientific Model Development*, 10, 585–607.

Compo, G. P., Whitaker, J. S., Sardeshmukh, P. D., Matsui, N., Allan, R. J., Yin, X., . . . Bessemoulin, P. (2011). The twentieth century reanalysis project. *Quarterly Journal of the Royal Meteorological Society,* 137(654), 1-28.

Contractor, S., Alexander, L. V., Donat, M. G., & Herold, N. (2015). How well do gridded datasets of observed daily precipitation compare over Australia? *Advances in Meteorology,* 2015, 325718.

Contractor, S., Donat, M. G., & Alexander, L. V. (2018). Intensification of the daily wet day rainfall distribution across Australia. *Geophysical Research Letters*, 45, 8568– 8576.

Dare, R. A., Davidson, N. E., & McBride, J. L. (2012). Tropical Cyclone Contribution to Rainfall over Australia. *Monthly Weather Review,* 140(11), 3606-3619.

Delworth, T. L., & Zeng, F. (2014). Regional rainfall decline in Australia attributed to anthropogenic greenhouse gases and ozone levels. *Nature Geoscience,* 7(8), 583-587.

Deser, C., Phillips, A. S., & Alexander, M. A. (2010). Twentieth century tropical sea surface temperature trends revisited. *Geophysical Research Letters,* 37(10), L10701.

Dey, R., Lewis, S. C., & Abram, N. J. (2018). Investigating observed northwest Australian rainfall trends in Coupled Model Intercomparison Project phase 5 detection and attribution experiments. *International Journal of Climatology.*, 39: 112– 127.

Dey, R., Lewis, S. C., Arblaster, J. M., & Abram, N. J. (2019). A review of past and projected changes in Australia's rainfall. *Wiley Interdisciplinary Reviews: Climate Change,* 10(3), e577.

Dittus, A. J., Karoly, D. J., Lewis, S. C., & Alexander, L. V. (2015). A Multiregion Assessment of Observed Changes in the Areal Extent of Temperature and Precipitation Extremes. *Journal of Climate*, 28(23), 9206-9220.

Donat, M. G., Alexander, L. V., Yang, H., Durre, I., Vose, R., & Caesar, J. (2013b). Global Land-Based Datasets for Monitoring Climatic Extremes. *Bulletin of the American Meteorological Society*, 94(7), 997-1006.

Donat, M. G., Alexander, L. V., Yang, H., Durre, I., Vose, R., Dunn, R. J. H., . . . Kitching, S. (2013a). Updated analyses of temperature and precipitation extreme indices since the beginning of the twentieth century: the HadEX2 dataset. *Journal of Geophysical Research: Atmospheres,* 118(5), 2098-2118.

Donat, M. G., Angélil, O., & Ukkola, A. M. (2019). Intensification of precipitation extremes in the world's humid and water-limited regions. *Environmental Research Letters,* 14(6), 065003.

Dong, B., & Dai, A. (2015). The influence of the Interdecadal Pacific Oscillation on temperature and precipitation over the globe. *Climate Dynamics,* 45(9-10), 2667-2681.

Dong, L., & Zhou, T. (2014). The Indian Ocean sea surface temperature warming simulated by CMIP5 models during the twentieth century: Competing forcing roles of GHGs and anthropogenic aerosols. *Journal of Climate,* 27(9), 3348-3362.

Drobinski, P., Alonzo, B., Bastin, S., Silva, N. D., & Muller, C. (2016). Scaling of precipitation extremes with temperature in the French Mediterranean region: What explains the hook shape? *Journal of Geophysical Research: Atmospheres,* 121(7), 3100-3119.

Drobinski, P., Da Silva, N., Panthou, G., Bastin, S., Muller, C., Ahrens, B., . . . Giorgi, F. (2018). Scaling precipitation extremes with temperature in the Mediterranean: past climate assessment and projection in anthropogenic scenarios. *Climate Dynamics,* 51(3), 1237-1257.

Du, H., Alexander, L. V., Donat, M. G., Lippmann, T., Srivastava, A., Salinger, J., . . . Wu, Z. (2019). Precipitation From Persistent Extremes is Increasing in Most Regions and Globally. *Geophysical Research Letters,* 46(11), 6041-6049.

Easterling, D. R., Evans, J. L., Groisman, P. Y., Karl, T. R., Kunkel, K. E., & Ambenje, P. (2000). Observed Variability and Trends in Extreme Climate Events: A Brief Review. *Bulletin of the American Meteorological Society,* 81(3), 417-426.

Evans, J., Pepler, A., Di Luca, A., Ji, F., Alexander, L., & Argueso, D. (2015). *Future changes in extreme East coast lows.* Paper presented at the 36th Hydrology and Water Resources Symposium: The art and science of water. Barton, ACT: Engineers Australia,1131-1138

Evans, J. P., Argueso, D., Olson, R., & Di Luca, A. (2017). Bias-corrected regional climate projections of extreme rainfall in south-east Australia. *Theoretical and Applied Climatology,* 130(3-4), 1085-1098.

Evans, J. P., & Boyer-Souchet, I. (2012). Local sea surface temperatures add to extreme precipitation in northeast Australia during La Niña. *Geophysical Research Letters,* 39(10), L10803.

Fenby, C., & Gergis, J. (2013). Rainfall variations in south-eastern Australia part 1: consolidating evidence from pre-instrumental documentary sources, 1788–1860. *International Journal of Climatology,* 33(14), 2956-2972.

Feng, J., Li, J., & Li, Y. (2010). Is there a relationship between the SAM and southwest Western Australian winter rainfall? *Journal of Climate,* 23(22), 6082-6089.

Fischer, E. M., & Knutti, R. (2016). Observed heavy precipitation increase confirms theory and early models. *Nature Climate Change,* 6(11), 986.

Fisher, R. A. (1953). Dispersion on a sphere. *Proceedings of the Royal Society of London. Series A. Mathematical and Physical Sciences,* 217(1130), 295-305.

Flato, G., Marotzke, J., Abiodun, B., Braconnot, P., Chou, S. C., Collins, W., . . . Eyring, V. (2014). Evaluation of climate models. In Climate change 2013: the physical science basis. Contribution of Working Group I to the Fifth Assessment Report of the Intergovernmental Panel on Climate Change (pp. 741-866): Cambridge University Press.

Fogt, R. L., & Bromwich, D. H. (2006). Decadal variability of the ENSO teleconnection to the high-latitude South Pacific governed by coupling with the southern annular mode. *Journal of Climate,* 19(6), 979-997.

Fogt, R. L., Bromwich, D. H., & Hines, K. M. (2011). Understanding the SAM influence on the South Pacific ENSO teleconnection. *Climate Dynamics,* 36(7-8), 1555-1576.

Fowler, A. M., Boswijk, G., Gergis, J., & Lorrey, A. (2008). ENSO history recorded in Agathis australis (kauri) tree rings. Part A: kauri's potential as an ENSO proxy. *International Journal of Climatology: A Journal of the Royal Meteorological Society,* 28(1), 1-20.

Frederiksen, J. S., & Frederiksen, C. S. (2007). Interdecadal changes in southern hemisphere winter storm track modes. *Tellus Series a-Dynamic Meteorology and Oceanography,* 59(5), 599-617.

Freund, M., Henley, B. J., Karoly, D. J., Allen, K. J., & Baker, P. J. (2017). Multi-century cool- and warm-season rainfall reconstructions for Australia's major climatic regions. *Climate of the Past,* 13(12), 1751-1770.

Gallant, A. J., Hennessy, K. J., & Risbey, J. (2007). Trends in rainfall indices for six Australian regions: 1910-2005. *Australian Meteorological Magazine,* 56(4), 223-241.

Gallant, A. J., & Karoly, D. J. (2010). A combined climate extremes index for the Australian region. *Journal of Climate,* 23(23), 6153-6165.

Gergis, J., & Ashcroft, L. (2013). Rainfall variations in south-eastern Australia part 2: a comparison of documentary, early instrumental and palaeoclimate records, 1788–2008. *International Journal of Climatology,* 33(14), 2973-2987.

Gergis, J., Gallant, A. J. E., Braganza, K., Karoly, D. J., Allen, K., Cullen, L., . . . McGregor, S. (2012). On the long-term context of the 1997–2009 'Big Dry'in South-Eastern Australia: insights from a 206-year multi-proxy rainfall reconstruction. *Climatic Change,* 111(3-4), 923-944.

Gillett, N., & Fyfe, J. (2013). Annular mode changes in the CMIP5 simulations. *Geophysical Research Letters,* 40(6), 1189-1193.

Goswami, B. N., Venugopal, V., Sengupta, D., Madhusoodanan, M., & Xavier, P. K. (2006). Increasing trend of extreme rain events over India in a warming environment. S*cience,* 314(5804), 1442-1445.

Groisman, P. Y., Karl, T. R., Easterling, D. R., Knight, R. W., Jamason, P. F., Hennessy, K. J., . . . Fortuniak, K. (1999). Changes in the probability of heavy precipitation: important indicators of climatic change. In *Weather and Climate Extremes* (pp. 243-283): Springer.

Groisman, P. Y., Knight, R. W., Easterling, D. R., Karl, T. R., Hegerl, G. C., & Razuvaev, V. N. (2005). Trends in Intense Precipitation in the Climate Record. *Journal of Climate,* 18(9), 1326-1350.

Grose, M., Barnes-Keoghan, I., Corney, S., White, C., Holz, G., Bennett, J., . . . Bindoff, N. (2010). Climate Futures for Tasmania: general climate impacts technical report.

Grose, M., Timbal, B., Wilson, L., Bathols, J., & Kent, D. (2015). The subtropical ridge in CMIP5 models, and implications for projections of rainfall in southeast Australia. *Australian Meteorological and Oceanographic Journal,* 65, 90-106.

Grose, M. R., Risbey, J. S., Moise, A. F., Osbrough, S., Heady, C., Wilson, L., & Erwin, T. (2017). Constraints on southern Australian rainfall change based on atmospheric circulation in CMIP5 simulations. *Journal of Climate,* 30(1), 225-242.

Guerreiro, S. B., Fowler, H. J., Barbero, R., Westra, S., Lenderink, G., Blenkinsop, S., . . . Li, X.-F. (2018). Detection of continental-scale intensification of hourly rainfall extremes. *Nature Climate Change,* 8(9), 803.

Handmer, J., Ladds, M., & Magee, L. (2018). Updating the costs of disasters in Australia. *Australian Journal of Emergency Management, The,* 33(2), 40.

Hardwick Jones, R., Westra, S., & Sharma, A. (2010). Observed relationships between extreme sub-daily precipitation, surface temperature, and relative humidity. *Geophysical Research Letters,* 37(22), L22805.

Haustein, K., Otto, F., Uhe, P., Schaller, N., Allen, M., Hermanson, L., . . . Cullen, H. (2016). Real-time extreme weather event attribution with forecast seasonal SSTs. *Environmental Research Letters,* 11(6), 064006.

Hawkins, E., Frame, D., Harrington, L., Joshi, M., King, A., Rojas, M., & Sutton, R. (2020). Observed emergence of the climate change signal: from the familiar to the unknown. *Geophysical Research Letters,* 47(6), e2019GL086259.

Hawkins, E., & Sutton, R. (2009). The potential to narrow uncertainty in regional climate predictions. *Bulletin of the American Meteorological Society,* 90(8), 1095-1107.

Haylock, M., & Nicholls, N. (2000). Trends in extreme rainfall indices for an updated high quality data set for Australia, 1910-1998. *International Journal of Climatology,* 20(13), 1533-1541.

Hegerl, G. C., Hoegh-Guldberg, O., Casassa, G., Hoerling, M. P., Kovats, R., Parmesan, C., . . . Stott, P. A. (2010). Good practice guidance paper on detection and attribution related to anthropogenic climate change. Paper presented at the Meeting Report of the

Intergovernmental Panel on Climate Change Expert Meeting on Detection and Attribution of Anthropogenic Climate Change.
Held, I. M., & Soden, B. J. (2006). Robust responses of the hydrological cycle to global warming. *Journal of Climate,* 19(21), 5686-5699.
Hendon, H. H., Lim, E.-P., Arblaster, J. M., & Anderson, D. L. T. (2014). Causes and predictability of the record wet east Australian spring 2010. *Climate Dynamics,* 42(5), 1155-1174.
Henley, B. J. (2017). Pacific decadal climate variability: Indices, patterns and tropical-extratropical interactions. *Global and Planetary Change,* 155, 42-55.
Henley, B. J., Gergis, J., Karoly, D. J., Power, S., Kennedy, J., & Folland, C. K. (2015). A tripole index for the Interdecadal Pacific Oscillation. *Climate Dynamics,* 45(11-12), 3077.
Hennessy, K. J., Suppiah, R., & Page, C. M. (1999). Australian rainfall changes, 1910-1995. *Australian Meteorological Magazine,* 48(1), 1-13.
Hewson, T. D. (1998). Objective fronts. *Meteorological Applications,* 5(1), 37-65.
Hill, K. J., Santoso, A., & England, M. H. (2009). Interannual Tasmanian rainfall variability associated with large-scale climate modes. *Journal of Climate,* 22(16), 4383-4397.
Ho, M., Kiem, A. S., & Verdon-Kidd, D. C. (2015a). A paleoclimate rainfall reconstruction in the Murray-Darling Basin (MDB), Australia: 1. Evaluation of different paleoclimate archives, rainfall networks, and reconstruction techniques. *Water Resources Research,* 51(10), 8362-8379.
Ho, M., Kiem, A. S., & Verdon-Kidd, D. C. (2015b). A paleoclimate rainfall reconstruction in the Murray-Darling Basin (MDB), Australia: 2. Assessing hydroclimatic risk using paleoclimate records of wet and dry epochs. *Water Resources Research,* 51(10), 8380-8396.
Holman, K. D., & Vavrus, S. J. (2012). Understanding Simulated Extreme Precipitation Events in Madison, Wisconsin, and the Role of Moisture Flux Convergence during the Late Twentieth and Twenty-First Centuries. *Journal of Hydrometeorology,* 13(3), 877-894.
Hope, P., Abbs, D., Bhend, J., Chiew, F., Church, J., Ekström, M., . . . McInnes, K. (2015a). Southern and south-western flatlands cluster report. *Climate change in Australia projections for Australia's natural resource management regions.* CSIRO and Bureau of Meteorology, Canberra, ACT, Australia.
Hope, P., & Ganter, C. (2010). Recent and projected rainfall trends in south-west Australia and the associated shifts in weather systems. Paper presented at the Managing climate change: papers from the Greenhouse 2009 Conference. CSIRO, Collingwood, Victoria, Australia.
Hope, P., Grose, M. R., Timbal, B., Dowdy, A. J., Bhend, J., Katzfey, J. J., . . . Whetton, P. H. (2015b). Seasonal and regional signature of the projected southern Australian rainfall reduction. *Australian Meteorological and Oceanographic Journal,* 65(1), 54-71.
Hope, P., Timbal, B., & Fawcett, R. (2010). Associations between rainfall variability in the southwest and southeast of Australia and their evolution through time. *International Journal of Climatology,* 30(9), 1360-1371.
Hope, P. K. (2006b). Projected future changes in synoptic systems influencing southwest Western Australia. *Climate Dynamics,* 26(7), 765-780.
Hope, P. K., Drosdowsky, W., & Nicholls, N. (2006). Shifts in the synoptic systems influencing southwest Western Australia. *Climate Dynamics,* 26(7-8), 751-764.
Hsu, P. c., Li, T., Murakami, H., & Kitoh, A. (2013). Future change of the global monsoon revealed from 19 CMIP5 models. *Journal of Geophysical Research: Atmospheres,* 118(3), 1247-1260.

Huang, Y., Chameides, W. L., & Dickinson, R. E. (2007). Direct and indirect effects of anthropogenic aerosols on regional precipitation over east Asia. *Journal of Geophysical Research: Atmospheres,* 112(D3), 112, D03212.

Hudson, D., Alves, O., Hendon, H. H., Lim, E.-P., Liu, G., Luo, J.-J., . . . Wang, G. (2017). ACCESS-S1: the new Bureau of Meteorology multi-week to seasonal prediction system. *Journal of Southern Hemisphere Earth Systems Science,* 67(3), 132-159.

Hughes, N., Galeano, D., & Hattfield-Dodds. (2019). The effects of drought and climate variability on Australian farms. *Australian Bureau of Agricultural and Resource Economics and Sciences,* Canberra.

Hutchinson, M. F. (1998). Interpolation of rainfall data with thin plate smoothing splines. Part I: Two dimensional smoothing of data with short range correlation. *Journal of Geographic Information and Decision Analysis,* 2(2), 139-151.

Hwang, Y.-T., & Frierson, D. M. W. (2013). Link between the double-Intertropical Convergence Zone problem and cloud biases over the Southern Ocean. *Proceedings of the National Academy of Sciences,* 110(13), 4935-4940.

Jackson, T., Hatfield-Dodds, S., & Zammit, K. (2018). Snapshot of Australian agriculture. Australian Government, Department of Agriculture and Water Resources, *Australian Bureau Agriculture and Resource Economics: Canberra*.

Jakob, D., Karoly, D. J., & Seed, A. (2011a). Non-stationarity in daily and sub-daily intense rainfall – Part 1: Sydney, Australia. *Natural Hazards and Earth System Sciences,* 11(8), 2263-2271.

Jakob, D., Karoly, D. J., & Seed, A. (2011b). Non-stationarity in daily and sub-daily intense rainfall – Part 2: Regional assessment for sites in south-east Australia. *Natural Hazards and Earth System Sciences,* 11(8), 2273-2284.

Jakob, D., Su, C.-H., Eizenberg, N., Kociuba, G., Steinle, P., Fox-Hughes, P., & Bettio, L. (2017). An atmospheric high-resolution regional reanalysis for Australia. *The Bulletin of The Australian Meteorological and Oceanographic Society,* 30, 16-23.

Jakob, D., & Walland, D. (2016). Variability and long-term change in Australian temperature and precipitation extremes. *Weather and Climate Extremes,* 14, 36-55.

Ji, F., Evans, J. P., Argueso, D., Fita, L., & Di Luca, A. (2015). Using large-scale diagnostic quantities to investigate change in East Coast Lows. *Climate Dynamics,* 45(9-10), 2443-2453.

Jones, C., & Carvalho, L. M. (2006). Changes in the activity of the Madden–Julian oscillation during 1958–2004. *Journal of Climate*, 19(24), 6353-6370.

Jones, D. A., Wang, W., & Fawcett, R. (2009). High-quality spatial climate data-sets for Australia. *Australian Meteorological and Oceanographic Journal,* 58(4), 233.

Jourdain, N. C., Gupta, A. S., Taschetto, A. S., Ummenhofer, C. C., Moise, A. F., & Ashok, K. (2013). The Indo-Australian monsoon and its relationship to ENSO and IOD in reanalysis data and the CMIP3/CMIP5 simulations. *Climate Dynamics*, 41(11), 3073-3102.

Jourdain, N. C., Lengaigne, M., Vialard, J., Izumo, T., & Gupta, A. S. (2016). Further Insights on the Influence of the Indian Ocean Dipole on the Following Year's ENSO from Observations and CMIP5 Models. *Journal of Climate,* 29(2), 637-658.

Kahru, M., Marinone, S., Lluch-Cota, S., Parés-Sierra, A., & Mitchell, B. G. (2004). Ocean-color variability in the Gulf of California: scales from days to ENSO. *Deep Sea Research Part II: Topical Studies in Oceanography*, 51(1-3), 139-146.

Kajikawa, Y., Wang, B., & Yang, J. (2009). A multi-time scale Australian monsoon index. *International Journal of Climatology,* 30(8), 1114-1120. doi:10.1002/joc.1955

Kalnay, E., Kanamitsu, M., Kistler, R., Collins, W., Deaven, D., Gandin, L., . . . Joseph, D. (1996). The NCEP/NCAR 40-Year Reanalysis Project. *Bulletin of the American Meteorological Society*, 77(3), 437-471.

Keenan, T., & Carbone, R. (2008). Propagation and diurnal evolution of warm season cloudiness in the Australian and Maritime Continent region. *Monthly Weather Review,* 136(3), 973-994.

Kent, D. M., Kirono, D. G., Timbal, B., & Chiew, F. H. (2013). Representation of the Australian sub-tropical ridge in the CMIP3 models. *International Journal of Climatology,* 33(1), 48-57.

Kiem, A. S., & Franks, S. W. (2004). Multi-decadal variability of drought risk, eastern Australia. *Hydrological Processes,* 18(11), 2039-2050.

Kiem, A. S., Franks, S. W., & Kuczera, G. (2003). Multi-decadal variability of flood risk. *Geophysical Research Letters,* 30(2),1035.

King, A. D., Alexander, L. V., & Donat, M. G. (2013). Asymmetry in the response of eastern Australia extreme rainfall to low-frequency Pacific variability. *Geophysical Research Letters,* 40(10), 2271-2277.

King, A. D., Alexander, L. V., & Donat, M. G. (2013a). The efficacy of using gridded data to examine extreme rainfall characteristics: a case study for Australia. *International Journal of Climatology,* 33(10), 2376-2387.

King, A. D., Donat, M. G., Alexander, L. V., & Karoly, D. J. (2015). The ENSO-Australian rainfall teleconnection in reanalysis and CMIP5. *Climate Dynamics,* 44(9-10), 2623-2635.

King, A. D., Lewis, S. C., Perkins, S. E., Alexander, L. V., Donat, M. G., Karoly, D. J., & Black, M. T. (2013b). Limited evidence of anthropogenic influence on the 2011-12 extreme rainfall over Southeast Australia. *Bulletin of the American Meteorological Society,* 94(9), S55.

King, A. D., Pitman, A. J., Henley, B. J., Ukkola, A. M., & Brown, J. R. (2020). The role of climate variability in Australian drought. *Nature Climate Change,* 10(3), 177-179.

Kociuba, G., & Power, S. B. (2015). Inability of CMIP5 models to simulate recent strengthening of the walker circulation: implications for projections. *Journal of Climate,* 28(1), 20-35.

Ladds, M., Keating, A., Handmer, J., & Magee, L. (2017). How much do disasters cost? A comparison of disaster cost estimates in Australia. *International journal of disaster risk reduction,* 21, 419-429.

Lamarque, J.-F., Kyle, G. P., Meinshausen, M., Riahi, K., Smith, S. J., van Vuuren, D. P., . . . Vitt, F. (2011). Global and regional evolution of short-lived radiatively-active gases and aerosols in the Representative Concentration Pathways. *Climatic Change,* 109(1), 191-212.

Latif, M., Kleeman, R., & Eckert, C. (1997). Greenhouse warming, decadal variability, or El Nino? An attempt to understand the anomalous 1990s. *Journal of Climate,* 10(9), 2221-2239.

Lavender, S., & Walsh, K. (2011). Dynamically downscaled simulations of Australian region tropical cyclones in current and future climates. *Geophysical Research Letters,* 38(10), L10705.

Lavender, S. L., & Abbs, D. J. (2013). Trends in Australian rainfall: contribution of tropical cyclones and closed lows. *Climate Dynamics,* 40(1-2), 317-326.

Lavery, B., Joung, G., & Nicholls, N. (1997). An extended high-quality historical rainfall dataset for Australia. *Australian Meteorological Magazine,* 46(1), 27-38.

Lavery, B., Kariko, A., & Nicholls, N. (1992). A historical rainfall data set for Australia. *Aust. Met. Mag*, 40, 33-39.

Lee, S.-H., & Seo, K.-H. (2011). A multi-scale analysis of the interdecadal change in the Madden-Julian Oscillation. *Atmosphere*, 21(2), 143-149.

Lenderink, G., & Attema, J. (2015). A simple scaling approach to produce climate scenarios of local precipitation extremes for the Netherlands. *Environmental Research Letters*, 10(8), 085001.

Lenderink, G., Barbero, R., Loriaux, J. M., & Fowler, H. J. (2017). Super-Clausius–Clapeyron Scaling of Extreme Hourly Convective Precipitation and Its Relation to Large-Scale Atmospheric Conditions. *Journal of Climate*, 30(15), 6037-6052.

Lenderink, G., Barbero, R., Westra, S., & Fowler, H. J. (2018). Reply to comments on "Temperature-extreme precipitation scaling: a two-way causality?". *International Journal of Climatology*, 38(12), 4664-4666.

Lenderink, G., & van Meijgaard, E. (2008). Increase in hourly precipitation extremes beyond expectations from temperature changes. *Nature Geoscience*, 1, 511.

https://www.nature.com/articles/ngeo262#supplementary-information

Lewis, S. C., & Karoly, D. J. (2015). Are estimates of anthropogenic and natural influences on Australia's extreme 2010–2012 rainfall model-dependent? *Climate Dynamics*, 45(3-4), 679-695.

Li, J., Feng, J., & Li, Y. (2012). A possible cause of decreasing summer rainfall in northeast Australia. *International Journal of Climatology*, 32(7), 995-1005.

Li, X.-F., Yu, J., & Li, Y. (2013). Recent summer rainfall increase and surface cooling over Northern Australia since the late 1970s: A response to warming in the Tropical Western Pacific. *Journal of Climate*, 26(18), 7221-7239.

Li, Y., Cai, W., & Campbell, E. (2005). Statistical modeling of extreme rainfall in southwest Western Australia. *Journal of Climate*, 18(6), 852-863.

Li, Z., Cai, W., & Lin, X. (2016). Dynamics of changing impacts of tropical Indo-Pacific variability on Indian and Australian rainfall. *Scientific reports*, 6, 31767.

Lim, E.-P., Hendon, H. H., Zhao, M., & Yin, Y. (2017). Inter-decadal variations in the linkages between ENSO, the IOD and south-eastern Australian springtime rainfall in the past 30 years. *Climate Dynamics*, 49(1-2), 97-112.

Lim, E. P., Hendon, H. H., Arblaster, J. M., Delage, F., Nguyen, H., Min, S. K., & Wheeler, M. C. (2016). The impact of the Southern Annular Mode on future changes in Southern Hemisphere rainfall. *Geophysical Research Letters*, 43(13), 7160-7167.

Lin, Z., & Li, Y. (2012). Remote Influence of the Tropical Atlantic on the Variability and Trend in North West Australia Summer Rainfall. *Journal of Climate*, 25(7), 2408-2420. doi:10.1175/jcli-d-11-00020.1

Liu, S. C., Fu, C., Shiu, C.-J., Chen, J.-P., & Wu, F. (2009). Temperature dependence of global precipitation extremes. *Geophysical Research Letters*, 36(17), L17702.

Lucas, C. (2010). *A High-quality Historical Humidity Database for Australia [electronic resource]*.

Luo, J.-J., Sasaki, W., & Masumoto, Y. (2012). Indian Ocean warming modulates Pacific climate change. *Proceedings of the National Academy of Sciences*, 109(46), 18701-18706.

Marelle, L., Myhre, G., Hodnebrog, Ø., Sillmann, J., & Samset, B. H. (2018). The changing seasonality of extreme daily precipitation. *Geophysical Research Letters*, 45(20), 11,352-311,360.

Marshall, G. J. (2003). Trends in the Southern Annular Mode from observations and reanalyses. *Journal of Climate,* 16(24), 4134-4143.

McIntosh, P. C., & Hendon, H. H. (2017). Understanding Rossby wave trains forced by the Indian Ocean Dipole. *Climate Dynamics*, 50, 2783–2798.

Meneghini, B., Simmonds, I., & Smith, I. N. (2007). Association between Australian rainfall and the southern annular mode. *International Journal of Climatology,* 27(1), 109-121.

Menne, M. J., Durre, I., Vose, R. S., Gleason, B. E., & Houston, T. G. (2012). An Overview of the Global Historical Climatology Network-Daily Database. *Journal of Atmospheric and Oceanic Technology,* 29(7), 897-910.

Meyers, G., McIntosh, P., Pigot, L., & Pook, M. (2007). The years of El Niño, La Niña, and interactions with the tropical Indian Ocean. *Journal of Climate,* 20(13), 2872-2880.

Miao, C., Sun, Q., Borthwick, A. G. L., & Duan, Q. (2016). Linkage Between Hourly Precipitation Events and Atmospheric Temperature Changes over China during the Warm Season. *Scientific reports,* 6, 22543.

https://www.nature.com/articles/srep22543#supplementary-information

Micevski, T., Franks, S. W., & Kuczera, G. (2006). Multidecadal variability in coastal eastern Australian flood data. *Journal of Hydrology,* 327(1-2), 219-225.

Michailidi, E. M., Antoniadi, S., Koukouvinos, A., Bacchi, B., & Efstratiadis, A. (2018). Timing the time of concentration: shedding light on a paradox. *Hydrological sciences journal,* 63(5), 721-740.

Mishra, V., Wallace, J. M., & Lettenmaier, D. P. (2012). Relationship between hourly extreme precipitation and local air temperature in the United States. *Geophysical Research Letters,* 39(16), L16403.

Moise, A., & Colman, R. (2010). *Tropical Australia and the Australian monsoon: general assessment and projected changes.* Paper presented at the Managing Climate Change: Papers from the Greenhouse 2009 Conference.

Moise, A., Colman, R., & Brown, J. (2012). Behind uncertainties in projections of Australian tropical climate: analysis of 19 CMIP3 models. *Journal of Geophysical Research: Atmospheres,* 117(D10), D10103.

Moise, A., Smith, I., Brown, J. R., Colman, R., & Narsey, S. (2019). Observed and projected intra-seasonal variability of Australian monsoon rainfall. *International Journal of Climatology,* 40, 2310– 2327.

Montzka, S., Reimann, S., Engel, A., Kruger, K., Sturges, W., Blake, D., . . . Jucks, K. (2011). Scientific assessment of ozone depletion: 2010. *Global Ozone Research and Monitoring Project-Report No. 51*.

Mukherjee, S., Aadhar, S., Stone, D., & Mishra, V. (2018). Increase in extreme precipitation events under anthropogenic warming in India. *Weather and Climate Extremes ,* 20, 45-53.

Murphy, B. F., & Timbal, B. (2008). A review of recent climate variability and climate change in southeastern Australia. *International Journal of Climatology,* 28(7), 859-879.

Narsey, S. Y., Brown, J. R., Colman, R. A., Delage, F., Power, S. B., Moise, A. F., & Zhang, H. (2020). Climate Change Projections for the Australian Monsoon From CMIP6 Models. *Geophysical Research Letters,* 47(13), e2019GL086816.

Narsey, S., Reeder, M. J., Ackerley, D., & Jakob, C. (2017). A midlatitude influence on Australian monsoon bursts. *Journal of Climate,* 30(14), 5377-5393.

Nawi, N. M. (2009). *Development of a climate-based computer model to reduce wheat harvest losses in Australia.* University of Southern Queensland.

Ng, B., Walsh, K., & Lavender, S. (2015). The contribution of tropical cyclones to rainfall in northwest Australia. *International Journal of Climatology,* 35(10), 2689-2697.

Nicholls, N. (2006). Detecting and attributing Australian climate change: a review. *Australian Meteorological Magazine,* 55(3), 199-211.

Nicholls, N., Chambers, L., Haylock, M., Frederiksen, C., Jones, D., & Drosdowsky, W. (1999). Climate variability and predictability for south-west Western Australia. *Towards Understanding Climate Variability in south western Australia, Research reports on the First Phase of the Indian Ocean Climate Initiative*, 1-52.

Nicholls, N., & Collins, D. (2006). Observed Climate Change in Australia over the past Century. *Energy & Environment,* 17(1), 1-12.

Nicholls, N., Drosdowsky, W., & Lavery, B. (1997). Australian rainfall variability and change. *Weather,* 52(3), 66-72.

Nicholls, N., Landsea, C., & Gill, J. (1998). Recent trends in Australian region tropical cyclone activity. *Meteorology and Atmospheric Physics,* 65(3-4), 197-205.

O'Donnell, A. J., Cook, E. R., Palmer, J. G., Turney, C. S., Page, G. F., & Grierson, P. F. (2015). Tree rings show recent high summer-autumn precipitation in northwest Australia is unprecedented within the last two centuries. *PloS one,* 10(6), e0128533.

O'Gorman, P. A., & Schneider, T. (2009). The physical basis for increases in precipitation extremes in simulations of 21st-century climate change. *Proceedings of the National Academy of Sciences,* 106(35), 14773-14777.

O'Gorman, P., & Muller, C. (2010). How closely do changes in surface and column water vapor follow Clausius–Clapeyron scaling in climate change simulations? *Environmental Research Letters,* 5(2), 025207.

O'Gorman, P. A. (2012). Sensitivity of tropical precipitation extremes to climate change. *Nature Geoscience,* 5(10), 697.

Pall, P., Allen, M., & Stone, D. A. (2007). Testing the Clausius–Clapeyron constraint on changes in extreme precipitation under CO 2 warming. *Climate Dynamics,* 28(4), 351-363.

Palmer, J. G., Cook, E. R., Turney, C. S., Allen, K., Fenwick, P., Cook, B. I., . . . Baker, P. (2015). Drought variability in the eastern Australia and New Zealand summer drought atlas (ANZDA, CE 1500–2012) modulated by the Interdecadal Pacific Oscillation. *Environmental Research Letters,* 10(12), 124002.

Pendergrass, A. G. (2018). What precipitation is extreme? *science,* 360(6393), 1072-1073.

Pendergrass, A. G., & Hartmann, D. L. (2014). Changes in the distribution of rain frequency and intensity in response to global warming. *Journal of Climate,* 27(22), 8372-8383.

Pendergrass, A. G., & Knutti, R. (2018). The uneven nature of daily precipitation and its change. *Geophysical Research Letters,* 45(21), 11,980-911,988.

Pepler, A., Coutts-Smith, A., & Timbal, B. (2014). The role of East Coast Lows on rainfall patterns and inter-annual variability across the East Coast of Australia. *International Journal of Climatology,* 34(4), 1011-1021.

Pepler, A., Hope, P., & Dowdy, A. (2019). Long-term changes in southern Australian anticyclones and their impacts. *Climate Dynamics*, 53, 4701–4714.

Pepler, A. S., Di Luca, A., Ji, F., Alexander, L. V., Evans, J. P., & Sherwood, S. C. (2015). Impact of identification method on the inferred characteristics and variability of Australian East Coast Lows. *Monthly Weather Review,* 143(3), 864-877.

Pepler, A. S., Di Luca, A., Ji, F., Alexander, L. V., Evans, J. P., & Sherwood, S. C. (2016). Projected changes in east Australian midlatitude cyclones during the 21st century. *Geophysical Research Letters,* 43(1), 334-340.

Perry, S. J., McGregor, S., Gupta, A. S., & England, M. H. (2017). Future changes to El Niño–Southern Oscillation temperature and precipitation teleconnections. *Geophysical Research Letters*, 44(20), 10,608– 10,616.

Pfahl, S., O'Gorman, P. A., & Fischer, E. M. (2017). Understanding the regional pattern of projected future changes in extreme precipitation. *Nature Climate Change*, 7(6), 423.

Philip, P., & Yu, B. (2020). Interannual variations in rainfall of different intensities in South West of Western Australia. *International Journal of Climatology*, 40(6), 3052-3071.

Pitman, A., & Perkins, S. (2008). Regional projections of future seasonal and annual changes in rainfall and temperature over Australia based on skill-selected AR4 models. *Earth Interactions*, 12(12), 1-50.

Pitman, A. J., Narisma, G. T., Pielke, R., & Holbrook, N. (2004). Impact of land cover change on the climate of southwest Western Australia. *Journal of Geophysical Research: Atmospheres*, 109(D18), D18109.

Plummer, N., Salinger, M. J., Nicholls, N., Suppiah, R., Hennessy, K. J., Leighton, R. M., . . . Lough, J. M. (1999). Changes in climate extremes over the Australian region and New Zealand during the twentieth century. *Climatic Change*, 42(1), 183-202.

Power, S., Casey, T., Folland, C., Colman, A., & Mehta, V. (1999). Inter-decadal modulation of the impact of ENSO on Australia. *Climate Dynamics*, 15(5), 319-324.

Power, S., Haylock, M., Colman, R., & Wang, X. (2006). The predictability of interdecadal changes in ENSO activity and ENSO teleconnections. *Journal of Climate*, 19(19), 4755-4771.

Power, S. B., & Delage, F. P. D. (2019). Setting and smashing extreme temperature records over the coming century. *Nature Climate Change*, 9(7), 529-534.

Prein, A. F., Rasmussen, R. M., Ikeda, K., Liu, C., Clark, M. P., & Holland, G. J. (2017). The future intensification of hourly precipitation extremes. *Nature Climate Change*, 7(1), 48-52.

Preston, B. J. (2009). Water and ecologically sustainable development in the courts. *Macquarie J. Int'l & Comp. Envtl. L.*, 6, 129.

Rahman, A., Weinmann, P. E., Hoang, T. M. T., & Laurenson, E. M. (2002). Monte Carlo simulation of flood frequency curves from rainfall. *Journal of Hydrology*, 256(3-4), 196-210.

Randall, D. A., Wood, R. A., Bony, S., Colman, R., Fichefet, T., Fyfe, J., . . . Srinivasan, J. (2007). Climate models and their evaluation. In *Climate change 2007: The physical science basis. Contribution of Working Group I to the Fourth Assessment Report of the IPCC (FAR)* (pp. 589-662): Cambridge University Press.

Rauniyar, S. P., & Walsh, K. J. (2011). Scale interaction of the diurnal cycle of rainfall over the Maritime Continent and Australia: Influence of the MJO. *Journal of Climate*, 24(2), 325-348.

Raut, B. A., Jakob, C., & Reeder, M. J. (2014). Rainfall Changes over Southwestern Australia and Their Relationship to the Southern Annular Mode and ENSO. *Journal of Climate*, 27(15), 5801-5814.

Rayner, N., Parker, D. E., Horton, E., Folland, C., Alexander, L., Rowell, D., . . . Kaplan, A. (2003). Global analyses of sea surface temperature, sea ice, and night marine air temperature since the late nineteenth century. *Journal of Geophysical Research: Atmospheres*, 108(D14).

Rehman, S. U., Khan, K., & Simmonds, I. (2019). Links between Tasmanian precipitation variability and the Indian Ocean subtropical high. *Theoretical and Applied Climatology*, 138, 1255–1267.

Reid, K. J., Simmonds, I., Vincent, C. L., & King, A. D. (2019). The Australian Northwest Cloudband: Climatology, Mechanisms, and Association with Precipitation. *Journal of Climate*, 32(20), 6665-6684.

Risbey, J. S., McIntosh, P. C., & Pook, M. J. (2013). Synoptic components of rainfall variability and trends in southeast Australia. *International Journal of Climatology*, 33(11), 2459-2472.

Risbey, J. S., Pook, M. J., McIntosh, P. C., Wheeler, M. C., & Hendon, H. H. (2009). On the Remote Drivers of Rainfall Variability in Australia. *Monthly Weather Review*, 137(10), 3233-3253.

Roderick, T. P., Wasko, C., & Sharma, A. (2019). Atmospheric moisture measurements explain increases in tropical rainfall extremes. *Geophysical Research Letters*, 46, 1375– 1382.

Rogers, C. D. W., & Beringer, J. (2017). Describing rainfall in northern Australia using multiple climate indices. *Biogeosciences*, 14(3), 597.

Rotstayn, L. D., Cai, W., Dix, M. R., Farquhar, G. D., Feng, Y., Ginoux, P., . . . Wang, M. (2007). Have Australian rainfall and cloudiness increased due to the remote effects of Asian anthropogenic aerosols? *Journal of Geophysical Research*, 112(D9), D09202.

Rotstayn, L. D., Jeffrey, S. J., Collier, M. A., Dravitzki, S. M., Hirst, A. C., Syktus, J. I., & Wong, K. K. (2012). Aerosol- and greenhouse gas-induced changes in summer rainfall and circulation in the Australasian region: a study using single-forcing climate simulations. *Atmospheric Chemistry and Physics*, 12(14), 6377-6404.

Rouillard, A., Skrzypek, G., Turney, C., Dogramaci, S., Hua, Q., Zawadzki, A., . . . Grierson, P. (2016). Evidence for extreme floods in arid subtropical northwest Australia during the Little Ice Age chronozone (CE 1400–1850). *Quaternary Science Reviews*, 144, 107-122.

Saji, N., Goswami, B., Vinayachandran, P., & Yamagata, T. (1999). A dipole mode in the tropical Indian Ocean. *Nature*, 401(6751), 360-363.

Salzmann, M. (2016). Global warming without global mean precipitation increase? *Science advances*, 2(6), e1501572.

Santoso, A., McGregor, S., Jin, F.-F., Cai, W., England, M. H., An, S.-I., . . . Guilyardi, E. (2013). Late-twentieth-century emergence of the El Niño propagation asymmetry and future projections. *Nature*, 504(7478), 126.

Schär, C., Ban, N., Fischer, E. M., Rajczak, J., Schmidli, J., Frei, C., . . . Zwiers, F. W. (2016). Percentile indices for assessing changes in heavy precipitation events. *Climatic Change*, 137(1), 201-216.

Seidel, D. J., Fu, Q., Randel, W. J., & Reichler, T. J. (2008). Widening of the tropical belt in a changing climate. *Nature Geoscience*, 1(1), 21.

Shaw, S. B., Royem, A. A., & Riha, S. J. (2011). The relationship between extreme hourly precipitation and surface temperature in different hydroclimatic regions of the United States. *Journal of Hydrometeorology*, 12(2), 319-325.

Shepherd, T. G. (2016). A Common Framework for Approaches to Extreme Event Attribution. *Current Climate Change Reports*, 2(1), 28-38.

Shi, G., Cai, W., Cowan, T., Ribbe, J., Rotstayn, L., & Dix, M. (2008). Variability and Trend of North West Australia Rainfall: Observations and Coupled Climate Modeling. *Journal of Climate*, 21(12), 2938-2959.

Sillmann, J., Kharin, V. V., Zhang, X., Zwiers, F. W., & Bronaugh, D. (2013a). Climate extremes indices in the CMIP5 multimodel ensemble: Part 1. Model evaluation in the present climate. *Journal of Geophysical Research: Atmospheres*, 118(4), 1716-1733.

Sillmann, J., Kharin, V. V., Zwiers, F. W., Zhang, X., & Bronaugh, D. (2013b). Climate extremes indices in the CMIP5 multimodel ensemble: Part 2. Future climate projections. *Journal of Geophysical Research: Atmospheres,* 118(6), 2473-2493.

Smith, I., McIntosh, P., Ansell, T., Reason, C., & McInnes, K. (2000). Southwest Western Australian winter rainfall and its association with Indian Ocean climate variability. *International Journal of Climatology,* 20(15), 1913-1930.

Smith, I. N., & Timbal, B. (2012). Links between tropical indices and southern Australian rainfall. *International Journal of Climatology,* 32(1), 33-40.

Speer, M. S., Leslie, L. M., & Fierro, A. O. (2011). Australian east coast rainfall decline related to large scale climate drivers. *Climate Dynamics,* 36(7-8), 1419-1429.

Stephens, G. L., & Ellis, T. D. (2008). Controls of global-mean precipitation increases in global warming GCM experiments. *Journal of Climate,* 21(23), 6141-6155.

Sugiyama, M., Shiogama, H., & Emori, S. (2010). Precipitation extreme changes exceeding moisture content increases in MIROC and IPCC climate models. *Proceedings of the National Academy of Sciences,* 107(2), 571-575.

Sun, Q., Miao, C., Duan, Q., Ashouri, H., Sorooshian, S., & Hsu, K. L. (2018). A review of global precipitation data sets: Data sources, estimation, and intercomparisons. *Reviews of Geophysics,* 56(1), 79-107.

Suppiah, R., & Hennessy, K. J. (1996). Trends in the intensity and frequency of heavy rainfall in tropical Australia and links with the Southern Oscillation. *Australian Meteorological Magazine,* 45(1), 1-17.

Suppiah, R., Macadam, I., & Whetton, P. (2007). Climate change projections for the tropical rainforest region of North Queensland. *Cairns: Reef and Rainforest Research Centre Limited,* 38.

Swart, N., & Fyfe, J. C. (2012). Observed and simulated changes in the Southern Hemisphere surface westerly wind-stress. *Geophysical Research Letters,* 39(16).

Taschetto, A. S., & England, M. H. (2009a). An analysis of late twentieth century trends in Australian rainfall. *International Journal of Climatology,* 29(6), 791-807.

Taschetto, A. S., & England, M. H. (2009b). El Niño Modoki Impacts on Australian Rainfall. *Journal of Climate,* 22(11), 3167-3174.

Taylor, K. E., Stouffer, R. J., & Meehl, G. A. (2012). An Overview of CMIP5 and the Experiment Design. *Bulletin of the American Meteorological Society,* 93(4), 485-498.

Thompson, D. W., Solomon, S., Kushner, P. J., England, M. H., Grise, K. M., & Karoly, D. J. (2011). Signatures of the Antarctic ozone hole in Southern Hemisphere surface climate change. *Nature Geoscience,* 4(11), 741.

Timbal, B. (2004). Southwest Australia past and future rainfall trends. *Climate Research,* 26(3), 233-249.

Timbal, B. (2009). The continuing decline in South-East Australian rainfall: update to May 2009. *CAWCR Research Letters,* 2(4-11).

Timbal, B., Abbs, D., Bhend, J., Chiew, F., Church, J., Ekström, M., . . . McInnes, K. (2015). Murray basin cluster report. *Climate Change in Australia Projections for Australia's Natural Resource Management Regions: Cluster Reports. CSIRO and Bureau of Meteorology, Australia, Australia*.

Timbal, B., & Arblaster, J. M. (2006b). Land cover change as an additional forcing to explain the rainfall decline in the south west of Australia. *Geophysical Research Letters,* 33(7), L07717.

Timbal, B., Arblaster, J. M., & Power, S. (2006a). Attribution of the late-twentieth-century rainfall decline in southwest Australia. *Journal of Climate,* 19(10), 2046-2062.

Timbal, B., & Drosdowsky, W. (2013). The relationship between the decline of Southeastern Australian rainfall and the strengthening of the subtropical ridge. *International Journal of Climatology,* 33(4), 1021-1034.

Tozer, C., Kiem, A., Vance, T., Roberts, J., Curran, M., & Moy, A. (2018). Reconstructing pre-instrumental streamflow in Eastern Australia using a water balance approach. *Journal of Hydrology,* 558, 632-646.

Tozer, C. R., Vance, T. R., Roberts, J. L., Kiem, A. S., Curran, M. A., & Moy, A. D. (2016). An ice core derived 1013-year catchment-scale annual rainfall reconstruction in subtropical eastern Australia. *Hydrology and Earth System Sciences,* 20(5), 1703.

Trenberth, K. E. (2012). Framing the way to relate climate extremes to climate change. *Climatic Change,* 115(2), 283-290.

Trenberth, K. E., Dai, A., Rasmussen, R. M., & Parsons, D. B. (2003). The changing character of precipitation. *Bulletin of the American Meteorological Society,* 84(9), 1205-1217.

Trenberth, K. E., & Shea, D. J. (2005). Relationships between precipitation and surface temperature. *Geophysical Research Letters,* 32(14), L14703.

Ummenhofer, C. C., England, M. H., McIntosh, P. C., Meyers, G. A., Pook, M. J., Risbey, J. S., . . . Taschetto, A. S. (2009). What causes southeast Australia's worst droughts? *Geophysical Research Letters,* 36(4), L04706.

Utsumi, N., Seto, S., Kanae, S., Maeda, E. E., & Oki, T. (2011). Does higher surface temperature intensify extreme precipitation? *Geophysical Research Letters,* 38(16), L16708.

Vance, T., Roberts, J., Plummer, C., Kiem, A., & Van Ommen, T. (2015). Interdecadal Pacific variability and eastern Australian megadroughts over the last millennium. *Geophysical Research Letters,* 42(1), 129-137.

Verdon-Kidd, D. C., & Kiem, A. S. (2009). Nature and causes of protracted droughts in southeast Australia: Comparison between the Federation, WWII, and Big Dry droughts. *Geophysical Research Letters,* 36, 6.

Verdon, D. C., Wyatt, A. M., Kiem, A. S., & Franks, S. W. (2004). Multidecadal variability of rainfall and streamflow: Eastern Australia. *Water Resources Research,* 40(10), W10201.

Viney, N. R., & Bates, B. C. (2004). It never rains on Sunday: the prevalence and implications of untagged multi-day rainfall accumulations in the Australian high quality data set. *International Journal of Climatology,* 24(9), 1171-1192.

Wang, B., Liu, J., Kim, H.-J., Webster, P. J., & Yim, S.-Y. (2012). Recent change of the global monsoon precipitation (1979–2008). *Climate Dynamics,* 39(5), 1123-1135.

Wang, G., Cai, W., & Purich, A. (2014). Trends in Southern Hemisphere wind-driven circulation in CMIP5 models over the 21st century: Ozone recovery versus greenhouse forcing. *Journal of Geophysical Research: Oceans,* 119(5), 2974-2986.

Wang G. G., Wang, D., Trenberth, K. E., Erfanian, A., Yu, M., Bosilovich, Michael G., & Parr, D. T. (2017). The peak structure and future changes of the relationships between extreme precipitation and temperature. *Nature Climate Change,* 7, 268.

https://www.nature.com/articles/nclimate3239#supplementary-information

Wang, H., Kumar, A., Murtugudde, R., Narapusetty, B., & Seip, K. L. (2019). Covariations between the Indian Ocean dipole and ENSO: a modeling study. *Climate Dynamics,* 53(9), 5743-5761.

Wang X., X., Jiang, D., & Lang, X. (2017). Future extreme climate changes linked to global warming intensity. *Science Bulletin,* 62(24), 1673-1680.

Wardle, R., & Smith, I. (2004). Modeled response of the Australian monsoon to changes in land surface temperatures. *Geophysical Research Letters,* 31(16), L16205.

Wasko, C., Lu, W. T., & Mehrotra, R. (2018). Relationship of extreme precipitation, dry-bulb temperature, and dew point temperature across Australia. *Environmental Research Letters,* 13(7), 074031.

Wasko, C., & Nathan, R. (2019). The local dependency of precipitation on historical changes in temperature. *Climatic Change,* 1-16, 156, 105–120.

Wasko, C., & Sharma, A. (2015). Steeper temporal distribution of rain intensity at higher temperatures within Australian storms. *Nature Geoscience,* 8, 527–529.

https://www.nature.com/articles/ngeo2456#supplementary-information

Westra, S., Fowler, H., Evans, J., Alexander, L., Berg, P., Johnson, F., . . . Roberts, N. (2014). Future changes to the intensity and frequency of short-duration extreme rainfall. *Reviews of Geophysics,* 52(3), 522-555.

Whan, K., Timbal, B., & Lindesay, J. (2014). Linear and nonlinear statistical analysis of the impact of sub-tropical ridge intensity and position on south-east Australian rainfall. *International Journal of Climatology,* 34(2), 326-342.

Wheeler, M. C., & Hendon, H. H. (2004). An all-season real-time multivariate MJO index: Development of an index for monitoring and prediction. *Monthly Weather Review,* 132(8), 1917-1932.

Wheeler, M. C., Hendon, H. H., Cleland, S., Meinke, H., & Donald, A. (2009). Impacts of the Madden–Julian Oscillation on Australian Rainfall and Circulation. *Journal of Climate,* 22(6), 1482-1498.

Whetton, P. H., Grose, M. R., & Hennessy, K. J. (2016). A short history of the future: Australian climate projections 1987–2015. *Climate Services,* 2, 1-14.

White, C., Franks, S., & McEvoy, D. (2015). Using subseasonal-to-seasonal (S2S) extreme rainfall forecasts for extended-range flood prediction in Australia. *IAHS-AISH Proceedings and Reports,* 370, 229-234.

White, C., Sanabria, L., Grose, M., Bennett, J., Holz, G., McInnes, K., . . . Bindoff, N. (2010). Climate Futures for Tasmania: extreme events technical report, Antarctic Climate and Ecosystems Cooperative Research Centre, Hobart, Tasmania.

Wilcox, L., Highwood, E., Booth, B., & Carslaw, K. (2015). Quantifying sources of inter-model diversity in the cloud albedo effect. *Geophysical Research Letters,* 42(5), 1568-1575.

Wright, P. B. (1974). Seasonal rainfall in southwestern Australia and the general circulation. *Monthly Weather Review,* 102(3), 219-232.

Wright, W. J. (1997). Tropical–extratropical cloudbands and Australian rainfall: I. climatology. *International Journal of Climatology,* 17(8), 807-829.

Ye, H., Fetzer, E. J., Wong, S., Behrangi, A., Yang, D., & Lambrigtson, B. H. (2015). Increasing atmospheric water vapor and higher daily precipitation intensity over northern Eurasia. *Geophysical Research Letters,* 42(21), 9404-9410.

Yim, S.-Y., Wang, B., Liu, J., & Wu, Z. (2014). A comparison of regional monsoon variability using monsoon indices. *Climate Dynamics,* 43(5-6), 1423-1437.

Zhang, W., Villarini, G., & Wehner, M. (2019). Contrasting the responses of extreme precipitation to changes in surface air and dew point temperatures. *Climatic Change,* 154, 257–271.

Zhang, X., Alexander, L., Hegerl, G. C., Jones, P., Tank, A. K., Peterson, T. C., . . . Zwiers, F. W. (2011). Indices for monitoring changes in extremes based on daily temperature and precipitation data. *Wiley Interdisciplinary Reviews: Climate Change,* 2(6), 851-870.

Zhang, X., Zwiers, F. W., Li, G., Wan, H., & Cannon, A. J. (2017). Complexity in estimating past and future extreme short-duration rainfall. *Nature Geoscience*, 10(4), 255-259.

Zhao, M., Hendon, H. H., Alves, O., Liu, G., & Wang, G. (2016). Weakened eastern Pacific El Niño predictability in the early twenty-first century. *Journal of Climate*, 29(18), 6805-6822.

Zheng, F., Li, J., Clark, R. T., & Nnamchi, H. C. (2013). Simulation and projection of the Southern Hemisphere annular mode in CMIP5 models. *Journal of Climate*, 26(24), 9860-9879.

Zillman, J. W. (2001). *A Hundred Years of Science and Service: Australian Meteorology Through the Twentieth Century*: Bureau of Meteorology.